

Trinity College Dublin
Coláiste na Tríonóide, Baile Átha Cliath
The University of Dublin

The Gut-Lung Axis and Butyrate-Mediated Immunomodulation: A Study on Pneumococcal Pneumonia Severity and Vaccine Efficacy

Kate Roche

Supervisors – Research Assistant Professor Natalia Muñoz-Wolf and co-supervisor Professor Ed Lavelle

2026

A PhD thesis submitted to Trinity College Dublin for the degree of Doctor of Philosophy

I declare that this thesis has not been submitted as an exercise for a degree at this or any other university and it is entirely my own work with help from those accredited[1] and with acknowledgement of resources provided by our collaborators[2]. I confirm that the work has been completed in full compliance with relevant university policies, including the Academic Integrity policy, the Trinity Policy on Good Research Practice, and the guidance on AI and GenAI in Teaching, Learning, Assessment and Research. I agree to deposit this thesis in the University's open access institutional repository or allow the Library to do so on my behalf, subject to Irish Copyright Legislation and Trinity College Library conditions of use and acknowledgement. I consent to the examiner retaining a copy of the thesis beyond the examining period, should they so wish (EU GDPR May 2018).

22/12/2025

Kate Roche

[1] Acknowledgement to the following for their contributions to this work:

- Research Assistant Prof. Kiva Brennan for performing intramuscular injections and the polysaccharide specific anti-body ELISAs (**Fig. 4.8 D, H**), (**Fig. 4.18 G, H**) and (**Fig. 4.22 A-D**).
- MSc. Jeremy Aboagye for performing the ELISpot assays (**Fig. 4.10**), (**Fig. 4.19**).
- BSc. Melanie Fidel, for assisting with the optimisation of the protocols used in the clinical pipeline at Tallaght University Hospital.
- MSc. Filza Masood for performing the *Streptococcus pneumoniae* growth curves shown in **Fig. 3.1** and contributing to the gentamicin protection assays on primary human alveolar macrophage (**Fig. 3.14 B, C**).
- Research Assistant Prof. Natalia Muñoz-Wolf for generation of the mouse adapted D39 strain and helping with processing of tissues and bacterial enumeration (**Fig. 3.22 D, E**).

- Dr. Fiona Mary Roche and Dr. Karsten Hokamp for the primary EdgeR analysis of bulk RNA sequencing data and for providing R Studio scripts for the generation of heatmaps, gene set enrichment analysis and volcano plots (**Fig. 3.4-3.11**). I generated all final graphs based on these resources myself with the exception of Principal Component Analysis plots (**Fig. 3.6 A**) and (**Fig. 3.7 A**) and **Fig. 3.8**.

[2] Acknowledgement of resources provided by collaborators:

- Prof. Suzanne Cloonan, Trinity College Dublin, and Prof. Susan Carpenter, University of California, San Francisco, for their contribution of the Foetal liver derived alveolar macrophage (FLAM) cell line.
- Prof. Analía Ríal and Prof. Jose Alejandro Chabalgoity, University of La Republica - Uruguay, for their contribution of the *S. pneumoniae* strains E1586 and TIGR4 and the *S. pneumoniae* bacterial lysates.
- Research Assistant Prof. Kiva Brennan for sourcing and providing the clinical pneumococcal vaccine Prevnar13®.
- Prof Ed Lavelle, Prof. Jacob Bitoun and Prof. James McLachlan for providing the adjuvant Double mutant heat-labile toxin (dmLT).
- Prof. Seamas Donnelly and Prof Patrick Mitchell and all physicians involved in sample collection and T.J. Butler the lab manager at Tallaght University Teaching Hospital for providing access to the clinical and research facilities and assisting with human sample collection and processing.
- A heartfelt acknowledgement to all the patients who kindly agreed to participate in the clinical study and donated their samples to research.
- Dr Barry Moran for providing advice and access to the Flow Cytometry Facility at Trinity Biomedical Sciences Institute.

Acknowledgements

I would first like to thank my supervisors, Research Assistant Prof. Natalia Muñoz-Wolf and Prof. Ed Lavelle. I truly couldn't have asked for better supervisors and want to start by thanking you both for the opportunities you have granted me. Thank you, Natalia, for originally giving me this opportunity; none of this would have been possible without you. Your passion, expertise, and determination in your work are an inspiration. Thank you for your guidance and support over the last four years. Thanks, Ed, for your continued support and patience with us dropping by your office every other day! Thank you for integrating me into the lab at the start of this PhD. I've been extremely fortunate to have spent the last four years in a great working environment with fantastic people.

To everyone in the lab, both past and present, I want to say a huge thank you, and it was an absolute pleasure working with each and every one of you. Roisin, you mentioned our co-dependency in your own thesis acknowledgements, and I fear it has only gotten worse; thank you for being one of my best friends. Jorge – My science sibling, you are the hardest-working and most deserving person I know. You have always raised the bar and encouraged me to do the same. Nicole R – Mo chúpla, mo chara, go raibh maith agat as na gáirí go leir. Dorian – "If you want a job done, ask Dorian Dederko"; thank you for all the laughs and for sharing the burden of isolation trauma! Jeremy – Your ELISpot expertise, unwavering positivity, and your passion for good food has made the gloomiest days in TBSI exciting. Nicole O'S – It's been a pleasure working with you in the last two years, I've found community in someone who loves Pompompurin as much as I do. Liam – Ádh mór agat leis an PhD, is eolaí dochreidte tú! Fay – I could write about you for 200 pages; I look up to you in so many ways personally and professionally. Thank you for all your encouragement, kindness and treats, which have kept me going this last year. Lorena – Thank you for keeping the lab running. I don't know where we would all be without your efficiency and hard work. Yukta – It has been lovely getting to know you this last year, and very best of luck with your future endeavours. Filza (The microbiology queen) – Thank you for everything (especially Chrissy) in the last year, you are so talented and have an incredibly bright future ahead of you! Melanie – Thank you for your support last year, and all the laughs in Barcelona!

Ross – The lab really hasn't been the same since you've left, I miss the afternoon Gerard's coffees and talking to the swans in the Liffey. To past members of the Lavelle Lab, Joanna, Alex and Grainne, it has been a pleasure working with you all!

Cian and Alanna, it's been 8 long years in Trinity, and we've made it to the other side. I couldn't be prouder of both of you! It's been an honour watching you both achieve incredible PhDs.

A huge thank you to the Cloonan Lab, who have been extremely supportive collaborators throughout this project. Suzanne – thank you for all your guidance during the PhD. Lynne – I've thoroughly enjoyed our abstract chats and giggles in the Cat2, thank you for all your support! Sarah – Of the many positive takeaways from the last four years, gaining you as a friend has been at the top of the list. Thank you for always being there! I would like to acknowledge the physicians and our collaborators at Tallaght University Teaching Hospital, for facilitating the clinical pipeline, which has been fundamental in our work. I would also like to acknowledge those who contributed to this work by kindly agreeing to donate their samples to research.

Kiva, thank you for all your expertise with the Prevnar studies. It has been a pleasure working with you! Craig, thank you for your IgA advice!

Myriam, thank you for supporting me through the last four years and listening with open ears to every trial, tribulation and sporadic success. Your own fascination in science triggered mine, and this thesis wouldn't have been at all possible without your unwavering belief in me (or teaching me what a cell was). To my grandparents, G and P, love you lots, thank you for blindly believing in me! Sammy, my deepest appreciation for all the lifts to and from TBSI, chicken dinners and positive affirmations! To my friends, thank you all for your patience. I am making my re-introduction to social society this Spring 2026!

Abstract

Lower respiratory tract infections (LRTI) remain a leading cause of mortality worldwide. Community-acquired pneumonia (CAP) accounts for a significant burden of LRTI cases, with *Streptococcus pneumoniae* being the primary aetiological agent of CAP globally and also causing other forms of invasive disease (IPD), namely otitis media, meningitis, bacteraemia and sepsis. Despite the availability of pneumococcal vaccines, the global burden of pneumococcal pneumonia and IPD remains high. The gut microbiota has emerged as a significant regulator of chronic respiratory diseases and infections through the gut-lung axis of immune regulation. Short-chain fatty acids (SCFA) are highly pleiotropic immunomodulatory microbiota-derived metabolites, produced exclusively by microbial commensals through the saccharolytic fermentation of dietary fibre. Acetate, propionate and butyrate are the three most abundant short-chain fatty acids in the intestinal tract, the peripheral circulation and the lung.

Dysbiosis, the imbalance or depletion of the microbiota, increases susceptibility to respiratory infection and is noted in patients with chronic respiratory disease. However, the exact mechanisms behind how the gut microbiota modulates lung immunity remain to be fully elucidated. SCFAs, as systemic messengers of the microbiota, alleviate respiratory infections in murine models of *Influenza*, *Klebsiella pneumoniae,* and recently, *S. pneumoniae* under eubiotic conditions*.* Potentially therapeutic links have been identified between intake of the prebiotic agent of SCFA, fermentable fibre and outcomes of respiratory infection and disease. Here, we examine whether the therapeutic potential of butyrate can be harnessed to alleviate pneumococcal pneumonia in a highly susceptible model of antibiotic-induced dysbiosis. Bulk RNA sequencing revealed that butyrate treatment altered the transcriptomic profile of alveolar macrophages (AMs) *in vitro*, enhancing antimicrobial pathways and significantly upregulating genes associated with several antimicrobial peptides. Gentamicin protection assays in both murine and human AMs further highlighted the ability of butyrate to enhance intracellular containment of *S. pneumoniae* while limiting IL-6 production. *In vivo* butyrate treatment effectively alleviated the severity of

pneumococcal infection in highly susceptible dysbiotic mice, attenuating manifestations of disease such as hypothermia and reducing local and systemic bacterial burden.

Our current understanding of how gut commensal composition and microbiota-derived metabolites impact vaccine immunogenicity and efficacy could underpin heterogeneity in vaccine performance amongst the global population. Current conjugated pneumococcal vaccines have proved successful in limiting the burden of IPD; however, limitations still remain, such as serotype replacement, limited protection against pneumonia and limited induction of mucosal immunity. The modulatory impact of SCFA on vaccine immunogenicity and efficacy remains to be elucidated and has not been studied in the context of pneumococcal vaccination or intranasal vaccination. Here, the effect of oral butyrate supplementation on the response to the licensed pneumococcal vaccine Prevnar13® is investigated. Additionally, the effects of butyrate supplementation on a trivalent pneumococcal vaccine formulated with heat-killed whole-cell lysed *S. pneumoniae* combined with the adjuvant double-mutant heat-labile toxin (dmLT) were studied. Conversely to the initial hypothesis, butyrate supplementation limited antigen-specific humoral responses locally in the lung, with reductions in antigen-specific IgA and systemically with reductions in serum antigen-specific IgG subclasses. Additionally, butyrate supplementation modulated antigen-specific cellular-mediated immunity, altering lymphocyte dynamics and functional characteristics. Collectively, these findings open new avenues for harnessing the gut-lung axis against pneumococcal pneumonia, while emphasising the need to optimise and rationalise the use of widely consumed butyrate supplements to selectively boost protective immunity against pneumococcal infection without compromising the efficacy of future novel mucosal pneumococcal vaccines.

Publications:

Intratumoral delivery of the chitin-derived C100 adjuvant promotes robust STING, IFNAR and CD8+ T cell dependant anti-tumour immunity Joanna L. Turley, Ross W. Ward, Jorge Huete-Carrasco, Natalia Muñoz-Wolf, **Kate Roche**, Lei Jin, Andrew Bowie, Mats Andersson, Ed C. Lavelle

Biodegradable microparticles promote anti-inflammatory innate immune memory though a size- and mTOR dependent process. Roisin I. Lynch, Aoife L. Gorman, Sean McCluskey, Cian J.H. Horneck-Johnston, **Kate Roche**, Natalia Muñoz-Wolf, Frederick J. Sheedy, Ed C. Lavelle

Abbreviations

A2B	Adenosine A2B regulator
AAI	Allergic airway inflammation
AhR	Aryl hydrocarbon receptor
Aim2	Absent in melanoma 2
AM	Alveolar macrophage
AMP	Adenosine monophosphate
Apoa	Apolipoprotein
ASC	Apoptosis-associated speck-like protein
ATT	Anti-tubercular therapy
BAL	Bronchiolar lavage
BALF	Bronchoalveolar lavage fluid
BMDM	Bone marrow derived macrophage
CAP	Community acquired pneumonia
CARD	Caspase recruitment domain
CbpA	Choline binding protein A
CCL	Chemokine ligand
CCR	Chemokine receptor
CD	Cluster of differentiation
CD	Crohn's disease
CF	Cystic fibrosis
CMIS	Common mucosal immune system
COPD	Chronic obstructive pulmonary disease
CRAMP	Cathelicidin-related antimicrobial peptide
CRM	Corynebacterium diphtheriae protein
CXCL	C-X-C motif chemokine ligand
CXCR	C-X-C motif chemokine receptor
DC	Dendritic cell
dmLT	Double mutant heat labile toxin
DNA	Deoxyribonucleic acid
DSS	Dextran sulfate sodium
EGR	Early growth response
ERK	Extracellular signal-regulated kinase
FFAR	Free fatty acid receptor
FLAM	Foetal liver derived alveolar macrophage
FMT	Fecal microbial transplant
FoxP3	Forkhead box P3
GALT	Gut associated lymphoid tissue
GATA	GATA binding protein
GM-CSF	Granulocyte colony stimulating factor
GPR	G-coupled protein receptor
HCAR2	Hydroxycarboxylic receptor 2

HDACi	Histone deacetylase inhibitor
HLA	Human leukocyte antigen
HSE	Health Services Executive
Hyl	Hyaluronate lyase
IBD	Inflammatory bowel disease
IFN	Interferon
Ig	Immunoglobulin
IL	Interleukin
ILC	Innate lymphocyte
iNKT	Inducible natural killer cell
iNOS	Inducible nitric oxide synthase
IP-10	Interferon-gamma induced protein 10
IPD	Invasive pneumococcal disease
IRAK	Interleukin-1 receptor associated kinase
Irf	Interferon regulatory factor
JNK	c-Jun-N-terminal kinase
Ki-67	Antigen Kiel 67
KLF	Krüppel-like factor
LAIV	Live attenuated influenza vaccine
Lcn	Lipocalin
LL-37	Cathelicidin antimicrobial peptide LL-37
LPS	Lipopolysaccharide
LTF	Lactoferrin
Ly	Lymphocyte antigen
LytA	Autolysin
MAdCAM-1	Mucosal vascular addressin cell adhesion molecule-1
MAIT	Mucosal associated invariant T cell
MAPK	Mitogen activated protein kinase
MCT1	Monocarboxylate transporter 1
MDM	Monocyte derived macrophage
MHC	Master histocompatibility complex
MIP	Macrophage inflammatory protein
MMP	Matrix-metalloproteinase
moDC	Monocyte derived dendritic cell
MPO	Myeloperoxidase
mTOR	Mechanistic target of rapamycin
mTORC1	Mechanistic target of rapamycin complex 1
MUC	Mucin
MyD88	Myeloid differentiation primary response 88
NEMO	NFkB essential modulator
NET	Neutrophilic extracellular trap
NFkB	Nuclear factor kappa-light-chain-enhancer of activated B cells

NLRC4	NLR family CARD domain containing 4
NLRP3	NLR family pyrin domain containing 3
NOD	Not-like receptor
Nrf2	Nuclear factor erythroid 2-relateed factor
P38	Mitogen-activated protein kinase 14
p53	Tumor protein p53
PavA	Pneumococccal adherence and virulence factor A
PCV	Pneumococcal conjugate vaccine
PepO	Endopeptidase O
PhtD	Pneumococcal histidine triad protein D
PigR	Polyspecific immunoglobulin receptor
PLY	Pneumolysin
PMN	Polymorphonuclear cells
PPAR	Peroxisome proliferator-activated receptor
PpmA	Putative proteinase maturation protein A
PspA	Pneumococcal surface protein A
RANTES	Regulated upon activation normal T-cell expressed and secreted
RelmB	Resistin-like molecule beta
RNA	Ribonucleic acid
RORγt	Retinoic acid receptor-related orphan receptor gamma t
ROS	Reactive oxygen species
SCFA	Short-chain fatty acid
SFB	Segmented filamentous bacteria
sIg	Secretory immunoglobulin
SMCT1	Sodium-coupled monocarboxylate transporter 1
SP	Surfactant protein
STAT	Signal transducer and activator of transcription
STING	Stimulator of interferon genes
Tab	TGF-β activated kinase 1 (MAP3K7) binding protein
Tak	Transforming growth factor-β-activated kinase 1
Tbet	T-box expressed in T cells
TECK	C-X-C motif chemokine ligand 25
TGF	Tumor growth factor
Th	T helper
TLR	Toll like receptor
TNF	Tumor necrosis factor
TNFR2	Tumor necrosis factor receptor 2
TRAF	Tumor necrosis factor receptor-associated factor
TRIF	TIR domain-containing adaptor-inducing interferon-β
TSLP	Thymic stromal lymphoprotein
UC	Ulcerative colitis
URT	Upper respiratory tract

Table of Contents

1.1 The Mucosal Immune System 19
1.1.1 The Gastrointestinal Immune System 20
1.1.2 The Respiratory Immune System 24

1.2 The Microbiota 28
1.2.1 Intestinal Microbiota 30
1.2.3 Dysbiosis 31
1.2.4 Microbiota-derived metabolites 36
1.2.5 Production of Short-chain Fatty Acids 37
1.2.6 Mechanisms of Short-chain Fatty Acids 39
1.2.7 The Respiratory Microbiota 42

1.3 The gut-lung axis and respiratory pathology and infection 43
1.3.1 Microbiota-derived metabolites as messenger and immunomodulators beyond the intestine. 47

1.4 *Streptococcus pneumoniae* 49
1.4.1 Epidemiology 49
1.4.2 Bacteria 51
1.4.3 Innate Response to Streptococcus pneumoniae 51
1.4.4 Adaptive Response to Streptococcus pneumoniae 59

1.5 Vaccination 62
1.5.1 Vaccination 62
1.5.2 Intranasal Vaccination 65
1.5.2 Pneumococcal Vaccination 66
1.5.3 Limitations of Pneumococcal Vaccines 67
1.5.4 Considerations in Pneumococcal Vaccine Development 69

1.6 The gut-lung axis and vaccination 74
1.6.1 Dysbiosis and Vaccine Performance 74
1.6.2 Ability of the microbiota and microbiota derived metabolites to modulate lymphocytes 76
1.6.3 The role of microbiota derived metabolites in vaccination 80

Chapter 2 ..... *Error! Bookmark not defined.*

Materials and Methods 84

2.1 Cell Culture 90
2.1.1 THP-1 cells 91
2.1.2 *Ex vivo* culture of human alveolar macrophages (hAMs) 91
2.1.3 Foetal liver derived alveolar macrophages (FLAMs) 92
2.1.4 Culture of L929 for M-CSF enriched media 92
2.1.5 *Ex vivo* culture of bone marrow derived macrophages (BMDMs) 93
2.1.6 *Ex vivo* culture of splenic cells 94
2.1.7 *Ex vivo* culture of primary lung cell suspensions cells 94
2.1.8 Treatment of cells *in vitro* with sodium butyrate 95
2.1.9 Stimulation of bone marrow derived macrophage and foetal liver derived alveolar macrophage 95
2.1.10 Stimulation of splenocytes and lung cells *ex vivo* to quantify cytokine production 96

2.2 *In vivo* 96
2.2.1 Mice 96
2.2.2 Dietary supplementation with SCFA 96
2.2.3 Induction of antibiotic-induced dysbiosis 97
2.2.4 Induction of pneumococcal pneumonia 97
2.2.5 Preparation of intranasal vaccines 98

2.2.6 Intranasal immunisation 99

2.3 Bacteria **99**

2.3.1 Bacterial strains 99

2.3.2 Adaptation of bacterial strains for *in vivo* infection 100

2.3.3 Preparation of bacterial stocks 100

2.3.4 Quantification of bacteria 101

2.3.5 Infection of foetal liver derived macrophage in vitro 101

2.3.6 Evaluation of intracellular killing using a gentamicin protection assay 102

2.4 General **103**

2.4.1 Crystal violet viability assay 103

2.4.2 Phenotypic characterisation of myeloid lung cellularity by flow cytometry 103

2.4.3 Phenotypic characterisation of lung lymphocyte populations by flow cytometry 105

2.4.4 Quantification of cytokine by enzyme liked immunoglobulin assay (ELISA) 107

2.4.5 Quantification of antibody by enzyme liked immunoglobulin assay (ELISA) 107

2.4.6 Quantification of pneumococcal polysaccharide specific antibody by enzyme liked immunoglobulin assay (ELISA) 108

2.4.7 Quantification of pneumococcal specific IgA^+ B cells in lung cells by ELISpot 109

2.4.8 SDS-PAGE 109

2.4.9 Semi-dry membrane transfer 110

2.4.10 Staining of membranes 111

2.4.11 RNA Isolation 111

2.4.12 Data Analysis 111

3. The effects of butyrate on host response to pneumococcal infection. 113

3. Introduction 114

3.1 Butyrate does not have any direct anti-microbial properties. 119

3.2 Butyrate is not cytotoxic at selected working concentrations. 121

3.3 Butyrate acts as a histone deacetylase inhibitor in FLAMs. 123

3.4 *S. pneumoniae* and the synthetic TLR2 agonist, Pam3Csk4, induce global transcriptomic changes in foetal liver derived macrophages (FLAMs). 125

3.6 Butyrate enhances antimicrobial pathways in AM upon infection. 131

3.7 Butyrate modulates cytokine milieu of alveolar-like macrophage in response to inflammatory stimuli. 140

3.8 Butyrate selectively limits IL-6 production in FLAMs in response to infection. ... 143

3.9 Butyrate enhances the antimicrobial activity of alveolar macrophages. 145

3.10 *In vivo* Effects of the Short-chain Fatty Acid, Butyrate, on Outcomes of Invasive Pneumococcal Pneumonia. 148

***3.11 In vivo S. pneumoniae* infection is marked by an early depletion of AMs and rapid infiltration of neutrophils. 150**

3.12 Antibiotics do not elicit direct immunomodulatory effects on THP-1 macrophage. 153

3.13 Antibiotics cause a reduction of polyspecific IgA in the intestine. 155

3.14 Dysbiosis contributes to an increased susceptibility to pneumococcal pneumonia. 157

3.15 Butyrate ameliorates the effects of dysbiosis-driven exacerbation of invasive pneumococcal infection. 159

3.16 Dietary supplementation with butyrate attenuates neutrophil recruitment during invasive pneumococcal infection. 162

Discussion 165

4. Exploring the immunomodulatory effects of butyrate on pneumococcal vaccination outcomes. 169

4. Introduction 170

4.1 Designing a polyvalent intranasal pneumococcal vaccine. 175

4.2 Nasal immunisation with the adjuvanted polyvalent whole-cell pneumococcal vaccine, SpnL(dmLT), generates antigen-specific IFN-γ and IL-17A in both the lung and spleen. 177

4.3 Immunisation with the intranasal experimental polyvalent pneumococcal vaccine, SpnL(dmLT) results in increased lymphocyte populations in the lungs and drives $CD44^+CD4^+$ T effector/memory cells. 179

4.4 Intranasal SpnL(dmLT) does not increase splenic total lymphocyte populations but leads to increased splenic effector/memory $CD4^+CD44^+$ T cell populations. 184

4.5 Immunisation with SpnL(dmLT) promotes serum antigen-specific IgG antibodies. 187

4.6 SpnL(dmLT) promotes local antigen-specific IgA in the nasal tract and lungs..... 190

4.7 Exploring the effects of SCFA-mediated modulation on pneumococcal vaccine responses. 194

4.8 Oral butyrate supplementation alters basal levels of lung and splenic IL-17A in the lung in naïve mice. 195

4.9 Butyrate supplementation alters lymphocyte populations in the lungs of immunised mice. 197

4.10 Butyrate supplementation increases lymphocyte populations in the spleens of immunised mice. 201

4.11 Dietary supplementation with butyrate results in reduced levels of antigen-specific antibodies in the serum of immunised mice. 205

4.12 Butyrate supplementation results in reduced levels of antigen-specific IgA in the lung and nasal cavity of immunised mice. 207

4.13 Butyrate supplementation did not suppress antigen-specific serum IgG in mice immunised intramuscularly with the conjugated polyvalent pneumococcal vaccine, Prevnar13® but did decrease antigen-specific Th1 responses. 210

Discussion 212

5. General Discussion 218

Future Work 227

List of Figures:

Figure 1.1 The structure of the intestinal immune system.
Figure 1.2 Mechanisms of IgA class switching in the intestine
Figure 1.3 The immune architecture of the URT and LRT.
Figure 1.4 Factors influencing the host microbiota.
Figure 1.5 Biosynthesis pathways of SCFAs.
Figure 1.6 Mechanisms of SCFA engagement with host eukaryotic cells.
Figure 1.7 The gut-lung axis in respiratory infection
Figure 1.8 The activation of PRRs and subsequent intracellular responses in response to *S. pneumoniae.*
Figure 1.9 Innate immune response to *S. pneumoniae.*
Figure 1.10 Current types of vaccines and those in development.
Figure 1.11 Pneumococcal Vaccines.
Figure 1.11 The Impact of the Intestinal Microbiota on Vaccine Efficacy and Lymphocyte phenotype

Figure 2.1 Standard curves of cytokine ELISAs.

Figure 3.1 Butyrate does not have direct antimicrobial effects against *S. pneumoniae*.
Figure 3.2 Butyrate marginally affects the viability of FLAMs but BMDMs appear more susceptible to cytotoxicity.
Figure 3.3 Butyrate elicits histone deacetylase inhibitory activity at low millimolar concentrations in FLAMs.
Figure 3.4 FLAMs upregulate expression of inflammatory pathways in response to *S. pneumoniae in vitro*.
Figure 3.5 FLAMs upregulate expression of inflammatory pathways in response to TLR2 stimulation *in vitro*.
Figure 3.6 Differentially regulated pathways in FLAMs in response to *S. pneumoniae* live infection *versus* TLR2 stimulation.
Figure 3.7 Butyrate treatment alone influences the transcriptional regulation of the cell cycle.
Figure 3.8 Butyrate stimulates the expression of genes involved in host innate defence, while regulating cell cycle in AM.
Figure 3.9 Butyrate stimulates the expression of genes involved in host innate defence, while regulating cell cycle in cells infected with *S. pneumoniae*, D39.
Figure 3.10 Butyrate stimulates the expression of genes involved in host innate defence, while regulating cell cycle in cells stimulated with the TLR2 ligand, Pam3Csk4. FLAMs
Figure 3.11 Butyrate upregulates genes implicated in interferon signalling pathways.
Figure 3.12 Butyrate preferentially suppresses IL-6 in both bone marrow derived macrophage (BMDM) and FLAM (FLAM).

Figure 3.13 Butyrate preferentially suppresses IL-6 in both bone marrow derived macrophage (BMDM) and FLAMs.
Figure 3.14 Butyrate limits IL-6 production in alveolar-like macrophages during *S. pneumoniae* infection.
Figure 3.15 *Butyrate promotes intracellular clearance of S. pneumoniae in murine and human alveolar macrophage*.
Figure 3.16 Pilot study to evaluate dose escalation in optimising the lethal infectious dose of *S. pneumoniae* (serotype 2, D39).
Figure 3.17 Flow cytometry gating strategy for the phenotypic characterisation of innate immune infiltrates during pneumococcal infection.
Figure 3.18 Pneumococcal infection is characterised by an early depletion of AM and swift infiltration of neutrophils and monocytes.
Figure 3.19 Antibiotics do not significantly modulate inflammatory cytokine production upon stimulation in monocyte-derived macrophage.
Figure 3.20 Antibiotic treatment regimen and tracking of body weight in dysbiotic mice.
Figure 3.21 Antibiotic-induced dysbiosis of the microbiota increases susceptibility to pneumococcal pneumonia.
Figure 3.22 Butyrate alleviates the deleterious effects of antibiotic-induced dysbiosis on outcomes of pneumococcal infection.
Figure 3.23 Dietary supplementation with butyrate does not alter innate immune population in the lungs under basal conditions.
Figure 3.24 Antibiotic-induced dysbiosis alters innate immune infiltrates during pneumococcal infection.

Figure 4.1 Vaccination strategy for the experimental adjuvanted intranasal pneumococcal vaccine.
Figure 4.2 An experimental intranasal adjuvanted pneumococcal vaccine, SpnL(dmLT) generates robust IL-17A and IFN-γ in vaccinated animals in response to antigen recall.
Figure 4.3 Immunophenotyping of resident lymphocyte populations post immunisation.
Figure 4.4 Nasal vaccination with SpnL(dmLT) promotes increases in lymphocyte populations in the lung parenchyma.
Figure 4.5 Nasal vaccination with SpnL(dmLT) generates memory T cell populations in the lung capable of IL-17A and IFN-γ production upon antigen restimulation.
Figure 4.6 Nasal vaccination with SpnL(dmLT) does not increase total lymphocyte populations in the spleens of immunised animals.
Figure 4.7 Nasal vaccination with SpnL(dmLT) promotes memory T cell populations in the spleen capable of IL-17A and IFN-γ production upon antigen restimulation.
Figure 4.8 Nasal vaccination with SpnL(dmLT) promotes antigen-specific humoral immunity, enhancing antigen-specific serum total IgG, and IgG1 and IgG2c subclasses against the trivalent SpnL.
Figure 4.9 Nasal vaccination with SpnL(dmLT) generates local antigen-specific IgA in the nasal cavity.

Figure 4.10 Nasal vaccination with SpnL(dmLT)generates antigen-specific IgA in the lung parenchyma.
Figure 4.11 Dietary supplementation during pneumococcal immunisation.
Figure 4.12 Oral butyrate supplementation can alter resident T-cell derived lung IL-17A levels in naïve mice.
Figure 4.13 Lymphocyte populations are decreased in the lung in immunised animals receiving dietary oral butyrate supplementation.
Figure 4.14 Dietary intervention with butyrate results in lower numbers of IL-17A$^+$ and IFN-γ$^+$ CD44$^+$ memory T cells in the lungs of immunised mice.
Figure 4.15 Lymphocyte populations are unchanged in the spleen of immunised animals receiving dietary oral butyrate supplementation.
Figure 4.16 Dietary intervention with butyrate results in higher frequencies and numbers of IL-17A$^+$ and IFN-γ$^+$ CD44$^+$ T cells in the spleens of immunised mice.
Figure 4.17 Butyrate supplementation results in reduced splenic IFN-γ in immunised animals in response to antigen recall.
Figure 4.18 Butyrate supplementation limits nasal vaccine induced antigen-specific serum IgG responses.
Figure 4.19 Butyrate supplementation reduced vaccine induced antigen-specific IgA in lung parenchymal tissue.
Figure 4.20 Butyrate supplementation limits production of total IgA in the serum of immunised mice.
Figure 4.21 Butyrate supplementation reduced antigen-specific IgA in the nasal cavity of immunised mice.
Figure 4.22 Oral butyrate supplementation suppressed vaccine (Prevnar13)-induced antigen-specific splenic IFN-γ but not antigen-specific IgG, Prevnar.

1. Introduction

***Streptococcus pneumoniae* (*S. pneumoniae*) is a major human respiratory pathogen. This work focuses on harnessing the gut-lung axis of immune regulation, through the use of butyrate, a microbiota-derived short-chain fatty acid (SCFA), in alternative therapeutic and prophylactic strategies to target *S. pneumoniae*.** The gut-lung axis of immune regulation defines the bi-directional immunological crosstalk that exists between the gut microbiota and the respiratory immune system. Indeed, there are other axes of immune regulation highly dependent on the immunomodulatory nature of the gut microbiota, namely the gut-brain axis, the gut-liver axis and the gut-heart axis. Here we provide a comprehensive overview of the core immunology and microbiology concepts that underpin this work starting with the intestinal and respiratory mucosal immune systems, the microbiota, SCFAs, host response to *S. pneumoniae* and pneumococcal vaccination. Here we will also examine the current literature in this field demonstrating links between the gut-lung axis of immune regulation, host response to respiratory infection and the potential links between the gut-lung axis of immune regulation and vaccination immunogenicity and efficacy.

1.1 The mucosal immune system

The mucosal immune system is a highly complex collection of connected yet anatomically distinct immune sites which function to support immunity at barriers with environmental exposure. The mucosal immune system is stratified based on anatomical location, such as the oral mucosa, the nasopharyngeal mucosa, the respiratory mucosa, the urinogenital mucosa and the largest mucosal immune niche, the gastrointestinal mucosa. While these mucosal niches are spatially segregated, the immunological crosstalk that exists between these sites, constitutes the common mucosal immune system (CMIS). The mucosal immune system has effector and inductor sites. Effector sites are where the immune cells elicit functions against pathogens and insults while tolerating innocuous antigens. Inductor sites are where adaptive immune processes are initiated, e.g. Peyer's patches in the intestinal tract and local draining lymph nodes (LNs) such as mesenteric and mediastinal LNs in the intestine and lung respectively. The mucosal immune system is heavily influenced by the commensal microorganisms which

inhabit these anatomical barriers and requires highly specialised immune mechanisms to regulate immune tolerance, protection against pathogenic insult and communication with the adjacent microbiota and other mucosal niches via the CMIS. The gut-lung axis of immune regulation, defined in the opening section, is a rapidly emerging field of research. Furthermore, additional axes of immune regulation have been identified between the commensal gut microbiota and the liver, heart and brain, coined the gut-liver axis, gut-heart axis and gut-brain axis respectively. The mucosal immunology that underpins the gut-lung axis will be discussed below.

1.1.1 The gastrointestinal immune system

The gastrointestinal mucosa is subject to a continuous exposure of innocuous antigens, pathogens and benign microorganisms. Neutralising noxious stimuli while tolerating innocuous antigen requires highly refined mechanisms of immune regulation at the intestinal mucosa to maintain immunological homeostasis while retaining the ability to engage in inflammatory and targeted responses upon encountering insults such as infection or injury.

The glycocalyx is the exterior layer of the mucosa which is on the luminal side of the epithelial barrier [1]. The glycocalyx is composed of an exterior and interior mucoid layer, containing heavily glycosylated mucins, namely MUC1, MUC2, MUC3, MUC4, MUC12, MUC13 and MUC17 produced by goblet cells in the underlying intestinal epithelium [2], [3], [4], [5]. The underlying cellular barrier layer is the intestinal epithelium, which is composed of enterocytes, colonocytes, Paneth cells, microfold (M) cells and intestinal stem cells (**Fig. 1.1**). Paneth cells are exclusively found in the small intestine and secrete antimicrobial peptides, particularly α-defensins, which functions to regulate the resident commensal communities and provide innate defence functions [6], [7]. Microfold cells (M) cells have antigen presenting functions and continuously sense the intestinal luminal contents, processing and presenting antigen on the basolateral side of the epithelial border, to underlying inductive sites such as Peyer's patches or isolated lymphoid follicles. M cells have an apical brush border which hosts a wide range of pathogen recognition receptors (PRR), namely toll like receptors (TLR),

lectin receptors and integrins and is covered by a characteristically thin glycocalyx to facilitate antigen sensing [8]. Intestinal stem cells are found in crypts and give rise to colonic epithelial cells. Beneath the intestinal epithelium, a layer of connective tissue hosts an abundance of resident immune cells, collectively known as the lamina propria. The gut associated lymphoid tissue (GALT) is composed of the isolated lymphoid follicles, Peyer's patches, and mesenteric lymph nodes. A schematic overview of the special organisation of the gastrointestinal immune system is depicted below in **Fig. 1.1**.

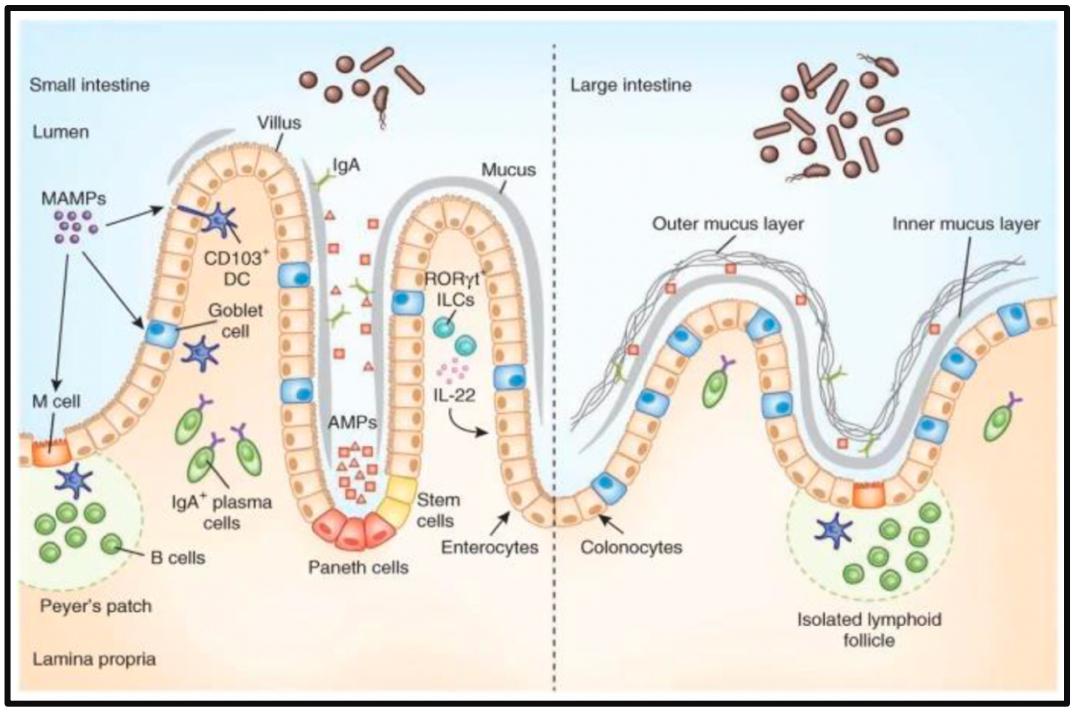


Fig. 1.1The structure of the intestinal immune system. Diagram by Brown et al. 2013 [1]

The lamina propria hosts a range of inductive and effector sites, with a plethora of innate and adaptive responses occurring *in situ*. Intestinal monocytes express high CCR7 and can elicit antigen presentation at draining mesenteric lymph nodes [9], [10]. Intestinal macrophages are considered to be monocyte derived macrophage arising from circulating Ly6C^{hi} progenitors in the lamina propria [11]. Tissue resident intestinal macrophage express high levels of fractalkine receptor CX3CR1, and scavenger receptors CD163 and F4/80 [11]. The fractalkine receptor CX3CR1 has implicated roles in barrier function, with *Cx3cr1*$^{-/-}$ mice having increased bacterial epithelial translocation and an increased susceptibility to dextran sulfate sodium (DSS) induced colitis [9]. The

close proximity between the antigen sensing compartment and the inductive sites allows for rapid imprinting of antigen presenting effector and regulatory T cells. Intestinal macrophages can directly participate in antigen presentation, with $CX3CR1^{hi}$ exhibiting the ability to directly transfer processed antigen to dendritic cells (DCs) *in situ* [9], [10], [12]. Intestinal DCs localise in the lamina propria at resting state and can be stratified into $CD103^{+}CD11b^{+}$ and $CD103^{-}CD11b^{+}$ [13]. These DCs can sample luminal antigen and migrate to the GALT sites upon stimulation, participating in antigen presentation to effector lymphocytes [14]. Additionally, intestinal DCs can sample antigen through transepithelial dendrites [15]. Intestinal and peripheral DCs can travel in the circulation to imprint distal T cell populations in the lungs and skin which have intestinal homing functions [16]. This is dependent on a retinoic acid-dependent mechanism involving upregulation of CCR9 and α4β7 integrin which are the cognate receptors of TECK and MAdCAM-1 respectively on the luminal intestinal epithelial surface [16], [17], [18].

The sheer volume of innocuous antigens that the intestinal immune system is exposed to, requires highly sophisticated mechanisms of immune homeostasis, to prevent redundant inflammation and pathology. Antigen-specific responses are mounted against these dietary and environmental innocuous antigens and those found in the commensal microbiota [13]. These antigen-specific lymphocytes mainly produce an anti-inflammatory secondary cytokine milieu and promote plasma B cells capable of producing polyspecific secretory IgA. Intestinal regulatory T cells (Treg) express high levels of CD25 and are $FoxP3^{+}$ [19]. Type 1 regulatory (Tr1) cells produce IL-10 and transforming growth factor (TGF)-β at mucosal surfaces [20], [21]. There are reports of T helper (Th1) regulatory population which also participate in intestinal homeostasis through production of interleukin (IL)-10 [22]. IL-10 is known to downregulate antigen presenting machinery in antigen presenting cells (APCs) resulting in reduced major histocompatibility complex (MHC)-II expression and reduced expression of the co-stimulatory CD86 receptor [23]. Similarly, IL-10 can suppress toll like receptor (TLR)-dependent activation cues in macrophage and dendritic cells [23]. However, IL-10 does not exclusively rely on immunosuppressive mechanisms to support intestinal homeostasis. IL-10 has demonstrated roles in enhancing goblet cell function, promoting

the production of intestinal mucus, particularly MUC2, MUC3 and MUC4 expression [24], [25]. Innate lymphocyte (ILC) populations and alternative lymphocyte populations, such as $\gamma\delta$ T cells, MAIT cells and $CD8^{+}\alpha\beta^{+}$ effector populations are also abundant in the intestinal mucosa which readily respond to infection and facilitate homeostatic processes [26], [27], [28], [29].

Production of polyspecific secretory IgA (sIgA) is another mechanism by which the host adaptive immune system maintains intestinal homeostasis. Intestinal IgA has roles in maintaining eubiosis of the resident microbiota and protecting mucosal surfaces from pathobiont invasion. There are two structurally different types of IgA in the intestinal tract, IgA1 found almost exclusively in the small intestine and IgA2 found in the large intestine. As previously mentioned, IgA^{+} plasma cells in the underlying GALT produce this secretory IgA. This polyspecific secretory IgA is transported to the lumen by binding to the polyspecific immunoglobulin receptor (PigR) which acts as a transporter on the basolateral membrane of the epithelial border, facilitating transcytosis of sIgA to the apical membrane, where PigR is subsequently cleaved. Dendritic cell and Treg cell derived tumour growth factor (TGF-β) supports T-cell dependent class switching to immunoglobulin (Ig)A in local inductive sites such as Peyer's patches (**Fig. 1.2**). This T-cell dependent IgA class switching is dependent on inducible nitric oxide (iNOS) production in local DCs; which then promotes upregulated TGF-βR on Peyer's patch B cells [30]. Induction of the α4β7 integrin on DCs, which facilitates intestinal homing of these cells is mechanistically regulated by TGF-β and retinoic acid [18]. This highlights a critical role of TGF-β in regulating intestinal innate cellularity.

Type 3 or Th17 cells in the intestine are characterised by expression of the transcription factor RORγt and characteristically produce IL-21, IL-22 and IL-17 [31]. While IL-17 is essential for transport of secretory IgA across the epithelial barrier, via activity of PigR, IL-17 appears dispensable for production of IgA in Peyer's patches [32]. This implies an alternative or perhaps additional T-cell independent mechanism of IgA class-switching in the context of intestinal B cells, which is orchestrated by dendritic cells, as shown in **Fig. 1.2** [33]. T-cell independent IgA class switching generates lower affinity antibodies and requires auxiliary TLR stimulation of B cells and stimulation of transmembrane activator and CAML interactor (TACI) by B-cell activating factor (BAFF) and A-

proliferation inducing ligand (APRIL) during antigen presentation [34]. However, follicular helper T cells can also be generated from T_{regs} and Th17 cells and promote T-cell dependent IgA class-switching in B cells [35], [36].

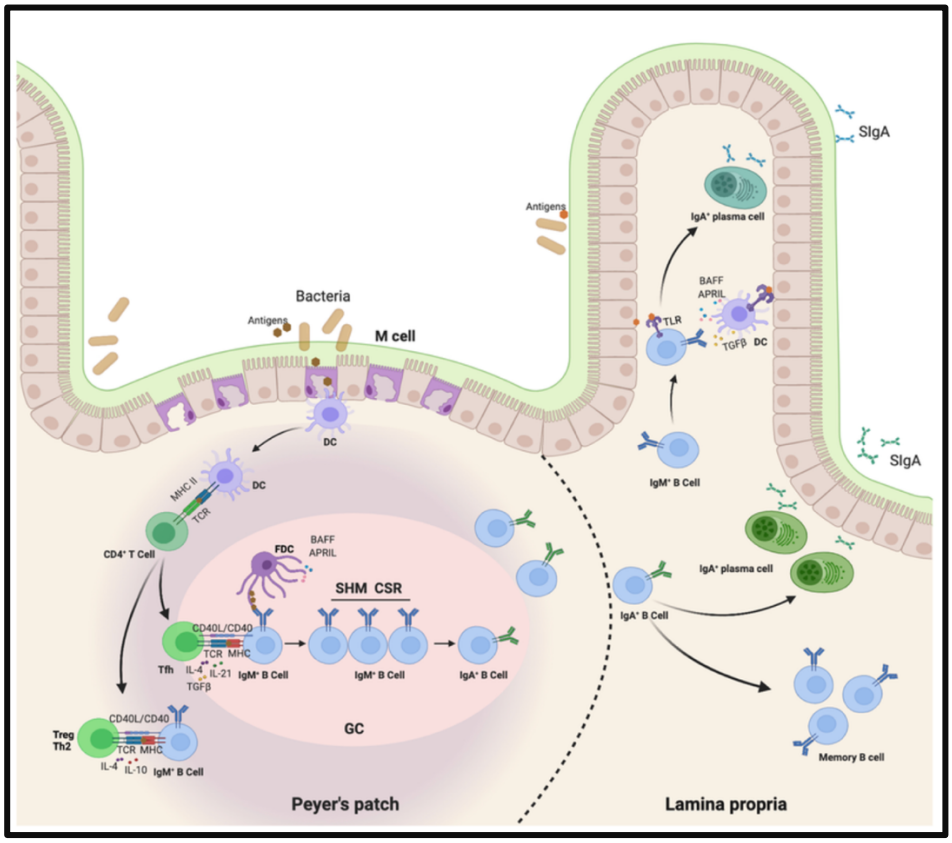


Fig. 1.2 Mechanisms of IgA class switching in the intestine. Adapted from Zhong et al. 2021 [37].

1.1.2 The respiratory immune system

The respiratory immune system is one of the largest mucosal niches by surface area. Barrier functions in the **upper respiratory tract (UTR)** play a significant role in protection, with the epithelial barrier containing ciliated epithelial cells, cuboidal epithelial cells, basal cells (**Fig. 1.3**). The airway epithelium serves as a physical barrier protecting from environmental insults and pathogens. The cuboidal epithelium has additional auxiliary innate immune functions producing antimicrobial peptides, reactive oxygen and nitrogen species and production of cytokines [38]. Cuboidal epithelial cells produce high concentrations of heavily glycosylated mucins, namely Muc1, Muc2, Muc5ac, Muc5b, Muc4 and Muc16 which contribute to the upper airway glycocalyx,

Muc5b has essential roles in host defence against bacterial infection in the murine URT [39], [40], [41]. There is evidence of local DC and macrophage populations crossing the epithelial border by transcytosis to sense antigen at the apical membrane and home to upper airway local inductive sites, such as the cervical and mandibular lymph nodes [38], [42]. Additionally, respiratory epithelial cells can participate in antigen presentation. This was noted in murine nasal epithelial cells which exhibit a marked increase in MHCII and CD80 in an allergic airway model of OVA-sensitisation [43]. This was also supported by a heightened frequencies of $CD69^{+}CD4^{+}$ T cells and IL-13 in human T cells co-cultured with human nasal epithelial cells derived from allergic rhinitis patients [43]. Similarly, epithelial cells of the lower airways can additionally participate in antigen presentation and express MHCII in both human and murine lung epithelial cells [42]. Inductive sites in the UTR include the nasal associated lymphoid tissue (NALT) and draining lymph nodes, in particular the adenoids, palatine, lingual and tubule tonsil in humans, collectively known as Waldeyer's ring and broadly lymphoid follicles in the nasal cavity and cervical and mandibular lymph nodes in rodents [44]. The inductive sites of the URT host tissue resident memory T cells which are characterised by expression of CD69 and CD103 for cytotoxic $CD8^{+}$ T_{rm} and CD69 in combination with differing expression levels of CD103 for helper CD4+ T_{rm} [45].

The epithelial borders of the lower bronchioles are similar in structure to the conducting airways. The alveolar niche is the main site of recruitment of resident and infiltrating innate immune cells during insult. The alveolar pocket is lined with type I and type II pneumocytes. These pneumocytes function in gas exchange however have primary functions in producing pulmonary surfactant, which reduces alveolar surface tension to preserve structural integrity of the lung and facilitate the alveolar macrophage (AM) niche, through the action of surfactant protein B (SP-B) and (SP-C) [46]. Additionally alveolar pneumocytes produce antimicrobial peptides and provide barrier defences [47].

Resident innate immune granulocyte populations are the first to respond during infection or injury, one such population are AMs. Alveolar macrophages are derived from yolk sack progenitors; however, a complex protein milieu is required for sustaining

AM populations. Granulocyte-macrophage colony stimulating factor (GM-CSF), drives PPARγ signalling in AMs, whereas SP-A, suppresses AM function in resting state and stimulates production of GM-CSF in local epithelial cells and TGF-β all of which have implicated roles in maintaining AM populations [48], [49]. Murine AMs are characterised by high expression of Siglec-F or/and MerTK and CD11c and are positive for macrophage and myeloid markers CD64, F4/80 and CD11b respectively [50]. Human AMs are characterised by varying expression of CD206, CD86 and CD163 in combination with CD11c and CD11b [51], [52]. Murine AM phenotype is regulated by transcription factors PPAR-γ, KLF4 and EGR4 [53], [54], [55], [56]. While AMs at basal state could be considered to adopt an "alternative" or of an M2 phenotype, these cells exhibit a high degree of plasticity and can readily adopt an inflammatory profile in response to infection [57]. AMs express high degrees of scavenger receptor expression, namely Marco (SR-A6), Siglec-F and CD206 [50]. Interstitial macrophages found in the extra-alveolar lung parenchyma are characterised by high expression of CD11c in combination with macrophage-based markers CD64, MerTK and F4/80; however, are negative for Siglec-F [58]. Lung monocyte-derived macrophage are characterised by expression of Ly6C, which is lost upon terminal differentiation into macrophages *in situ*, in combination with macrophage markers CD64, CD11b, MHC II however do not typically express CD11c [59]. The dynamics of monocytes and macrophage populations in the lung are complex and highly dependent on the inflammatory environment [60], [61], [62], [63]. Circulating monocytes, are characterised by high expression of CD115 and low expression of Ly6C, in both human and mouse [64].

Effector T cell responses in the lung parenchyma are essential for pathogen recognition, supporting the effector functions of the innate immune system and promoting homeostasis. However, the lung is constantly exposed to environmental particles aswell as pathogens and must distinguish innocuous insults from pathogenic threats. In the case of allergic airway inflammation (AAI), Th2 (GATA3+) responses in the lungs are mediated in part by the innate contributions of respiratory pneumocytes and lung fibroblasts which produce thymic stromal lymphopoietin (TSLP), IL-25 and IL-33 [65]. Furthermore, Th2 derived cytokine IL-4, IL-5 and IL-13 directly contribute to allergic airway responses as demonstrated in models of house dust mite induced AAI [66]. While

Th2 responses are imperative in targeting parasitic and helminth infection, these responses are generally seen as aberrant inflammatory responses in the lungs and a sign of atopic disease. Th1 (Tbet+) responses in the lung are imperative for protection against bacterial and viral pathogens. Th1 derived cytokines such as interferon (IFN)-γ, tumor necrosis factor (TNF)-α and IL-2 are imperative in combatting intracellular pathogens, induction of necroptosis or apoptosis of infected cells and sustaining effector T cells responses through autocrine signalling of IL-2 [67]. The importance of Th1 responses in mediating the immune response to bacterial infection has been identified in the case of intracellular pathogens such as *Mycobacterium tuberculosis* infection [68]. These cells are also critical for the generation of CD8+ effector T cells, which in turn are critical for cross-protection against viral pathogens. Respiratory CD8+ T cells can be characterised as $CD62L^{low}CCR7^{low}CD44^{high}$, establishing respiratory CD8+ cells as effector memory cells [69]. Th17 responses in the lungs are critical for clearance of respiratory bacterial pathogens, such as *Bordetella pertussis* and *S. pneumoniae* [70], [71]. Th17 (RORγt+) cells produce a plethora of inflammatory cytokines such as IL-17 family cytokines, IL-22, IL-26, TNF-α and GM-CSF [31]. This suggests that Th17 effector lymphocytes have a role in promoting functions of recruited neutrophils through TNF-α and IL-17 signalling and sustaining AM responses through IL-17 mediated GM-CSF signalling [72], [73]. Respiratory Tregs (CD4+, CD25+ FoxP3+) produce TGF-β, which is critical in resolving inflammation and supporting AM differentiation [74].

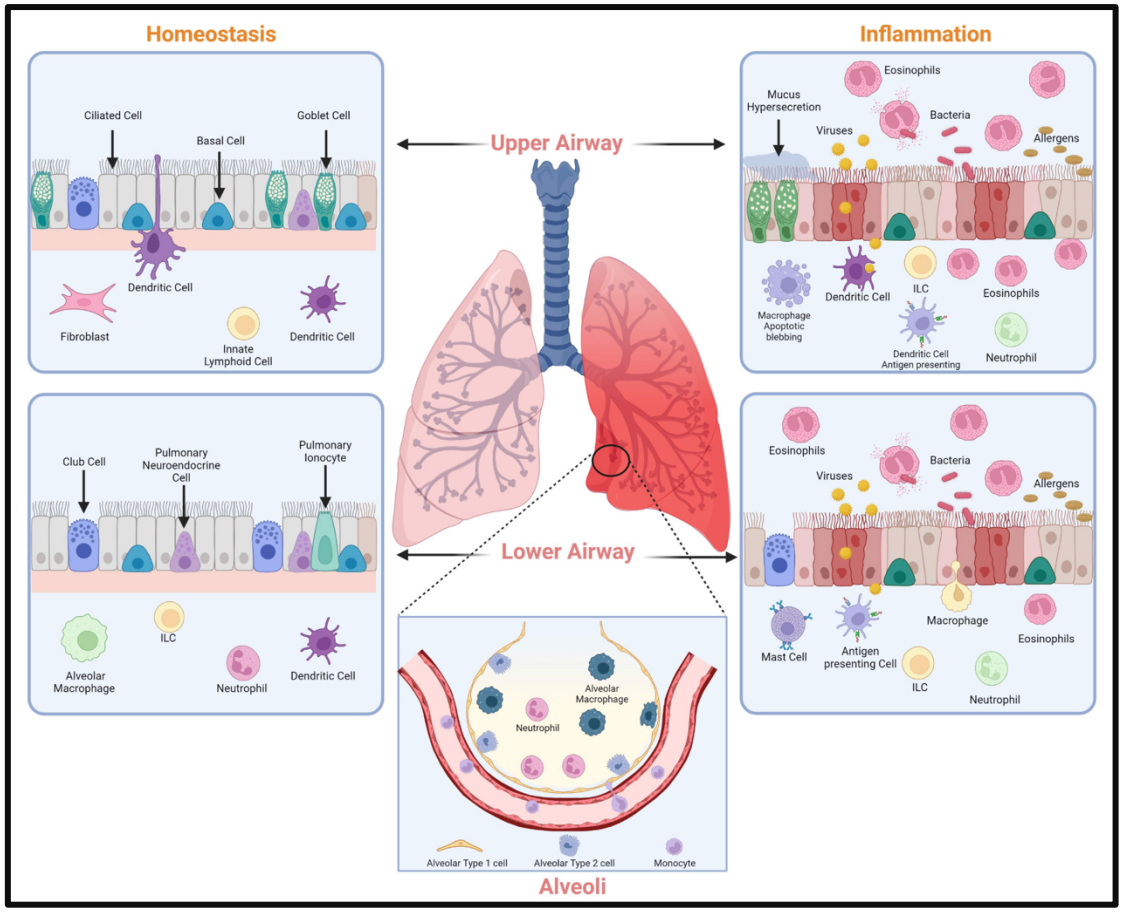


Fig. 1.3 The immune architecture of the URT and LRT. Diagram made by Gopallawa et al. 2023.

1.2 The microbiota

As discussed in section 1.1, mucosal immune sites harbour an abundant and diverse community of commensal microorganisms. The mucosal immune system has evolved to synergistically exist with these microorganisms through complex immunological mechanisms. The mammalian host contains an abundant and diverse collection of bacteria, fungi, viruses and protozoa, which is termed the microbiota. The *microbiota* has evolved with the host establishing a symbiotic relationship between the host and microbiota which has been referred to as a "superorganism". The *microbiome* is another term which refers to the complete collection of genes contained in the commensals of the mammalian host. These two terms, while often used interchangeably, distinguish the genealogical landscape of the microorganisms inhabiting the human body from phenotypic characterisation of these microorganisms. The scale of the human

microbiota was fully characterised by Turnbaugh *et al.* in The Human Microbiome Project in 2007, which is widely considered the genesis of microbiome research [75]. The development of next generation sequencing platforms, facilitating global metagenomic and phenotypic analytical methods have broadened this field of research.

Characterisation of the microbiota can be achieved through different methods. One such method is 16S sequencing, which consists of a targeted transcriptomic sequencing approach to characterise bacterial species within a community. 16S (rRNA) is the RNA component of the bacterial 30S ribosomal subunit, the 16S gene contains heterogenous regions which allow for genotypic characterisation of the bacterial species. Shotgun metagenomic sequencing, is a more sophisticated sequencing method, which involves fragmentation of the total DNA content in a sample which is sequenced and re-assembled *in silico* to obtain information on the individual bacterial communities within a sample and the potential functionality of these organisms. In addition, metaproteomic analysis has allowed for the analysis of the microbiota-derived protein milieu and metabolomics, where mass-chromatography and spectrometry methods have been utilised for this. Finally bulk RNA sequencing or alternative meta transcriptomic approaches have allowed for the total transcriptional activity of a single microbiota-derived organism to be characterised.

“Eubiosis” refers to the basal state of the microbiota and is generally considered a healthy microbiota. “Dysbiosis” refers to a microbiota which has deviated in abundance or diversity from the eubioitic microbiota, due to host-driven endogenous factors or external exogenous factors, including antibiotics, immunosuppressive and anti-inflammatory medication, changes in diet and autoimmune conditions, amongst others. Experimentally dysbiosis can be artificially induced *in vivo* through the use of antibiotic cocktails or through oral administration of polyethylene glycol. Evidence that the microbiota has key roles in host nutrition, physiology, behaviour and immune regulation have emerged from clinical longitudinal observational studies but also the use of germ-free animal models and models of induced intestinal dysbiosis. Studies involving germ-free animals which lack any commensal microorganisms have been invaluable in the understanding of the microbiota. Germ-free animals have altered physiological,

metabolic, behavioural and immune responses compared to wild-type specific pathogen free mice harbouring a conventional microbiota. Similarly mono- and poly-colonisation studies have identified key symbiotic commensal communities in regulating host processes.

The microbiota can be stratified into the anatomical niches of commensal colonisation such as the gastrointestinal tract, the nasopharyngeal tract, the respiratory tract, the oropharyngeal tract, the genitourinary tract and the skin. These anatomical niches are mucosal sites, in which the microbiota shapes the resident mucosal immune system. However, the ability of the microbiota to shape the immune system is not limited to the adjacent mucosal anatomical niche, highlighting the complex dynamic between the microbiota and host common mucosal immune system (CMIS).

1.2.1 The intestinal microbiota

The human intestine harbours over 10^{14} bacterial commensals and represents the most abundant and diverse microbial niche in the body [76]. The intestinal microbiota has critical nutritional functions, such as the metabolism of fermentable dietary fibre and the production of microbiota-derived metabolites such as amino acids, short-chain fatty acids (SCFA) and vitamins. The intestinal microbiota can produce vitamins independently of host metabolism, such examples being production of vitamin K and B12, as well as other vitamin B derivatives [77], [78]. Regulatory T cell-mediated tolerance is critical in maintaining immune homeostasis in the intestines, preventing inflammation and reactivity to innocuous antigen [79], [80]. Symbiotic bacteria not only have auxiliary nutritional functions but also prevent the proliferation of pathobionts through competition for resources [81]. Often in the case of dysbiosis, complete ablation of symbiotic communities or dysregulated frequencies in global commensal competition, can result in the opportunistic expansion of pathobionts resulting in enteric pathology.

There are four main bacterial phyla in the intestinal microbiota, *Firmicutes*, *Bacteroidetes*, *Proteobacteria* and *Actinobacteria,* with *Firmicutes* and *Bacteroidetes*

accounting for more than 90% of bacterial commensals [75], [82], [83], [84]. Murine species are coprophagic, which is fundamental in inflammatory homeostasis and social behaviour [85]. This generally results in higher homogeneity in commensal signatures in cohoused animals; for this reason, co-housing and FMTs are effective methods of microbiota study in rodents. Furthermore, laboratory animals are kept under controlled dietary and environmental conditions. However, humans do not exhibit coprophagy and many exogenous and endogenous factors influence the human microbiota, resulting in heterogeneity between commensal signatures.

1.2.3 Dysbiosis

Dysbiosis can happen as a result of significant ablation of microbial communities or shifts in the abundance of certain commensals. It is widely recognised that the microbiota is dynamic and can change to support the host physiology and immune processes. Dysbiotic shifts in the endogenous microbiota are seen as deleterious and can negatively impact the host immune system, exacerbating autoimmune and inflammatory conditions and impairing host response to infection [86], [87], [88]. The causes of dysbiosis can be broadly stratified into two categories: intrinsic factors, host mediated factors and extrinsic factors, those outside the host which can impact on the endogenous microbiota (**Fig. 1.4**). Intrinsic factors include host genetics, biological sex, age, birth delivery method and co-morbidities. Extrinsic factors include environmental conditions, socio-economic factors, geography and climate, cohabitation with animals, diet, use of xenobiotics, socio-economic factors and lifestyle factors, such as smoking status, alcohol consumption, sleep patterns and stress, hygiene practices and exercise [88]. One differentiating factor is that there is a certain element of self-governance or control over the status of the microbiota with regard to extrinsic factors, in comparison to intrinsic factors are those which cannot be changed. This suggests a key role of the intestinal microbiota in maintaining intestinal health.

Host genetics are an endogenous factor which influences the stability of the microbiota. Clinical evaluations and *in vivo* murine studies have identified a set of genes in which mutations appear to increase susceptibility to dysbiosis. The intricacy of interactions

between the host immune system and the microbiota suggests that many genetic determinants of dysbiosis could be host immune genes. Mutations in these genes, namely *Nod2, Tlr4* and *HLA-DRB1,* are also identified as associated genetic determinants of inflammatory enteric conditions such as ulcerative colitis (UC) and Crohn's disease (CD), collectively under the umbrella term inflammatory bowel disease (IBD) [89], [90]. It is widely recognised that toll like receptor genes, namely, *Tlr4* can have significant roles in dysbiosis [90]. Single nucleotide polymorphisms in CARD genes, particularly *Card9* resulted in increased susceptibility in an *in vivo* model of dextran sulfate induced colitis by altered regulation of enteric innate inflammatory responses [91]. Under aberrant conditions, the microbiota is capable of potentiating intestinal inflammation in animal models of inflammatory bowel disease (IBD) and in the clinical case [84]. Intestinal macrophages from *Il10*$^{-/-}$ mice have an increased capacity to respond to intestinal bacteria compared to wild-type controls. This signature was coupled to increased production of IL-12, IL-23 and particularly IL-12p40 upon restimulation with intestinal bacteria, suggesting a polarised an inflammatory Th1 signature in a murine model of colitis [92]. Furthermore, deficiencies in the microbiota are associated with pathological outcomes in dextran sodium sulphate (DSS) induced colitis. Germ-free animals lacking a conventional microbiota had increased severity in disease outcomes, in comparison to conventional wild-type mice. Fecal microbial transplant (FMT) from conventional mice can alleviate pathology in affected germ-free mice, through antagonization of the free fatty acid receptor FFAR2 (GPR43), a key receptor for microbiota derived short-chain fatty acids [93].

As previously mentioned, the known genetic heterogeneity in host immune genes, could be considered a caveat in studies of dysbiosis in the human population, such examples being the toll like receptor family genes. However, there are genes which are recognised to influence microbiota dynamics, such as *Apoa1*, *Myd88*, *Nod2*, *RelmB* and *Hla* genes [88], [94], [95], [96], [97]. Nod-like receptor 2 senses bacterial-derived muramyl-dipeptide and mediates eubiosis in the microbiota and has implemented roles in maintaining intestinal homeostasis. Mutations in the *Nod2* gene are associated with lower commensal diversity and a dysbiotic signature in Crohn's disease [94]. Secretory IgA (sIgA) is crucial in maintaining eubiosis, particularly in the intestinal tract and *Nod2*

mutations have been associated with retrograde transport of sIgA and subsequent dysbiosis [95]. *Tlr5*$^{-/-}$ mice exhibit symptoms of metabolic disease and lower levels of *Bacteroidetes* and *Lachnospiraceae* both of which are recognised as beneficial commensal groups [96]. MyD88 was demonstrated to interact with the commensal microbiota in the development of type I diabetes, demonstrating *Myd88*$^{-/-}$ mice have an altered microbiota profile [97]. Other alternative intrinsic host factors, such as mode of delivery at birth can influence basal the microbiota. Clinical evaluations investigating mode of delivery on infant microbiota identified a lower abundance of maternal derived commensals such as *Corynebacterium* spp., *Moraxella* spp. And *Dolosigranulum* spp. [98]. Nabhani et al. 2019 found that a window was observed in infant mice in which a 10- to 100- fold increased abundance of *Clostridia* and *Bacteroidia* which founded the composition of the adult microbiota was observed during weaning. Inflammatory T cell-derived TNF-α and IFN-γ were increased during the weaning period. Additionally antimicrobial genes were increased during this period, further indicating a critical window in which the infant microbiota can be permanently altered by extrinsic factors, contributing to future pathology [99].

Antibiotics are a primary cause of dysbiosis, causing major ablations in commensal communities and often reduction in microbial diversity. The extent of dysbiosis will result on the type of antibiotic used and the duration of antibiotic treatment, with some cases of microbial ablation never recovering to eubiosis. The use of antibiotics has increased by 65% over the period 2000-2015, with increased consumption particularly in lower- and middle-income countries [100]. Longitudinal clinical studies carried out by Pajella et al. 2018 and collegues investigated the use and subsequent effect of antibiotic usage and prevalence of dysbiosis in an adult cohort of 12 participants. Use of the broad-spectrum antibiotics meropenem, gentamicin and vancomycin results in significant dysbiotic signatures in the faecal microbiota in all participants. A particular signature of antimicrobial genes was associated with the enhanced survival of some commensal families. These antimicrobial genes provided resistance to aminoglycosides and glycopeptide antibiotics, namely gentamicin and vancomycin respectively. Overtime many commensal were restored, albeit the total ablation of some commensal communities was noted after the course of study [101]. The severity of dysbiotic

signatures will have differential impacts on host physiological and immune processes. Antibiotics which have a tropism for gram positive bacteria, particularly gram-positive anaerobes may be more detrimental to host homeostasis and immunity, due to their importance in producing immunomodulatory metabolites. Vancomycin and clindamycin were both found to significantly reduce the α-diversity in the intestinal microbiota in murine studies [102]. While dysbiosis can cause permanent changes in the resident microbiota, it is known that the microbiota can return to equilibrium over time [101]. Immunocompromised individuals and paediatric cohorts can suffer from sustained dysbiotic consequences, with dysbiotic shifts have detrimental outcomes on host immune function. Many studies have identified links between an altered microbiota profile and increased prevalence of disease with higher risk of obesity, asthma, food allergies and intestinal bowel disease in children [103], [104], [105], [106]. While the microbiota heavily influences the host immune system, host immune factors are also required for the stability of the microbiota. Gibson et al. 2016, demonstrated that antibiotic therapy induced alterations in the intestinal microbiota of pre-term infants with antibiotic treatment regiments linked to particular enrichment for antibiotic resistance genes. This is especially detrimental if the commensal communities acquiring these antibiotic resistance genes are potential pathobionts. Antibiotic-induced dysbiosis also results in a significantly decreased production of SCFA [107].

Diet is a significant modulatory factor in the composition of the microbiota [108], [109], [66], [110], [111]. This is evident from global clinical evaluations in microbiota profiles and corresponding dietary patterns and *in vivo* models of selective dietary interference [109]. The “Westernised diet” is associated with a deficiency in fermentable dietary fibre sources and higher intake of dietary protein and fat. Clinical evaluations on the commensal profiles of paediatric cohorts from West Africa and Southern Europe had an increased abundance of the general Prevotella and Xylanibacter which participates in the catabolism of cellulose and xylan. This was in line with a reported diet higher in carbohydrates, fibre and protein in West African children with an intake of 10 grams of dietary fibre daily compared to Southern European children with an average daily consumption of 5.6 grams of dietary fibre [109]. Dietary consumption of fermentable

dietary fibre favours the production of microbiota-derived metabolites which have potent modulatory properties on host physiology and immunity [112], [66].

Some studies have demonstrated that artificial dietary sweeteners can induce dysbiotic shifts in the host intestinal microbiota. However, studies on artificial sweeteners such as aspartame, acesulfame potassium, saccharine, and sucralose have yielded conflicting results, demonstrating either no significant effect on microbiota biodiversity or significant dysbiotic changes [113]. Studies by Rodriguez-Palacios and collegues demonstrated that dietary administration of the sweetener Splenda in murine models of Bacteroidetes-enriched ileal Crohn's disease induced a dysbiotic signature with elevated levels of Proteobacteria in both healthy and CD mice and higher biological myeloperoxidase levels in CD mice, indicative that dietary-induced dysbiotic shifts can alter the inflammatory microenvironment during enteric disease [114]. Food preservatives can also contribute to dysbiosis and therefore an inflammatory microenvironment. One murine study investigated the potential role of food preservatives, namely sodium benzoate, sodium nitrite and potassium sorbate on microbiota composition in wild-type and *Nod2*$^{-/-}$ deficient mice. As mentioned, genetic alterations in *Nod2*$^{-/-}$ are associated with deleterious outcomes in IBD and an increased risk of dysbiosis. *Nod2*$^{-/-}$ were disproportionally affected by the dietary administration of food preservatives compared to wild-type mice. While shifts in alpha diversity index were significant in wild-type compared to *Nod2*$^{-/-}$, *Nod2*$^{-/-}$ mice exhibited a larger shift in beta-diversity index and significant enrichments in *Proteobacteria, Bacteroidetes* and *Verrrucamicrobia* with a loss of *Proteobacteria* [114]. Alcohol is also widely recognised to have dysbiotic effects on the composition of the gut microbiota, with no overall changes in microbiota abundance but reduction of Lactobacillus and an increase in the relative abundance of *Allobacum* [115]. Excessive or chronic alcohol intake can also directly result in chronic dysregulation of gut epithelial permeability. Fibre is seen as the main dietary governing factor of the microbiota. Consumption of dietary fibre is crucial in maintaining eubiosis and supporting the ability of the microbiota to support immune function. Dietary fibre can be stratified into non-digestible or structural fibre and digestible or fermentable fibre, both of which have separate functions in gut health.

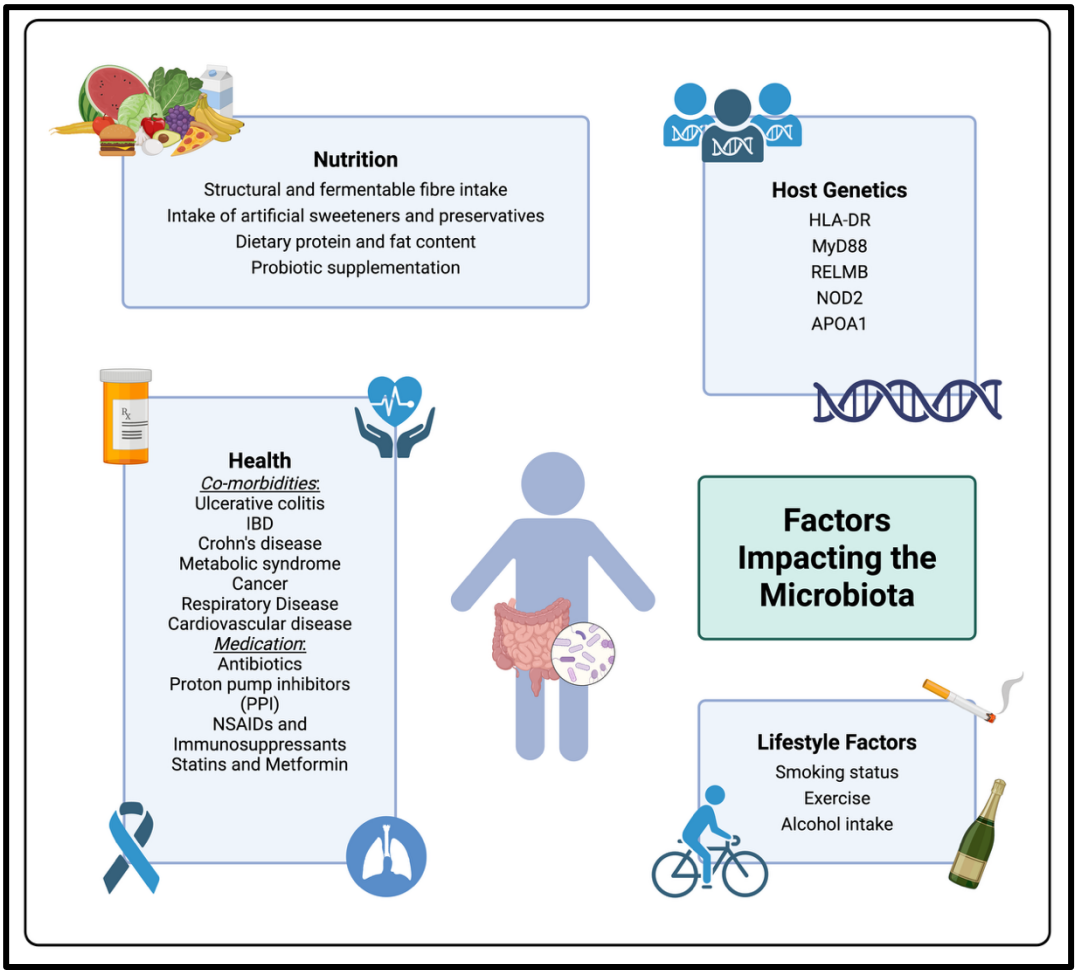


Fig. 1.4 Factors influencing the host microbiota. The microbiota is highly dynamic and shaped by a number of factors. Exogenous factors (those outside the host which influence the microbiota) include diet and lifestyle factors (exercise, xenobiotic use, stress, alcohol intake and smoking). Endogenous factors (those which are intrinsic to the host and cannot generally be changed) include host genetics and comorbidities [88]. Diagram made using Biorender.

1.2.4 Microbiota-derived metabolites

Before proceeding to discuss the production, mechanisms and roles of SCFAs in health and disease, it is important to recognise the full extent of microbiota-derived metabolites. SCFAs are the most abundant family of microbiota-derived metabolites, however, primary and secondary bile acids, amino acid-based metabolites and tryptophan derivatives, namely indoles are all additional products of the commensal metabolome [116]. Indoles are ligands of the aryl-hydrocarbon receptor (AhR) [117]. These metabolites similarly have immunomodulatory roles. Indole-3-propionic acid alters the energetic profile of human $CD4^+$ T cells, enhancing fatty acid oxidation, amino

acid, mitochondrial metabolism and inhibiting glycolysis, in a mechanism independent of AhR engagement. This promoted an anti-inflammatory phenotype in these CD4+ T cells, highlighting a potentially crucial role of Indole-3-propionic acid in intestinal homeostasis [118]. The roles of bile acids in intestinal health are still emerging, however interesting clinical observations have emerged implicating the presence of bile acids in the LRT with changes in the airway microbiota of COPD patients, however presence of bile acids didn't correlate to disease status or progression [119]. The field of microbiota derived metabolites and their roles in health and pathogenesis is rapidly emerging.

1.2.5 Production of short-chain fatty acids

SCFAs contain an aliphatic hydrocarbon tail of varying lengths, up to six carbon units, attached to a carboxylic acid group. There are 8 characterised SCFAs formate (C1), acetate (C2), propionate (C3), butyrate (C4), isobutyrate (C4), valerate (C5), isovalerate (C5), 2-methylbutanoate (C5) and caproic acid (C6). SCFAs are the by and end-products of saccharolytic fermentation of soluble dietary fibre. However, limited evidence suggests that metabolism of both mucins and amino acids can give rise to production of SCFAs, particularly branched SCFAs [120], [121], [122]. SCFA production mainly occurs in the intestinal tract through metabolic and substrate cross-feeding, given the higher microbial richness in this intestinal niche. SCFA concentrations differ anatomically and by reported concentration, with murine serum SCFA concentrations reported in the range of 1-2 mM [66], [123]. SCFAs disseminated systemically through the portal vein from the distal colon are 250μM acetate, 20-200μM propionate and 15-65μM butyrate. This same study found peripheral blood concentrations of SCFA were 20-150μM acetate, 1-13μM propionate and 1-12μM butyrate [124]. However, other studies have reported higher concentrations in the peripheral blood, with reported total serum SCFA concentrations as high as 1mM [66]. SCFAs exist in the murine lung at micromolar concentrations under basal circumstances ~45μM acetate, ~10μM propionate and ~1-2μM butyrate. These concentrations were strikingly similar to those found in the human lung [125]. Human serum concentration of SCFA have been reported between 0-5μmol/L, however, can rise to 1mM in disease states [126]. Total SCFA concentration

ranges from 20-17mM in the human proximal colon to 70-140mM in the distal colon [127]. Prebiotic soluble or fermentable fibre such as inulin, pectin, arabinoxylans, β-glucans and complex oligosaccharides are fed into cross-feeding to produce SCFAs [128], [112], [129], [130], [131]. The type of prebiotic can influence the SCFA produced, pectin has been associated as a prebiotic precursor for the production of propionate, while inulin has been associated with butyrate production *in vivo* [132], [133], [112]. While guar gum has been associated with production of acetate [134].

Metabolic cross-feeding involves the utilisation of end-products of anabolic metabolism to produce further complex metabolites. Substrate cross-feeding involves the further anabolic synthesis of alternative metabolites from by-products of anabolic pathways. A comprehensive review by Lange *et al.* 2023, outlined the main pathways involved in SCFA synthesis, the Wood-Ljungdahl pathway which leads to the production of acetate and acetyl-CoA (**Fig. 1.5**). Both acetate and acetyl-CoA are then utilised through metabolic cross feeding to produce butyrate by activity of the phosphotransbutyrylase/butyrate kinase pathway or alternatively the butyryl-CoA: acetate CoA-transferase pathway. Propionate is then produced by the acrylate, succinate and propanediol pathways which convert acrylate, methylmalonate and propane-1,2-diol respectively into propionate [135], [136], [137].

SCFAs are produced predominantly by gram positive bacteria, *Clostridial* clusters XIVa and are recognised to have predominant roles in SCFA production, particularly butyrate [138], [122]. Production of acetate is mainly mediated by *Bifidobacterium*, *Lactobacillus* and *Streptococcus spp.,* Clostridial genera such as *Roseburia*, *Eubacterium* and *Faecalibacterium* are the main producers of butyrate, while *Lachnospiraceae, Prevotella, Ruminococcus* and *Roseburia* are the main producers of propionate [132], [136], [137], [122], [139].

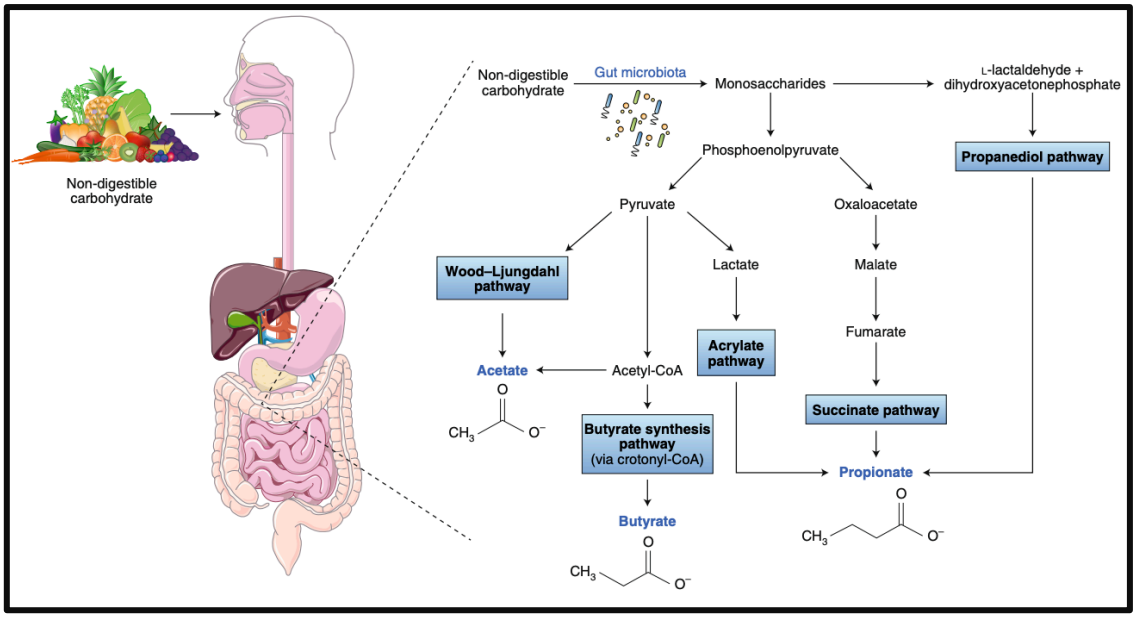


Fig. 1.5 Biosynthesis pathways of SCFAs. Diagram made by Frampton *et al.* 2020 [140].

1.2.6 Mechanisms of short-chain fatty acids

Short-chain fatty acids have pleiotropic modulatory properties in host immunity and physiology. These pleiotropic immunomodulatory effects are likely attributed to the ability of SCFA to alter the phenotype of immune cells through different mechanisms and the bioavailability of SCFA *in situ* (**Fig. 1.6**). A pioneering study by Le Poul et al. 2003, demonstrated that SCFAs bind orphan family G-coupled protein receptors, GPR41 (Ffar3) and GPR43 (Ffar2) which are expressed at varying levels in human tissues [141]. Later GRP109a (HCAR2) was identified as a cognate receptor for β-hydroxybutyrate and subsequently butyrate [142], [143]. Limited evidence suggests Olfactory receptor 78 serves as an additional receptor for acetate and propionate [144]. Alternative to exogenous interaction with cell surface receptors, SCFAs can be internalised and utilised intracellularly through active transport by monocarboxylate transporters, MCT1 (Slc5a8) and SMCT1 (Slc16a1) or internalisation by passive transport via the cell membrane [145], [146], [147].

SCFA can act as an inhibitor of histone deacetylases (HDACi), prevention of HDAC results in an accumulation of poly-acetylated histones and a relaxed chromatin structure

accessible for transcription. Inhibition of HDAC is not the sole mechanism of SCFA mediated epigenetic modification. In addition to acetylation of histones, butyrylation, propionylation, succinylation, crotonylation, hydroxyisobutyrylation and β-hydroxybutyrylation have been identified as alternative mechanisms of histone modification [148], [149], [150], [151]. SCFAs in addition to acetylation can elicit histone 3 and 4 crotonylation, a process linked to cell cycle regulation. This crotonylation of histones was facilitated by direct inhibition of class I and II HDACs by butyrate [152].

Short-chain fatty acids can act through a plethora of mechanisms to elicit effects on host metabolism, immunity and health. Butyrate acts as an energy source for colonocytes which rely on fatty acid oxidation and oxidative metabolism as main pathways of catabolic metabolism [153], [154], [155], [156]. Butyrate can also enhance antioxidant mechanisms under oxidative stress through regulation of Nrf2 [157]. Similarly, SCFAs can regulate cell proliferation and apoptosis. The less abundant butyrate derivative β-hydroxybutyrate can promote cell survival through attenuation of p53 by enhanced mitochondrial metabolism, marked by increased oxidative phosphorylation and beta-oxidation [158]. However, in other cancer cell lines butyrate elicits highly differential activities from promotes apoptosis through engagement of p53 to promoting the survival of resident lymphocytes and increasing “stemness”, emerging recently as an attractive supplement to potentially compliment cancer therapies [159], [160]. Downstream of GPRs SCFAs can elicit MAPK-p38 signalling to modulate the immune phenotype of innate immune cells [161].

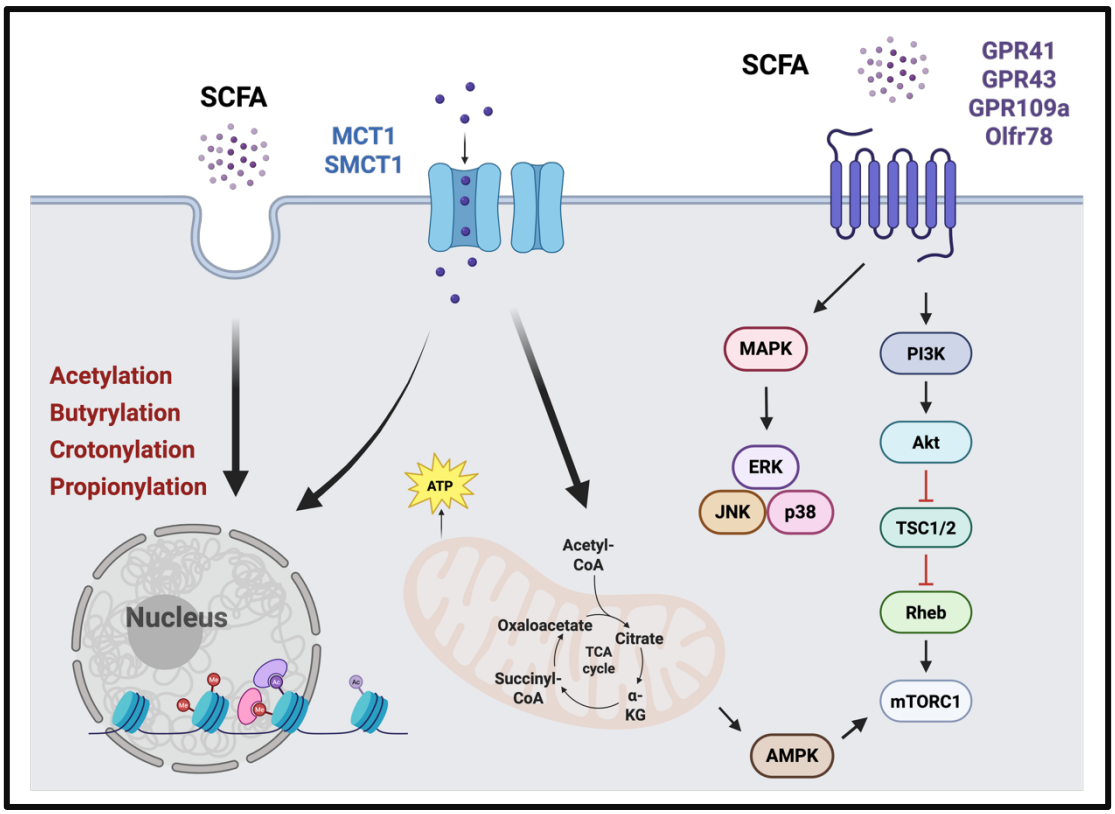


Fig. 1.6 Mechanisms of SCFA engagement with host eukaryotic cells. Diagram made using Biorender.

1.2.7 The respiratory microbiota

The respiratory tract is a mucosal surface exposed to the environment and therefore has a commensal microbiota, composed of bacteria, fungi and viruses, similar to the gut. However, this commensal niche is significantly less abundant and diverse by comparison. The relative biomass of the respiratory tract has been reported as between 10^2-10^3 per gram of tissue or 10^3-10^5 colony forming units/mL in bronchiolar lavage (BAL) samples [162], [125]. There are limitations involved in current methods of respiratory microbiota sampling. Clinical sampling via bronchoscopy remains the conventional method of BAL collection for sampling of the lower respiratory tract microbiota, however these samples can be contaminated with upper respiratory tract (UTR) and oropharyngeal derived commensals [163]. Similarly, the basal resident nasal and URT microbiota is heavily influenced by the oral commensal microbiota, through micro aspiration events. For this reason, a comprehensive evaluation of studies investigating the spatial relationship between commensal niches and persistent species helps to fully understand the respiratory tract microbiota [164]. However, one study by Odendaal et al. 2024, highlighted that the human URT is dominated by *Corynebacterium, Moraxella, Staphylococcus, Dolosigranulum, Haemophilus* and *Anaerococcus* amongst others less abundant genera [165]. This same study demonstrated that the oral microbiota was dominated with *Streptococcus, Prevotella, Veillonella, Leptotricia, Actinomyces* and *Rothia* demonstrating that despite the risk of sampling contamination and aspiration the oral microbiota and URT have different commensal landscapes [165]. Indeed, other human cohort studies sampling the URT have identified *Streptococcus, Corynebacterium, Moraxella, Staphylococcus* and *Lachnospiraceae* as abundant genera [166]. However, studies highlight that the composition of the URT is highly influenced by age, differing between children and adults and geographical variations in sampled cohorts [165], [166], [167]. The LRT microbiota broadly contains *Streptococcus, Prevotella* and *Veillonella* [163].

The respiratory microbiota has implicated roles in lung health and disease. Dysregulation of the respiratory microbiota is seen in chronic respiratory conditions

such as cystic fibrosis, chronic obstructive pulmonary disease, idiopathic pulmonary fibrosis and lung cancer [168], [169], [170], [171], [172].

1.3 The gut-lung axis and respiratory pathology and infection

The immunological crosstalk that exists between the intestinal microbiota and the respiratory immune system is defined as the "*gut-lung axis of immune regulation*". The role of the intestinal microbiota as a regulatory of respiratory immunity emerged through clinical cohort studies in respiratory pathologies [173]. Dysregulation of the gut microbiota is seen in chronic respiratory diseases, namely chronic obstructive pulmonary disease (COPD), cystic fibrosis (CF), idiopathic pulmonary fibrosis (IPF) and asthma and allergic airway disease (AAI), [87], [174], [175], [176], [177]. Murine models have supported this clinical evidence, validating these correlation studies, demonstrating links between intestinal dysbiosis and COPD and IPF, using smoke exposure and bleomycin induced lung pathology respectively [174], [66]. Bowerman et al. 2020 demonstrated that in individuals with COPD show depletion of *Bacteroidetes* and broader *Clostridia* families namely *Roseburia, Ruminococcaceae* and *Lachnospiraceae* in the faecal microbiota, both of which are associated with SCFA production. On the other hand, *Streptococcus* and *Rothia* spp. were increased [87]. A chronic partial ablation in SCFA-producing bacteria could imply a role pathogenesis of COPD. Similarly, COPD patients present with chronic enteric co-morbidities such as IBD and UC [178].

Conversely, germ-free animals are protected against bleomycin-induced pulmonary fibrosis and a decrease in gut microbiota diversity was associated with reduced disease pathology, indicating a potential deleterious role of the gut-lung axis in IPF. This reported effect was due to an increased frequency of PL-1^{+}IL-17^{+} and IL-6^{+} T cells with higher commensal microbial richness [174]. An ablated lung microbiota is a known feature of CF, however potential links between a dysbiotic intestinal phenotype and outcomes of CF pathogenesis is less explored. Significant enrichment of *Bacteroidetes*, *Lachnospiraceae*, *Clostridium* and *Enterococcus* were associated with diverse metabolic functions including fatty acid oxidation, β-oxidation, fatty acid biosynthesis and fatty

acid elongation, alongside tryptophan and arginine degradation and the lactose utilisation pathway in the microbiota of CF patients compared to healthy controls [175]. The link between the intestinal microbiota and host respiratory immunity extends to host responses to infection. Antibiotic-induced dysbiosis has been associated with increased respiratory bacterial burden and increased lethality in murine models of pneumococcal pneumonia [179], [73]. Similarly, in murine models of *Staphylococcus aureus* and *Klebsiella pneumoniae* mediated bacterial pneumonia, antibiotic-induced dysbiosis has resulted in higher bacterial burdens compared to eubioitic controls [73], [107], [180].

The ability of the intestinal microbiota to set the "immune tone" in the lung through ameliorations in respiratory cytokine milieu has been explored [125]. Gut-derived LPS has been identified as an immunomodulator in the lung. Liu et al. and collegues, demonstrated that gut-derived LPS synergises with SCFA to regulate the immune tone in the lung through modulation of the innate cell-derived alveolar cytokine mileu, particularly AM-derived IL-1β [125]. Ruane et al. 2016 demonstrated that lung $CD103^+$ and $CD24^+$ DCs regulate IgA class switching in a retinoic acid and TGF-β dependent mechanism. Production of these mediators was dependent on the microbiota, with germ-free animals exhibiting significantly reduced levels of lung DC-derived TGF-β, similar to *Trif*$^{-/-}$*Myd88*$^{-/-}$ when compared to conventional SPF controls [18]. This further implicates the importance of sensing microbiota derived PAMPs in priming host immunity. The similarities between germ-free response and *Trif*$^{-/-}$*Myd88*$^{-/-}$ in this context highlight that engagement of these pathways by microbiota derived PAMPs contributes to TGF-β production and subsequent effects on DC phenotype. This effect could further regulate inflammatory infiltrates during lung infection or insult.

Similarly, TLR stimulation of gut microbiota derived PAMPs, particularly LPS, is the key factor governing the protective effect of the gut-lung axis during influenza A infection. This was further stratified by selective antibiotic treatment, to a reliance on neomycin-sensitive commensal bacteria [181]. Antibiotic-induced dysbiosis resulted in a reduced capacity of primed lung dendritic cells to travel to mediastinal lymph nodes, which was restored with exogenous LPS inoculation, implying a crucial role of microbiota-derived LPS sensing in providing auxiliary immunoregulatory functions in host immunity [181].

Likewise, the gut microbiota has been shown to play an important role in models of viral infection, with antibiotic-mediated ablation of the microbiota resulting in impaired type II IFN in $CD4^+$ and $CD8^+$ lymphocytes, a reduction in antigen-specific and higher pulmonary viral titres in a model of type A influenza infection [181]. Segmented filamentous bacteria (SFB) are gram positive, anaerobic, bacteria which inhabit the gut [182]. Ngo et al. 2024 demonstrated that SFB^- mice had an increased susceptibility to influenza A infection. SFB appeared responsible for the stability of AM populations, marked by reduced caspase-3 and increased CD71 and Ki-67 expression, implying not only are these AMs viable but also proliferative [183]. The ablation of AMs due to cell death during respiratory infection is typically associated with influenza A infection, however, is also apparent in the case of pneumococcal infection [184], [185], [61], [62], [63], [60].

In the context of lung bacterial infections, Schuijt et al. and collegues demonstrated that AMs isolated from dysbiotic animals had an altered phenotype with a lower bactericidal capacity. Pulmonary cytokine milieu was also altered in these animals with significantly higher neutrophil chemoattractants IL-6, CXCL1 and decreased IL-10. This upregulation in inflammatory cytokines was in conjunction with significantly worsened organ damage in dysbiotic animals. While this study did not highlight further effects of altered cytokine and chemoattractant production, it is plausible that this could have contributed to increased infiltration of neutrophils and lung injury [179]. Conversely, Brown et al. and collegues reported lower CXCL1 and CXCL2 in dysbiotic animals, in response to *S. pneumoniae* and *K. pneumoniae* infection, however crucially acknowledged that GM-CSF production, required for AM function, is dependent on IL-17A in a microbiota-dependent manner [73]. Cumulative evidence indicates the gut-lung axis is a defining factor of bacterial pneumonia. Similiarly, deleterious outcomes of antibiotic-induced dysbiosis have been noted in *Escherichia coli* pneumonia [186]. Chen et al. 2010 highlighted that mice receiving antibiotics prior to infection had higher bacterial burdens in the lung and blood during E. coli infection, in addition to abrogated myeloperoxidase (MPO) levels in the lung. In addition to this, AMs in mice receiving antibiotic had an altered phenotype with reduced bactericidal functions and heightened production of IL-6 and IL-1β [186].

Additionally, SCFAs have contrasting effects on cytokine production. SCFAs have been shown to inhibit NFκB transcriptionally regulated cytokines and alleviates colitis via histone deacetylation [187]. One study by Säemann et al. 2000 and collegues demonstrated that butyrate was capable of inhibiting TNF-α, IL-12p35 and IL-12p40 mRNA in human PBMC-derived monocytes [188]. A comprehensive evaluation of SCFA (acetate, butyrate, propionate) mediated effects on cytokine production on human PBMCs was published by Asarat et al. 2016. This study highlighted that protein levels of IL-1β, IL-2, IL-6, IL-17, IL-21 and IL-23 were decreased in LPS-stimulated PBMCs in the presence of butyrate, however IL-10 levels were increased in the presence of SCFA [189]. Additionally, SCFA-mediated enhancement of IL-10 was seen in Th1 cells [190]. In converse to this, other studies have reported a positive regulation of SCFAs on inflammatory cytokine production, highlighting the ability of propionate to increase TNF-α production in human mesenchymal stem cells via MAPK induced p38 activation, this then lead to increased IL-6 and CXCL8 [161].

An immunological axis of regulation between the gut microbiota and specifically AMs is supported by studies which identify gut microbiota, specifically SFB-mediated protection in pneumococcal infection in *Rag*$^{-/-}$ mice which lack T or B lymphocytes [191]. Another study by Khan et al. 2019 and collegues demonstrated the standard line anti-tubercular antibiotic therapy (ATT) for treatment of *Mycobacterium tuberculosis*, administration of rifampicin, isoniazid and pyrazinamide resulted in a dysregulation in the gut microbiota associated with increased spread of *M. tuberculosis* upon challenge [192]. This was not dependent on T cell contributions but rather an impaired AM, exhibiting a reduced capacity to ex vivo [192]. In conclusion there are crucial links between the commensal microbiota and the functional phenotype of AMs, with many of these studies suggesting an “ineffective” or reduced bactericidal phenotype of AM in the incidence of dysbiosis. In addition to this there appears to be a phenotype of uncontrolled inflammation in dysbiotic cohorts during respiratory infection.

1.3.1 Microbiota-derived metabolites as messenger and immunomodulators beyond the intestine.

Short-chain fatty acids, tryptophan metabolites and amino acid derivatives are all by or end products of commensal metabolism. These metabolites can act locally in the intestine to modulate host immunity and physiology, however, are also known to travel in the systemic circulation and elicit immunological effects at distal sites, such as the brain, lungs and liver. SCFAs as described in section **1.3**, are produced predominantly by gram-positive anaerobes through the saccharolytic fermentation of prebiotic soluble dietary fibre. Furthermore, causative links have been identified between the therapeutic potential of dietary fibre and outcomes of respiratory pathology, further supporting a therapeutic potential of SCFA in respiratory infection and pathogenesis [193], [194].

Acetate has been investigated in the context of pneumococcal infection. Machado et al. and collegues have demonstrated that acetate can increase reactive nitrogen species in an IL-1β dependent mechanism to increase bactericidal activity in MH-S macrophages *in vitro*. This mechanism further relied on an increase in glycolytic metabolism which increased HIF-1α activity and promoted NLRP3-dependent IL-1β production. Mice administered acetate in drinking water had a significantly lower bacterial burden in the lung compared to controls *in vivo* [195]. Propionate synergises with gut-derived LPS to elicit immunomodulatory functions in the lung. Free fatty acid receptors 2 (FFAR2) and 3 (FFAR3), receptors of SCFAs, expression is induced on MH-S and MLE12 cells, *in vitro* models of alveolar macrophage and alveolar epithelial type 2 cells respectively, in response to LPS exposure, indicating a synergistic relationship between both gut-microbiota-derived products. Furthermore, IL-1β co-localised with FFAR2 and FFAR3 expression in $CD11c^{+}$, $MRC1^{+}$ AMs, in *in situ* mRNA probing of human lung tissue resections, providing primary evidence that SCFAs can act directly on AM *in vivo* [125]. SCFAs have demonstrated an ability to augment anti-viral immunity in the respiratory tract.

Crucially SCFAs appear to support the anti-microbial functionality of tissue resident macrophages. Schulthess et al. 2018 and collegues demonstrated that butyrate could enhance the antimicrobial functions of intestinal macrophages against enteric pathogens *Salmonella typhimurium*, *Eschericha coli*, *Citrobacter rodentium* and *Staphylococcus aureus*. Butyrate treatment appeared to enhance glycolytic metabolism, reduced mTOR kinase activity and antimicrobial peptide production, while increasing LC3 associated activity. Butyrate enhances expression of calprotectin, *S100A8* and *S100A9*, *S100A12*, *LYZ*, *FCN1* in human PBMCs. Synergistically, LC3-mediated clearance of intracellular bacteria and increased cellular ROS was detected in butyrate treated macrophage in response to infection [196]. Indeed, similar effects have been investigated in the case of lung resident macrophages. Wu et al. 2020 demonstrated that combined treatment with acetate, butyrate and propionate enhanced the antimicrobial activity of RAW264.7 macrophage against *K. pneumoniae* by promoting LAMTOR2, an mTOR activated mediator of lysosomal activity [107]. Similarly, an *in vivo* murine model published recently by Kullberg et al. 2025 and collegues demonstrated that mice receiving i.p. butyrate exhibited lower levels of IL-6 and CXCL1 which correlated to lower neutrophil influx in the BALF and lower MPO activity in the lung when challenged with *K. pneumoniae* [197]. This attenuation of neutrophil mediated inflammatory response corresponded to a decreased bacterial burden in the lung and limited systemic bacterial spread to the blood, liver and spleen [197]. These results were recapitulated using the butyrogenic probiotic *Faecalibacterium prausnitizii* albeit the significant depletion of total neutrophils selectively occurred in mice receiving butyrate compared to those colonised with *Faecalibacterium prausnitizii* [197]. It is worth noting that the immunomodulatory effects of SCFAs are not limited to acetate, butyrate and propionate, but also extend to branched SCFAs. Isovalerate a less abundant SCFA, found at sub-micromolar concentrations in human lung tissue [125]. *Prevotella copri*, a producer of branched SCFAs, isovaleric and isobutyric, acids demonstrated protectivity during H9N2 influenza infection. Isovaleric acid when delivered as an oral dietary supplement in murine H9N2 influenza infection ameliorated disease, reducing viral load in the lung while reducing NFκB governed cytokines TNF-α, IL-6 and IL-1β, which translated to a reduced tissue pathology score [198].

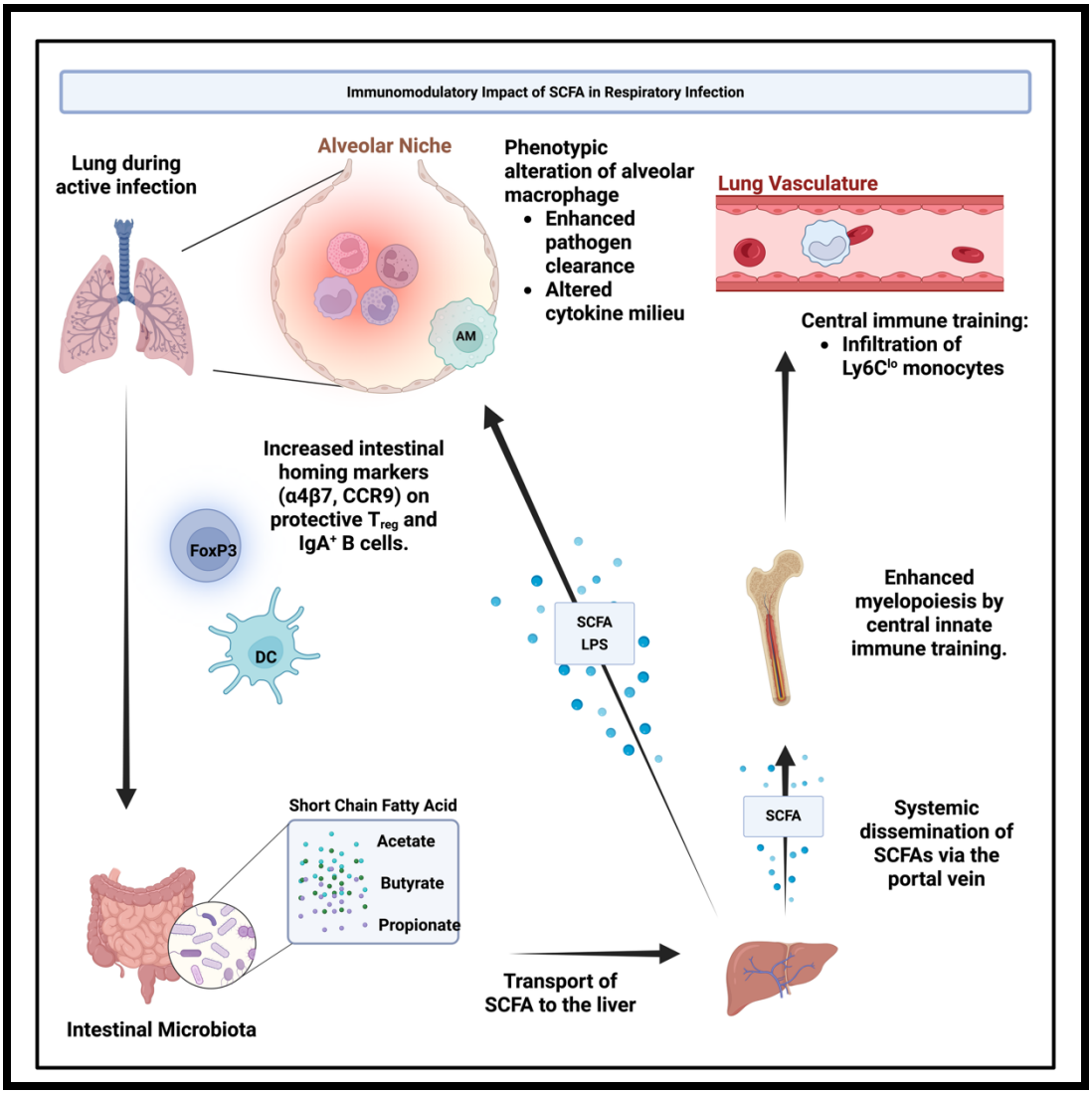


Fig. 1.7 The gut-lung axis in respiratory infection

1.4 *Streptococcus pneumoniae*

1.4.1 Epidemiology

S. pneumoniae is a significant cause of communicable disease associated morbidity and mortality [199], [200]. *S. pneumoniae* can also manifest as otitis media, as well as other life-threatening invasive infections that include bacteraemia, sepsis, invasive pneumococcal pneumonia, myocarditis, among others, collectively known as invasive pneumococcal disease (IPD) [201]. Children under 5 years, older adults over 65 years and individuals suffering from chronic respiratory conditions or immunosuppression are particularly susceptible to IPD. Additional risk factors for IPD include being male, having

cardiovascular disease, intake of xenobiotic agents such as antibiotics drinking and smoking. *S. pneumoniae* can exist as part of the basal microflora in the nasopharyngeal microbiota, with higher rates of asymptomatic carriage typically seen in paediatric cohorts [201].

There are currently over 100 circulating serotypes of disease characterised by the outer polysaccharide capsule which represents the main pneumococcal antigen [202], [203]. While pneumococcal vaccines are available worldwide and are integrated into the Health Service Executive (HSE), Ireland childhood immunisation scheme, there is still an important prevalence of pneumococcal infections [204]. The current line of standard treatment recommended under HSE guidelines for the treatment of CAP involves amoxicillin, doxycycline or clarithromycin as phase I antibiotics [204]. While *S. pneumoniae* is not considered one of the ESKAPE pathogens, antibiotic resistance is still a growing concern. ESKAPE pathogens are multi-drug-resistant bacterial spp. which are the cause of many hospital acquired infections, these pathogens are *Enterococcus faecium, Staphylococcus aureus, Klebsiella pneumoniae, Acinetobacter baumannii, Pseudomonas aeruginosa* and *Enterobacter spp.* [205]. The World Health Organization (WHO) Bacterial Priority Pathogens List establishes the top antibiotic-resistant (AMR) bacteria categorized by priority level [206]. While *S. pneumoniae* is not part of the ESKAPE bacteria, it is considered as *'Medium Priority'*. Several reports highlight the AMR issue for pneumococci, where resistance to β-lactam, cephalosporin and macrolide antibiotics in infective pneumococcal strains has been found [207], [208], [209]. A systematic review of global studies on pneumococcal serotype prevalence by Darkwah et al. 2025 identified that IPD patients carrying pneumococcal serotypes 3, 6A, 11A, 15A, 19F, and 31 were at a higher risk of morbidity [210]. One caveat in comprehensive studies correlating pneumococcal serotypes and bacterial genetics to pathogenesis and antimicrobial resistance is the geographical difference in serotype prevalence [211]. Infective serotypes commonly reported in cases of severe pneumococcal infection include serotype 3, which is considered an extremely adaptable serotype during host infection [212].

1.4.2 Bacteria

S. pneumoniae is a gram-positive facultative anaerobe. It can exist as either as a capsulated or non-capsulated bacterium both of which have potential virulence, albeit capsulated bacteria are associated with clinical pneumococcal disease cases. *S. pneumoniae* exhibits alpha haemolysis when cultivated on blood agar and is catalase negative. Pneumococci can form diploid clusters or long chains, which can be serotype dependent. Tettelin et al. 2001 characterised the genome of TIGR4, a serotype 4 pneumococcal strain, demonstrating the genome is ~2.1 million base pairs in length, with a significant portion of the genome exhibiting genetic plasticity [213], [214]. *S. pneumoniae* has a high replication rate, as fast as 30 minutes and can undergo genetic changes in order to adapt to environment or host; a distinct relationship between doubling time and genetic variation exists, with delays in replication associated with preservation of genetic integrity [215]. Capsular polysaccharide is attached to the cell wall through peptidoglycan interactions. In some invasive serotypes bacteria can shed the outer polysaccharide capsule evading opsophagocytosis, in the case of serotype 3, the capsular polysaccharide is non-covalently adherent [216]. *S. pneumoniae* is highly adaptable and utilities quorum sensing to readily change genomic structure benefiting colonisation of the host and biofilm formation in the environmental niche [217]. For this reason, it can be considered a pathobiont. *S. pneumoniae* readily colonises the nasopharynx and upper airways, mainly in paediatric cohorts.

1.4.3 Innate response to *Streptococcus pneumoniae*

Early and controlled inflammatory responses are required for successful elimination of infection and positive infection outcomes. Many signalling pathways are engaged downstream of PRR engagement during pneumococcal infection as out lined in **Fig. 1.8**. Lipoteichoic acid residues on the surface of *S. pneumoniae* interact with toll like receptor 2 (TLR2) on resident immune cells, while engaging in downstream signalling and engagement of NFκB [218], [219], [220], [221], [222]. The role of TLR2 in direct AM mediated anti-microbial defence has been disputed, however TLR2 engagement is required to produce inflammatory cytokine production [223], [224]. In converse, *Tlr*$2^{-/-}$

Nod2$^{-/-}$ mice have increased susceptibility to *S. pneumoniae* implying a critical role of TLR2 in synergising with Nod2 in host defence to *S. pneumoniae* with other studies utilising *Tlr2*$^{-/-}$ support the role of TLR in protection against *S. pneumoniae* [225], [226]. Unmethylated CpG residues on pneumococcal DNA activate toll-like receptor 9 (TLR9) intracellularly in endocytic vesicles, which requires uptake of the bacterium by host cells or sensing of host DNA release during episodes of cell stress [227], [228]. Toll-like receptor 4 (TLR4) has an implied but debated role in the innate response to pneumococcal infection [229]. Pneumolysin (PLY), a cytolytic protein made by many pneumococcal isolates forms pores on the eukaryotic cholesterol-rich membranes acting as another important virulence factor and promoting inflammation. PLY has been reported to interact with the NLR family pyrin domain containing 3 (NLRP3) inflammasome, albeit in a TLR4-independent manner [230] disputing previous evidence which suggested the TLR4 pathway was involved in PLY recognition.

Ligated toll-like receptors signal through MyD88 to activate downstream canonical NFκB activation. This involves activation of complexed Tumor necrosis factor receptor-associated factor (TRAF)6, Interleukin-1 receptor-associated kinase (IRAK) 1, IRAK 2 and IRAK4 which facilitates the downstream activation of TGF- activated kinase 1 and MAP3K7-binding protein (Tab)2/3 and TGF-activated kinase 1(Tak)1 further activating NFκB essential modulator (NEMO), IκB kinase (IKK)α and IKKβ which then facilitates transcriptional regulation by active nuclear factor kappa-light-chain-enhancer of activated B cells (NFκB). Activation of NFκB results in the production of a myriad of inflammatory cytokines and engagement of cell survival pathways [231]. Pahl et al. 1999 published a comprehensive list of NFκB transcriptional targets including of a plethora of inflammatory cytokines, namely IFN-γ, IL-1α, IL-1β, IL-1Rα, IL-2, IL-6, IL-8, IL-12p40, IL-15, IP-10, IFN-β, MCP-1, MIP-1α, MIP-2, RANTES and TNF-α [232]. Nod2 interacts with peptidoglycan degradation products, also resulting in the downstream activation of NFκB [225]. The Aim2 inflammasome is activated through recognition of pneumococcal DNA and has in imperative role in host defence against pneumococcal infection, with Aim2 mice exhibiting an increased susceptibility to lethal pneumococcal infection [233]. Both peptidoglycan mediated activation of the NLRP3 inflammasome and nucleic acid-

mediated activation of the Aim2, interact through ASC and result in the downstream cleavage of pro-caspase 1. Active caspase 1 facilitates production of IL-1β and IL-18 through the proteolytic cleavage of pro-IL-1β and pro-IL-18 [234]. Similarly, pneumolysin (PLY) is a potent stimulator of inflammatory cytokines, TNF-α and IL-1β in monocytes [235].

Stimulator of interferon genes (STING) has recently been recognised as a potential crucial signalling mediator in host pneumococcal defence. Koppe et al. 2012 demonstrated that the ability to produce type I IFN, namely IFN-β, was retained in the absence of TLR2, TLR3, TLR4, TLR7, TLR9, Rig-I-like receptor (RLR), Mitochondrial antiviral signalling protein (MAVS) and Nod2, however appeared dependent on sensing of bacterial DNA and subsequent STING-mediated Interferon regulatory factor (Irf)3 activity. Furthermore, this production of type I IFN was dependent on phagocytosis and downstream lysosomal acidification [236]. This STING-dependent production of type I IFNs stimulated autocrine production of the monocyte chemoattractant Regulated upon activation, Normal T cell expressed and Secreted (RANTES) [236]. This could imply a mechanistic axis *in vivo* between early type I IFN production and subsequent infiltration of monocytes. Infection of polymorphonuclear cells (PMNs) with *S. pneumoniae* lacking superoxide dismutase (sod-/-) exhibited heightened mitochondrial reactive oxygen species (ROS) production compared to those infected with WT bacteria [237]. *S. pneumoniae* induces the production of ROS in host mammalian cells. While the mechanism of *S. pneumoniae* mediated ROS induction in host mammalian cells is unclear, it appears independent of both pneumolysin (PLY) and capsular polysaccharide [237]. PLY has been reported to induce a respiratory burst in PMNs, which in turn was required for bacterial clearance. MyD88 appeared to contribute to mitochondrial ROS induction, which was negatively regulation by A2B adenosine receptor [237].

Antimicrobial peptides (AMPs) have an imperative role in early defence against *S. pneumoniae* infection. This is clear from *in vivo* murine studies in which knockout animals; lacking AMPs have a higher susceptibility to pneumococcal infection [238]. S100 family members, S100a8 and S100a9, which are primarily produced by but not limited to neutrophils, can dimerise to form the calprotectin complex which is released

during NETosis [239]. Calprotectin is often elevated in cases of pneumococcal infection and functions to regulate granulocyte colony stimulating factor and subsequently increase neutrophil numbers [240]. S100a9 is a critical antimicrobial peptide in early response to pneumococcal infection, *S100a9*$^{-/-}$ mice had higher BALF and lung bacterial burden, higher inflammation by histological scoring and a decreased survival upon induction of pneumococcal pneumonia [238]. Lactoferrin is an antimicrobial peptide with direct bactericidal and immunomodulatory functions. Lactoferrin functions by sequestering iron sources from bacteria, mechanistically this has been proven by investigating the direct bacterial effects of hololactoferrin (iron chelated) versus apolactoferrin (no iron chelation) [241]. Lactoferrin is capable of disaggregating biofilms, which is of particular importance in controlling *S. pneumoniae* quorum sensing and subsequent biofilm formation in colonisation [242].

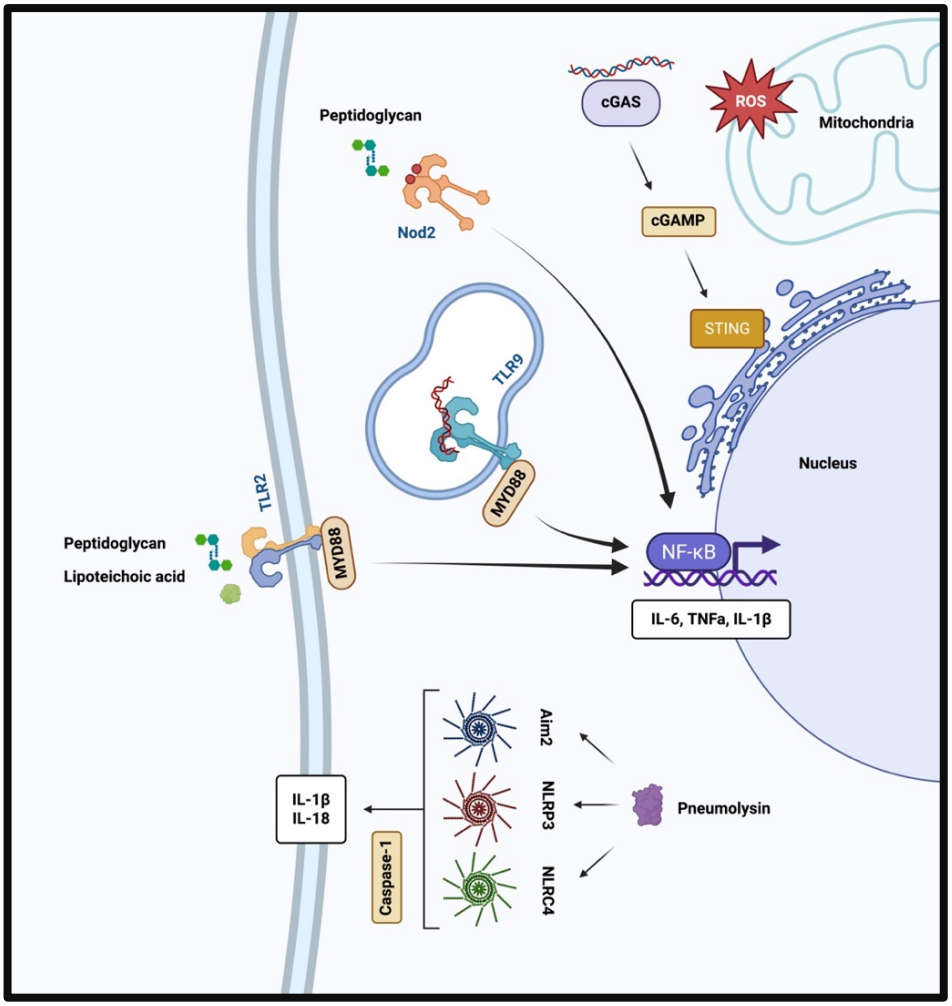


Fig. 1.8 The activation of PRRs and subsequent intracellular responses in response to *S. pneumoniae*. Pneumococcal antigens such as lipopeptides, peptidoglycan, pneumolysin and bacterial unmethylated CpG DNA, readily agonise TLR2, TLR4, TLR9, Nod1 and Nod2 which facilitate the downstream activation of NFκB and inflammatory cytokines TNF-α and IL-6. Activation of the NLRP3, NLRC4 and Aim2 inflammasome complexes results in the downstream release of pyroptotic cytokines. Finally, release of cellular DNA by oxidative damage, results in the activation of the cGAS-STING pathway and downstream production of type I IFNs [243]. Diagram made using Biorender.

Pneumococci can also form biofilms, bacterial communities which form aggregates by producing and secreting extracellular polymeric substances and allow bacteria to colonise surfaces [244]. Lactoferrin can inhibit this through direct DNAse activity [242]. Lactoferrin also synergises with lysosomal pathways to facilitate further antibacterial activity. While not directly demonstrated in the response to *S. pneumoniae* the synergistic effect of lactoferrin with the lysozyme has been investigated in response to other gram-positive bacteria such as *Staphylococcus aureus* and gram-negative bacteria [245], [246], [247]. Lipocalins are a family of carrier proteins, predominantly secretory proteins with a wide array if functions [248]. Lipocalin 2 has a reported pathological role in pneumococcal infection, increasing the early inflammatory response to infection and impairing macrophage response to infection [249], [250]. Cathelicidins, are another family of antimicrobials peptides with crucial roles in innate defence against pneumococcal infection, as demonstrated in a model of pneumococcal meningitis. LL-37 in humans and CRAMP in murine animals act as neutrophil chemoattractants [251]. *Cramp*$^{-/-}$ mice exhibited a higher susceptibility profile in a model of pneumococcal mediated bacterial meningitis, reflected by a higher local and systemic bacterial burden and decreased survival index [252].

Alveolar macrophages (AMs) are the first population of resident innate cells to engage in host pneumococcal defences. AMs recognise pneumococci in the distal airway and produce S100a9, S100a8, both of which have roles in neutrophil chemotaxis [253], [254]. However, it is also known that AMs are crucial in the resolution of apoptotic neutrophils during pneumococcal pneumonia controlling inflammation in the alveolar niche [255]. AMs are crucial in clearance of pneumococci in the lung [256], [73], [179]. AM phenotype changes throughout the course of infection. The resident population of murine AM in the uninfected lung are typically characterised by high synergistic

expression of CD11c and SiglecF (CD207) [50], while in the human lung CD206 in synergistic expression with CD86 mark AM populations [51]. However, these populations are depleted early in infection and are replaced by a population of infiltrating AM-like cells which are higher in expression of MHCII and lower in SiglecF [62], [60]. This turnover in the resident airway macrophage population is widely recognised as the macrophage disappearance act appears dependent on IFN-γ. Albeit the contributions of $CD4^+$ T cells appears to be arbitrary for this process [60]. Alveolar macrophages undergo broad scale transcriptional changes during pneumococcal infection characterised by an increase in antimicrobial genes and inflammatory cytokines genes [253].

Zec et al. 2023, identified that AMs exhibit increased CD11b expression during pneumococcal infection which correlates to an altered phenotypic profile. Amongst the highly expressed genes in this study, CD11b was associated with increases in *Ccl9*, *Cxcl1, Cxcl2, Cxcl3, Lcn2, S100a8* and *S1009* all of which have roles in neutrophil recruitment [253]. This evidence implies AMs can act in an auxiliary capacity during pneumococcal infection by recruiting neutrophils and peripheral inflammatory monocytes as opposed to engaging in a direct antimicrobial capacity (**Fig. 1.8**). In this same study AMs derived from animals infected with *S. pneumoniae* were capable of producing CXCL1 and myeloperoxidase (MPO) *ex vivo* [253]. This study by Zec et al. 2023 and colleagues provided a fundamental insight into the phenotypic changes AMs take on to combat pneumococcal infection.

Neutrophils act in a dichotomous capacity during pneumococcal infection. Early neutrophil infiltration is crucial for bacterial clearance however attenuated activity can result in lung parenchymal damage; however, an impairment of neutrophil infiltration can be deleterious in pneumococcal infection outcomes, [257], [258], [259], [260], [261]. Neutrophils and specifically neutrophil elastase have been associated with cleavage of NFκB regulated cytokines, exacerbated infection and higher bacterial loads in the BALF and blood [260], [261]. However, other publications highlight the crucial role of neutrophils in host protection during pneumococcal challenge. Muñoz-Wolf et al. 2016 demonstrated that sublingual administration of flagellin protected mice during pneumococcal challenge in a mechanism mediated by neutrophils [258]. Similiarly,

Ivanov *et al.* 2011, Kawakami *et al.* 2003 and Nakamatsu et al. 2007 demonstrate that neutrophils are essential for protection downstream of iNKT cell activation during pneumococcal infection [259], [262], [263]. Kinetics of neutrophil infiltrate underlie this dichotomy over whether neutrophils are seen as deleterious or beneficial during pneumococcal infection. Neutrophils are attracted to the lung via chemotactic CXCL1, CXCL5, MIP1α (CCL3), and CXCL8 which encourages extravasation to the alveolar spaces through the lung [264], [265], [266]. Neutrophils emit extracellular traps (NETs) which are composed of single stranded DNA. Neutrophil elastase release appears to be heavily induced by pneumolysin [238]. Neutrophil elastase in response to *S. pneumoniae* binds the surface of pneumococci and directly elicits cell wall aminopeptidase A degradation.

Monocytes require CCR2 signalling to migrate to the site of infection from peripheral sites such as the bone marrow during lung infection [267]. However, *Ccr2*$^{-/-}$ mice that had recovered from *Influenza A* infection (IAV) had a reported lower susceptibility to pneumococcal challenge than wild-type counterparts implying a potentially dual role of monocytes in the innate response to pneumococcal infection [268]. Monocytes that are recruited during infection can differentiate *in situ* to monocytes derived dendritic cells (moDC) or monocyte derived macrophage (MDM), dependent on the local cytokine milieu [10]. Monocytes can also support the functional capacity of CD4^{+} T cells by promoting IL-17A and IFN-γ during *in vitro* co-cultures [269]. Some studies suggest that MDMs can adopt an AM like phenotype, however Arafa et al. 2022 demonstrated that AMs are not dependent on CCR2 and are functionally different from MDMs [225].

Dendritic cells bridge the gap between the innate and adaptive immune responses and are fundamental in presenting pneumococcal antigen to local and systemic adaptive cell populations. DCs are activated through ligands and pathways previously described. However, the cytokine profile of the dendritic cells will dictate the polarisation of the CD4^{+} response generated. McNeela et al. 2010 demonstrated that DCs when stimulated with pneumolysin synergistically with TLR ligands, upregulate production of IL-12, IL-23, IL-6, IL-1β, IL-1α and TNF-α [230]. IL-23 and IL-1β are crucial cytokines in polarising CD4+ T cells towards a Th17 subtype, which is crucial in pneumococcal defences. While IL-12 and IL-6 encourage differentiation of CD4^{+} Th1 cells. Simultaneously, early induction of

$CD103^+$ type 2 DCs appears crucial in eliminating bacteria. Studies by Ivanov *et al.* 2012 have demonstrated that the iNKT agonist, a-galactosylceramide, when delivered prophylactically promoted an induction of $CD103^+$ DCs which promoted iNKT activation and production of IFN-γ and IL-17A, both of which cytokines are essential in sustaining the AM and neutrophil populations respectively during infection [259].

Innate T cells, such as invariant natural killer T (iNKT) participate in host response to pneumococcal infection [270], [259], [262], [263], [271]. iNKT cells have been recognised as a source of IFN-γ and IL-17 in mice, administered the iNKT cell agonist α-galactosylceramide (α-GalCer) intranasally, during pneumococcal infection, produced by the two resident subsets of iNKT cells, NKT1 and NKT17 respectively [259]. While all subsets, namely NKT1, NKT2 and NKT17 are recruited to the lungs early in infection, only NKT17 cells alongside γδT cells received TCR signalling post infection. Supporting this, IL-17A was detected in both NKT17 cells and more abundantly γδT cells post infection, albeit levels of $GM\text{-}CSF^+NKT1^+$ populations were not significantly increased by post infection [271]. Additionally, Ivanov *et al*. 2012 identified that αGalCer-meditated protection during pneumococcal intranasal challenge was completely dependent on iNKT cell-derived IFN-γ and IL-17A mediated neutrophil activity [259]. As IFN-γ does not have direct neutrophil chemotactic properties, it is likely that this neutrophil infiltration was dependent on IL-17A-mediated chemotaxis, however IFN-γ promotes opsonophagocytic uptake of bacteria enhancing neutrophil function, implicating synergy in the two lymphocyte derived cytokines in relation to neutrophil mediated defence.

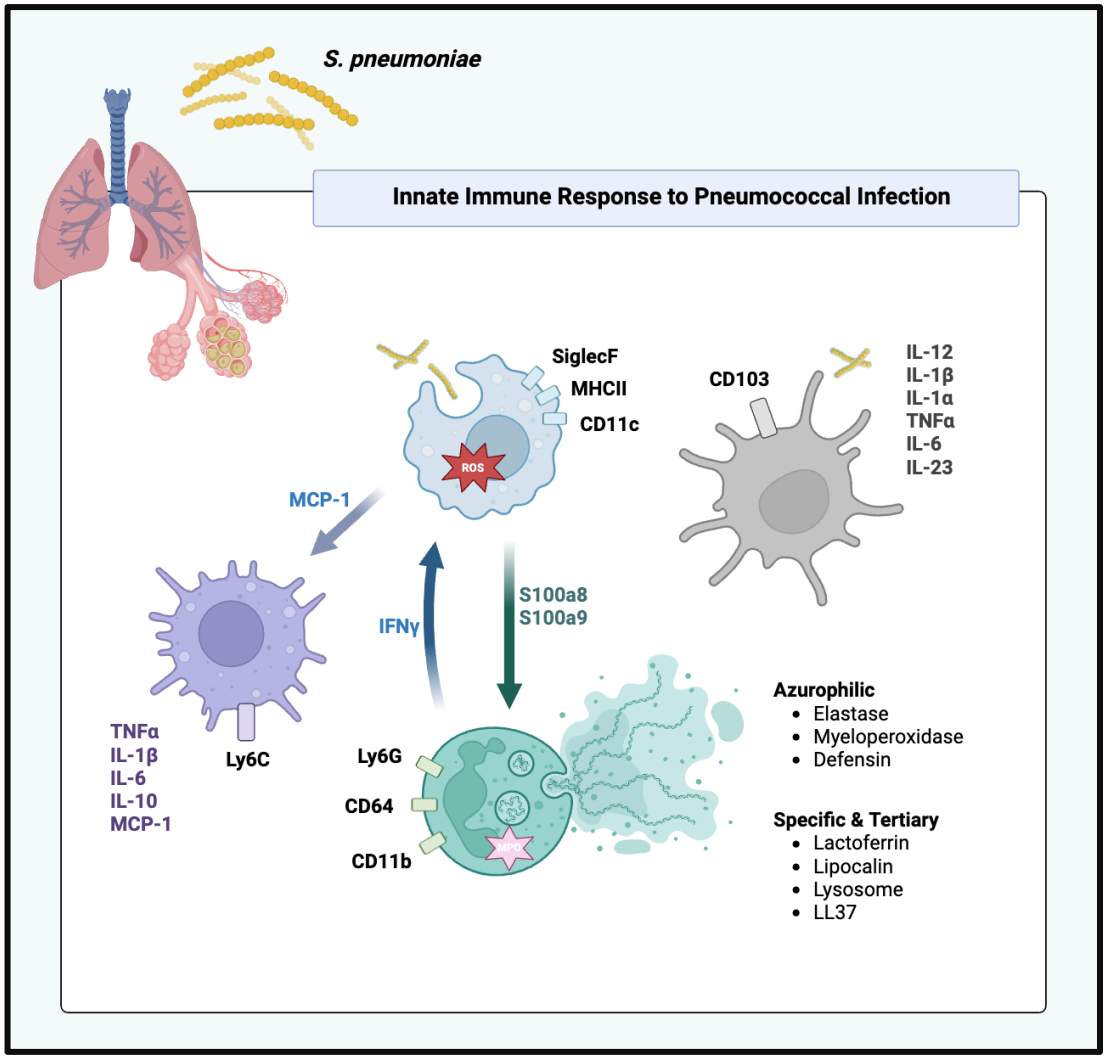


Fig. 1.9 Innate immune response to *S. pneumoniae*. The early host response to S. pneumoniae involves immediate engagement with the innate immune compartment, as outlined in section 1.4.3. Diagram made using Biorender.

1.4.4 Adaptive response to *Streptococcus pneumoniae*

Tissue resident helper T cell ($CD4^+$) populations are crucial in host defence against pneumococcal pneumonia. Regulatory T cells (T_{regs}) are implicated in host defence against pneumococcal infection mainly through regulating the degree of inflammation. It was demonstrated that both $FoxP3^+$ and $TNFR2^+$ T_{regs} were crucial in host defence during bacterial pneumonia, with both *Foxp3*$^{-/-}$ and *Tnfr2*$^{-/-}$ animals exhibiting a decreased survival profile compared to wild-type controls [272]. This population of respiratory $TNFR2^+$ T_{regs} limited T cell-derived IL-17, which in turn limited neutrophil chemotaxis and excessive inflammation [273]. Furthermore, it is known in the case of

influenza infection, that TNF-α promotes local production of neutrophil derived matrix metalloprotease 9 (MMP9) which facilitates extravasation in the airways [273]. Albeit IL-10 can impair clearance of *S. pneumoniae* if the degree of IL-10 mediated neutrophil suppression limits their functional capacity. Horn *et al*. 2024, demonstrated that IL-10 receptor (IL-10R) deficient mice had a higher local and systemic bacterial burden, neutrophil infiltration and functional capacity, namely ROS and proteolytic enzyme production were limited in wild-type mice compared to *Il10r*$^{-/-}$. Ultimately no significant effect on immunopathology was observed in response to knockout of IL-10R [274].

Regulatory T cells, specifically $CD4^+$, $CD25^+$, $FoxP3^+$ regulatory T cells have a reported protective role in host response to pneumococcal infection [275]. Regulatory T cells (T_{reg}) and their cytokine milieu, namely IL-10 and TGF-β are crucial for inflammatory resolution during pneumococcal infection [275]. This is supported by studies showing that pneumococcal whole cell antigen induces proliferation of $FoxP3^+$ and $FoxP3^-$ T_{reg} populations *ex vivo* in human NALT adenoid tissue [276].

Th1 populations are important in host response to intracellular pathogens. Th1 development requires polarising cytokines IL-12 and IFN-γ and are phenotypically characterised by production of secondary cytokines TNF-α, IFN-γ and IL-2 and expression of the transcription factor, T-bet or TBX21 [277], [278], [279]. Th1 cells are of particular importance in host anti-pneumococcal immunity and interact with the pulmonary innate immune system to promote bacterial clearance. Th1 cells act as sources of IFN-γ which can polarise resident and infiltrating macrophages to transition to an activated or "M1" profile [280], [281]. Similarly, IFN-γ producing $CD4^+$ T cells participate in protection against pneumococcal re-challenge together with IL-17 [282].

Th17 cells also play an imperative role in adaptive host immunity against pneumococcal infection and require IL-23 and IL-1β [283], [284], [285], [31]. Th17 cells are significant producer of IL-17A, which is necessary for PigR mediated transport of secretory IgA across mucosal barriers [286]. Th17 cells are also potent producers of IL-17F, GM-CSF, IL-21, IL-22 and TNF-α [283], [31]. Similarly, IL-17A can synergise with TNF-α and IL-22 to promote expression of antimicrobial peptide genes, particularly defensins, mucins

and lipocalin (Lcn2) in the case of TNF-α and calprotectin components S100a8 and S100a9 in the case of IL-22 [287].

Human challenge models have revolutionised our ability to characterise host responses to pneumococcal infection in a translational context. The importance of robust humoral immunity in the URT had been demonstrated in the human setting in which CPS-specific IgG in the serum and nasal wash mediates agglutination of pneumococci [288]. Additionally, CPS-specific IgG in the nasal cavity and serum is associated with reduced colonisation rates [289]. Human challenges involving the inoculation of live pneumococci have been carried out using both serotype 3, serotype 23F, and serotype 6B [290], [288], [291], [292], [293]. As aforementioned, serotype 3 is a classically highly invasive serotype while 6B [290] is reported as a less invasive strain [294], [295], [212], [296], [210]. However, serotype 6B has been isolated from blood and cerebrospinal fluid of a paediatric cohort, highlighting the ability of this serotype as an aetiological agent of IPD in children [297]. Furthermore, the increased ability of serotype 6B to form pneumococcal biofilms likely contributes to its heightened ability to colonise the nasopharyngeal tract [298]. Studies by Robinson *et al*. 2021 characterised the response of symptomatic individuals to *S. pneumoniae* serotype 3 colonisation in comparison to those presenting with no symptoms. Expression of IL-6 was significantly increased in the symptomatic cohort at day 2 and day 7 post-colonisation while RANTES (CCL5) was negatively associated with presentation of symptoms [290]. In this same study differential cytokine expression was observed in nasal lavages of individuals colonised with *S. pneumoniae* serotype 3 and 6B, in which consistent expression of RANTES (CCL5) and IL-2 was higher in the cohort challenged with *S. pneumoniae* serotype 6B, suggesting increased engagement of monocytes and T cells in the nasal cavity during serotype *S. pneumoniae* serotype 6B infection [290]. This highlights that while we can have a general understanding of cellular engagement in host response to *S. pneumoniae* it may differ between pneumococcal serotypes. This has broader implications particularly in pneumococcal vaccine design, where the selection of an appropriate adjuvant might favour certain protection against certain pneumococcal serotypes, such as those associated with higher risk of manifesting in IPD.

1.5 Vaccination

1.5.1 Vaccination

Vaccination is one of the most significant medical inventions, significantly reducing morbidity due to communicable disease over time. The initial concept of taking prophylactic action to prevent disease by variolation can be seen in ancient history. However, the genesis of modern vaccinology was the successful immunisation of a child to smallpox in 1796, the work of the physician Edward Jenner. The fundamental principal of immunity is that exposure to a pathogenic agent can result in the generation of specific immune memory, which establishes future protection against the pathogen. Eradication of a disease by vaccination requires herd immunity, in which the majority are not permissive to transmission and invasive infection of the pathogen and subsequently the biological niche for the pathogen is diminished. The eradication of smallpox in 1977 has demonstrated that ablation of a pathogenic agent can be achieved through global immunisation to achieve complete herd immunity. The importance of vaccination was further emphasised during the Severe Acute Respiratory Syndrome Coronavirus 2 (SARS-CoV2) pandemic in which a global study conducted by Watson *et al.* 2022 highlighted a global reduction of 63% of SARS-CoV2 mediated deaths thanks to vaccination, equivalent to an estimated 19.8 million lives [299].

As previously discussed, AMR is an increasing concern, critical for the bacterial species that compose the ESKAPE group and the high and medium priority pathogens indicated by the WHO. Vaccines against these pathogens must rely on their ability to drive potent cellular mediated and humoral immunity to boost efficacy, longevity of the response and overcome AMR. This highlights an immediate need for next generation vaccines that can not only prevent disease but also target the bacterial reservoirs in the population preventing colonisation and transmission. Indeed, acquisition of antibiotic-resistance in circulating *S. pneumoniae* strains highlights the need for improved pneumococcal vaccination platforms [300].

There are many different types of vaccines as outlined in **Fig. 1.9** [301]. Live-attenuated or inactivated vaccines are those in which a viable form of the pathogen is used to generate immunity. Live attenuated and inactivated vaccines, examples being the live attenuated Flu vaccine (LAIV) and Dukarol respectively, are generally quite immunogenic and can generate protective immunity without the inclusion of an adjuvant. However, vaccines composed of subunit antigens, capsular vaccines and recombinant vaccines are less immunogenic and sometimes require an auxiliary immunostimulant to facilitate the generation of long-term robust immunity. Such examples are the pneumococcal conjugate vaccines Prevnar13® (Pfizer) and *Haemophilus influenzae B* vaccine, in which poorly immunogenic polysaccharide capsular antigen is conjugated to the immunogenic diphtheria-derived carrier proteins [302]. Alternative or in combination to carrier proteins, adjuvants, substances which modulate the immune response to a vaccine, are incorporated.

An adjuvant is an immunostimulatory substance which enhances the immunogenicity of a vaccine to the target vaccine antigen [303]. Adjuvant research has revolutionised the scope of vaccines used, since the early 20th century where the incorporation of aluminium salts in vaccine preparations was introduced. Aluminium salts, commonly Alum, is still the most widely used vaccine adjuvant. However, it is now acknowledged that adjuvants can be tactically utilised to drive specific long-lived cellular and humoral signatures in both communicable and non-communicable diseases. Such examples can be seen in recombinant subunit vaccines containing AS01B: Shingrix targeting varicella zoster virus and RTS,S/AS01 (Mosquirix™) targeting *Plasmodium falciparum* malaria, the aetiological agents of chickenpox/shingles and malaria respectively [304], [305]. AS01 composed of the synthetic TLR4 agonist MPL in combination with a saponin QS-21, which drives early IL-12 and IL-18 by resident macrophage, mediating IFN-γ production and facilitating antigen presenting cell activation in the draining lymph nodes [306].

Vaccination has been utilised to target non-communicable disease. Therapeutic and prophylactic vaccination has demonstrated efficacy as off-shelf therapeutic options in cancer treatment and allergy. Additionally, the *E. coli*-derived adjuvant double mutant

heat labile toxin (dmLT) has been harnessed in development of a fentanyl conjugate vaccine to combat drug challenge [307].

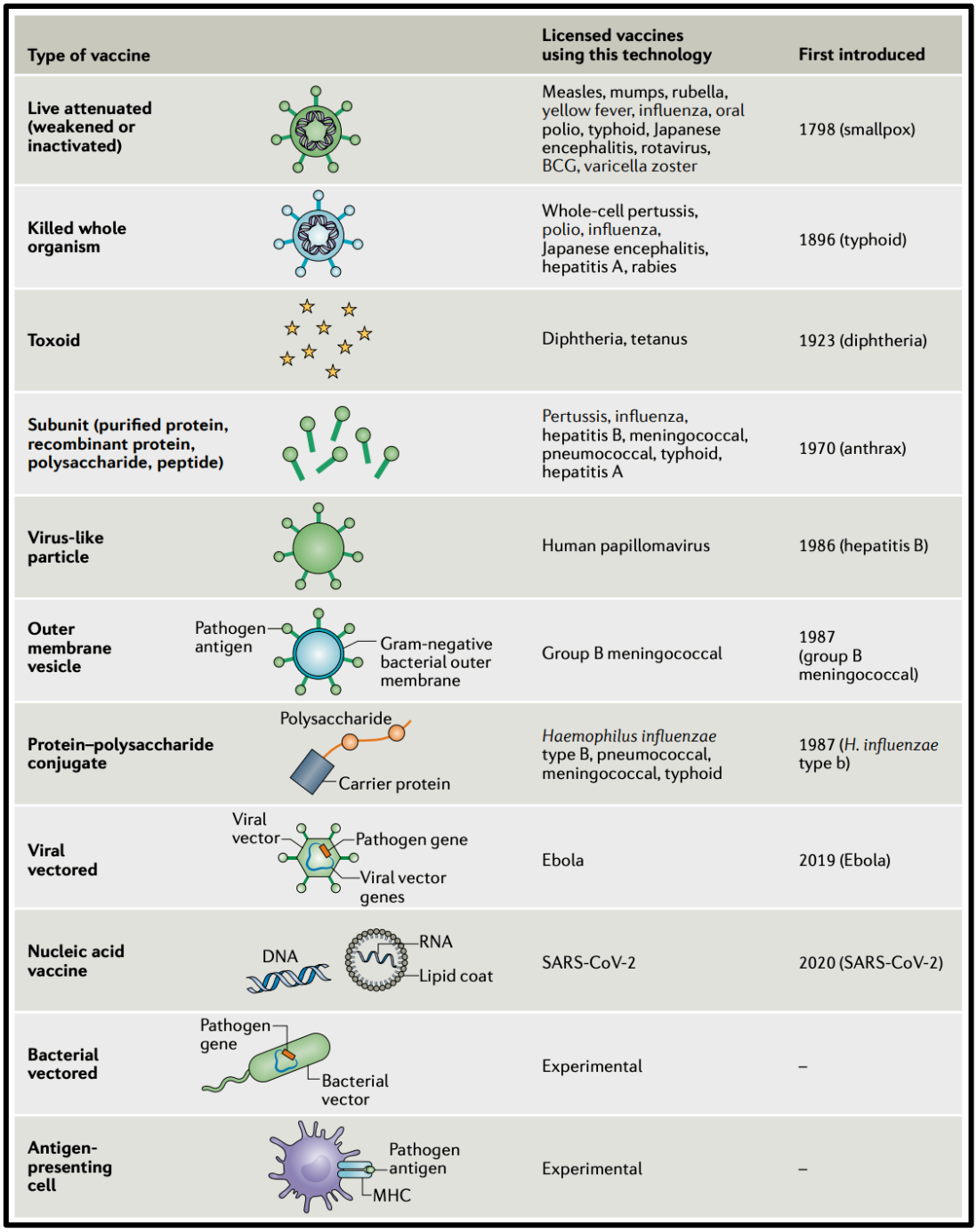


Fig. 1.10 Current types of vaccines and those in development. Figure by Pollard et al. 2021 [301].

1.5.2 Intranasal vaccination

Most licensed human vaccines are administered parenterally. Parenteral vaccines can elicit systemic humoral responses in the form of immunoglobulin which can protect against invasive disease, however, the ability of parenteral vaccines to generate mucosal immunity is limited. Mucosal immunisation has a potential advantage over parenteral immunisation in preventing transmission through the generation of neutralising site-specific mucosal responses. Particularly, mucosal immunisation promotes the production of neutralising IgA and IgG at mucosal surfaces, which are often sites of pathogen entry, as well as potent cellular mediated immunity. Intranasal vaccines have therefore the potential to elicit strong, enduring immunological memory locally in the respiratory mucosa, compared to parenterally administered counterparts in the form of secretory mucosal IgA which confers protection against transmission [308].

Intranasal vaccines are, however, more difficult to design, primarily due to the higher level of immunogenicity required to overcome mucosal tolerance and the lack of translatable models. Furthermore, the immune anatomy of the nasal tract differs heavily between humans and murine species [44]. While generation of regulatory immune responses at these sites is an endogenous method of maintaining immune homeostasis, this can present as a challenge as typically initial inflammatory responses are required to initiate the adaptive immune responses. Overcoming this tolerogenic barrier can be achieved by various means such as using the more immunogenic live attenuated or inactivated whole cell vaccines or through the incorporation of immunostimulatory mucosal adjuvants.

All currently licensed mucosal vaccines are targeted at enteric pathogens, while only one mucosal vaccine on market targets a respiratory pathogen, the licensed intranasal vaccine, FluMist (US) or Fluenz Tetra (EU) [308]. This is a non-adjuvanted live attenuated influenza vaccine (LAIV), against seasonal strains of influenza A and influenza B. FluMist is live attenuated and replicating, which facilitates its effectivity in inducing immune responses in the nasal cavity where generally a stronger stimuli is required to generate

robust immune responses. However, LAIV is temperature restricted, which allows it to replicate in the URT eliciting adaptive immunity, but does not replicate in the warmer LRT [309]. However, to date no intranasal vaccines targeting respiratory bacterial pathogens have been licensed.

1.5.2 Pneumococcal vaccination

Pneumococcal vaccines have successfully reduced the burden of invasive pneumococcal disease cases globally [310]. There are currently five pneumococcal vaccines approved in the European Union, Prevnar 13 (PCV13) and Prevnar 20 (PCV20) (Pfizer Inc, NY, USA), Pneumovax (Merck), Synflorix (GlaxoKleineSmith) and Capvaxive 21 (Merck & Co., Inc., NJ, USA). Pneumovax23 (Merck & Co., Inc., NJ, USA) was the first approved pneumococcal vaccine, covering 23 serotypes of *S. pneumoniae*. This was the mainstream pneumococcal vaccine until the induction of conjugate pneumococcal vaccines in 2007. Synflorix (GlaxoSmithKline, Brentford, UK) is a polysaccharide conjugate vaccine covering 10 pneumococcal serotypes. Vaxneuvance (Merck & Co., Inc., NJ, USA) covers 15 pneumococcal serotypes and the new formulation Capvaxive (Merck & Co., Inc., NJ, USA) covers 21 pneumococcal serotypes. Here, the pneumococcal polysaccharides are conjugated to *Haemophilus influenzae* derived protein D, diphtheria and tetanus toxoid carrier proteins and adsorbed on alum.

The Prevnar family of vaccines are multivalent polysaccharide conjugate vaccines collectively cover pneumococcal serotypes 1, 3, 4, 5, 6A, 6B, 7F, 8, 9V, 10A, 12F, 14, 15B, 18C, 19A, 19F, 22F, 23F and 33F. PCV7 was the first commercially available pneumococcal conjugate vaccine and performed with increased effectivity compared to previous unconjugated purified capsular polysaccharide pneumococcal vaccines. Serotype coverage was expanded with European Medicine Agency (EMA) approval of PCV13 in 2009 with Food and Drug Administration, USA (FDA) approval following in 2011. PCV20 was then granted FDA approval in 2021 followed by EMA approval in 2022. The expansion of the Prevnar family of conjugated pneumococcal vaccines to include emerging pathogenic serotypes resulted in it being the leading pneumococcal vaccine used globally.

While the success of pneumococcal vaccines at reducing pneumococcal disease burden cannot be disputed, Troeger *et al*. 2018 conducted a longitudinal study from 1990-2016 on global dynamics of lower respiratory tract infections. Over 1.1 million *S. pneumoniae* related deaths were estimated globally in 2016, in which over 340,000 IPD of these were in paediatric cohorts under 5 years of age [200]. These estimated infection rates and *S. pneumoniae* related mortality are still cause for concern and calls for a rational re-evaluation on how to improve pneumococcal vaccine strategies.

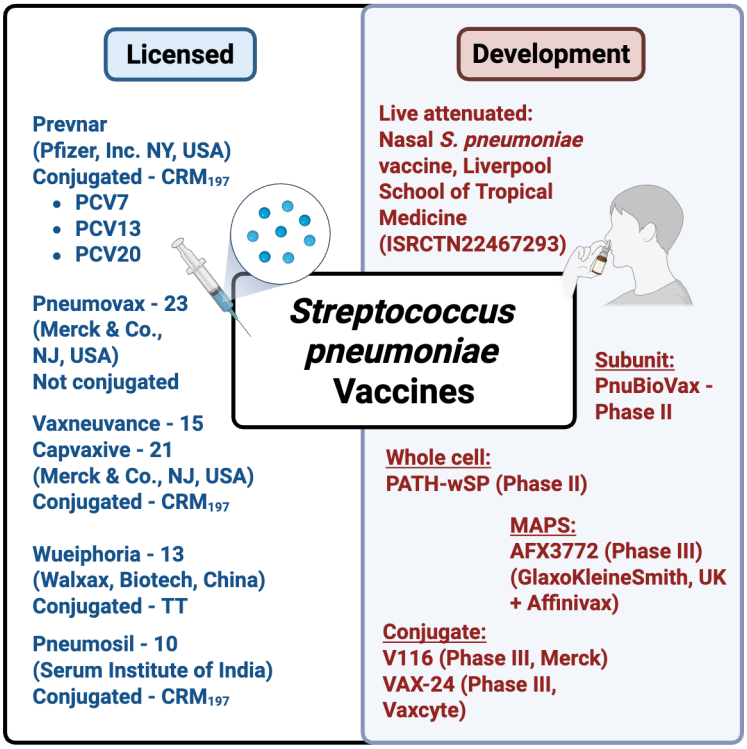


Fig. 1.11 Pneumococcal Vaccines. Diagram made using Biorender.

1.5.3 Limitations of pneumococcal vaccines

Before focussing on the current limitations surrounding pneumococcal vaccination strategies, it is important to recognise the fundamental impact pneumococcal immunisation has had in limiting the global burden of pneumococcal disease. Pneumococcal disease prevalence has dramatically declined since the implementation of PCV7 in childhood immunisation regimes [310], [311].

There are several limitations associated with the current approach to pneumococcal immunisation. From an epidemiological standpoint polysaccharide-based vaccines are complex and costly to produce, store and transport, which has resulted in a lower roll-out of pneumococcal vaccination in lower income countries. Serotype prevalence is geographically variable, where invasive serotypes in lower income countries may not reflect those in higher-middle income countries [312]. A socioeconomic bias in vaccine efficacy globally can result from, ethical biases in the dissemination and efficacy of pneumococcal vaccines globally [313]. This is reflected in higher burden of pneumococcal disease in lower income countries, demonstrated by Wahl *et al*. 2018 demonstrated in global estimates that approximately 50% of pneumococcal related deaths in 2015 occurred in India, Nigeria, Democratic Republic of Congo and Pakistan [314].

Breakthrough infections are an immediate cause for concern in relation to pneumococcal vaccine efficacy. *S. pneumoniae* undergoes significant genetic changes to modify capsular expression in response to vaccine-driven selective pressure. Cross-protective immunity with current pneumococcal vaccines has been observed, individuals receiving the 21-valent vaccine V116 which covers serotypes 6A and 15C demonstrated reactivity against serotypes 6C and 15B, not found in the formulation [315]. However, whether this serotype cross-reactivity provides an adequate degree of protection in the case of invasive infection remains to be seen. Albeit challenges in targeting non-capsulated and certain capsulated pneumococcal strains remain such as serotype 3 in which the bacteria can shed the outer capsule to evade host defences [294], [216].

Furthermore, it is well established that capsular polysaccharides are poorly immunogenic and present as T cell-independent antigens [295]. Capsular polysaccharides do not induce T-cell engagement in promoting class-switching, affinity maturation or memory T and B cell generation. The main protective mechanism of CPS vaccines is the induction of T-independent B cells capable of producing IgM, which also does not provide long-lived immunity [295]. However, the introduction of conjugated formulations improved pneumococcal vaccine immunogenicity through the

engagement of T-cells. Carrier proteins, namely CRM_{197}, an attenuated mutant of diphtheria toxin facilitates activity of Tfh cells [316] as it covalently attached to the polysaccharide and facilitates the intracellular degradation of the complete conjugated formulation for CPS antigen presentation on MHC-II. This promotes not only CPS-specific IgG class switching, and somatic hypermutation but also long-lived immunity through B cell differentiation [316]. This formulation is more immunogenic and exhibits better efficacy particularly in paediatric cohorts than the previous T-independent formulation [316], [311]. However, studies conducted by Clutterbuck et al. 2008 demonstrated that while children and adults mounted responses to the heptavalent conjugate vaccine (PCV7), the responses were significantly lower in children than adults and that despite the observation of class-switching to IgG in immunised children, IgM was still the dominant subclass for serotypes 14 and 23F, while IgG was the dominant subclass for serotype 4 [317]. This implies a need for rationalised pneumococcal vaccine design to target non-capsular antigens and re-evaluate immunisation strategies for paediatric cohorts.

1.5.4 Considerations in pneumococcal vaccine development

While conjugation methods, such as the implementation of CRM_{197} in vaccine preparations overcame this caveat, targeting protein-based antigens would serve in generating superior cellular and humoral immunity to pneumococcal infection. Additionally, targeting a broader scope of pneumococcal antigens could potentially circumvent vaccine redundancy by serotype replacement. Secretory proteins could be targeted such as pneumolysin (PLY), IgA protease or endopeptidase O (PepO) [318]. In response to pneumococcal infection, non-capsular antigen-specific IgG in the serum and bronchoalveolar lavage fluid (BALF) included putative proteinase maturation A (PpmA), pneumococcal histidine triad protein (PhtD) and pneumococcal surface protein A (PspA) [319]. Alternative pneumococcal virulence factors such as pneumococcal adhesion and virulence A (PavA), autolysin (LytA), hyluronatelyase (Hyl), fructose-1,6-biphsphate and choline binding protein (CbpA) could prove effective in providing protein antigens which would generate improved humoral and cellular mediated immunity [318].

This is especially crucial as many of these virulence factors are involved in escaping neutralisation and subsequent opsophagocytosis, which is the main mechanism of host defence against pneumococcal infection. Pneumolysin is arguably the most important pneumococcal virulence factor, demonstrated in the case of *ply*$^{-/-}$ pneumococcal strains which have attenuated virulence compared to wild-type *S. pneumoniae in vivo* [320], [321]. Many pneumococcal vaccines in early phase clinical trials (NCT00896064), (NCT01444352), (NCT01764126), (NCT01446962), (NCT03803202), (NCT04525599), (NCT04087460) and (NCT01262872) have included genetically modified attenuated variants of pneumolysin as primary target antigens [295]. *S. pneumoniae* exhibits a high degree of genetic heterogeneity, considering this, a reverse vaccinology approach could distinguish conserved proteins sequences which could pose as novel antigenic targets. Arguably the ideal approach would be a whole cell preparation, where a myriad of pneumococcal antigens could be targeted.

The first live attenuated approach to pneumococcal immunisation yielded successful results. Hill et al. 2023, demonstrated in a human study (ISRCTN22467293) that nasal inoculation with wild-type Spn6B and the genetically modified SpnA1 generated IgG in the serum and nasal cavity. Additionally, inoculation of these two strains was associated with reduced carriage upon re-challenge [289].

Another approach in improving vaccine efficacy is through adjuvants, which drive a potent T cell immunity. There is still a blind spot in the mechanism of action of aluminium-based adjuvants. Alum is known to preferentially induced T_h2 responses and can increase IL-10 production which in turn limits T_h1 responses [322], [323]. As mentioned, the adaptive responses to *S. pneumoniae* rely heavily on contributions of humoral immunity however, robust cellular mediated immunity could be the key to superior pneumococcal vaccine efficacy, through the action of novel adjuvants. Early induction of Th1 cytokines IL-2, TNF-α and IFN-γ, is crucial in supporting humoral response and early anti-bacterial immunity by resident innate phagocytes. IFN-γ enhances opsophagocytosis, by promoting class switching to IgG2a and IgG2c subtypes, influencing Fcγ expression on host phagocytes and maintaining the highly phagocytic

lung resident macrophage pool [324], [325], [326]. While IL-2 supports proliferation and clonal expansion of memory T cells.

Many potential adjuvants could support these functions. Poly-deacetylated chitin polymers, namely chitosan, exhibit potent immunostimulatory activity. Chitosan is currently being explored for its potential efficacy as an adjuvant in vaccines targeting LRTI pathogens, including *S. pneumoniae* [327], [328], [329]. Chitosan when delivered i.n. in experimental pneumococcal vaccines has demonstrated an ability to protect against nasopharyngeal colonisation, implying an ability of this preparation to drive sterilising immunity at the site of pathogen entry. Indeed, this study demonstrated in mice receiving Chitosan-DNA nanoparticles expressing pneumococcal surface protein A, higher levels of serum IgG2 and bronchiolar lavage derived IgA were detected, similarly, significantly increased IL-17A and IFNγ were quantified in splenic tissue. This corresponded to a significantly lower nasal burden of *S. pneumoniae* upon rechallenge and higher IL-17A detected in BAL fluid [329]. Similarly, Carrol et al. 2016, demonstrated that chitosan proved effective in a model of intranasal pneumococcal immunisation by boosted anti-PspA IgG2c and IgG1 and enhanced IFNγ in lung restimulations from immunised animals [330]. Another experimental mucosal adjuvant α-galactosylceramide has demonstrated effectivity when delivered in the context of oral vaccines targeting Helicobacter pylori and Vibrio cholerae [331], [332]. Furthermore, α-galactosylceramide has demonstrated prophylactic efficacy in *S. pneumoniae* infection, highlighting it's potential efficacy as a pneumococcal vaccine adjuvant [259], [270], [263], [262].

Flagellin, a TLR5 agonist found in the motility machinery of bacteria, has demonstrated potential efficacy as a pneumococcal vaccine adjuvant [333]. One study by Muñoz-Wolf et al. 2010 demonstrated that administration of flagellin i.n. could protect from lethal pneumococcal challenge. Flagellin promoted production of *Cxcl1*, *Cxcl2*, *Ccl20*, *Tnfa* and *Il6* in the lungs of infected animals and initially exacerbated inflammatory cellularity, in the lung which was resolved by seven days post infection. The protective activity of flagellin appears to be mediated by the increase in inflammatory lung cellularity, particularly Gr1 dependent cells [334]. There are other accounts of the prophylactic

activity of flagellin in response to pneumococcal infection alone or in synergy with other treatments [258], [335].

Double mutant heat liable toxin (dmLT) toxoid-based adjuvants have demonstrated efficacy in mucosal formulations such as *Escherichia* coli derived heat-labile toxin (LTA1) [308]. Due to safety concerns on the nasal delivery of LTA1, an attenuated derivative was developed, which demonstrated high efficacy in generating mucosal and systemic humoral responses [336], [337], [338], [339], [340]. Studies by Estupiñan and collegues have recently explored dmLT as an effective intranasal adjuvant in the setting of pneumococcal immunisation. This study demonstrated that delivery of dmLT alongside diphtheria toxin-conjugated serotype 1 pneumococcal capsular polysaccharide (Pn1-CRM_{197}) dramatically enhanced germinal centre formation and enhanced induction and retention of antibody secreting cells in both the spleen and bone marrow, as well as increasing Pn1 specific IgA^+ antibody secreting cells in the bone marrow and IgA in the serum and salivary secretions [341].

Adjuvant:	Effect:	Publication:	Delivery:
α-galactosylceramide	• Promoted IFNγ and IL-17A producing iNKT populations in a model of pneumococcal re-challenge. • Promoted induction of	[259], [270]	*Intranasal*
Double mutant heat-liable toxin (dmLT/LTA1)	• Drives NLRP3 inflammasome activity in antigen presenting cells, IL-1β promotes Th17 polarisation. • Drives Th1 and Th17 responses. • Promotes serum IgG subclasses. • Promotes antigen-specific IgA at mucosal surfaces.	[341], [340], [338], [342]	*Intranasal*
Chitosan	• Promoted neutralising IgA at the site of immunisation. • Promoted serum IgG, IgG1 and IgG2c in the serum of immunised animals. • Demonstrated significant but not complete protection against nasopharyngeal colonisation. • Promoted induction of antigen-specific IFNγ and IL-17A in the lung and spleens of immunised animals.	[329], [330]	*Intranasal*
Retinoic Acid Based Compounds	• Promotes class switching to IgA in B cells in mucosal inductive sites.	[18], [16], [343]	*Intranasal*
Flagellin	• Promotes expression of granulocyte chemoattractant, Cxcl1, Cxcl2, Ccl20 and induction of Gr1+ neutrophils which mediated protection against *S. pneumoniae.* • Enhances expression of *Tnfa* and *Il6* in the lung upon *S. pneumoniae* infection	[258], [333], [335], [334]	*Intranasal* *Sublingual*

Table 1.1 Pre-clinical studies indicating a potential avenue for adjuvant use in pneumococcal immunisation.

1.6 The gut-lung axis and vaccination

Vaccines are arguably the most important medical intervention second only to water sanitation. While vaccination has been highly successful in the prevention and control of communicable disease, vaccine performance varies between individuals, a phenomenon which is incompletely elucidated. Multiple factors govern vaccine performance such as host genetics, comorbidities, level of immunocompetence, socioeconomic factors, and nutrition and lifestyle habits, such as smoking and exercise [344]. However, one outstanding factor is the contribution of the host microbiota to outcomes of vaccine efficacy and immunogenicity. The contributions of the gut microbiota to outcomes of immunisation are rapidly developing fields of research. The microbiota is a critical regulator of vaccine performance [345], [346]. The exact mechanisms by which the host microbiota dictates outcomes of vaccine immunogenicity and efficacy remain unclear. However, suggested mechanisms by which the microbiota can influence vaccine efficacy include the microbiota exhibiting properties as an endogenous adjuvant, the immunomodulatory activity of microbiota derived metabolites, namely SCFAs and molecular mimicry of microbiota derived antigens [344]. While these mechanisms are all plausible, there is still a deficit in the understanding of the role of microbiota derived metabolites such as SCFAs, in vaccination.

1.6.1 Dysbiosis and Vaccine Performance

In vivo models of antibiotic-induced dysbiosis have highlighted the role of the microbiota in vaccine efficacy. A pivotal study conducted by Swaminathan *et al*. 2021, examined the differential effects of antibiotic classes on signatures of induced dysbiosis. Vancomycin and clindamycin administration *in vivo* induced the highest degrees of dysbiosis which correlated to the lowest serum antigen-specific IgG titres in a model of parenteral ovalbumin immunisation [102]. As previously mentioned, vancomycin and clindamycin target gram positive anaerobes, *Lachnospiraceae*, *Ruminococcaceae* and *Clostridiaceae*, which are crucial for the production of SCFA, [137], [122]. Dysbiotic mice immunised with a model OVA-subunit vaccine exhibited lower antigen-specific antibody titres to eubioitic mice, with OVA-specific IgG negatively correlated with the degree of

microbial disruption. These results were recapitulated in non-human primates [102]. Similarly, studies by Lamouse-Smith *et al*. 2011 demonstrated that the intestinal flora is essential in supporting humoral responses in infant and germ-free mice. However, this study demonstrated that dysbiosis during a specific window of life, in this case *in utero* and the neonatal period resulted in worsened vaccine performance, however this improved to comparative levels to gnotobiotic mice over time [346]. An adult clinical cohort study, investigating the impact of the commensal microflora on Rotavirus vaccine performance, an oral live attenuated formulation, demonstrated that narrow spectrum antibiotic use results in enhanced immunogenicity of the prime Rotavirus vaccination [347]. Lynn et al. 2021 has highlighted proposed mechanisms by which the microbiota can influence vaccine efficacy, such as innate sensing of the microbiota by pathogen recognition receptors, by enhanced antigen presentation by dendritic cells, immunomodulatory microbiota-derived metabolites and B and T-cell cross-reactive epitopes which are encoded by the microbiota [344]. These mechanisms are highly reflective of those proposed in the context of the role of the microbiota in host response to infection. Interestingly, broad-spectrum antibiotics did not have the same effect in the case of the parenteral formulations, Pneumo23 and tetanus toxoid, in which no immunomodulatory effect of the microflora on vaccine performance was seen [347]. Conversely, alternative studies have suggested a negative correlative relationship between antibiotic use in a paediatric cohort and suboptimal responses to diphtheria toxin, pertussis toxin and Spn6B, Spn14 and Spn23F antigens within the polyvalent PCV formulation in children under 9 months of age [348]. These studies collectively imply that the effects of the microbiota on vaccine immunogenicity and efficacy are heavily context dependent. Dysbiosis is a defining factor in outcomes of immunisation in early life, where deleterious outcomes on vaccine performance are not as prevalent in adult cohorts.

1.6.2 Ability of the microbiota and microbiota derived metabolites to modulate lymphocytes

A well-recognised feature of the microbiota is the ability to direct or "prime" resident lymphocytes. Short-chain fatty acids have reported differential effects on antigen-specific humoral responses. Acetate and butyrate support mucosal immune responses in the intestine by increasing IgA^+ B cells and subsequently enteric mucosal IgA in a T-cell independent manner, implying an ability to either modulate the profile of the antigen presenting cell interacting with the B cell, or alternatively, directly alter the phenotype of the B cell [349], [350], [343]. The ability of acetate, to increase IgA+ B cells in the intestinal tract of dysbiotic mice was abrogated in *Grp43*$^{-/-}$, acetate acted directly on DCs to enhance Aldh1a2 in a GPR43 dependent manner which promoted B-cell IgA production [350]. Butyrate also acts on dendritic cells, specifically $CD103^+CD11b^+$ to enhance TGF-β, αvβ8 integrin expression and all-trans retinoic acid in a GPR41, GPR109a and HDACi dependent manner [343]. Similiarly, Ruane et al. 2014 demonstrated that the commensal microbiota is essential for the migration of IgA-expressing B cells in the lung to the intestine by lung dendritic cells (lDC) in animals delivered cholera toxin i.n. This effect was due to lDC cell-mediated upregulation of $\alpha4\beta7$ and CCR9 on these IgA^+ B cells. This effect was dependent on a retinoic acid induced mechanism in B cells mediated by lung dendritic cells [18]. While the microbiota appears implicated in "priming" lymphocyte trafficking from the lung to the intestinal mucosa. The reverse, lymphocytes being "primed" in the intestinal tract to migrate to the lung parenchyma in a microbiota dependent mechanism.

Influential studies of the effects of SCFA on lymphocyte phenotypes identified roles between commensal microbiota derived metabolites and regulation of colonic regulatory T cell populations [22], [351], [352]. Furusawa et al. 2013 identified that butyrate was crucial for the differentiation of T_{reg} in the colonic lamina propria, this was a result of a high degree of acetylation at the *Foxp3* locus, supporting a role of SCFA-mediated HDACi in modulation lymphocyte responses [351]. Arpaia et al. 2013 similarly confirmed that cells treated with butyrate had increased acetylation at the Foxp3 locus via HDACi activity, corresponding to a functional increase in $FoxP3^+$ regulatory T cells

[352]. A diet enriched in soluble fibre has been shown to reduce pathology of allergy induced airway inflammation, marked by gut-lung axis mediated suppression of Th2 immunity. Further investigation highlighted in this model of house dust mice (HDM)-induced allergic airway inflammation, that propionate delivered as a dietary supplement had a marked reductive effect on type 2 cytokine mileu, IL-5, IL-5 and IL-13, significantly reduced DC maturation markers, total IgE and HDM-specific IgG1 [66].

The effects of SCFA on outcomes of Th1 immunity is not well investigated. In fact, there is discourse in the literature regarding the effects of SCFA on lymphocyte production of type III IFNs. Natural killer (NK) cells exposed to butyrate display a reduced phenotype due to SCFA-mediated abrogation of NK cell metabolism, however whether this was mechanistically dependent on FFAR ligation, HDACi or via. internalisation and usage of SCFA in catabolic metabolism was not discussed [353]. Butyrate induced IL-10 production in colonic Th1 $CD4^+$ cells. In *Rag*$^{-/-}$ mice receiving allogenic transfer of Th1 cells from butyrate treated mice had lower IFN-γ production than those recipient of Th1 cells from controls. However, number of IFN-γ $^+$ T cells was unaffected between groups, implying butyrate represses the ability of Th1 cells to produce IFN-γ but does not affect overall IFN-γ^+ T cell frequencies [190]. Butyrate appears to differentially modulate $CD4^+$ polarisation in a concentration dependent manner, with sub millimolar butyrate concentrations promoting regulatory T cell polarisation and higher concentrations promoting a Th1 phenotype.

At millimolar concentrations *Ifng* and *Tbx21* mRNA transcription was significantly enhanced a feature dependent on the inhibition of histone 3 deacetylation [22]. SCFAs, butyrate and pentanoate appear to positively regulate phenotypic functions of $CD8^+$ T cells, increasing anti-tumor functionality in a HDACi-dependent mechanism [354]. Similarly, Trompette *et al.* 2018 demonstrated *in vivo* that a high-fibre diet leading to bioavailable millimolar serum concentrations of SCFA, improved $CD8^+$ cell functions in response to influenza infection through alterations of lymphocyte metabolism [112]. Cytotoxic $CD8^+$ T cells and NK cells, despite different mechanisms of activation have similar functions, both being cytotoxic lymphocytes, producing granzymes in response to insults and are sources of IFN-γ [355]. However, the reported effects of SCFAs on

these cell types differ dramatically. Butyrate can suppress the NK cell response to activating cytokine IL-12 and IL-15 and expression of NK cell proteins, these effects were attributed to a significant reduction in phosphorylation S6 levels implying a suppression of mTORC1 in butyrate treated NK cells. Butyrate suppressed energetic metabolism in NK cells eliciting the aforementioned effects [353]. In converse to this recent studies demonstrate that butyrate induced $CD56^{bright}$ and $CD69^{+}CD56^{dim}$ NK cells but not classical NK cells via HDACi activity [356]. Similiarly, low dose acetate, butyrate and propionate enhanced the anti-tumor cytotoxic effects of NK-92 cells *in vitro* but did not elicit outstanding effects on the NK cell secretome [357].

Short-chain fatty acids again exhibit differential effects on alternative IL-17 producing innate lymphocyte populations, namely γδT cells. SCFA can repress IL-17 production by caecal γδT cells *ex vivo*, this effect was not dependent on GPR43 as demonstrated in *Ffar2*$^{-/-}$ or internalisation of SCFA, as demonstration by inhibition of MCT1, however was dependent on HDACi [358]. It is likely that SCFAs differentially influence lymphocyte function based on the differentiation state of the cells, particularly in the case of T cells.

The intestinal helminth parasite *Nippostrongylus brasiliensis* was associated with a reduction in segmented filamentous bacteria (SFB) and broadly a global reduction in Firmicutes in the gut. This corroborated with a suppression of IL-17 in ileal tissue, which was not recapitulated in SFB^{-} mice, implying a direct reliance on SFB for generation of type 17 immunity locally in the intestinal tract [359]. However, SFB is now recognised as a mediator of peripheral, specifically respiratory type 17 immunity [360], [361]. Bradley et al. 2017 demonstrated that gut resident SFB could prime autoreactive Th17 cells in the lung of K/BxN mice, a murine model of rheumatoid arthritis. Using vancomycin for the specific ablation of SFB commensals, the priming effect of the gut on autoreactive Th17 lung resident cells was abrogated. Similarly, Th1 signatures as measured by IFNγ production were not impacted by ablation of SFB communities [360]. This collectively suggests that the gut microbiota provides cues for the migration of primed gut resident T cells to migrate peripherally to the lung and elicit effector functions. While this has exclusively been demonstrated in the context of autoimmunity it is plausible, by definition of the common mucosal immune system (CMIS), where cells primed at one

mucosal site can home to peripheral mucosal sites and elicit effector functions, that this effect could occur during vaccination, particularly vaccination by mucosal route [44]. SFB have additionally demonstrated induction of type 17 pulmonary immunity in the setting of bacterial pneumonia, with SFB^- animals having reduced IL-22 and increased IL-6 comparative to SFB^+ counterparts. Similarly in this study, IL-17A production in SFB- mice was boosted upon co-housing with SFB^+ mice [361]. Ngo et al. 2024 and collegues recently demonstrated that SFB mediated protection during influenza A infection was independent of type 17 immunity as demonstrated in *Il17a*$^{-/-}$ and *Il22*$^{-/-}$ mice, in fact this protection did not rely on the adaptive arm of the immune system at all but rather SFB-dependent modulation of AM responses, in converse to the studies previously mentioned [183]. However, the protective effects were lost in *Csf2*$^{-/-}$ mice the conventional knockout model of GM-CSF, a crucial cytokine in AM functionality, implying SFB stimulates production of respiratory GM-CSF, albeit this was not further investigated in this study [183]. Segmented filamentous bacteria fall under the broader category of *Clostridia*, the same class as many SCFA producing bacteria. Currently there is no evidence that SFB can produce SCFA, let alone alternative immunomodulatory metabolites, however the exact mechanisms by which these gut resident commensals exert influence over systemic, namely respiratory, immunity remains unelucidated.

The commensal microbiota can provide auxiliary immunostimulatory signals during immunisation, acting as an endogenous pleiotropic adjuvant. Many studies have identified a crucial contribution of microbiota-mediated TLR5 signalling in the effectivity of systemic parenteral immunisation [362], [363], [364]. This was demonstrated by Lynn *et al*. 2018, in which infant mice exposed to antibiotics (dysbiotic) had lower antigen-specific IgG compared to controls (eubioitic) when immunised with the Bacillus Calmette-Guérin (BCG) vaccine, meningococcal B and C vaccine, Infranrix, also known as the 6-in-1 vaccine and Prevnar13® [363]. Antibiotic exposure in early life also led to a shift in the microbiota of these mice with a reduction in *Lachnospiraceae* and an apparent complete ablation or *Ruminococcaceae* and *Roseburia*, all of which are implicated in SCFA production [137]. This implies SCFAs could be crucial in mediated host response to parenteral immunisation, but specifically pneumococcal

immunisation. Additionally, Nod2 sensing of the microbiota is identified to have indispensable roles in the adjuvanticity of cholera toxin [365].

1.6.3 The role of microbiota derived metabolites in vaccination

To date the literature surrounding the roles of SCFA in vaccination is limited and much of what we understand is extrapolated from dietary intervention studies and models of antibiotic induced dysbiosis or studies of SCFA immune modulation on the direct phenotypic properties of lymphocytes and antigen presenting cells. However, studies investigating the modulatory properties of SCFA on lymphocytes in the setting of infection and autoimmunity allow us to extrapolate from these contexts and speculate mechanisms by which SCFAs could alter vaccine immunogenicity and efficacy. Swaminathan et al. 2021 conducted studies on the impact of both broad and narrow spectrum antibiotic administration on vaccination outcomes. Vancomycin induced the highest degree of dysbiosis-driven vaccine hypo response [102]. Vancomycin targets gram positive anaerobes and it could be speculated that vancomycin-driven hypo response is due to the depletion of SFB or SCFA-producing bacteria, which are gram-positive anaerobes belonging to *Firmicutes* [360], [137], [366]. Indeed, the importance of SCFA in mediating host response to immunisation was highlighted in studies by Wu et al. 2023, in which vaccine induced hypo response to the parenteral rabies vaccine was rescued through dietary administration of butyrate [367]. Mice receiving vancomycin has blunted Th1 immunity, reduced antigen-specific (anti-RABV) antibodies and decreased germinal centre (GC) B cells and plasma cells. Butyrate supplementation rescued this vancomycin-induced vaccine hypo response, restoring anti-RABV antibodies, Th1 cell frequencies and GC B cells and plasma cells [367].

SCFAs have differential modulatory effects on B cells. A majority of studies have disclosed a role of SCFAs in supporting B cell functions. Kim et al. 2016 demonstrated that SCFAs induce metabolic shifts in B cells promoting mitochondrial metabolism and fatty acid synthesis which are classically known to support plasma cell function [124], [368], [369], [370]. This SCFA-driven metabolic shift appeared to enhance production of

IgA, IgG1, IgG2a, IgG2b, IgG3 in a HDACi dependent mechanism, deduced as these effects were mimicked through the treatment of the HDACi trichostatin A. These results were recapitulated in human B cells *in vitro* [124]. Sanchez et al. 2020 published in converse to this, demonstrating that SCFAs can epigenetically regulation class-switching functions of B cells, by encouraging the production of micro RNAs (miRNAs) targeting the 3' prime region of class switching genes *Aicda* and *Prdm1* at high concentrations, however at lower concentrations can modestly promote class-switch recombination [371]. This translated to a suppression of antigen-specific antibodies in both the setting of parenteral and mucosal immunisation using T-dependent (ovalbumin and cholera toxin for oral immunisation or NP_{16}-CGG in combination with alum) or T-independent (NP-LPS) *in vivo* [371]. In converse, Wu et al. 2023 showed that butyrate enhanced mitochondrial function in vitro, activating the Akt-mTOR axis, promoting the generation of plasma cells [367]. In this study, butyrate upregulated CD138 expression on B cells, *Prdm1* mRNA expression and subsequent Blimp-1 expression at the protein level, implying an increased capacity for class switching while adopting a plasma cell phenotype [367]. These conflicting mechanistic studies highlight that the effects of SCFA on B cell phenotype and therefore humoral responses to vaccination remain to be fully elucidated.

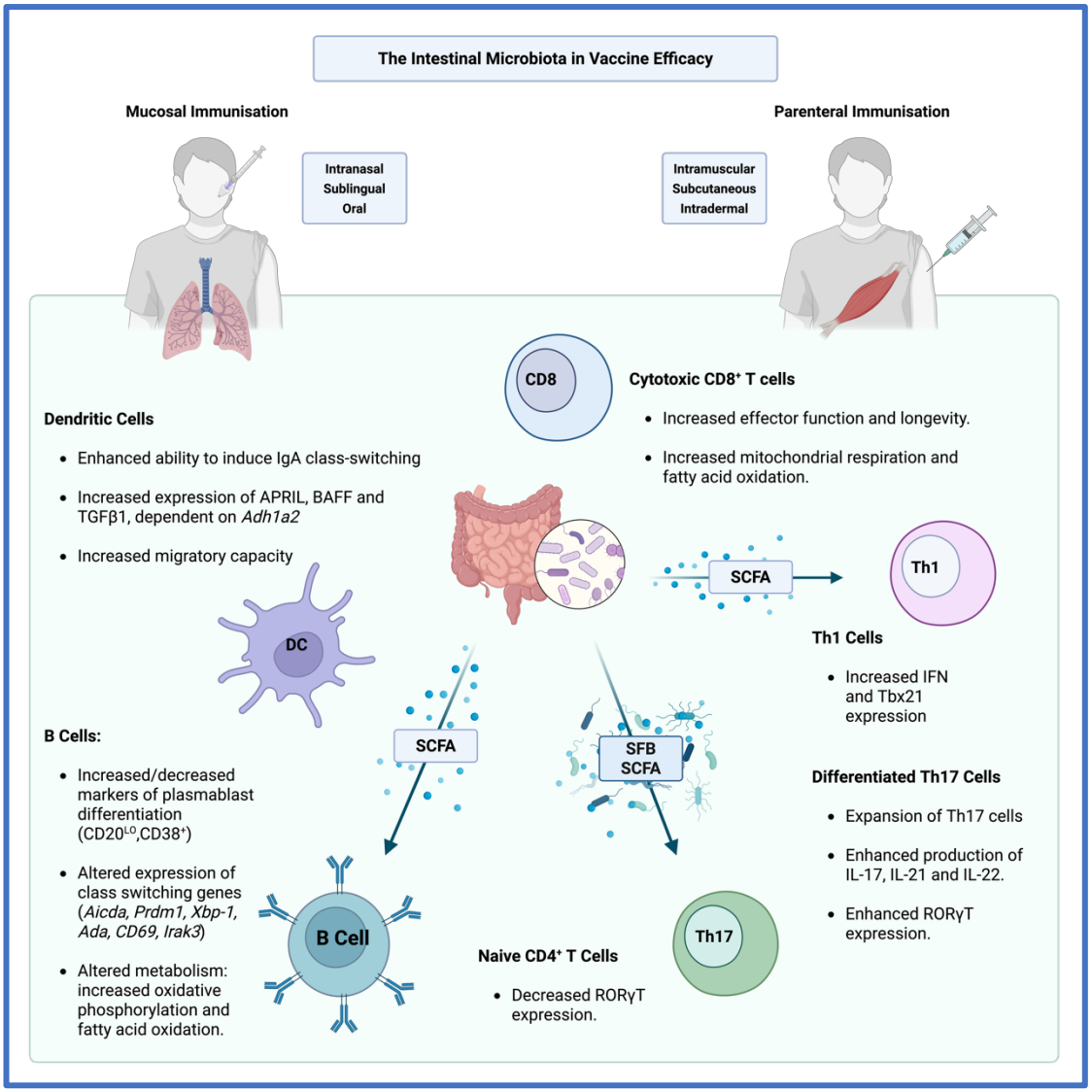


Fig. 1.12 The Impact of the Intestinal Microbiota on Vaccine Efficacy and Lymphocyte phenotype. Diagram made using Biorender.

Hypothesis:

Collectively, literature points towards an imperative role of the microbiota in both respiratory infection and immunisation. This in part is due to the metabolic contributions of the microbiota, through the generation of immunomodulatory metabolites, short-chain fatty acids.

The main hypotheses are:

"*The short-chain fatty acids, butyrate, can improve outcomes of acute pneumococcal pneumonia through pleiotropic immunomodulatory means in the setting of dysbiosis-induced susceptibility*"

"*The short-chain fatty acid, butyrate can improve the immunogenicity of intranasal and parenteral pneumococcal vaccines*"

2. Materials and Methods

Table 2.1 Materials

Cell Culture:		
RPMI-1640 GlutMAX	Gibco	61870036
DMEM	Gibco	D5671
Foetal Bovine Serum	Gibco	10270106
Type I Collagenase	Thermo Fisher	17100017
Deoxyribonuclease I Bovine Pancreas	Sigma Aldrich	D4513
Penicillin/Streptomycin	Gibco	15070063
b-mercaptoethanol	Gibco	31350010
Human TGF-β	Peprotech, Thermo Fisher	100-21
Murine GM-CSF	Peprotech, Thermo Fisher	315-03
Trypan Blue	Gibco	15250061
Phorbol 12-myristate-13-acetate	Sigma-Aldrich	P8139
Pam3Csk4	Invivogen	tlrl-pms
LPS E. coli serotype O (R515)	Enzo Life Science	ALX-581-007-L002
MEM Vitamins	Gibco	11120052
Sodium Pyruvate (100X)	Gibco	11360039
Non-essential MEM vitamins (100X)	Gibco	11140-035
L-Glutamine	Gibco	25030081
Sodium Butyrate	Sigma-Aldrich	B5887
In vivo:		
Ampicillin	Thermo Fisher Sigma-Aldrich	15493649 A1593
Neomycin	Sigma-Aldrich	N1876
Vancomycin	Sigma-Aldrich	V1130
Metronidazole	Sigma-Aldrich	M3761
Amphotericin	Gibco	15290018

***In vivo* (cont)**		
Soybean trypsin inhibitor	Sigma-Aldrich	T9128
Pefabloc®	Merck	76307
Complete Protease Inhibitor Cocktail	Roche	11836170001
Sodium Butyrate (99%)	Thermo Fisher	263195000
HyClone™Water Cell Culture Grade	Cytiva	11586271
Bacterial:		
Todd-Hewitt Broth	Sigma-Aldrich	T1438
Yeast Extract	Sigma-Aldrich	8013-01-2
Tryptone soy agar	BD Biosciences	11768822
Defibrinated sheep blood	Thermo Fisher	SR051B
TSA agar plates (5% sheep blood)	Fannin Themo Fisher	 10362223
ELISA		
TNF-α DuoSet Murine ELISA	R&D Biosystems	DY410
IL-6 DuoSet Murine ELISA	R&D Biosystems	DY406
IL-1β DuoSet Murine ELISA	R&D Biosystems	DY401
IL-10 DuoSet Murine ELISA	R&D Biosystems	DY417
IFN-γ DuoSet Murine ELISA	R&D Biosystems	DY485
IL-17A DuoSet Murine ELISA	R&D Biosystems	DY421
Purified Rat Anti-Mouse IgA	BD Pharmingen™	556969
Purified mouse IgA, κ-b-allotype isotype control	BD Pharmingen™	550924
Goat anti-mouse IgA-HRP	Southern Biotech	1040-05
Goat anti-mouse IgG-HRP	Southern Biotech	1030-05
Goat anti-mouse IgG2c-HRP	Bio-Rad	STAR135P
ELISA (cont)		

Biotin rat anti-mouse IgG1	BD Pharmingen™	553441
Streptavidin-HRP	BD Pharmingen™	51-9002813
BD OptEIA™ TMB Substrate Reagent Set	BD Pharmingen™	555214
Human IL-6 Uncoated ELISA Kit	Invitrogen	88-7066-88
Human IL-1β Uncoated ELISA Kit	Invitrogen	88-7261-88
Human TNF-α Uncoated ELISA Kit	Invitrogen	88-7346-88
Pneumococcal polysaccharide, type 3	Oxford Biosystems	76853
Pneumococcal polysaccharide, type 4	Oxford Biosystems	76855
Pneumococcal CWPS	Oxford Biosystems	3459
Flow Cytometry:		
1X PBS	Gibco	10010023
10X PBS	Gibco	
4% Paraformaldehyde	Santa Cruz Biotechnology	sc-281692
Ultrapure™ 0.5M Ethylenediaminetetraacetic acid	Invitrogen™	15575020
Zombie Aqua™ Fixable Viability Kit	BioLegend	423102
BD Horizon™ Fixable Viability Stain 510	BD Biosciences	564406
Purified rat anti-mouse CD16/32 (Mouse BD Fc Block™)	BD Pharmingen™	553142
OneComp eBeads™	Invitrogen™	01-1111-42
eBioscience™ FoxP3/Transcription Factor Staining Buffer Set	Invitrogen™	00-5523-00
Flourochromes:	See tables **2.4** and **2.5**	
Nucleic Acids:		
Direct-zol™ RNA MicroPrep Zymo-Spin™ IC Kit	Zymo Research	R2062

Western Blot:		
PageRuler™ Plus Prestained Protein Ladder	Thermo Fisher	11832124
Anti-Histone H3 Antibody	Abcam	#ab300641
Anti-Histone H4 Antibody	Abcam	#ab177790
IRDye 800CW Goat anti-mouse IgG	Odessey	#926-32211
IRDye 680CW Goat anti-mouse IgG	Odessey	#926-68070
Acrylamide/Bisacrylamide 30%	Merck	A3574

Table 2.2 Buffers

Ex VIvo	
Bronchiolar lavage buffer	PBS (1X) Gibco, 0.5% FBS, 2mM EDTA
Nasal lavage buffer	Protease inhibitor + PBS
Lung perfusion buffer	PBS (1X) Gibco, 5mM EDTA
Fecal pellet collection buffer	
Cell Culture	
Ammonium Chloride Lysis Buffer	8.8g ammonium chloride, 1L deionised water
ELISA	
Sodium Carbonate Buffer	4.2g $NaHCO_3$, 1.78g Na_2CO_3, distilled water
Phosphate Citrate Buffer	10.2g anhydrous citric acid, 14.6g Na_2HPO_4, distilled water
Reagent Diluent (DY485)	Trizma base (20mM), 150mM NaCl, 0.05% Tween-20, 0.1% BSA, pH 7.2-7.4
Wash Buffer	0.05% Tween-20, distilled water
Reagent Diluent (All other ELISAs)	PBS (1X) Gibco, 1% BSA
Flow Cytometry	
Permeabilization Buffer	PBS (1X) Gibco, eBioscience™ FoxP3/Transcription
FACS Buffer	1X PBS, 2% FBS, 2mM EDTA
Fixation Buffer	PBS (1X) Gibco, 2% PFA

Western Blot	
1.5M Tris pH 8.8	18.15g Trizma base, 100mL H2O, pH 8.8
1M Tris pH 6.8	12.1g Trizma base, 100mL H2O, pH 6.8
10% APS	10g Ammonium persulfate, 100mL H2O
10% SDS	10g Sodium dodecyl sulfate, 100mL H2O
10X Tris buffered saline (TBST)	80g NaCl, 2g KCl, 30g Trizma base, 10mL Tween-20, 990mL H2O
Transfer Buffer	10% Bolt™ Transfer buffer, H2O
Blocking and Reagent Buffer	3%w/v BSA, 1X TBST

2.1 Cell Culture

Table 2.3 Media components used for *in vitro* and *ex vivo* systems.

Cell type:	Base media:	Alteration:
In vitro:		
THP-1	cRPMI	50nM β-mercaptoethanol No antibiotics unless specified
FLAM	cRPMI	30ng/mL mGM-CSF 20ng/mL hTGF-β No antibiotics
L929	cDMEM	No antibiotics
hAM	cRPMI	1% Penicillin/Streptomycin, 2.5ug/mL Amphotericin B (Antibiotics and amphotericin were removed prior to infection, section 2.3.6)
Ex vivo:		
BMDM	cDMEM	25% L929 (Differentiation) 12.5% L929 (Maintenance)
Lung	cRPMI	50nM β-mercaptoethanol 0.1% penicillin/streptomycin 0.35% v/v MEM Vitamins 0.88% v/v non-essential amino acids 0.88mM Sodium Pyruvate
Spleen	cRPMI	50nM β-mercaptoethanol 0.1% penicillin/streptomycin 0.35% v/v MEM Vitamins 0.88% v/v non-essential amino acids 0.88mM Sodium Pyruvate

Source of reagents is outlined in Table 2.1. Complete media (cRPMI or cDMEM) was considered base media with the addition of 10% foetal bovine serum and antibiotics (100U/mL Penicillin/Streptomycin) unless otherwise specified. Cell lines were maintained in the absence of antibiotics. Derivations from base media for different cell cultures are listed.

2.1.1 THP-1 cells

THP-1, a cell line derived from a paediatric patient with acute monocytic leukaemia, were originally sourced from ATCC (TIB-202™). Cells were maintained in cRPMI (devoid of penicillin/streptomycin) in suspension at 37°C, 5% CO_2. Cells were passaged when 60-70% confluency was reached. Prior to stimulation cells were seeded at $1x10^6$/mL in 12 well plates and pre-treated with 100nM phorbol-myristate acetate (PMA) for 48 hours to generate monocyte-derived macrophage. Media was then refreshed, and cells were left to rest for 24 hours prior to treatment.

2.1.2 *Ex vivo* culture of human alveolar macrophages (hAMs)

All procedures regarding the use of human cells were performed under approved studies by the St James's/Tallaght University Hospital Joint Research Ethics Committees in compliance with the European Communities (Clinical Trials on Medicinal Products for Human Use) Regulations 2004 & ICH GCP guidelines, as well as the current General Data Protection regulation (GDPR), Health Research Regulations and the Data Protection Act 2018. Participants having a bronchoscopy as part of their clinical workup were invited to take part on the approved studies "Define Pathogenesis of patients both at risk and with defined pulmonary fibrosis" or " Harnessing the power of the Gut-Lung Axis: Metabolic and Inflammatory Outcomes in Chronic Obstructive Pulmonary Disease". After signed consent was obtained, bronchiolar lavage fluid (BALF) was acquired via bronchoscopy by the treating clinician and a portion of the BALF was transferred to the researcher on clinical sample duty rota on each day. The BALF sample was homogenised through gentle pipetting using a 25mL stripette and filtered through a mesh filter. The BALF sample was then centrifuged at 300g for 10 minutes at 4°C and supernatant was either stored at -80°C for downstream analysis or discarded.

For samples with heavy mucus content, freshly made DTT was added at a final concentration of 4% at room temperature (RT) and incubated for up to 10min at RT while homogenising gently by pipetting up and down with a 25mL pipette 5 times and

then with a 10mL pipette another 5 times. The BALF was then filtered through a sterile medical gauze before cells were washed and centrifuged at 300g for 10 minutes at 4°C. The resulting cell pellets were resuspended in 10mL hAM media (see table 2.1) and centrifuged again at 300g for 10 minutes at 4°C. Cells were resuspended in hAM media and counted using Trypan Blue exclusion assay. Cells were seeded at the appropriate density for the chosen assay and allowed to rest overnight at 37°C, 5% CO_2. Cells were washed once with hAM media prior to treatment.

2.1.3 Foetal liver derived alveolar macrophages (FLAMs)

FLAMs were kindly provided by the Cloonan Lab, TCD, these were sourced from the Carpenter lab, UCSC, primary progenitor cells were derived from C57BL6/J mice and FLAMs were established based on the protocol by Thomas *et al.* 2021. FLAMs were maintained in 10cm cell culture petri dishes at no less than 40% confluency in complete FLAM media at 37°C, 5% CO_2 (**Table 2.1**). FLAMs were split once 90% confluency had been reached. For cell splitting, supernatant was removed from cells and transferred to a sterile 50ml Falcon tube. Seven millilitres of sterile 1X PBS-1.5mM EDTA was added to cells and was allowed to incubate for 10 minutes at 37°C, 5% CO_2. Cells were then lifted by gently rinsing the dish and transferred to the 50mL Falcon tube containing the supernatant. Cells were centrifuged at 1500rpm for 5 minutes and resuspended in the appropriate volume of media to achieve 40-50% confluency. The resulting cell suspension was re-seeded in sterile petri dishes.

2.1.4 Culture of L929 for M-CSF enriched media

The aneuploidy fibrosarcoma (L929), murine cell line was transfected with an expression vector, of mammalian origin, containing the cloned murine gene encoding murine colony stimulating factor (M-CSF). Upon rederivation of L929 cells from frozen stocks, cells were initially cultured in 5mL of cDMEM, in the absence of antibiotics, in T25 flasks. On the second passage after rederivation from frozen stocks, cells were subsequently cultured in T75 or T175 flasks, depending on cell yields. Flasks were maintained

horizontally as L929 cells grow in adherent monolayers, at 5% CO_2, 37°C. Once 90% confluency was achieved, media was removed and cells were washed with 1X PBS. Trypsin-EDTA was added to flasks and cells were allowed to incubate for 5 minutes at CO_2, 37°C, lifting of cells was assisted by gentle agitation. Complete DMEM was added to trypsinised cells. This suspension was added to sterile 50mL tubes and centrifuged at 1200rpm for 5 minutes. Cell pellets were resuspended in cDMEM and counted using the trypan blue exclusion method. Cells were seeded in T175 flasks at $5x10^5$cells/mL in T75 or T175 flasks. Cells were allowed to incubate at CO_2, 37°C and supernatant, containing M-CSF, was collected 7 days later. Cells were split every 7 days when supernatant was removed, and cells had reached 90% confluency.

2.1.5 *Ex vivo* culture of bone marrow derived macrophages (BMDMs)

Male C57BL6/J mice were euthanised. Legs were removed and the femur and tibia were isolated. All tissue and muscle was removed from the bone and before further brief washes in 70% ethanol. The extremities of the femur and tibia were cut off, and the bones were flushed with 10mL cDMEM using a 27G needle, until complete isolation of the bone marrow was achieved. Bone marrow in cDMEM was repeatedly aspirated and expelled with a 19G needle to break up bone marrow into a cell suspension. This cell suspension was subsequently passed through a 40um cell strainer and centrifuged at 1200rpm for 5 minutes. The resulting cell pellet was resuspended in 1mL of ammonium chloride lysis buffer for 2 minutes. Ten millilitre of cDMEM was used to quench the lysis reaction and cells were again centrifuged at 1200rpm for 5 minutes. The resulting cell pellet was resuspended in 10mL of cDMEM and cells were counted using the trypan blue exclusion method. Cells were seeded in $10cm^2$ petri dishes at $1x10^6$cells/mL and supplemented with 25% L929 conditioned media, with a final volume of 10mL in each dish.

Cells were allowed to incubate at 5% CO_2, 37°C for 3 days. On day 3 an additional 10mL of cDMEM supplemented with 25% L929 conditioned media was added to petri dishes. Cells were incubated for a further 3 days at 5% CO_2, 37°C. On day 6, BMDMs were

terminally differentiated. Media was removed and cells were washed once gently with 1X PBS. Five millilitres of 0.1% EDTA-PBS to petri dishes was added to dishes which were incubated on ice or 5-10 minutes. BMDMs were lifted through gentle rinsing of the dish with 0.1% EDTA-PBS using a 5mL pipette. BMDMs were transferred to a sterile 50mL tube and resuspended in 10mL cDMEM and centrifuged at 400g for 5 minutes. BMDMs were counted using the trypan blue exclusion method and seeded at $1.5x10^5$cells/well in flat bottom 96-well cell culture plates. BMDMs were allowed to rest for a minimum of 24 hours once re-seeded before further treatment or stimulation.

2.1.6 *Ex vivo* culture of splenic cells

Spleens were isolated from vaccinated C57BL6/J mice and placed in 15ml falcon tubes containing 5ml cRPMI. Spleens were subsequently mashed through a 40uM mesh filter. Resulting suspension was centrifuged at 400g for 5mins. Supernatant was discarded and the cell pellet was resuspended in 1ml ACL lysis buffer and incubated for 2 minutes. 10mL of cRPMI was immediately added and suspension was again centrifuged at 400g for 5mins. Supernatant was discarded and pellets were resuspended in 2mL T cell media and counted.

2.1.7 *Ex vivo* culture of primary lung cell suspensions cells

Lungs were dissected from mice via exposure of the thoracic cavity. The aorta was cut just below the diaphragm; the lungs were perfused through injection of perfusion buffer (**Table 2.3**) through the right ventricle of the heart using a 27G needle. Lungs were then carefully removed and stored in 24-well plates containing RPMI-1640 containing antibiotics, devoid of FBS, on ice. Media was removed and lungs were processed into smaller tissue segments using sterile surgical scissors. Digestion media containing 20mg/mL collagenase type I and 100µg/mL DNAse I was added and allowed to incubate for 1 hour at 37°C, 5% CO_2 with gentle agitation at approximately 300rpm.

Digested tissue was passed through a 70μM filter and rinsed with 5mL of inhibition buffer (**table 2.3**). The resulting homogenous single cell suspension was then transferred to sterile 15ml falcon tubes and centrifuged at 400g for 5 minutes. Supernatant was discarded and cell pellets were resuspended in 1mL of ammonium chloride lysis buffer for 2 minutes. Ten millilitres of cRPMI was used to quench the lysis reaction. Cell suspensions were once again centrifuged as before and resuspended in 2mL of either cRPMI or T cell media to count (dependent on the use of cells). Cells were counted by dilution, first in complete T cell media and subsequently in trypan blue. Cells were resuspended to $1x10^6$/mL in complete T cell media for *ex vivo* culture and restimulation or phenotypic analysis of innate immune infiltrates post-infection. Cells were resuspended at $2x10^6$/mL in T cell media for *ex vivo* restimulation and subsequent analysis of intracellular cytokine production.

2.1.8 Treatment of cells *in vitro* with sodium butyrate

Cells were seeded at appropriate densities as per experimental layout. Sodium butyrate (B5578 Sigma) was weighed and diluted in the appropriate culture media to achieve a final concentration of 10-20mM as per experiment. The resulting solution was passed through a 0.22uM sterile membrane filter and further diluted in cell culture media to achieve required concentrations. Supplemented media containing butyrate was prepared fresh immediately before use for every experiment.

2.1.9 Stimulation of bone marrow derived macrophage and foetal liver derived alveolar macrophage

Cells were seeded at $1x10^5$ cells per well in flat-bottom 96 well cell culture plates in media appropriate to cell line and allowed to rest for 24 hours at 37°C, 5% CO_2 prior to stimulation or further treatment. The following stimuli were prepared in media: Pam3Csk4 (100ng/mL), (200ng/mL) or (500ng/mL). Stimuli were added to wells and cells were allowed to rest at 5% CO_2, 37°C.

2.1.10 Stimulation of splenocytes and lung cells *ex vivo* to quantify cytokine production

Lung parenchymal cells and splenocytes were seeded at in 96-well U bottom cell culture plates at densities indicated in section **2.1.6** and **2.1.7**. All stimulations were prepared in complete T cell media and delivered in a volume of 50µL. The stimulations were as follows media (negative control), polyvalent pneumococcal lysate, section **2.1.11**. (15µg/mL, 45µg/mL and 100µg/mL) or αCD3 (0.2µg/mL).

2.2 *In vivo*

2.2.1 Mice

Mice were sourced externally from Charles River, UK and maintained in the Comparative Medicines Unit (CMU), TCD in line with the EU Directive (2010/63/EU). All procedures were performed according to the protocols on licenses AE19136/P072 and AE19136/P172 approved by the Irish Health Product Regulatory Authority (HPRA) under the Irish Medicine's Board Acts 1995 and 2006 and under the European Union (Protection of Animals Used for Scientific Purposes) Regulations 2012 (S.I. No. 543 of 2012) and Directive 2010/63/EU of the European Parliament and of the Council of 22 September 2010. Animals were housed in individually ventilated cages, under SPF containment. Animals were allowed to acclimatise for a minimum of 1 week after transport and housing before the induction of any procedures. All wildtype mice used were C57BL6/J and were used between 8 and 35 weeks of age. Mice were administered food and water *ad libitum.*

2.2.2 Dietary supplementation with SCFA

Sodium butyrate (Thermo Fisher) was dissolved in sterile water at a concentration of 1M and subsequently filter sterilised. This concentrate was further dissolved in drinking water at a final concentration of 100mM. Supplemented drinking water was replaced

every 2-3 days. In the pneumococcal infection model animals were administered sodium butyrate in drinking water for two weeks prior to intranasal pneumococcal administration. In the vaccination model animals were administered sodium butyrate for 2 weeks prior to prime immunisation and throughout the entire course of immunisation. Supplement solutions of butyrate were prepared fresh each time.

2.2.3 Induction of antibiotic-induced dysbiosis

Dysbiosis was induced through daily oral administration of an antibiotic cocktail. Ampicillin 10g/L (Sigma A9393), neomycin 10g/L (Sigma N1876), metronidazole 10g/L (Sigma M361), vancomycin 5g/L (Sigma V1130) and 72.5-125µg/mL amphotericin A were dissolved in sterile water, to be delivered in a final volume of 200µL. Mice were administered this antibiotic cocktail once daily by oral gavage prior to pneumococcal challenge. Animals were scored daily to ensure excessive weight loss did not occur.

2.2.4 Induction of pneumococcal pneumonia

Bacterial inoculum was prepared immediately from frozen working stocks. Frozen stocks were thawed quickly and centrifuged at 6000g for 5 minutes. Bacterial pellets were resuspended in 1mL 1X PBS and centrifuged again as before. Bacteria were prepared at $1.5x10^{10}$-$2x10^{10}$ CFU/mL in 1X PBS in order to deliver a final dose of $7.5x10^{8}$-$1x10^{9}$ CFU in a volume of 40µL. Bacterial inoculum was stored on ice until required. Internal basal body temperature was recorded using an infra-red thermometer (Fluke 62 MAX plus IR Thermometer). Mice were anaesthetised by intraperitoneal injection with 110mg/kg ketamine (Ketimidor/Ketabel) and 5.5mg/kg xylazine (Chalazine), prepared in isotonic saline solution and delivered in a final volume of 100µL. Once under anaesthetic with regular respiratory rate and an absent pedal withdrawal reflex, mice were intranasally administered 40µL of bacterial inoculum. Mice were closely monitored after administration of inoculum for breathing difficulties and were returned to cages once respiratory rate had stabilised and animals were regaining consciousness.

Mice were then scored for disease severity, based on the scoring criteria listed in table 2.4, twice a day until humane endpoint was reached.

Table 2.4 Scoring guidelines for acute bronchopneumonia model.

Weight	No weight loss	0
	Weight loss between 5-10% from start of study	1
	Weight loss between 10-19% from start of study	2
	Weight loss between ≥ 20% from start of study	3
Activity	Normal activity	0
	Subdued behaviour with response to touch/provocation	1
	Isolated from other animals, less mobility and alertness observed	2
	Non-responsive to touch or provocation, weak labored movement	3
Condition/ Appearance	Normal	0
	Lack of grooming, ruffled fur	1
	Ocular/Nasal discharge, slight piloerection	2
	Hunched posture, severe piloerection and discharge	3

Mice will scored daily using the score sheet above following antibiotic administration.

Mice will be scored between 0-3 for each category.
*** Mice will be culled if they reach 3 in any individual category.

For additive scoring in different categories, it will be as follows:
0-3 Normal
4-5Monitor the animal carefully
6 Observe regularly, seek opinion of NACWO and consider termination of the animal
≥7 Terminate animal – Humane endpoint

2.2.5 Preparation of intranasal vaccines

Vaccines were prepared immediately prior to immunisation. Pneumococcal lysates used for immunisation were kindly provided by Adjunct Prof. Dr Analía Rial and Prof. Jose A. Chabalgoity, from the Laboratory for Vaccine Research, Department of Biotechnology, School of Medicine – Universidad de la República, Montevideo-Uruguay. A polyvalent pneumococcal lysate was prepared by combining appropriate amounts of bacterial lysate from three clinical pneumococcal strains, *S. pneumoniae* serotype 1 (E1586), *S. pneumoniae* serotype 3 (E1434) and *S. pneumoniae* serotype 4 (TIGR4 [JNR.7/87]). The polyvalent pneumococcal lysate was administered at 15ug/dose (5ug of each respective pneumococcal strain).

Double mutant heat liable toxin (dmLT) was kindly provided by Associate Prof. James McLachlan and Assistant Prof. Jacob P. Bitoun, Department of Microbiology and Immunology, University of Tulane. This was added to the polyvalent pneumococcal lysate at a concentration of 50µg/mL (1µg/dose).

2.2.6 Intranasal immunisation

Animals were anaesthetised by administration of inhalation anaesthesia. Anaesthesia was induced using 3-4% isoflurane. After induction of anaesthesia 1.5-2% isoflurane was used for maintenance. Mice were maintained at 1-1.5L/min oxygen to prevent respiratory depression. Depth of anaesthesia was monitored through rate of breathing and pedal withdrawal reflex. Once completely under anaesthesia mice were administered a 20µL volume of vaccine distributed between both nostrils. Mice were returned to a clean cage with extra bedding post-procedure. Mice were monitored for recovery immediately post procedure and 24 hours post procedure.

2.3 Bacteria

2.3.1 Bacterial strains

Serotype 2 (D39) was originally sourced from the National Collection of Type Cultures (NCTC), Public Health England, UK. *S. pneumoniae* serotype 1 (E1586), a clinical isolate originally derived from the blood of a paediatric pneumococcal pneumonia patient, and *S. pneumoniae* serotype 4 (TIGR4) ATCC BAA-334 were kindly provided to us by Prof. Analia Rial and Prof. Jose Alejandro Chabalgoity, University of La República, Uruguay. The clinical isolate TUH was provided to us by Natasha Sarwar, Clinical Microbiology, Trinity College Dublin. TUH is a wild-type strain was originally derived from the BALF of a bronchoscopy at Tallaght University Hospital, Dublin. It was confirmed to exhibit alpha haemolysis on blood agar;, however, it remains to be genotypically characterised and serotyped. All work involving the use of *S. pneumoniae* was carried out in biosafety level 2 facilities as per approved protocols by TCD Safety Office. A murine adapted variant of

this bacteria was previously generated by Assistant Research Prof. Natalia Muñoz-Wolf for use in infection of live animals and cells of murine origin.

2.3.2 Adaptation of bacterial strains for *in vivo* infection

Mice were infected with 10^3CFU/dose, *S. pneumoniae* serotype 2 D39 intraperitoneally. Blood from infected animals was recovered 20 hours post infection. Ten millilitre aliquots of Todd Hewitt Yeast Broth (THYB) were inoculated with blood and allowed to incubate for 8 hours at 37°C. Blood agar was then inoculated with these cultures and allowed to incubate at 5% CO_2, 37°C for approximately 20 hours. Fifteen millilitre Falcon tubes containing 10mL of fresh THYB were inoculated with 10-15 colonies from these blood agar plates and allowed to incubate under static conditions until an optical density at 600nm (OD_{600}) of 0.7-0.9 was achieved. Stocks were frozen as described in section 2.3.3.

2.3.3 Preparation of bacterial stocks

Tryptone soy agar plates, supplemented with 5% defibrinated sheep's blood (ThermoFisher) were inoculated with freshly thawed master stock and allowed to incubate overnight at 37°C, 5% CO_2. Fifteen millilitre falcon tubes, containing 10mL of freshly prepared Todd Hewitt Yeast Broth (THYB) were inoculated with 10-15 colonies of bacteria, taken from the plated master stocks. An additional three tubes were inoculated to act as positive controls and one tube of THYB was not inoculated to act as a negative control. Tubes containing inoculum were allowed to incubate under static conditions for approximately 6-12hrs in a water bath set to 37°C. Optical density was measured every 2hrs until a maximum OD_{600} of 1.1-1.3 was achieved. At this point the top 2-4mL of bacterial suspension was pooled from each tube. An equivalent volume of fresh THYB was added to the pooled bacterial suspension. For every 20mL of bacterial culture 7.6mL of 80% v/v glycerol was added. Stocks were then immediately aliquoted in either 1.5mL or 5mL volumes and stored at -80°C.

2.3.4 Quantification of bacteria

Working stocks of bacteria were thawed at 37°C and immediately centrifuged at the appropriate speed for each strained (6000g for D39 and TIGR4 for 8 min; 3000g for E1586 and TUH for 5 min), supernatant containing the freezing media was discarded. The equivalent volume of 1X PBS was added and bacteria were centrifuged again. Bacteria were resuspended in 1mL 1x PBS to count. A series of Eppendorf tubes was prepared with 900µL 1x PBS. One hundred microlitres of bacterial suspension was added to the first tube and vortexed. From this a series of 1:10 serial dilutions were prepared, ensuring to vortex gently or thoroughly mix between each successive dilution. A TSA plate containing 5% defibrinated sheep's blood was manually divided into six segments. Dilutions were plated in 20µL drops in triplicate on an individual segment and allowed to dry before returning to incubate at 37°C, 5% CO_2 for 18-24hrs. Dilutions were plated based on estimated bacterial count from OD_{600}. Dilutions were counted where between 3 and 30 colonies per 20µL drop were present. Colony forming units (CFU) per millilitre were calculated by the following:

(Colony forming units in triplicate/3) x **50** x 10^{x} = **CFU**/mL)

X = Factor of serial dilution
50 = Dilution factor corresponding to 20µL in 1mL of suspension
CFU = Mean CFU from technical triplicates

2.3.5 Infection of foetal liver derived macrophage in vitro

Foetal liver derived macrophages were plated at $1.5x10^{6}$/mL in 12-well cell culture plates and allowed to incubate overnight at 37°C, 5% CO_2. An aliquot of working stock of bacteria was counted as outlined in section 1.4, to have an estimate of bacterial count (CFU/mL). Cells were centrifuged at 300g for 5 minutes and washed 1X with PBS. Four hundred microlitres of fresh media was added to cells. Working stocks of bacteria were centrifuged at 6000g for 5 minutes. Supernatant was discarded and bacteria was washed with the equivalent volume of 1X PBS. Bacteria were again centrifuged and

resuspended at the required volume for required multiplicity of infection. Bacterial inoculum was added to cells in a final volume of 100µL, cells administered 100µL of 1X PBS devoid of bacteria acted as negative controls. Infected cells were centrifuged at 200g for 5 minutes to promote intermediate contact between the cells and bacteria. Infected cells were incubated for 1hr at 37°C, 5% CO_2. Cells were then centrifuged at 200g for 5 minutes and washed twice with 1X PBS. Cells were then returned to incubate at 37°C, 5% CO_2 for required time-points. After incubation, plates were centrifuged once more at 300g for 5 minutes and supernatant was stored at -20°C. Cells were washed once and 300µL of RNA lysis buffer was added to each well. Lysed cells were stored at -80°C prior to RNA isolation.

2.3.6 Evaluation of intracellular killing using a gentamicin protection assay

Foetal liver derived macrophages were plated at $1x10^5$/mL in 12-well cell culture plates and allowed to incubate overnight at 37°C, 5% CO_2. An aliquot of working stock of bacteria was counted as outlined in section **1.4**, to have an estimate of bacterial count (CFU/mL). Cells were centrifuged at 300g for 5 minutes and washed 1X with PBS. One hundred microlitres of fresh media was added to cells. Working stocks of bacteria were centrifuged at 6000g for 5 minutes. Supernatant was discarded and bacteria was washed with the equivalent volume of 1X PBS. Bacteria were again centrifuged and resuspended at the required volume for required multiplicity of infection. Bacterial inoculum was added to cells in a final volume of 100µL. Infected cells were centrifuged at 200g for 5 minutes to promote intermediate contact between the cells and bacteria. Infected cells were incubated for 1hr at 37°C, 5% CO_2. Cells were then centrifuged at 200g for 5 minutes and washed twice with 1X PBS. Cells were then returned to incubate at 37°C, 5% CO_2 for required time-points. After incubation, plates were centrifuged once more at 300g for 5 minutes and supernatant was discarded. Cells were washed once with 1X PBS. Two hundred microlitres of fresh media containing 100µg/mL gentamicin was added to each well and allowed to incubate at 37°C, 5% CO_2 for 30 minutes. Plates were centrifuged and supernatant was discarded. Infected cells serving as baseline controls were immediately lysed. Two hundred microlitres of 2% saponin in 1X PBS was

added to each well and incubated for 15 minutes at 37°C, 5% CO_2. Lysed cells were transferred to 1.5mL Eppendorf tubes and 800µL of 1X PBS was added. Lysed cells were centrifuged at 3000g for 5 minutes to recover intracellular bacteria. Recovered bacteria was washed twice with 1X PBS and resuspended in 100µL. Bacterial colony forming units were enumerated as outlined in section **2.3.4**. Remaining cells were incubated for a further 3 or 6 hours at 37°C, 5% CO_2. After this period of incubation cells were lysed as previously described and bacteria was counted.

2.4 General

2.4.1 Crystal violet viability assay

Protocol was provided by the Sheedy lab, TCD. Cells were washed once with 150µL 1X PBS. Fifty microlitres of 2% PFA was added to cells and incubated for 15 mins to fix cells. Cells were washed once more as before. Fifty microlitres of 0.1% crystal violet was added to wells and allowed to incubate for 30 mins with gentle agitation. Cells were washed twice as before using 1X PBS to remove residual stain. Plates were inverted and allowed to dry overnight. Following this, 50µL of 0.1% Triton-X was added to cells under gentle agitation to lyse stained cells. 30µL of cell lysate was added to a high binding ELISA plate. Absorbance was recorded at 592nm. Fluctuations in viable cells was calculated based on the change in absorbance normalised to the absorbance of the untreated control.

2.4.2 Phenotypic characterisation of myeloid lung cellularity by flow cytometry

A single cell suspension of lung homogenates was prepared as described in **2.1.7**, with the following exceptions. Media used during the collection of lung tissue was supplemented with 10% penicillin/streptomycin. Similarly, digestion media and all buffers used during the staining process were supplemented with 1% penicillin/streptomycin, with the exception of 2% paraformaldehyde (PFA). This was to

ensure complete antibiotic-mediated inactivation of viable bacteria before transfer of these cells to a biosafety level 1 (BSL1) environment.

Cells were resuspended at $1x10^6$/mL and 1mL was transferred to FACS tubes. Cells were centrifuged at 400g for 5 minutes and supernatant containing media was discarded. Cells were washed once in 1X PBS, centrifuged as before and supernatant was discarded. Cells were resuspended in 1mL of 1X PBS containing fixable viability stain 510 at a dilution of 1/1000. Cells were allowed to incubate on ice in the dark for 30 minutes. Cells were washed once more with 1mL 1X PBS. Cells were then resuspended in FACS buffer containing 0.5ug/sample of Fc block. An antibody mixture was prepared in advance for each individual antibody, with appropriate concentration of antibody (table **2.4**), BV buffer and FACS buffer. A master mix containing all the diluted fluorochromes outlined in table 2.4 was added to each sample (with a final volume of 10µL of each antibody per sample). Separately, a series of FMO controls were prepared for each fluorochrome, to determine the exact positive populations during analysis. A series of single stains using were additionally prepared using OneComp beads for compensation of the FACS instrument. Cells were allowed to incubate for 30 minutes at room temperature. Cells were washed with 1mL of 1X PBS and centrifuged as before, discarding supernatant. Cells were resuspended in 200µL of 2% paraformaldehyde (PFA) and allowed to incubate for 15 minutes at room temperature. Cells were washed again once with 1mL 1X PBS and centrifuged. Fixed cells were resuspended in 200µL of FACS buffer and stored in the dark at 4°C until acquisition. Fixed cells were acquired within 48 hours.

Table 2.4 Characterisation of lung innate immune infiltrates post pneumococcal infection.

Target:	**Fluorochrome:**	**Clone:**	**Catalogue No.:**	**Concentration of antibody**
CD45	FITC	30-F11	11045182	0.5
CD3	BV510	17A2	740147	0.2
B220	BV510	RA3-6B2	103248	0.2
CD11b	PE-Cy7	M1/70	552850	0.2

CD11c	BV605	HL3	563057	0.2
CD64	BV421	X54-5/7.1	139309	0.2
F4/80	AF700	BM8	MCA497A700	-
Ly6C	APC-Cy7	AL-21	560596	0.2
Ly6G	BV650	1A8	127641	0.2
MerTK	BV711	2B10C42	151515	0.2
Viability	BV510	-	423102	1:1000

2.4.3 Phenotypic characterisation of lung lymphocyte populations by flow cytometry

A single cell suspension of lung homogenates was prepared as described in **2.1.7,** from immunised mice. Cells were stimulated as outlined in section **2.1.10.** A pool of cells from varying treatment groups was prepared for FMO controls. Cells intended for FMO controls were stimulated with αCD3 (0.2µg/mL) to ensure similar forward and side scatter to cells isolated from immunised mice and detectable expression of IL-17A and IFN-γ. Two hours after the initial incubation of the stimuli, Golgi Plug was added at a concentration of 1µg/mL in addition to the stimuli, cells were allowed to incubate for a further 4 hours at 5% CO_2, 37°C. Cells were then centrifuged in plates at 400g for 5 minutes. Supernatants were removed and cells were washed with 180µL 1X PBS per well. Cells were again centrifuged as before and supernatant removed. One hundred microlitres of zombie aqua viability dye was added to cells at a final concentration of 1/1000 in 1X PBS and cells were incubated in the dark at RT. Cells were centrifuged and washed with 1X PBS as before. Cells were then resuspended in 100µL of FACS buffer containing 0.5µg/sample of Fc block. An antibody mixture was prepared in advance for each individual antibody, with appropriate concentration of antibody (table **2.5**), BV buffer and FACS buffer. One hundred microlitres of a master mix containing all the diluted fluorochromes outlined in table **2.5** was added to each sample. Half of the final concentration of CD4 and CD8 was included at this time, similarly fluorochromes targeting IL-17A and IFN-γ were not included in this step. Separately, a series of FMO controls were prepared for each fluorochrome, to determine the exact positive populations during analysis. A series of single stains using OneComp beads were

additionally prepared for compensation of the FACS instrument. Cells were allowed to incubate for 30 minutes at room temperature in the dark. Cells and beads were centrifuged and washed as before. One hundred microlitres of 2% PFA was added to each well and cells were allowed incubate for 15 minutes in the dark. Cells were centrifuged and washed as before. Cells were resuspended in 50µL of permeabilization buffer and incubated for approximately 8 hours. A second master mix containing half the concentration of CD4 and CD8 and the full concentration of IL-17A and IFN-γ was added to cells, which were incubated for 30 minutes. Cells were centrifuged and washed as before. Cells were once again fixed using 100µL of 2% PFA. Cells were centrifuged and washed as before and subsequently resuspended in 200µL of FACS buffer. Cells were then transferred to FACS tubes and stored in the dark at 4°C until analysis.

Table 2.5 Characterisation of lymphoid lung cellularity post immunisation by flow cytometry

Target:	**Fluorochrome:**	**Clone:**	**Catalogue No.:**	**Amount (ng/test):**
CD45	PerCP	30-F11	103130	125
CD44	AF488	IM7	103015	1:200
CD49b	APC-eFlour780	DX5	47-5971-82	1000
CD3	PE-Dazzle594	145-2C11	100347	500
CD4	BV785	BV785	100453	63
CD8	BV650	BV650	100741	1:200
CD19	BV605	6D5	115540	500
gdTCR	PerCP-eFlour710	GL-3	46-5711-82	63
NK1.1	BV570	BV570	108733	1000
IFNg	PE			
IL-17	BV421			
Viability	Zombie aqua	-		1:1000

2.4.4 Quantification of cytokine by enzyme liked immunoglobulin assay (ELISA)

Cytokine was quantified in cell supernatants using commercially available ELISA kits, protocol was carried out as per manufacturer's instructions, with a final volume of 50µL per well in each step, with the exception of the blocking step which was a final volume of 150 µL. These included R&D Mouse IL-6 DuoSet ELISA (#DY406), R&D Mouse TNF-α DuoSet ELISA (#DY410), R&D Mouse IL-1β DuoSet ELISA (#DY401), R&D Mouse IL-10 DuoSet ELISA (#DY417), Mouse IL-17A DuoSet ELISA (#DY417) and Mouse IFN-γ DuoSet ELISA (#DY485). ELISAs targeting cytokine were developed using TMB substrate reagent. Reaction was stopped by adding 25µL of 1M H_2SO_4 to each well and plates were read at 450nm. Standard curves **(Fig. 2.1)** were used to quantify the relative amount of cytokine.

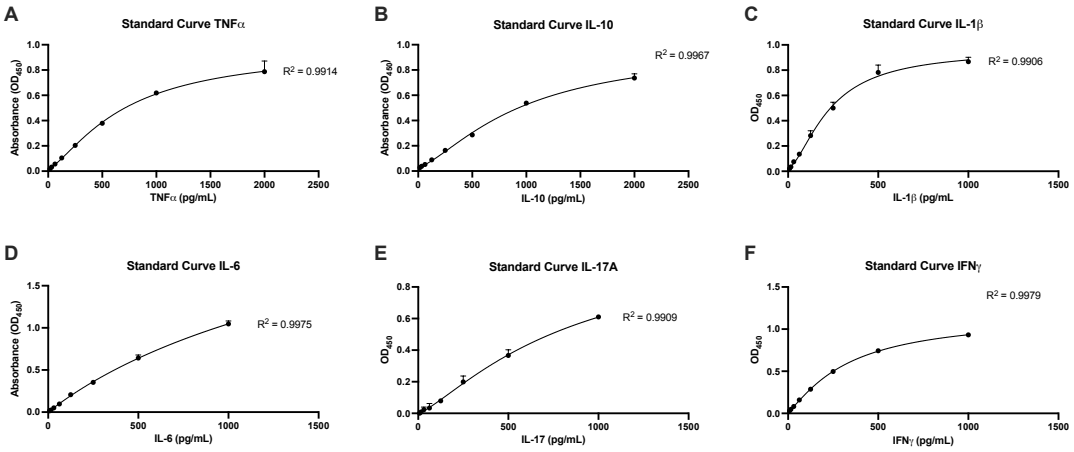


Fig. 2.1 Standard curves of cytokine ELISAs. R&D Mouse TNF-α DuoSet ELISA (#DY410) (**A**), R&D Mouse IL-10 DuoSet ELISA (#DY417) (**B**), R&D Mouse IL-1β DuoSet ELISA (#DY401) (**C**), R&D Mouse IL-6 DuoSet ELISA (#DY406) (**D**), Mouse IL-17A DuoSet ELISA (#DY417) (**E**) and Mouse IFN-γ DuoSet ELISA (#DY485) (**F**). Data displayed as n=3 technical triplicates ± SD, R^2 values were calculated based on non-linear regression fit to a sigmoidal curve XPL4 where X is representative of concentration, as recommended by manufacturer.

2.4.5 Quantification of antibody by enzyme liked immunoglobulin assay (ELISA)

A 20µg/mL solution of the polyvalent pneumococcal lysate described in **2.1.9** was prepared in sodium carbonate buffer. Ninety-six well medium binding ELISA plates were coated with 50µL of this solution and allowed to incubate overnight at 4°C. Coating

solution was removed, and plates were washed three times in PBS-0.5% Tween 20. Plates were blocked with 150µL 1% BSA-PBS per well and incubated at room temperature for 1-2hrs. Plates were again washed as before. Fifty microlitres of sample was added at two-fold serial dilutions prepared in 1% BSA-PBS and plates were allowed to incubate overnight at 4°C. Fifty microlitres of detection antibody was added and plates were incubated for 1-2hrs at room temperature. Detection antibody was prepared in 1% BSA-PBS at differing dilutions: IgG (1:5000), IgG2c (1:2000) and IgA (1:6000). Plates were once again washed as before and 50µL of developer was added per well. This was either *o*-phenylenediamine dihydrochloride (OPD) at 4mg/mL or TMB substrate reagent (TMB OptEIA™). OPD was prepared in phosphate citrate buffer 20 minutes prior to use; immediately before use 14µL of H_2O_2 was added. Reaction was stopped by adding 25µL of 1M H_2SO_4 to each well. Plates were read at either 450nm (TMB) or 490nm (OPD) using Thermo Scientific Multiscan FC plate reader using Skanit Multiskan software.

2.4.6 Quantification of pneumococcal polysaccharide specific antibody by enzyme liked immunoglobulin assay (ELISA)

Medium binding ELISA plates were coated with 10ug/mL pneumococcal polysaccharide 3 (PPS3) or PPS4 in 1X PBS in a 50uL. Plates were allowed to incubate overnight at 4°C. Plates were washed x3 in PBS-Tween 0.05%. Plates were then blocked with 150µL 1% BSA-PBS or 1 hours at RT. Serum samples were diluted based on the estimated level of detection. Serum samples were then neutralised using 500ug/mL CWPS for 30 minutes at RT. Plates were washed x3. Samples were added for 2 hours at RT. Plates were washed x3. The detection antibody, IgG (see table 2.1) was diluted in 1% BSA-PBS at a final concentration of 1:5000 and added to plates at 50uL/well. Detection antibody was incubated for a further 1hr at RT. Plates were washed x4 in PBS-Tween 0.05%. Plates were developed using TMB as previously described in **2.4.4**/**2.4.5**.

2.4.7 Quantification of pneumococcal specific IgA$^+$ B cells in lung cells by ELISpot

ELISpot plates were pre-treated as per kit protocol (IgA ELISpot Flex ALP, MabTech). ELISpot plates were then coated with either BSA (negative control), SpnL (20ug/mL), the target antigen or LPS (positive control). The ELISpot plate was washed x5 with sterile 1X PBS as outlined in kit protocol. The ELISpot plate was then blocked using 200uL/well of complete medium containing 10% FBS for 30 minutes at RT maintaining sterility. Media containing the blocking agent was removed. The lung parenchymal cell suspensions, prepared in section X, was added at $2x10^5$ cells/well and incubated overnight at 37°C, 5% CO_2. The medium containing the cell suspension was removed and the plate was washed x5 in 1x PBS. The detection antibody (mAb MT39A-biotin) was diluted in PBS-0.5% FCS and added to the plate at 100uL/well and incubated for 2 hours at RT. ELISpot plates were washes as before. One hundred microlitres of substrate solution (BCIP/NBT) was added. Once spots were faintly visible the reaction was stopped by washing plates with deionised water, the development time was approximately 10 minutes. The plate was allowed to dry completely in the dark before measurement using the Mabtech IRIS plate reader.

2.4.8 SDS-PAGE

Bis-acrylamide gels were prepared as described in table (2.6), with the percentage of bis-acrylamide dependent on the relative molecular weight of the protein of interest. All reagents listed in **table 2.6**, with the exception of APS and TEMED were combined. Apparatus was set up using 1.5mm glass cassettes (BioRad Mini-Protean). Immediately prior to pouring the gel, APS and TEMED were added to resolving and stacking gels respectively. Resolving gel was added leaving 1 inch of space left from the opening of the cassette. Five hundred microlitres of isopropanol was added to the top of the resolving gel immediately after pouring. Once set, stacking gel was added with a 10-well, 1.5mM width comb inserted and allowed to set.

Twenty microlitres of cell lysate was added to wells. A molecular weight standard was prepared by addition of 7µL (Pageruler™ Prestained Protein Ladder Invitrogen) to 13µL

of complete Laemelli buffer. Twenty microlitres of complete laemelli buffer was added to empty wells to ensure even running of protein bands in the gel. Cassettes were placed in electrophoresis tanks with wells orientated inwards and the reservoir was filled with running buffer. The gels were run using the PowerStation 200 (LabNet) at 80V for 30 mins, or until the bands had passed the stacking gel. The voltage was then increased to 115V until the band reached the bottom of the gel.

Table 2.6: Western Blot Reagents

Stacking Gel:	
H2O	**4.2mL**
Acrylamide/Bisacrylamide	**10.6mL**
1.5M Tris pH6.8	**5mL**
10% (w/v) SDS	**200µL**
10% (w/v) APS	**100µL**
TEMED	**14µL**
Resolving Gel:	
H2O	**5.5mL**
Acrylamide/Bisacrylamide	**1.3mL**
1M Tris pH6.8	**1mL**
10% (w/v) SDS	**80µL**
10% (w/v) APS	**80µL**
TEMED	**12µL**

2.4.9 Semi-dry membrane transfer

Gels were removed from cassettes, and the stacking gel was excised. Two pieces of Wattman filter paper were soaked in diluted Bolt™ transfer buffer and applied to the transfer apparatus. Nitrocellulose membranes were cut to the size of the gel and placed on the soaked filter paper. The gel was then applied to the membrane, and another piece of soaked filter paper was placed on top. Proteins were then transferred using the

(Biometra Fast Blot machine and Powerstation 200 powerpack) at 100mAmps for 1.5 hours.

2.4.10 Staining of membranes

Membranes were placed in 50mL Falcon tubes and blocked overnight at 4°C in TBST containing 3% BSA with rotation. Primary antibody was added as per table **2.7** and incubated overnight at 4°C with rotation. Nitrocellulose membranes were washed three times in TBST for 5 minutes per wash. Secondary antibody was added as per table **2.7** and incubated at RT for 1-2 hours. Membranes were analysed using the Odyssey XF system (LICOR). Densitometry was analysed using Empiria Studio Software (LICOR).

2.4.11 RNA Isolation

RNA extraction was performed as manufacturer's instructions using the Direct-zol™ RNA MicroPrep Zymo-Spin™ IC Kit (Zymo Research), as per manufacturer's instructions. Eluted RNA was collected and stored at -80°C. RNA quantity and quality was determined by A260/280 and A260/230 ratios prior to outsourcing for bulk RNA sequencing.

2.4.12 Data Analysis

Flow cytometry data was visualised using FlowJo Software™ (Treestar, Oregon, USA) v10.8. Data from western blots was analysed using Empiria Studio Software (LI-COR Biosciences, Nebraska USA). ELISA data was acquired and analysed using Scan-It Software (Thermo Fisher, Massachusetts, USA). ELISpot data was visualised and collected using Mabtech (Stockholm, Sweden) software.

Quantitative data was analysed using GraphPad Prism 9 and 10 Software. For data comparing one variable among two experimental treatment groups, student's t-tests were used to measure statistical significance. For all *in vivo* experiments, where one animal represents one biological replicate, and in the case of *in vitro* experiments where each passage of cells represents an individual biological replicate, unpaired t-tests were applied to test for statistical significance. For the comparison of more than two

experimental treatment groups, analysis of variance (ANOVA) was used. ANOVA functions of the assumption that the data is normally distributed or a Gaussian distribution. PRISM v.10 automatically applies the Geisser-Greenhouse correction to two-way ANOVA to account for normality. For one-way ANOVA, a Shapiro-Wilk test was used to test for normality, those which did not follow a normal distribution were analysed by the non-parametric equivalent of the test. All graphs within the same objective or method were analysed by consistent use of either parametric or non-parametric equivalents. P-values less than 0.05 were considered significant and are denoted in figure legends.

3. The effects of butyrate on host response to pneumococcal infection.

3. Introduction

As discussed, the commensal microbiota, particularly the intestinal microbiota, has a pivotal protective role during respiratory infection and lung pathology. Dysbiosis is associated with reduced lung function and increased susceptibility to respiratory infection. This effect has been demonstrated in empirical studies using models of antibiotic-induced dysbiosis, in which dysbiotic mice have poorer outcomes of respiratory infection with *K. pneumoniae*, *S. pneumoniae* and Influenza A [73], [179], [181]. *S. pneumoniae* is a pathogen of major clinical relevance in young children, the elderly and susceptible cohorts suffering from chronic respiratory diseases. Coincidentally, human clinical evaluations have highlighted that individuals suffering from COPD, CF or asthma appear to have a dysregulated intestinal microbiome. Likewise, individuals suffering from chronic inflammatory enteric conditions such as IBD commonly present a dysbiotic gut microbiota [372], [95], [373]. Concurrently, these individuals are at higher risk of obstructive airway disease and have an increased susceptibility to invasive lung disease [374], [375], [376], [377]. This susceptibility seen in IBD cohorts extends to a heightened risk of invasive pneumococcal disease (IPD) [378]. However, whether dysbiosis exacerbates the respiratory condition or *vice versa*, remains to be completely elucidated [87], [175], [176].

Schuijt *et al.* 2016 and Brown *et al.* 2017 have demonstrated that the intestinal microbiota plays a role in the host response to *S. pneumoniae* infection, in which mice undergoing antibiotic-induced intestinal dysbiosis presented with poorer outcomes of infection and decreased survival during invasive pneumococcal pneumonia [179], [73]. AMs are key phagocytes in the lung, essential for host defence against pneumococcal infection, as demonstrated by clodronate liposome mediated depletion of AMs resulting in a higher susceptibility to *S. pneumoniae*-mediated LRTI [73], [256]. Schuijt *et al.* showed that antibiotic exposure led to a dysregulated AM phenotype, with lower bactericidal functionality and decreased responses to lipoteichoic acid and lipopolysaccharide stimulation *ex vivo* which were not apparent in peritoneal macrophages [179]. The microbiota influences production of respiratory GM-CSF, and in the absence of a eubioitic microbiota, GM-CSF production and by proxy sustained AM

populations are abrogated affecting susceptibility to *S. pneumoniae* and *K. pneumoniae* [73]. The alteration of the AM phenotype in dysbiotic animals has been demonstrated in the context of other bacterial aetiological agents of respiratory infection. In animals receiving rifampicin, pyrazinamide and isoniazid, the standard antibiotic cocktail for treatment of *Mycobacterium tuberculosis* (ATT), a dysbiotic-driven dysregulation of AM phenotype was also seen. Mice receiving ATT exhibited higher *M. tuberculosis* dissemination and AMs isolated from the lungs of ATT-treated mice had a reduced capacity to clear intracellular *M. tuberculosis* [192]. Similarly antibiotic depletion of gut microbiota increases susceptibility to *Escherichia coli* pneumonia and abrogates the bactericidal activity and inflammatory cytokine milieu of AMs, increasing IL-6 and IL-1β but decreasing TNF-α production [186]. While the mechanistic features of the gut-lung axis of immune regulation remain to be fully elucidated. **These studies collectively highlight a mechanistic axis of immune regulation between the gut microbiota and AM phenotype, specifically in the context of host defence to bacterial LRTI.**

High intake of soluble dietary fibre, the main prebiotic precursor of highly pleiotropic immunomodulatory SCFA, has been linked to improved outcomes of respiratory disease and infection [112], [379], [193], [112]. Dietary supplementation studies with soluble dietary fibre increased bioavailable concentrations of SCFAs and improved outcomes of influenza [112]. Similarly longitudinal clinical observation studies investigating the impact of dietary fibre intake on outcomes of chronic obstructive pulmonary disease have yielded positive links between increased dietary fibre intake and improved disease outcomes [379], [193]. At the mechanistic level, Machado *et al.* 2022 demonstrated that acetate can enhance the antibacterial effects of AMs during *S. pneumoniae* infection, by enhancing nitric oxide (NO) synthesis dependent on NLRP3 activity and glycolysis driven HIF-1α activity [195]. Similarly, Wu *et al*. 2020, demonstrated that SCFAs can protect against *K. pneumoniae* driven bacterial pneumonia through upregulation of lysosomal pathways, albeit a cocktail of acetate (C2), propionate (C3) and butyrate (C4) was administered *in vivo* and the potential differential contributions of the individual SCFAs were not studied [107]. Conversely, Tian *et al.* 2019 demonstrated that high dose propionate, intratracheally administered shortly prior to infection could exacerbate lung inflammation and worsen outcomes of *S. aureus* mediated bacterial pneumonia,

while low dose propionate had opposing effects, implicating a highly concentration dependent effect of SCFA on modulatory outcomes [180]. In addition, some SCFA have been shown to have direct antibacterial effects on *S. pneumoniae* and *K. pneumoniae in vitro* which poses an additional potential contributing mechanism to their protective effects *in vivo*. This evidence indicates that the gut-lung axis of immune regulation can be harnessed in a therapeutic effort through dietary intervention. **In dysbiotic cohorts, commensal communities responsible for the production of SCFAs are ablated, resulting in lower levels of protective SCFAs. Through exogenous restoration of SCFA levels via dietary supplementation, the ability to combat respiratory infection could be restored.**

Here we first aimed to determine how butyrate affects the response of AMs during pneumococcal infection and the effects of oral butyrate supplementation in a model of invasive pneumococcal pneumonia. To determine the effects of butyrate *in vitro*, we first assessed how butyrate affected the growth of clinically relevant strains of *S. pneumoniae*. We then utilised a physiologically relevant model to study the response of AMs to *in vitro* stimulation with butyrate, while reducing the number of live animals that would be required to harvest primary AMs. For this we selected foetal-liver derived AM (FLAMs) as a permanent and sustainable model for examining the effects of butyrate on AM phenotype and function [380]. Bone-marrow derived macrophages were initially used for preliminary assays examining effects of butyrate on cytotoxicity and inflammatory cytokine production and for comparison purposes.

We established the threshold at which butyrate was cytotoxic for FLAMs and showed that butyrate was capable of eliciting histone deacetylase inhibitory functions concentrations that do not induce cell death. We subsequently identified that butyrate exposure prior to infection broadly promoted transcriptional regulation of pathways associated with innate immunity and defence against bacterial and viral pathogens. This was characterised by upregulated transcription of antimicrobial peptides and genes involved in interferon signalling. We showed that selective suppression of IL-6 at the protein level is a marked feature of butyrate-mediated immune modulation in both FLAMs and BMDMs. Butyrate pre-treatment additionally enhanced the clearance of

intracellular pneumococci in infected FLAMs. Crucially, butyrate also enhanced bacterial clearance in primary human AMs collected from BALF of patient cohorts suffering from respiratory illnesses.

Considering the promising results showing that butyrate enhances immune responses in AMs, we considered the potentially beneficial effects of butyrate in the context of acute pneumococcal infection, particularly in susceptible cohorts. To examine this, we utilised a murine model of antibiotic-induced dysbiosis, resulting in a susceptible phenotype to acute invasive pneumococcal infection. Dysbiotic animals were then administered butyrate in an effort to alleviate dysbiosis-driven susceptibility to infection. Butyrate supplementation was highly effective in reducing the burden of infection in dysbiotic mice which was accompanied by a reduced infiltration of neutrophils compared to mice that did not receive the SCFA.

Hypothesis

"*The short-chain fatty acid butyrate is a key driver of the gut-lung axis of immune regulation enhancing alveolar macrophage function and improving protection against invasive pneumococcal pneumonia*"

Aims:

1. To characterise the effect of butyrate on the transcriptional profile of alveolar macrophages using foetal liver derived macrophages under resting conditions or activation through TLR2 ligation or pneumococcal infection.

2. To assess the functional effects of butyrate on the bactericidal profile of FLAMs.

3. To investigate the ability of butyrate to circumvent antibiotic-induced dysbiosis driven hypo-response to acute pneumococcal infection *in vivo*.

3.1 Butyrate does not have any direct anti-microbial properties.

SCFA have direct microbial properties, acetic acid, propionic acid and butyric acid have free carboxyl groups and can readily donate protons (H^+) to acidify the intracellular environment of the bacteria. The metabolic production of SCFA from symbiotic commensal bacteria can inhibit pathobionts through the direct bacteriostatic activity of SCFA. At low pH SCFA can compromise the membrane integrity of some gram-negative species, namely *K. pneumoniae* and *E. coli,* eliciting bacteriostatic effects [381]. Additionally, SCFA-mediated bacteriostatic effects on *Salmonella typhimurium* have been identified [382]. However, other sources have suggested that SCFAs promote the growth and biofilm formation by some bacterial species, namely *Mycobacterium avium* [383]. Lim *et al*. 2024 recently examined the effects of SCFA bacteriostatic or bactericidal activity on a range of *S. pneumoniae* serotypes, finding serotype-specific differences in susceptibility [384]. However, the SCFA concentrations used in this study were not representative of physiological concentrations found in murine or human lung or serum [125], [66], [385].

To address whether the potential therapeutic benefit of butyrate was exclusively attributable to its capacity to modulate immune responses, it was first required that we demonstrated that butyrate has no direct antimicrobial effects on the bacteria. Here we used two collection strains of *S. pneumoniae* D39 (serotype 2), TIGR4 (serotype 4), a characterised human clinical isolate E1585 (serotype 1) and an un-characterised wild-type clinical isolate obtained from the BALF of a patient during bronchoscopy that we refer to as “TUH strain” of unknown serotype, to test whether butyrate had any direct effect on their growth. We established a series of bacterial cultures, in Todd-Hewitt yeast broth (THYB) supplemented with increasing concentrations of butyrate (0mM-30mM), in triplicate. These cultures were inoculated with 10 colonies of *S. pneumoniae* with a starting optical density of 0.01-0.05. These cultures were then incubated under static conditions at 37°C. Each hour, three tubes were taken and the OD_{600} of the top 1mL of the culture was measured until the plateau phase of bacterial growth had been reached.

No differential growth effects were observed between cultures incubated in the presence of butyrate at any of the tested concentrations for any of the strains compared to bacterial media alone (**Fig. 3.1**). It was then concluded that butyrate has no direct bacteriostatic or bactericidal properties on any of the *S. pneumoniae* strains used throughout the project.

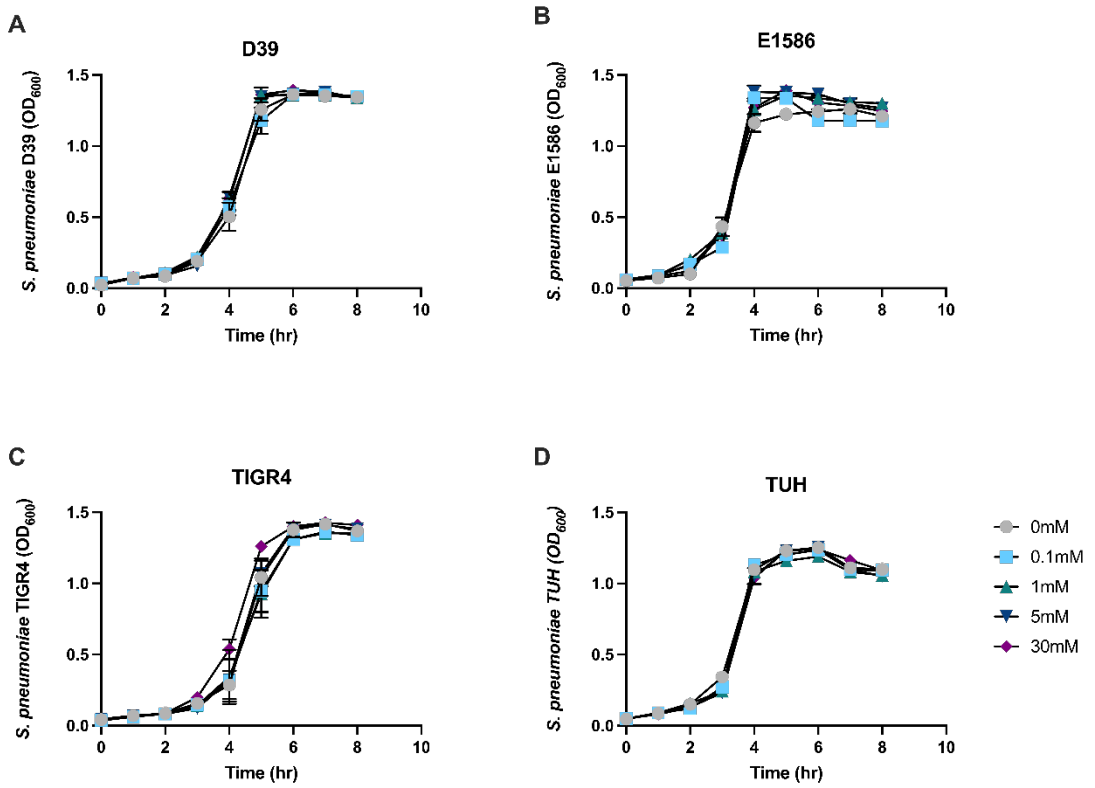


Fig. 3.1 Butyrate does not have direct antimicrobial effects against *S. pneumoniae*. THYB was supplemented with increasing concentrations of butyrate (0mM-30mM), culture containing THYB alone served as a negative control. Each supplemented aliquot of THYB was inoculated with *S. pneumoniae* of each selected serotype. The optical density of the butyrate supplemented cultures was recorded upon initial inoculation and every hour after for an 8-hour period until the stationary growth stage was reached. Data is representative of mean ± SEM where n=3 independent experiments. Data was analysed by one-way ANOVA, using Kruskal-Wallace test. No significant differences were seen. *With thanks to MSc. Filza Masood for performing the growth curves.*

3.2 Butyrate is not cytotoxic at selected working concentrations.

Having shown that butyrate had no direct bactericidal or bacteriostatic effects on any of the pneumococcal strains tested, we proceeded to investigate its effects on macrophages activated via TLR agonists. In early pneumococcal infection there is a shift in population dynamics of lung macrophages. Peripheral macrophages, particularly those from the bone marrow can migrate to the lung parenchyma and adopt an AM-like phenotype [60], [63]. This regeneration of the lung macrophage pool occurs as quickly as 24 hours post infection, so peripherally derived macrophages contribute to the local cytokine milieu later during infection, migrating from the bone marrow to the lung as monocytes and differentiating *in situ* [60], [63]. Therefore, we explored the effects of butyrate in two models: murine FLAMs and BMDMs.

FLAMs were generated by the Carpenter Lab, UCSC, as outlined in Thomas *et al.* 2021 [380], and kindly provided to us by the Cloonan Lab, TCD. The FLAMs served as a model closely recapitulating the phenotype of murine AM, which act in the early defence against pathogenic insult or injury in the lung; whereas murine BMDMs were used to represent monocyte-derived macrophages. Macrophages were seeded as outlined in **section 2.1.9** and allowed to rest overnight. Macrophages were then treated with increasing concentrations of butyrate (0mM to 5mM) overnight. Media containing butyrate was removed and macrophage were subsequently stimulated with the TLR2 ligand Pam3Csk4 (100ng/mL). It has been reported that butyrate, alongside other SCFAs, can exhibit cytotoxicity in the context of malignancy [386], [387], [388]. We wanted to ensure that the immunomodulatory effects of butyrate were not attributed to off-target cytotoxicity in FLAMs mainly as this had never been evaluated on these cells.

After overnight incubation, butyrate concentrations lower than 5mM did not significantly affect the viability of unstimulated FLAMs **(Fig. 3.2 A),** whereas BMDMs were more susceptible showing a dose-dependent increase in cell death from 1mM butyrate **(Fig. 3.2 C).** For both cell lines, TLR ligation after butyrate treatment marginally affected the viability compared to butyrate alone **(Fig. 3.2. B, D).**

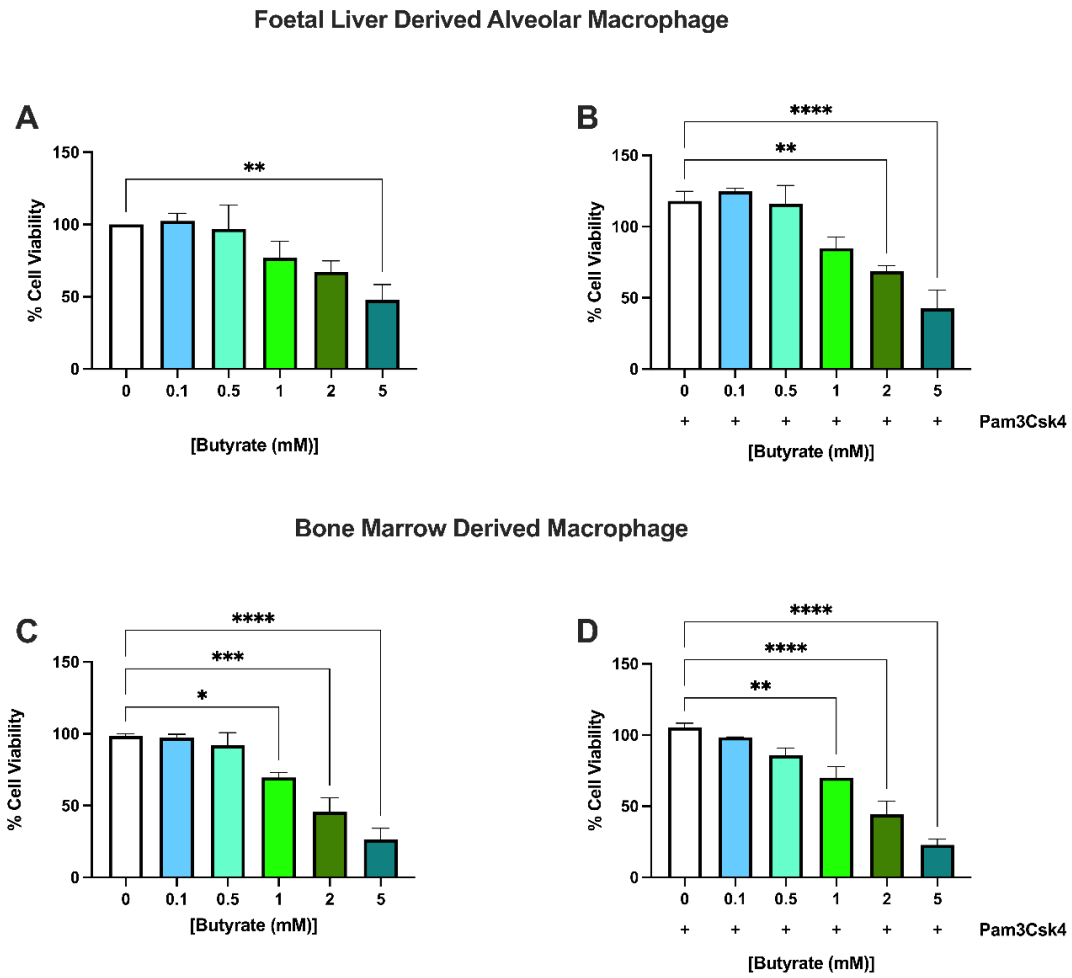


Fig. 3.2 Butyrate marginally affects the viability of FLAMs but BMDMs appear more susceptible to cytotoxicity. Macrophages were seeded as outlined in **section 2.1.9** and pre-treated with butyrate overnight prior to stimulation with Pam3Csk4 (100ng/mL) (**B, D**) for further 24 hours. Cell viability was subsequently measured by crystal violet viability assay. Viability was normalised based on optical density of treatment conditions against that of the negative control (no butyrate, no stimulation). Data is representative of mean ± SEM, where n=4 replicates per condition. Data is analysed by one-way ANOVA, * $p < 0.05$, ** $p < 0.01$, *** $p < 0.001$.

3.3 Butyrate acts as a histone deacetylase inhibitor in FLAMs.

A main mechanism by which butyrate elicits its immunomodulatory effects is through epigenetic regulation, namely through its activity as a histone deacetylase inhibitor (HDACi) [389]. Furthermore, SCFA-driven antimicrobial phenotypes in tissue resident macrophages are associated also with HDACi dependent mechanisms [196], [390], [391]. As this effect yet has to be demonstrated in the context of lung macrophages, we wanted to examine if butyrate could elicit HDACi functions in AMs. To assess this, FLAMs were treated overnight with two low doses (0.1mM and 1mM) of butyrate and were then left untreated or stimulated with the TLR2 agonist Pam3Csk4 (100ng/mL) to assess the HDACi potential of butyrate alone or in response to TLR2 stimulation. Suberoylanilide hydroxamic acid (SAHA) was used at 75nM, an inhibitor of histone deacetylases, served as a positive control in the assay. Total poly-acetylated histone 3 (K9, K14, K18, K23, K27) and 4 (K5, K8, K12, K16) in cellular lysates were then quantified by western blot, densitometry was normalised against β-actin as a reference protein.

Histone deacetylase inhibitor activity results in an accumulation of higher total histone poly-acetylation levels. At 0.1mM, butyrate had no effect on levels of poly-acetylated histones (**Fig. 3.3 A-D**), implying that at this concentration butyrate was not able to engage this pathway to modulate the immune profile of FLAMs. This effect was seen in both, the absence and presence of TLR2 stimulation. However, significant levels of poly-acetylated histone 3 were observed in cells treated with the higher 1mM concentration of butyrate. A significant increase in poly-acetylated histone 3 levels, comparable to that of the positive control was observed in FLAMs treated with 1mM butyrate in the absence of synergistic stimulation (**Fig. 3.3 A**). Of note, this effect was dampened in the presence of TLR2 stimulation (**Fig. 3.3 C**). Similarly, a trending increase ($p = 0.0677$) in poly-acetylated histone 4 was observed in FLAMs treated with 1mM butyrate at baseline (**Fig. 3.3 B**). This trending increase ($p = 0.0535$) in poly-acetylated histone 4 was further demonstrated in cells synergistically stimulated with Pam3Csk4 (**Fig. 3.3 D**). Therefore, 1mM butyrate proved to be an appropriate concentration which shows HDACi activity without noticeable cytotoxicity in FLAMs.

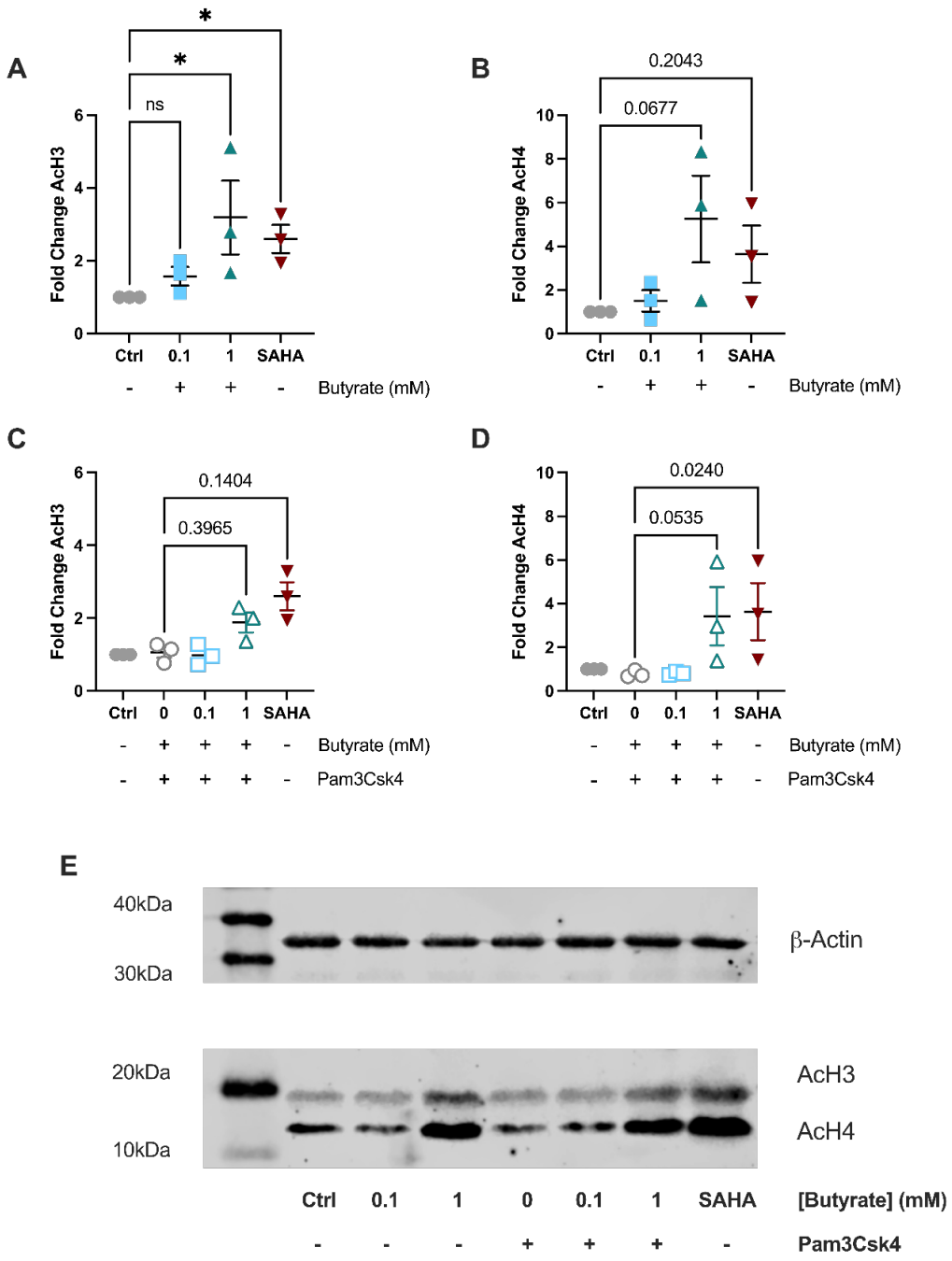


Fig. 3.3 Butyrate elicits histone deacetylase inhibitory activity at low millimolar concentrations in FLAMs. FLAMs were treated with increased concentrations of butyrate (0.1mM and 1mM) overnight in the absence or presence of Pam3Csk4 (100ng/mL). SAHA (75nM) was used as a positive control. Lysates were taken 24hrs post-treatment and analysed for poly-acetylated histone 3 and poly-acetylated histone 4 by western blot. Data shows fold change in acylated histone normalized to the reference protein β-actin, N=3 biological replicates, data analysed by Kruskal-Wallis test, using Dunnett's post-hoc test. Representative blot is from one of the biological replicates.

3.4 *S. pneumoniae* and the synthetic TLR2 agonist, Pam3Csk4, induce global transcriptomic changes in foetal liver derived macrophages (FLAMs).

Having characterised the direct effects of butyrate on *S. pneumoniae* growth or cytotoxicity on murine macrophages, the next step was to analyse the effects of the SCFA on the global transcriptional profile of FLAMs under resting conditions or stimulation with a TLR2 agonist or live *S. pneumoniae*. The transcriptomic profile of primary AMs and other AM cell lines to pneumococcal infection has been characterised [179], [195], [253]. However, the transcriptomic profile of FLAMs derived from the model established by Thomas *et al*. 2022, has not yet been characterised in the context of pneumococcal infection [380]. **Therefore, we first aimed to characterise the global transcriptomic signature of FLAMs in response to *S. pneumoniae*, D39 infection and TLR2 ligation before further analysing the effects of butyrate on their transcriptomic response to infection.**

FLAMs were seeded and rested for 24 hours prior to infection with *S. pneumoniae* serotype 2 D39 for one hour. Media containing bacteria was then removed and cells were allowed to rest in antibiotic-free media for a further 4 hours. In parallel, FLAMs were stimulated with the synthetic TLR2 agonist, Pam3Csk4 (500ng/mL) for 4 hours. Cells were then lysed and total RNA was isolated in house. Bulk mRNA sequencing was performed on Illumina NovaSeq platform using 150bp paired-end sequencing at Novogene headquarters UK. Data was normalised using EdgeR method, followed by Benjamini-Hochberg method of calculating FDR and identifying differentially expressed genes (DEGs) between samples. Highly significant DEGs were considered those demonstrating $p_{adj} < 0.05$, Log2FC ± 2, while trending DEGs were acknowledged as genes within the threshold of $p_{adj} < 0.05$, Log2FC ± 1.

Infection of FLAMs with *S. pneumoniae* resulted in an enhancement in inflammatory signalling pathways, as identified by GSEA enrichment analysis (**Fig. 3.4 C**), at 4 hours post-infection. We subsequently investigated expression of genes encoding inflammatory cytokines, monocyte and neutrophil chemoattractants, and PRRs which have reported to play roles in host response to pneumococcal infection [243], [221],

[392], [230], [232], [225], [226], [393], [394] as shown in the heatmaps in **Fig. 3.4 B** and **Fig. 3.5 B.** Genes were only considered for inclusion in heatmaps providing LogFC > 1 and p_{adj} < 0.05. Significant increases in *Tnf* (p_{adj} = < 0.001, Log2FC = 6.576), *Il1b* (p_{adj} = < 0.001, Log2FC = 7.571) and *Il6* (p_{adj} = < 0.001, Log2FC = 10.236) were found. Similarly, transcripts of inflammatory cytokines *Ccl2*, *Cxcl10*, *Cxcl9*, *Il12b*, *Ifnb1*, *Il1a* and *Cxcl1* were significantly upregulated in *S. pneumoniae* infected cells compared to controls (**Fig. 3.4 A, B**). Pattern recognition receptors, *Tlr2* (p_{adj} = < 0.001, Log2FC = 2.412) which serves as the cognate receptor for peptidoglycan and lipopeptide residues was significantly upregulated, as was *Nod2* (p_{adj} = < 0.001, Log2FC = 2.136) and *Nlrp3* (p_{adj} = < 0.001, Log2FC = 3.328), which can sense gram-positive lipoteichoic acid and peptidoglycan and pneumococcal derived pneumolysin respectively [225], [230], [221], [392].

Similarly, cells that were stimulated with the TLR2 ligand Pam3Csk4 exhibited global transcriptomic shift and enhancements in inflammatory signalling pathways (**Fig. 3.5 C**). Highly significant pathways enriched in cells treated with Pam3Csk4 broadly encompassed response to inflammatory stimuli, cellular stress, growth response and cytokine signalling (**Fig. 3.5 C**). Heightened expression of Tlr2 was detected in samples stimulated with Pam3Csk4, (p_{adj} = < 0.001, Log2FC = 2.261). Similarly, *Nod2* expression was increased (p_{adj} = < 0.001, Log2FC = 2.752), as was *Nlrp3* (p_{adj} = < 0.001, Log2FC = 3.964). Again, inflammatory cytokines *Ccl2*, *Cxcl10*, *Cxcl9*, *Il12b*, *Ifnb1*, *Il1a* and *Cxcl1*, were transcriptionally upregulated as were *Il6, Tnf* and *Il1b* (**Fig. 3.5 A, B**).

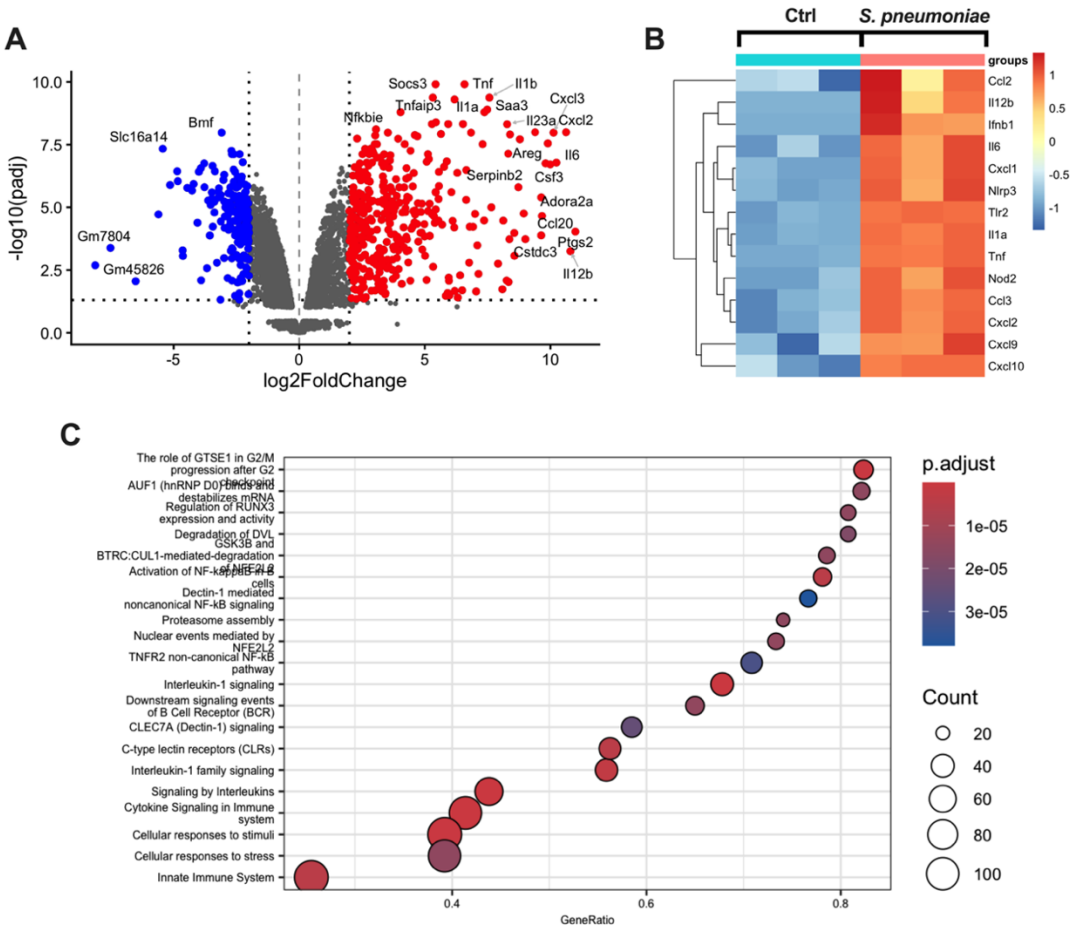


Fig. 3.4 FLAMs upregulate expression of inflammatory pathways in response to *S. pneumoniae in vitro*. FLAMs were infected with *S. pneumoniae* serotype 2 (D39) at an MOI of 5:1, as per the protocol outlined in the section (**2.3.2**) or left untreated (Ctrl). Total RNA was isolated from FLAMs and processed for bulk mRNA-sequencing. Data was processed using the EdgeR method of normalisation, adjusted p-values were determined using the Benjamini-Hochberg method. Parameters for significance were set to $P_{adj} > 0.05$ and logFC > 2, select genes crossing this threshold were included in the volcano plot and heatmap (**A, B**). GSEA enrichment analysis was completed with the threshold of pathway significance set to $P_{adj} < 0.05$, with 10 – 500 genes in reported pathways, the top 20 pathways are shown (**C**). Data is representative of 3 biological triplicates in each group.

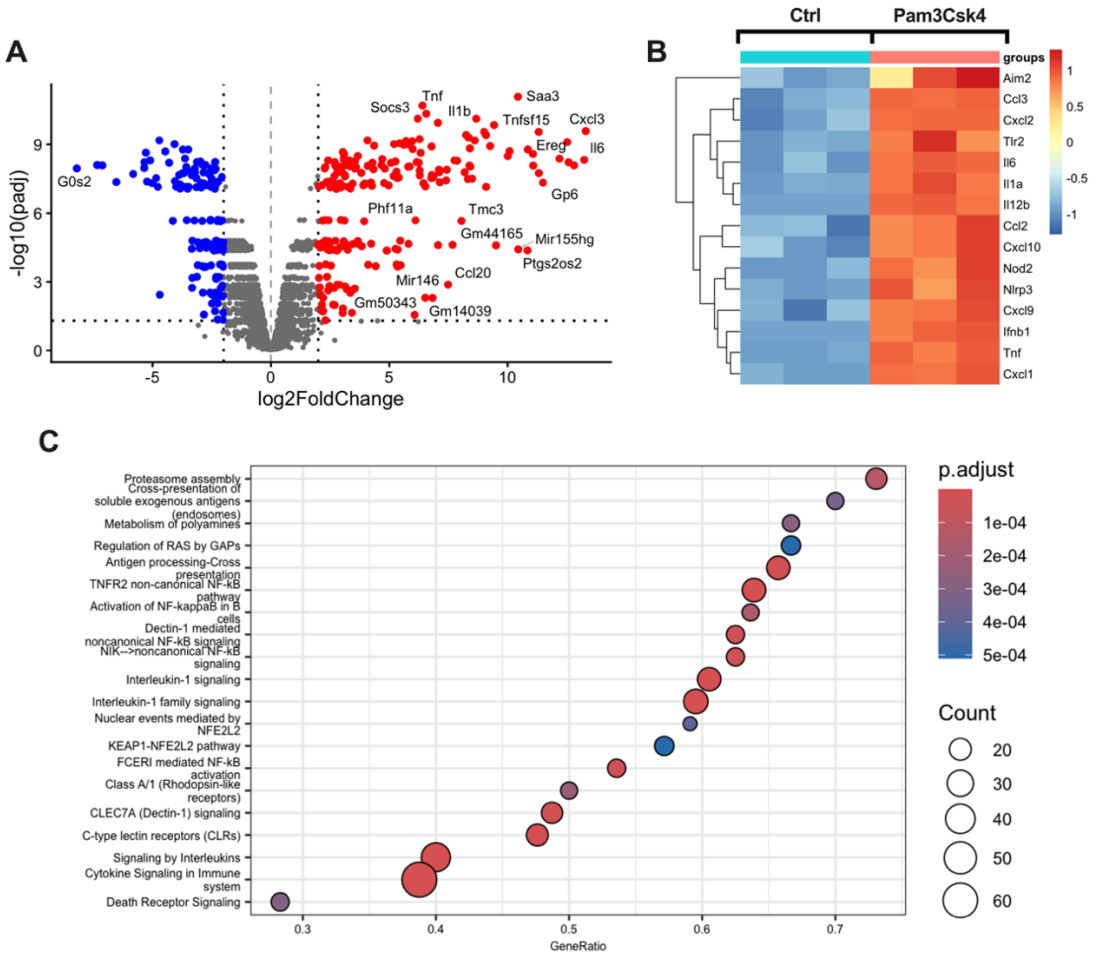


Fig. 3.5 FLAMs upregulate expression of inflammatory pathways in response to TLR2 stimulation *in vitro*. FLAMs were stimulated with Pam3Csk4 (500ng/mL) for 4 hours, as per protocol outlined previously (**2.3.2**) or left untreated (Ctrl). Total RNA was isolated from FLAMs and processed for bulk mRNA-sequencing. Data was processed using EdgeR method of normalisation, adjusted p-values were determined using the Benjamini-Hochberg method. Parameters for significance were set to $P_{adj} > 0.05$ and logFC > 2, select genes crossing this threshold were included in the volcano plot and heatmap (**A, B**). GSEA enrichment analysis was completed with the threshold of pathway significance set to $P_{adj} < 0.05$, with 10 – 500 genes in reported pathways, the top 20 pathways are shown (**C**). Data is representative of 3 biological triplicates in each group.

The role of TLR2 in pneumococcal infection is outlined in section 1.4.3. Therefore, we selected the potent synthetic TLR2 ligand Pam3Csk4, to further investigate the effects of butyrate-mediated immune modulation on AM response to specific engagement of TLR2 pathway. This additionally allowed us to compare live infection with a defined activator of the TLR2 pathway on FLAMs which has not been done before (**Fig. 3.6 A**). *S. pneumoniae* infected samples had a distinct transcriptomic signature from all other samples with PC3 variation accounting for 9% of total variation between samples (**Fig. 3.6 A**).

GSEA enrichment analysis was carried out as before, setting the threshold of pathway detection to $p_{adj} < 0.05$, with a minimum threshold of 10 to a maximum of 500 genes in select pathways. Gene set enrichment analysis (GSEA) comparing cells infected with *S. pneumoniae* versus stimulation with synthetic TLR2 ligation highlighted a range of pathways, some of which included the following: *ISG15 antiviral mechanism, respiratory electron transport, mitochondrial protein degradation and interferon signalling* (**Fig. 3.6 B**). The main mechanism of TLR2 ligation results in downstream signalling through the adaptor protein MyD88, however non-canonical signalling has been observed through engagement of TRAM and subsequent downstream production of type I IFNs [395], [396]. It is worth noting that a mechanism by which *S. pneumoniae* intracellularly induces production of type I IFN is the release of bacterial DNA which activates the cGAS-STING pathway, a mechanism which would only occur in the case of infection with live bacteria expressing intact pneumolysin [236]. However, it appears in this case that additional signals are required beyond TLR2 ligation for the engagement of IFN production. This also applied in the case of "*Interleukin-1 family signalling*", another pathway significantly differentially expressed between *S. pneumoniae* infected FLAMs and those stimulated purely though TLR2 (**Fig. 3.6 C**). Highly upregulated genes in *S. pneumoniae* infected cells compared to Pam3Csk4 stimulated counterparts include Krüppel-like factor 4 (*Klf4*) and Run and FYVE domain-containing protein 4 (*Rufy4*). *Klf4* has been implicated to have a central role in maintaining the AM phenotype [55]. Activity of *Rufy4* is implicated in autophagy and macro autophagy in dendritic cells and crucially AMs [397], [398].

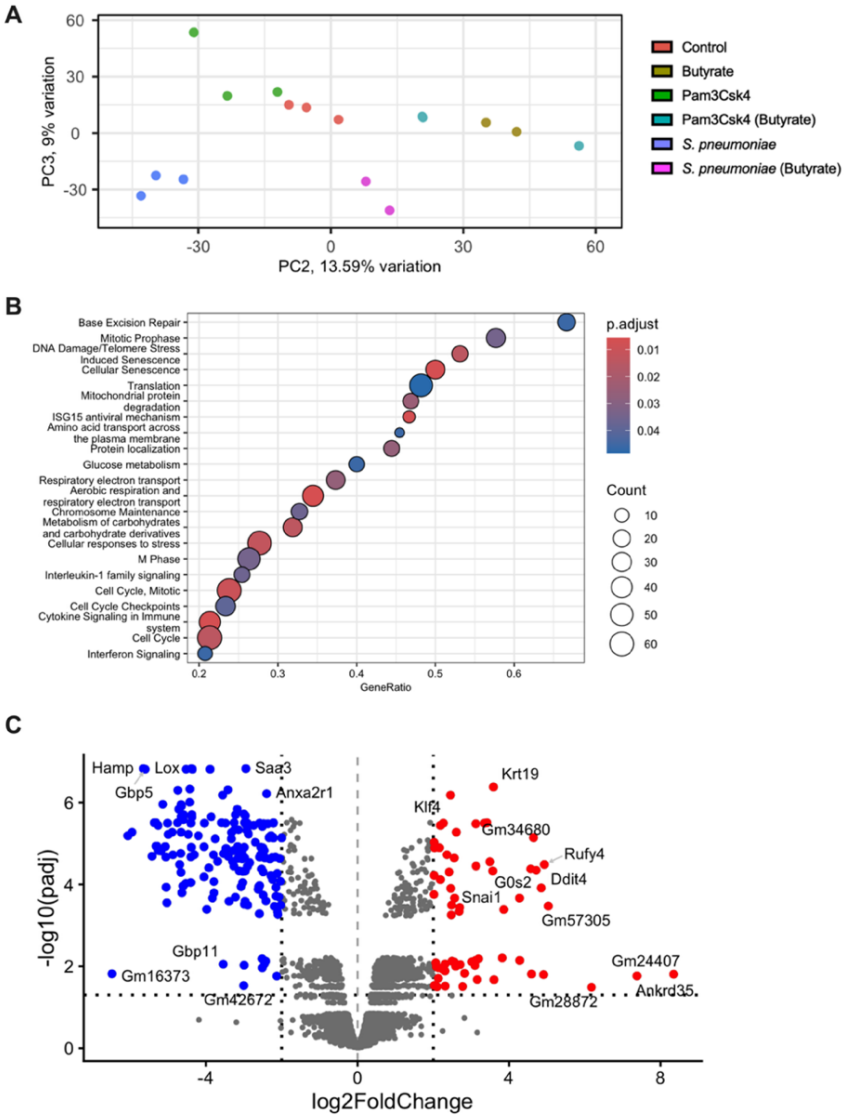


Fig. 3.6 Differentially regulated pathways in FLAMs in response to *S. pneumoniae* live infection *versus* TLR2 stimulation. FLAMs were stimulated with Pam3Csk4 (500ng/mL) for 4 hours, as per protocol outlined previously (**2.3.2**). Total RNA was isolated from FLAMs and processed for bulk mRNA-sequencing. Data was processed using EdgeR method of normalisation, adjusted p-values were determined using the Benjamini-Hochberg method. Parameters for significance were set to $P_{adj} > 0.05$ and logFC > 2, select genes crossing this threshold were included in the volcano plot (**C**). Heatmap is representative of distinction of variance in *S. pneumoniae* infected samples to all other samples, as represented on the y-axis (PC3) (**A**). from GSEA enrichment analysis was completed with the threshold of pathway significance set to $P_{adj} < 0.05$, with 10 – 500 genes in reported pathways, the top 20 pathways are shown (**B**). Data is representative of n=2/3 biological replicates in each group.

3.6 Butyrate enhances antimicrobial pathways in AM upon infection.

Next, we wanted to establish the effects of butyrate pre-treatment on FLAMs in their native state or subsequently infected with *S. pneumoniae* or stimulated with Pam3Csk4. FLAMs were pre-treated with butyrate (1mM) overnight as per protocol outlined in section **2.1.8**. Subsequently the cells were treated either with media alone (**Fig. 3.7**), infected with *S. pneumoniae*, D39 (**Fig. 3.9**) or stimulated with Pam3Csk4 (**Fig. 3.10**) as described previously. Bulk mRNA sequencing outputs were analysed as described and inclusion of DEGs in heatmaps conformed to thresholds outlined in section **3.2.6**.

We first wanted to determine the effects of butyrate treatment in the absence of an immunostimulant (**Fig. 3.7**). It was noted that butyrate treatment across all conditions induced a transcriptionally distinct profile, in which PC3 represents variation (13.59%) between all butyrate treated samples and untreated controls as outlined (**Fig. 3.7 A**). Additionally, pathways regulating the cell cycle were differentially negatively regulated across all treatments with butyrate in both, the unstimulated (media) and stimulated (*S. pneumoniae* infection and Pam3Csk4) settings, (**Fig. 3.7 C**), (**Fig. 3.8**). Stasis in cell cycle can be a sign of cellular senescence. Recent studies by Zhang *et al.* 2025, demonstrate that *in vivo* during infection with *S. pneumoniae* AMs can enter a senescent state, potentially unravelling the "macrophage disappearance" seen post lung infection or injury [63]. Senescence is generally associated with deleterious outcomes, as senescent macrophage can generate an inflammatory milieu, promoted by senescence associated proteins (SASP), which could contribute to an inflammatory microenvironment in the lung [399]. Senescent AMs have been additionally recognised to contribute to the lung tumour microenvironment [400]. However, several markers associated with AM cellular senescence were not differentially regulated (**Table 3.1**) [63].

Gene ontology (GO) GSEA highlighted that butyrate upregulated innate immune defence against gram-positive bacterial pathways: "*defence response to a Gram-positive bacterium*", "*defence response to a bacterium*", "*response to bacterium*", and "*regulation of innate immune response*" across all conditions treated with butyrate

treatments (**Fig. 3.8**). GSEA Kyoto encyclopaedia of genes and genomes (KEGG) similarly highlighted that "*NOD-like receptor signalling pathway*", "*chemical carcinogenesis – reactive oxygen species"* and "*lysosome"* were upregulated in butyrate treated samples across all conditions, while autophagy was only upregulated in butyrate treated unstimulated or infected samples (**Fig. 3.8**). For individual comparisons GSEA Reactome analysis was additionally run based on criteria outlined in **section 3.4**; butyrate-treated *versus* untreated *S. pneumoniae* samples and butyrate-treated *versus* untreated samples stimulated with Pam3Csk4 (Appendix).

We then investigated the transcriptional regulation of selected anti-microbial peptides (AMPs) and DEGs included in the categories "*Innate immune system*" and "*Neutrophil degranulation*" respectively (Appendix). We noted that butyrate treatment enhanced active transcription of multiple AMPs with dual roles in response to pneumococcal infection, namely Lactotransferrin (*Ltf*) and Neutrophil gelatinase protein, also known as lipocalin 2 (*Ngp*, also *Lcn2*) in cells stimulated with Pam3Csk4 or *S. pneumoniae* (**Fig. 3.9 B**), (**Fig. 3.10 B**). Lactotransferrin has a dual function in host response to pneumococcal infection, eliciting antimicrobial functionality through competitive iron sequestration and DNAse activity [401], [242].

Similiarly, we noted upregulation of several ribonucleases which have reported antimicrobial functions, *Rnase2a* (LogFC 2.968, $p_{adj} < 0.05$), *Rnase2b* (LogFC 3.7657, $p_{adj} < 0.001$), *Rnase6* (LogFC 1.5832, $p_{adj} < 0.05$), *Ear1* (LogFC 2.1176, $p_{adj} < 0.001$), *Ear2* (LogFC 1.3905, $p_{adj} < 0.01$) and *Ear6* (LogFC 1.7881, $p_{adj} < 0.001$) in butyrate-treated cells in response to pneumococcal infection and Pam3Csk4 stimulation (**Fig. 3.9 B**), (**Fig. 3.10 B**). An antimicrobial role of host RNases in infection has been recently characterised, extracellular RNA, which can arise in the setting of infection induced pyroptosis and necroptosis, has been shown to bind pneumococci and facilitate internalisation through pneumococcal enolase [402]. Internalisation can facilitate bacterial clearance; however it can also allow facultative intracellular invasion and survival of the bacteria. This same study highlighted that treatment with RNAse 1 inhibited this extracellular RNA-mediated invasion of host cells, indirectly implicating a potential role of RNAses in preventing pneumococcal invasion of host cells during active infection [402].

Additional antimicrobial genes in butyrate-treated macrophages infected with D39 that demonstrated increases were *S100a9* (LogFC 1.1903, $p_{adj} < 0.05$), lactoferrin (*Ltf*) (LogFC 2.052, $p_{adj} < 0.001$) and neutrophilic granule protein also known as lipocalin 2 (*Ngp*) (LogFC 3.418, $p_{adj} < 0.001$). Additionally, the lysosomal pathway was enriched in KEGG analysis (**Fig. 3.8 B**). Lysosomal activity is imperative in host response to pneumococcal infection through intracellular bacterial clearance. The recent literature supports an effect of butyrate in enhancing lysosomal function in response to bacterial infection [107].

GSEA gene ontology (GO) enrichment analysis highlighted that butyrate treatment upregulated pathways responsive to viral insult, namely "*defence response to virus*", "*negative regulation of viral process*" and "*response to virus*" (**Fig. 3.8**). Upon further investigation of the top hundred highly expressed genes, many genes coding guanylate binding proteins and those involved in IFN signalling were significantly enhanced. This signature appeared in butyrate-treated cells across both *S. pneumoniae* infected cells and those stimulated with Pam3Csk4 (**Fig. 3.8**). This was in fitting with the induction of transcriptional regulation of IFN-related pathways in *S. pneumoniae* infected cells compared to those stimulated with Pam3Csk4 (**Fig. 3.6**). Pattern recognition receptors known to activate downstream type I and type III IFN production, include STING (*Tmem173*), RIG-I (*Rigi*), MDA5 (*Ifih1*), TLR3 (*Tlr3*), TLR4 (*Tlr4*), TLR7/8 (*Tlr7, Tlr8*) and TLR9 (*Tlr9*) [403]. Therefore, we investigated these PRRs and downstream IRFs, the transcription factors responsible for induction of type I IFNs in the setting of butyrate pre-treatment and subsequent infection with *S. pneumoniae*. As outlined in the introduction, the cGAS-STING axis holds a mechanistic role in pneumococcal defence through recognition of host-DNA during cellular damage or inflammatory cell death or cGAS-mediated binding of bacterial DNA [236]. STING (*Tmem173*) (LogFC -1.3058, $p_{adj} < 0.001$) and downstream IRF elements of STING IRF3 (*Irf3*) (LogFC 0.291, $p_{adj} = 0.46066$) did not demonstrate any significant positive differential expression. Activation of STING via. cGAS recognition of cyclic dinucleotides or foreign or host DNA results in preferential activation of downstream IRF3, so we concluded that this pathway was not activated in the setting of butyrate modulation [404]. However positive differential expression was noted in the case of alternative dsDNA sensors, namely MDA5 (Ifih1)

(LogFC 1.9705, $p_{adj} < 0.01$) and RIG-I (*Rigi*) (LogFC 2.3615, $p_{adj} < 0.001$) (**Fig. 3.11**). While *Irf3* was not significantly differentially expressed, IRF7 (*Irf7*) (LogFC 2.7873, $p_{adj} < 0.01$) expression was significantly enhanced, similarly IRF7 is typically activated downstream of MAVS-TBK1 [405]. Transcription of IRF9 (*Irf9*) (LogFC 1.4732, $p_{adj} < 0.001$) was also significantly enhanced, implicating enhanced feedback of type I IFNs in an autocrine manner. Interferon signalling was increased in cells infected with pneumococci compared to TLR2 ligation, albeit we wanted to investigate if butyrate-driven transcriptional enhancement of IFN stimulated genes applied in response to stimulation with Pam3Csk4. Interestingly, trending increases in *Ifih1* (LogFC = 0.9771, $p_{adj} < 0.05$), *Rigi* (0.8325, $p_{adj} < 0.05$) and IRF7 (LogFC = 1.7043, $p_{adj} < 0.05$) was observed, while subtle but not trending effects were observed in *Irf9* (0.5366, 0.04654) expression, implicating a lower threshold of type I IFN-mediated autocrine signalling (**Fig. 3.11**).

In conclusion butyrate in the absence of an immunostimulant has modulatory roles in cell cycle processes as outlined in **Fig. 3.7**. However, butyrate treated cells, once stimulated or infected readily enhance transcriptional regulation of anti-microbial defences (**Fig. 3.8**), (**Fig. 3.9**), (**Fig. 3.10**).

Table 3.1 Genes associated with cellular senescence.

Gene	Media (Butyrate v. Control)		*S. pneumoniae* (Butyrate v. Control)		PamCSK4 (Butyrate v. Control)	
	LogFC	FDR	LogFC	FDR	LogFC	FDR
Cdnk1a	0.50214	0.51325	0.18945	0.85134	0.630287	0.065032
Cdnk2a	-0.03907	0.97335	0.74947	0.13504	-0.12472	0.59362
Sirt1	0.25208	0.65656	0.33430	0.49449	0.50282	0.09269
Sirt2	0.31174	0.52500	-0.05001	0.94682	-0.24671	0.42496
Ptsg1	-0.02734	0.96975	-0.11301	0.81059	-0.23275	0.31737

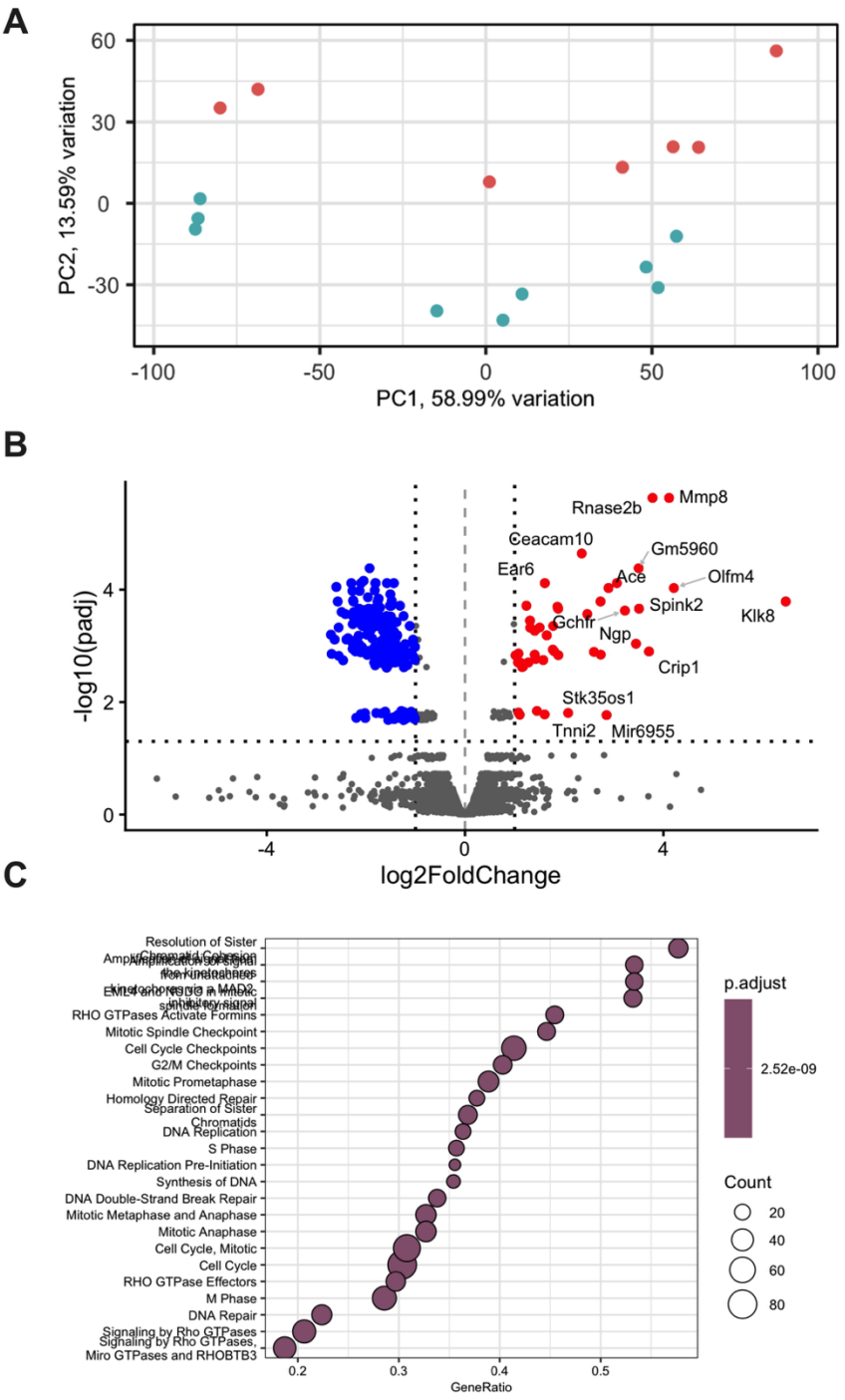


Fig. 3.7 Butyrate treatment alone influences the transcriptional regulation of the cell cycle. FLAMs were treated overnight with butyrate (1mM). Media containing butyrate was removed and cells were infected with *S. pneumoniae* D39, as per outlined protocol (**2.3.2**). Total RNA was isolated from FLAMs and processed for bulk mRNA-sequencing. Data was processed using EdgeR method of normalisation, adjusted p-values were determined using the Benjamini-Hochberg method. Parameters for significance were set to $P_{adj} > 0.05$ and logFC > 2, select genes crossing this threshold were included in the volcano plot (**A**), while the trending threshold was set to $P_{adj} > 0.05$ and logFC > 2 in inclusion of genes in the heatmap (**B**). GSEA enrichment analysis was completed with the threshold of pathway significance set to $P_{adj} < 0.05$, with 10 – 500 genes in reported pathways, the top 20 pathways are shown (**C**). Data is representative of n=2/3 biological replicates in each group.

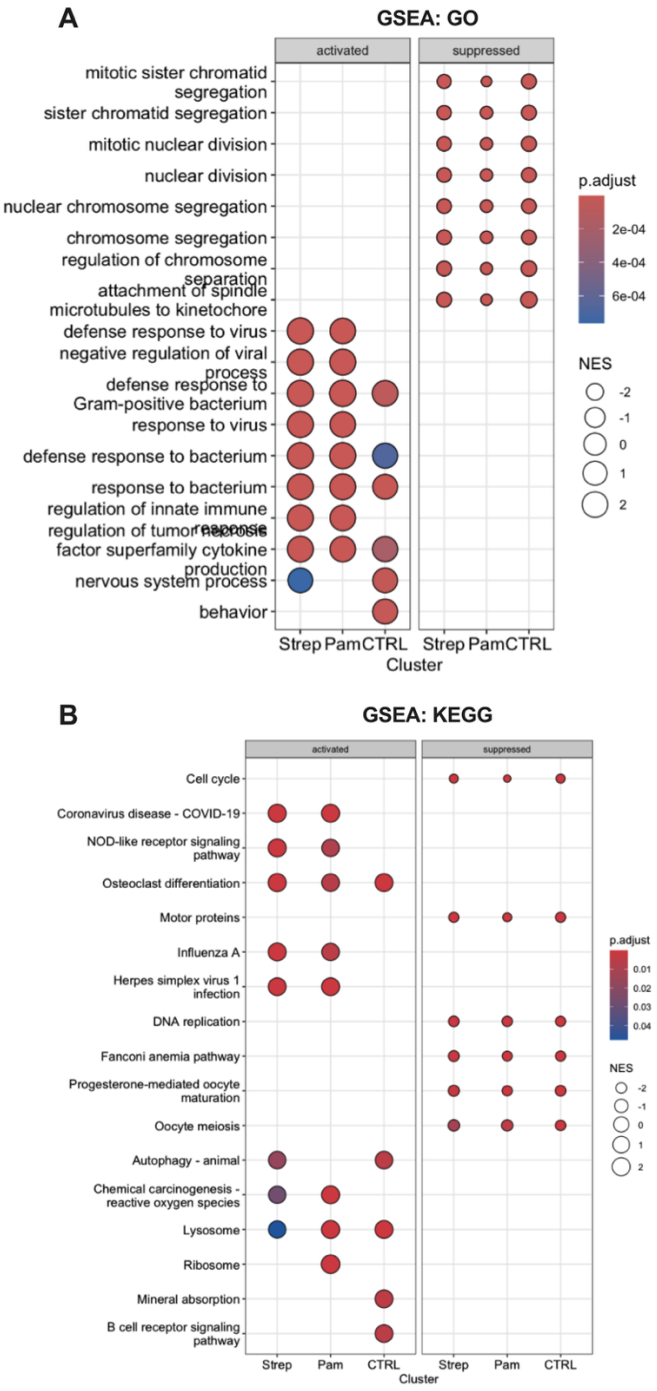


Fig. 3.8 Butyrate stimulates the expression of genes involved in host innate defence, while regulating cell cycle in AM. FLAMs were treated overnight with butyrate (1mM). Media containing butyrate was removed and cells were stimulated with media alone (CTRL), stimulated with Pam3CSk4 (500ng/mL) for 4 hours (Pam) or infected with *S. pneumoniae* D39 (Strep), as per outlined protocol (**2.3.2**). Total RNA was isolated from FLAMs and processed for bulk mRNA-sequencing. Data was processed using EdgeR method of normalisation, adjusted p-values were determined using the Benjamini-Hochberg method. KEGG and GO GSEA enrichment analysis was completed with the threshold of pathway significance set to $P_{adj} < 0.05$ (**C**). Data is representative of n=2/3 biological replicates in each group.

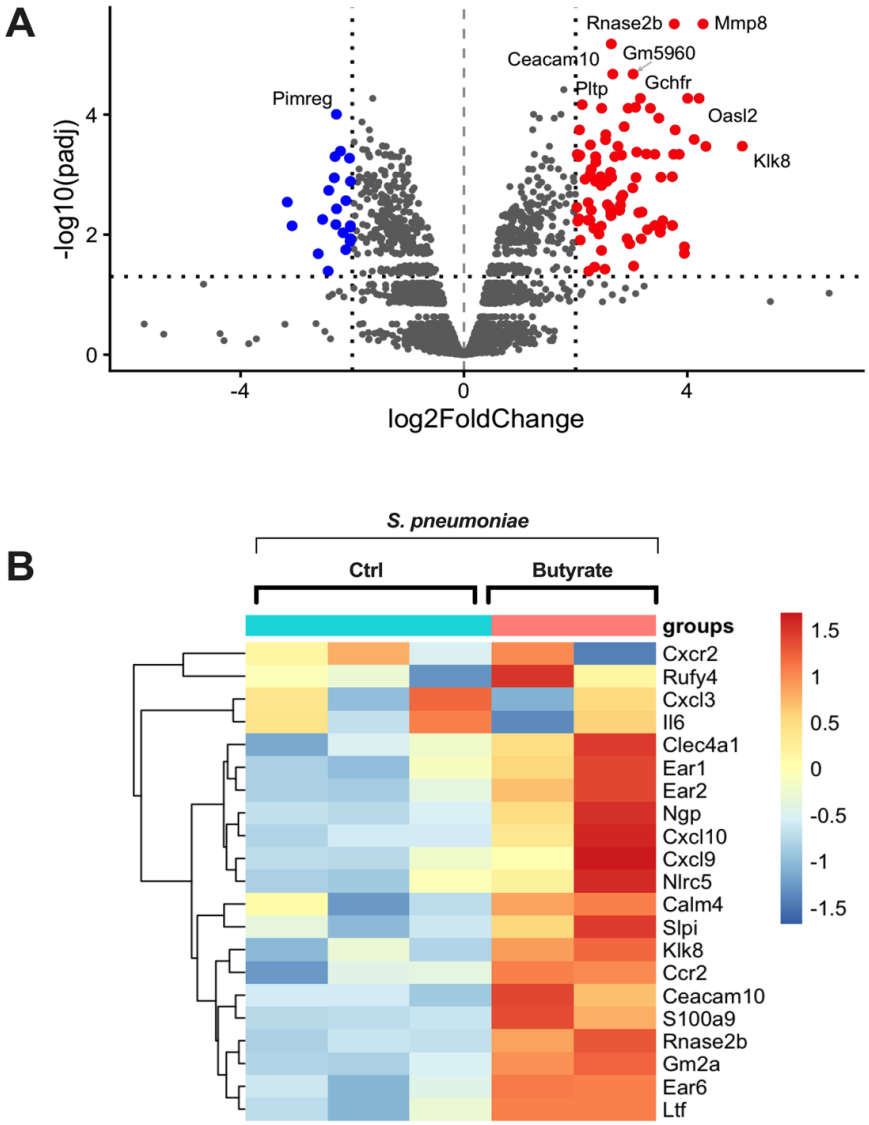


Fig. 3.9 Butyrate stimulates the expression of genes involved in host innate defence, while regulating cell cycle in cells infected with *S. pneumoniae*, D39. FLAMs were treated overnight with butyrate (1mM) and subsequently media containing butyrate was removed and cells were infected with *S. pneumoniae* D39, as per outlined protocol (**2.3.2**). Total RNA was isolated from FLAMs and processed for bulk mRNA-sequencing. Data was processed using EdgeR method of normalisation, adjusted p-values were determined using the Benjamini-Hochberg method. Parameters for significance were set to $P_{adj} > 0.05$ and logFC > 2, select genes crossing this threshold were included in the volcano plot (**A**), while the trending threshold was set to $P_{adj} > 0.05$ and logFC > 1 in inclusion of genes in the heatmap (**B**). Data is representative of n=2/3 biological replicates in each group.

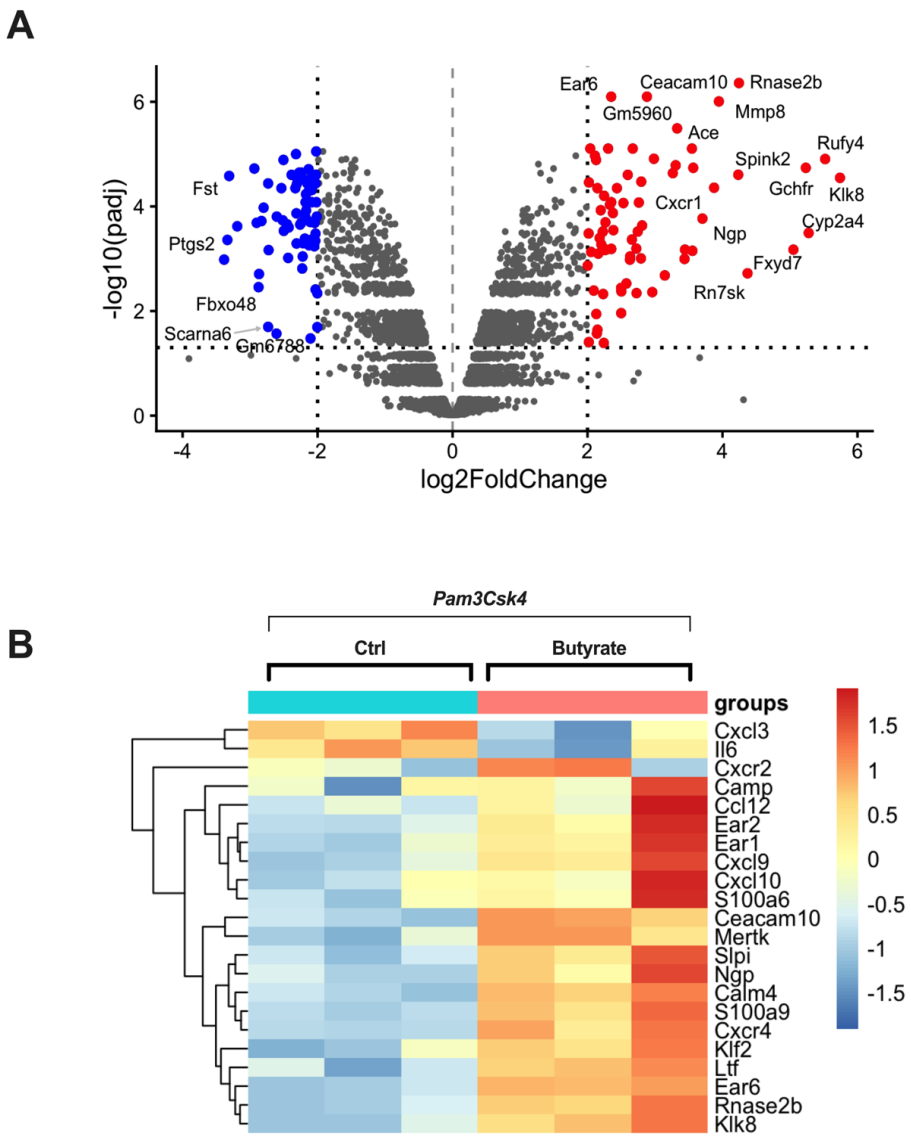


Fig. 3.10 Butyrate stimulates the expression of genes involved in host innate defence, while regulating cell cycle in cells stimulated with the TLR2 ligand, Pam3Csk4. FLAMs were treated overnight with butyrate (1mM) and subsequently media containing butyrate was removed and cells were stimulated with Pam3Csk4 (500ng/mL) for 4 hours. Total RNA was isolated from FLAMs and processed for bulk mRNA-sequencing. Data was processed in R studio using EdgeR method of normalisation, adjusted p-values were determined using the Benjamini-Hochberg method. Parameters for significance were set to $P_{adj} > 0.05$ and logFC > 2, select genes crossing this threshold were included in the volcano plot (**A**), while the trending threshold was set to $P_{adj} > 0.05$ and logFC > 1 in inclusion of genes in the heatmap (**B**). Data is representative of biological triplicates in each group.

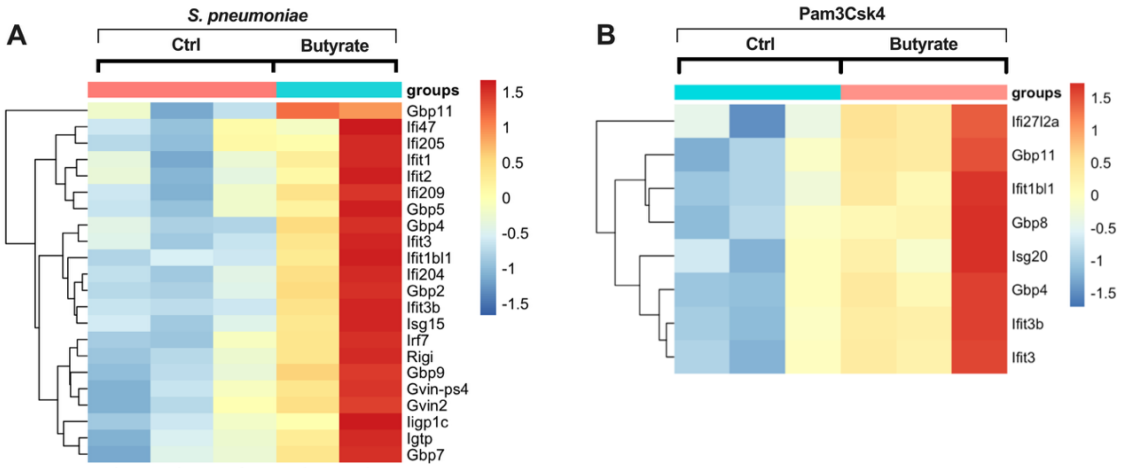


Fig. 3.11 Butyrate upregulates genes implicated in interferon signalling pathways. FLAMs were treated overnight with butyrate (1mM) and subsequently media containing butyrate was removed and cells were simulated with Pam3cSK4 (500ng/mL) for 4 hours (**B**) or infected with *S. pneumoniae* D39 (**A**), as per outlined protocol (**2.3.2**). Total RNA was isolated from FLAMs and processed for bulk mRNA-sequencing. Data was processed using EdgeR method of normalisation, adjusted p-values were determined using the Benjamini-Hochberg method. The trending threshold was set to $P_{adj} > 0.05$ and logFC > 1 for inclusion of genes in the heatmap (**B**). Data is representative of n=2/3 biological replicates in each group.

3.7 Butyrate modulates cytokine milieu of alveolar-like macrophage in response to inflammatory stimuli.

Short-chain fatty acids can alter the inflammatory profile of immune cells, as outlined in the introduction **section 1.6.1**. There is evidence that micromolar concentrations of butyrate can inhibit NFκB responses in a HDACi dependent manner in macrophages in which IL-6, IL-12 and TNF-α levels were reduced but not IL-10 [187]. Similar, results have been documented in human PBMCs in which butyrate gas inhibited NFκB dependent cytokines [189], [188]. SCFA-mediated modulation of inflammatory cytokines has been investigated in the AM cell line, MH-S. SCFAs were found to inhibit IL-6 upon LPS stimulation in a similar manner to trichostatin A treatment implicating a role of SCFA-mediated HDACi in reduction of IL-6 [180]. Notably, butyrate did not modify basal expression of IL-6 or TNF-α either FLAMs or BMDMs. No elevation in cytokine production was detected at any of the concentrations of butyrate pre-treatment (**Fig. 3.12**).

When stimulated with the TLR2 ligand, butyrate pre-treatment did not appear to modulate TNF-α or IL-6 production at any of the shown concentrations in FLAMs and BMDMs (**Fig. 3.12 A, B, C, D**). However, a significant suppression of IL-6 production by butyrate pre-treatment was observed in both cell types stimulated with the TLR2 ligand Pam3Csk4 at concentrations that did not affect viability **(Fig. 3.13 B, D),** but not TNF-α (**Fig. 3.13 A, C**). These data suggest that butyrate has an anti-inflammatory effect on both BMDMs and FLAMs, with selective suppression of IL-6 as a characteristic signature of butyrate-mediated modulation of cytokine production in both FLAMs and BMDMs. It is important to highlight that this result is in line with published studies on intestinal macrophages, the RAW267.4 macrophage cell line, human PBMCs and MH-S AM [390], [188], [187], [189], [190], [125].

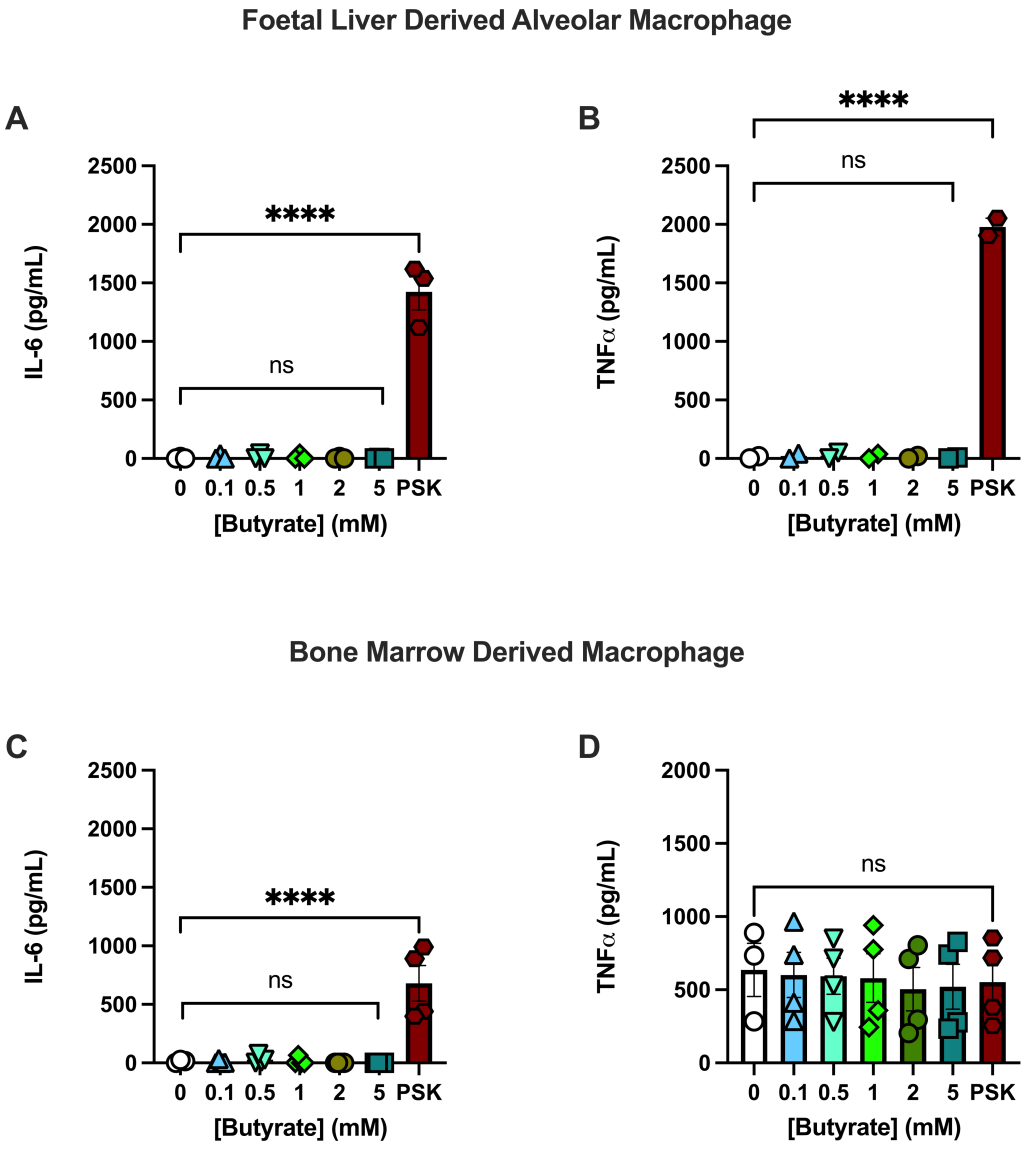


Fig. 3.12 Butyrate preferentially suppresses IL-6 in both bone marrow derived macrophage (BMDM) and FLAM (FLAM). Macrophages were seeded and pre-treated with increasing concentrations of butyrate overnight (0mM-5mM). Macrophages were subsequently rested for a further 24 hours in complete media. Supernatants were collected for downstream analysis of cytokines TNF-α and IL-6 by ELISA. PSK represents cells stimulated with Pam3Csk4 (100ng/mL) as a positive control. Graphs are representative of FLAMs (**A, B**) and BMDMs (**C, D**). Data is representative of mean ± SEM, where n=2-4 experimental replicates per group. Data was analysed using one-way ANOVA with Dunnett's post-hoc test.

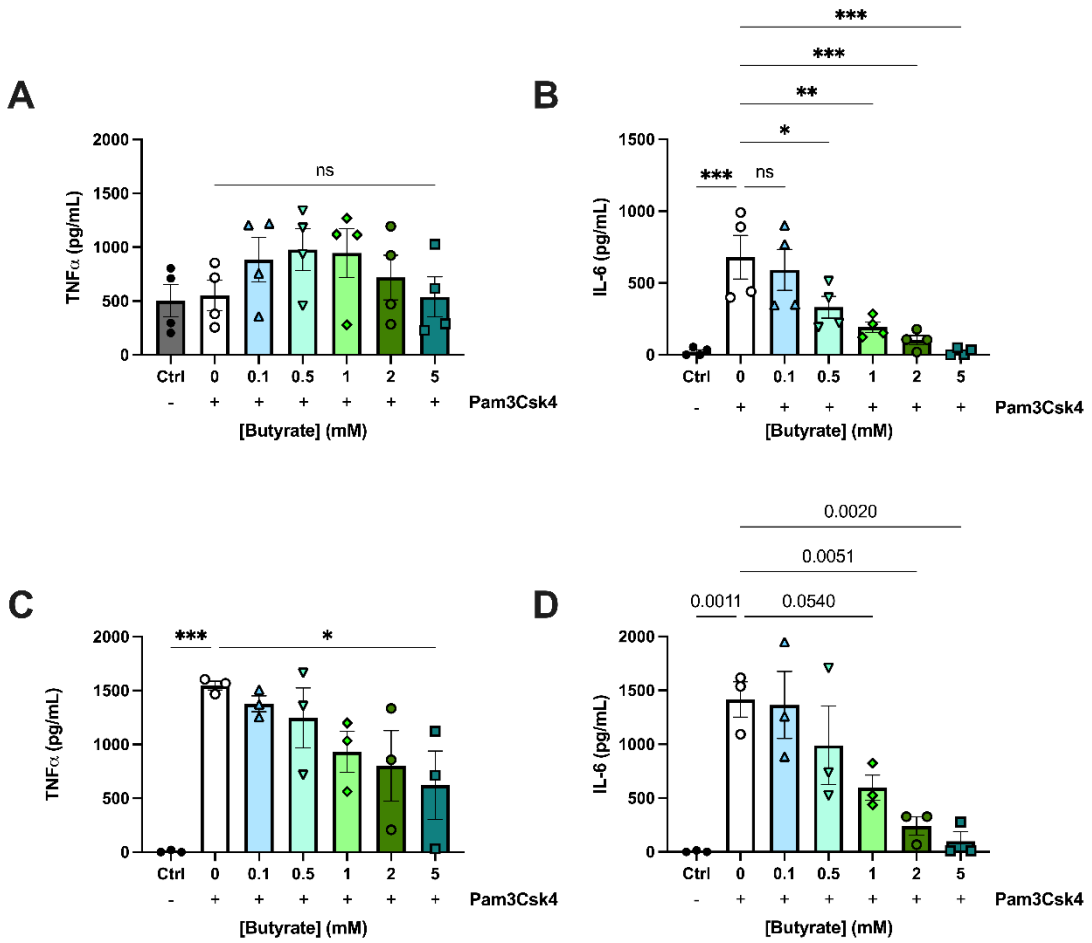


Fig. 3.13 Butyrate preferentially suppresses IL-6 in both bone marrow derived macrophage (BMDM) and FLAMs. Macrophages were seeded and pre-treated with increasing concentrations of butyrate overnight (0mM-5mM). Macrophages were subsequently stimulated with Pam3Csk4 (100ng/mL) for 24 hours. Supernatants were collected for downstream analysis of the cytokines TNF-α, IL-6 and IL-10 by ELISA. Graphs are representative of BMDMs (A-F) and FLAMs (G, H). Data is representative of mean ± SEM, where n=2/4 experimental replicates per group. Data was analysed using one-way ANOVA with Dunnett's post-hoc test. * $p < 0.05$, ** $p < 0.01$, *** $p < 0.005$.

3.8 Butyrate selectively limits IL-6 production in FLAMs in response to infection.

Based on the ability of butyrate to downregulate IL-6 in FLAMs in response to TLR2 ligation, we wanted to investigate if this effect extended to live pneumococci. FLAMs were seeded and pre-treated with butyrate (1mM) as per the protocol outlined **section 2.1.8**, and subsequently infected with *S. pneumoniae*, D39 at an MOI of 5:1 for 1 hour. Bacteria were removed and cells were further incubated for either 4 hours (**Fig. 3.14 A, B, C**) or 8 hours (**Fig. 3.14 D, E, F**). One millimolar butyrate was chosen for pre-treatment, as at this concentration no off-target effects of cytotoxicity were observed (**Fig. 3.2 A, B**), and IL-6 was significantly reduced in Pam3Csk4 stimulated cells (**Fig. 3.13 B, D**). Inflammatory cytokines IL-6, TNF-α in addition to IL-1β were quantified in cell supernatants collected at these timepoints by ELISA.

We observed that significant suppression of IL-6 was maintained in FLAMs pre-exposed to butyrate prior to pneumococcal infection, both at 4 and 8 hours post infection (**Fig. 3.14 A, D**). On the contrary, no significant differences were observed for TNF-α **(Fig 3.14 B, E)** or IL-1β **(Fig. 3.14 C, F)** at any timepoint. The suppression of IL-6 seen at the protein level in response to butyrate treatment was recapitulated at the transcriptional level in butyrate-treated FLAMs stimulated with Pam3Csk4 (LogFC -1.8726, $p_{adj} < 0.05$) (**Fig. 3.10**).

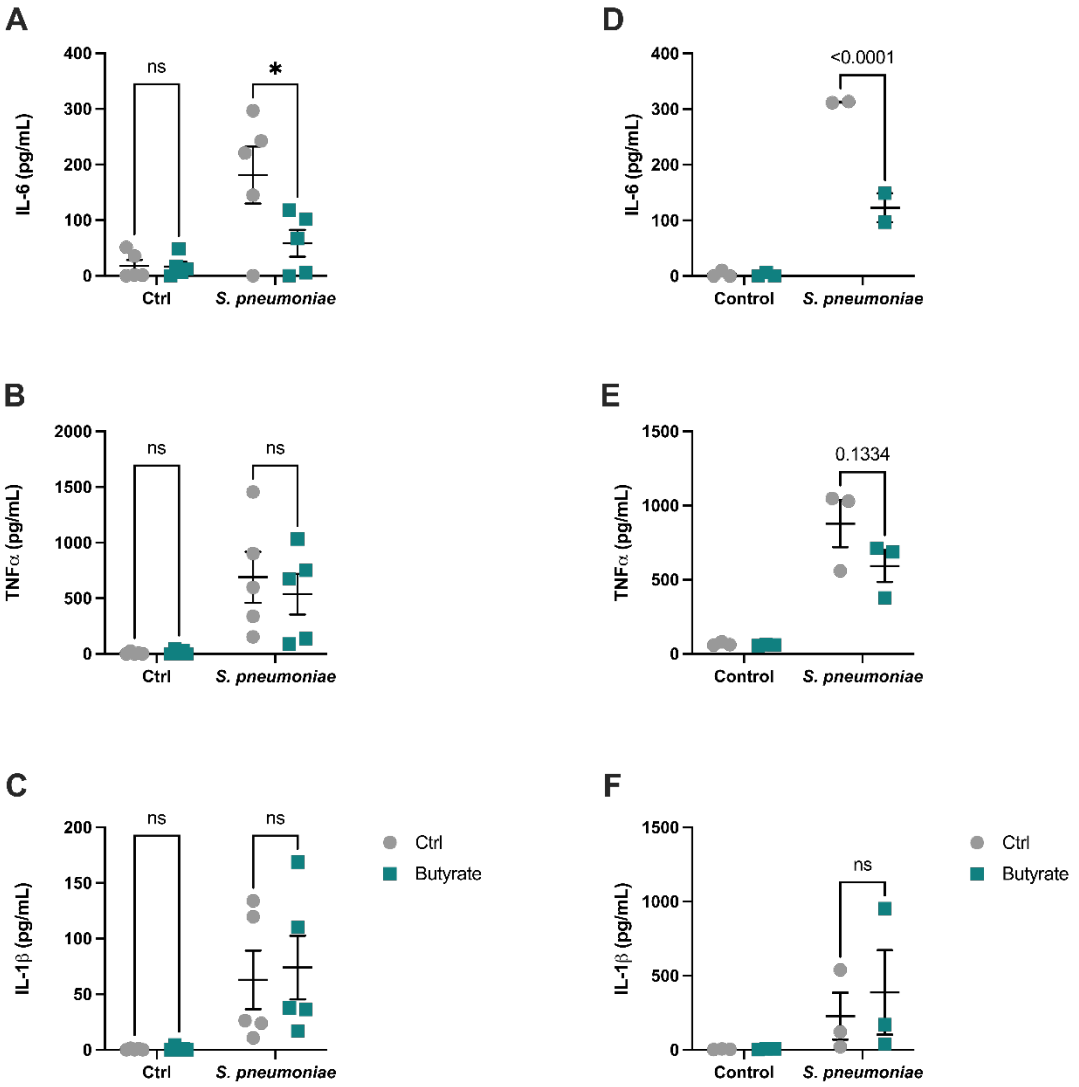


Fig. 3.14 Butyrate limits IL-6 production in alveolar-like macrophages during *S. pneumoniae* infection. FLAMs were pre-treated with butyrate for 24hrs prior to infection with *S. pneumoniae* D39 at an MOI of 5:1 for 1hr. Bacteria were removed, and cells were incubated for a further 4hrs **(A), (B), (C)** or 8hrs **(D), (E), (F)**. Cytokine, IL-6 **(A)**, TNF-α **(B)** and IL-1β **(C)** levels were quantified in cell supernatants. Data is representative of 5 biological replicates and two independent experiments, **(A), (B), (C)** and three biological replicates from three separate experiments **(D), (E), (F)**. Data was analysed by two-way ANOVA, using Bonferroni post hoc test, * $p < 0.05$, ** $p < 0.01$

3.9 Butyrate enhances the antimicrobial activity of alveolar macrophages.

Bulk transcriptomic signalling results highlighted genome-wide transcriptomic changes in both PamC3sk4 stimulated and infected cells pre-treated with butyrate. Four common categories of interest were upregulated: *Tumor necrosis factor superfamily production*, *Tumor necrosis factor production*, *defence response to bacterium, response to molecule of bacterial origin* and *defence response to a gram-positive bacterium* (**Fig. 3.7**). Ultimately subtle engagement of innate immune signatures was seen across all treatments exposed to butyrate, common significantly and trending upregulated genes included RNAse (*RNase2b*) and eosinophil associated ribonucleases 1, 2 and 6 (*Ear1, Ear2, Ear6*), antimicrobial peptides, lipocalin (*Ngp*), lactoferrin (*Ltf*) and *S100a9*. To examine if the enriched innate immune signatures seen in the transcriptomic data correlated with a functional change in FLAMs, we examined the bactericidal activity of FLAMs pre-treated with butyrate *in vitro* by gentamicin protection assays. In addition, to confirm if butyrate effects on murine AMs were pertinent to human AMs (hAMs), gentamicin protection assays were performed in hAMs isolated from bronchoalveolar lavage from patients subject to diagnostic bronchoscopies.

FLAMs and human AMs (hAM) were seeded and allowed to rest overnight. Cells were then pre-treated with butyrate (1mM) overnight for murine FLAMs (**Fig. 3.15 A**) or 3 hours in the case of hAMs to avoid cell death induced by prolonged *ex vivo* culture of the primary cells. Additionally, a 3-hour incubation period of butyrate pre-treatment was included for FLAMs (**Fig. 3.15 C**). FLAMs were subsequently infected with *S. pneumoniae* serotype 2 D39 at an MOI of 100:1 for 45 minutes. Human AMs were infected with either the characterised clinical isolate *S. pneumoniae* serotype 1 (E1586) (**Fig. 3.15 B**) or the clinical-derived wild-type strain, TUH of unknown serotype (**Fig. 3.15 C**). Cells were then treated with gentamicin to remove extracellular bacteria. Cells were immediately lysed at the 0hr time-point to determine basal number of intracellular bacterial post-infection or allowed to incubate in fresh media for a further 6 hours to enumerate bacterial colonies replicating/surviving intracellularly.

No significant differences were observed at the 0-hour time point, implying that butyrate did not alter the phagocytic capacity of FLAMs or hAMs (**Fig. 3.15 A, B, C**). In line with the RNA sequencing results, a trending decrease ($p = 0.0976$) was associated with intercellular bacterial load at 6 hours post infection in FLAMs pre-treated with butyrate (**Fig. 3.15**), implying butyrate treatment enhances intracellular bacterial clearance. It is known that *S. pneumoniae* can replicate intracellularly in AMs, as demonstrated by Nyazika *et al.* 2022 [406]. While it can't be confirmed here that butyrate treatment of AMs attenuates intracellular pneumococcal replication, these results do demonstrate that butyrate treatment increases the bactericidal activity in AMs, promoting bacterial clearance (**Fig. 3.15 A-D**).

Importantly, we also identified a significant reduction in intracellular bacterial load in hAMs at the 3-hour time point post infection, confirming that butyrate can significantly enhance the anti-bacterial activity of hAMs. This was a particularly crucial finding as these AMs were derived from individuals with chronic respiratory conditions including COPD, sarcoidosis, pulmonary fibrosis (**Fig. 3.15 B, C**).

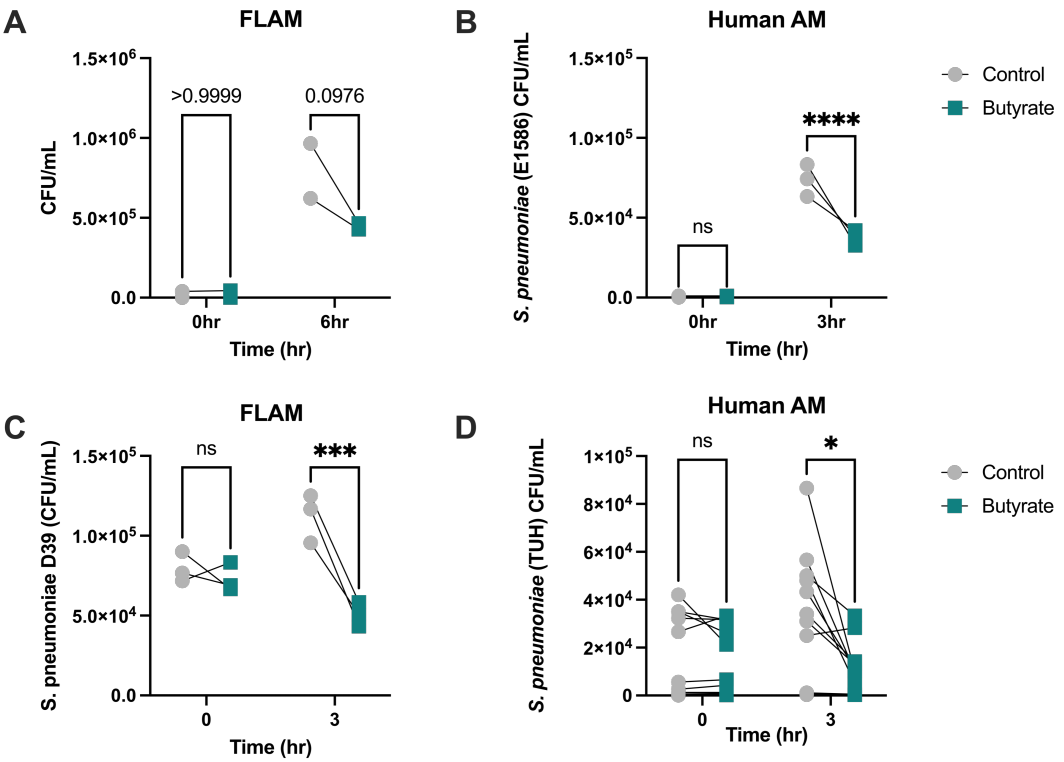


Fig. 3.15 ***Butyrate promotes intracellular clearance of S. pneumoniae in murine and human alveolar macrophage*.** FLAMs or hAMs were seeded and allowed to rest overnight. FLAMs were then pre-treated with butyrate (1mM) and incubated overnight, while hAMs were treated for 3 hours prior to infection. FLAMs were then infected with *S. pneumoniae* serotype 2 D39 at an MOI of 100:1 for 45 minutes. hAMs were infected with *S. pneumoniae* serotype 1 E1586 or an a clinical wild-type strain of unknown serotype ("TUH") obtained from human bronchoalveolar lavage at an MOI of 100:1 for 45 minutes. Bacteria were completely removed from cells and cells were treated with gentamicin (100µg/mL) for 30 minutes. Media containing antibiotics was removed and cells were either lysed immediately, and intracellular bacteria were enumerated (0hrs) or cells were allowed to further incubate for 3 hours (hAMs) or 6 hours (FLAMs) and lysed to plate intracellular bacteria. Data is representative of mean ± SEM, where n=2 experimental replicates. Statistics was performed by unpaired students T-test. With thanks to MSc Filza Masood for her contribution to the gentamicin protection assays in human AMs (**B, C**).

3.10 *In vivo* Effects of the Short-chain Fatty Acid, Butyrate, on Outcomes of Invasive Pneumococcal Pneumonia.

Based on our *in vitro* data, suggesting that the short-chain fatty acid butyrate can modulate macrophage phenotype, we wanted to examine the effect of butyrate in a murine model of respiratory infection. For this an *in vivo* model of acute invasive bronchopneumonia was optimised. Lethargy and piloerection are early indicators of disease progression and are followed by occasional ocular discharge, fluctuations in respiration and decreases in body temperature. Upon installation of a lethal dose of *S. pneumoniae*, animals typically progress to humane endpoint within a week post infection. It is well established in the literature that male mice are at an increased risk of invasive pneumococcal disease [407]. This also extends to the human context in which male patients suffering from invasive pneumococcal disease have poorer outcomes of infection [408], [409]. Here we used male C57BL/6 mice to examine the potential protective effects of butyrate on acute pneumococcal infection in what would represent the most at-risk individuals based on biological sex [407].

Three groups of mice were administered increasing doses of *S. pneumoniae*, serotype 2, strain D39 intranasally. Mice were then scored based on the criteria outlined in **table 2.5** twice a day post infection. All mice exhibited an initial temperature drop, six hours post infection, however mice administered the highest dose of bacteria were unable to recover body temperature post infection and progressed to hypothermia, a proxy for bacterial invasion into the bloodstream [410] and terminal disease. Mice administered a low ($4x10^8$ CFU/mice) and middle ($8x10^8$ CFU/mouse) doses of bacteria appeared to progress to hypothermia at a slower rate (**Fig. 3.16 A**) compared with mice administered the highest ($1.5x10^9$ CFU/mouse) dose of bacteria. Mice receiving the highest dose of pneumococci exhibited a swift increase in their illness behavioural and appearance score which continue to trend steadily upwards until terminal disease. Similar to external body temperature, mice receiving the low and intermediate doses of bacteria overcame the initial increase in illness behavioural and appearance score by 24 hours post initial infection and relapsed post 32 hours. Based on these preliminary results, the

intermediate dose (8x10^8 CFU/dose) was used as the target dose for following *in vivo* infections.

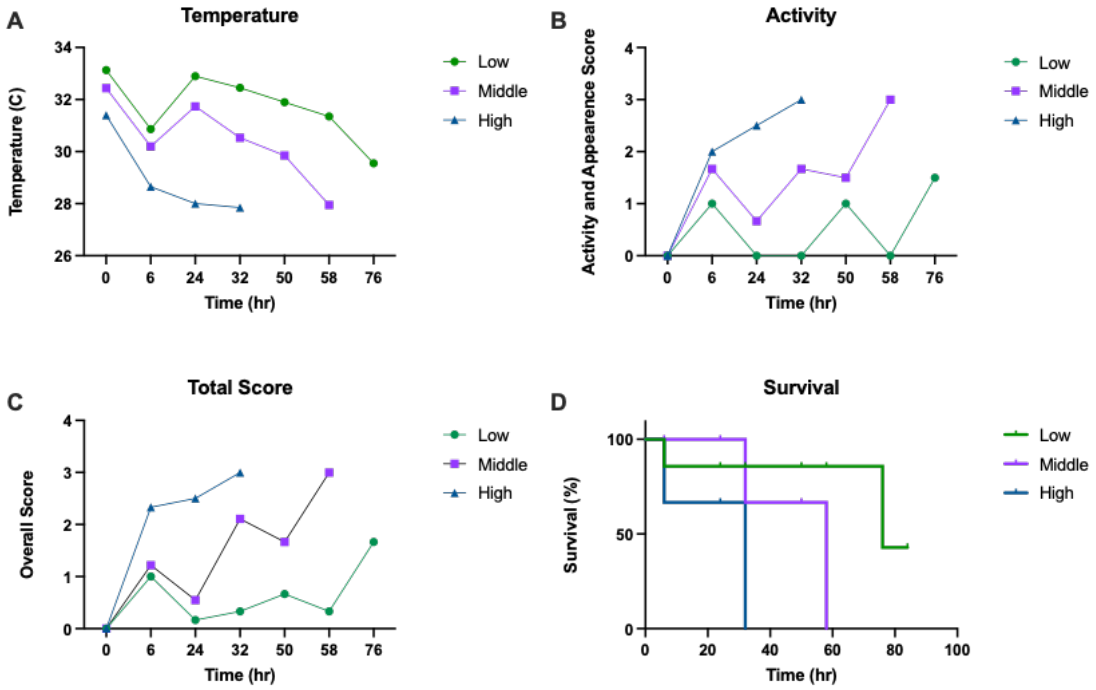


Fig. 3.16 Pilot study to evaluate dose escalation in optimising the lethal infectious dose of *S. pneumoniae* (serotype 2, D39). C57BL6/J mice were infected with increasing doses of *S. pneumoniae* serotype 2, strain D39, corresponding to a retrospective low dose of 4x10^8 CFU/dose, a middle dose of 8x10^8 CFU/dose and a high dose of 1.5x10^9 CFU/dose. Disease severity was measured by behavioural and body condition scoring and measurement of surface body temperature. Scoring was based on the criteria outlined in **table 2.4**. Data is representative of mean, with 2-3 mice/group.

3.11 *In vivo S. pneumoniae* infection is marked by an early depletion of AMs and rapid infiltration of neutrophils.

To establish the effects of microbiome interference and dietary intervention on lung cellularity during infection we first needed to characterise the typical recruitment dynamics of innate populations in the lung parenchyma, under the basal state and during infection. A common feature of acute pneumococcal infection is the early changes in resident and infiltrating phagocyte dynamics, marked by a characteristic depletion in AM [61], [62], [63], [60]. Mice were intranasally instilled with *S. pneumoniae* as per the protocol outlined in **section 2.2.4**. Four or 24 hours post infection mice were sacrificed and lungs were isolated for immunophenotypic analysis. Single cell suspensions of lungs were stained with fluorochromes outlined in and gated as per the workflow shown in **Fig. 3.17A**.

Lungs from infected mice had an overall increased cellularity at 24 hours post infection (p.i.) but not at the 4-hour timepoint, quantified by trypan blue viability assay (**Fig. 3.17 B**). This is likely attributed to the increased infiltration of neutrophils and inflammatory monocytes/macrophages (**Fig. 3.18 C**). At 4 hours post infection a significant depletion of AMs ($CD11b^{+}$, $CD11c^{hi}$, MHC^{lo}, $CD64^{+}$, $MerTK^{hi}$) and a decreasing trend in dendritic cells in both frequency and total numbers ($CD11b^{+}$, $CD11c^{+}$, MHC^{hi}, $CD64^{lo}$) was seen in the lungs of infected animals (**Fig. 3.18 A, B**). Similarly, a trending decrease was observed in the frequency of interstitial macrophage which was significant in terms of total number of cells ($CD11b^{+}$, $CD11c^{lo}$, MHC^{lo}, $CD64^{+}$, $MerTK^{hi}$) (**Fig. 3.18 A, B**). At this timepoint however no change in neutrophils ($CD11b^{+}$, $CD11c^{-}$, $Ly6C^{+}$, $Ly6G^{+}$) or monocytes ($CD11b^{+}$, $CD11c^{-}$, $Ly6C^{+}$, $Ly6G^{-}$) was observed (**Fig. 3.18 A, B**).

However, 24 hours post infection, a sustained decrease in frequency of AMs was observed, while there was an increase in both the frequency and total cell number of interstitial macrophages (**Fig. 3.18 C, D**). A significant increase in neutrophils was observed at 24 hours p.i. in frequency and total numbers (**Fig. 3.18 C, D**), whereas numbers of DCs and monocytes were also significantly increased (**Fig, 3.18 D**).

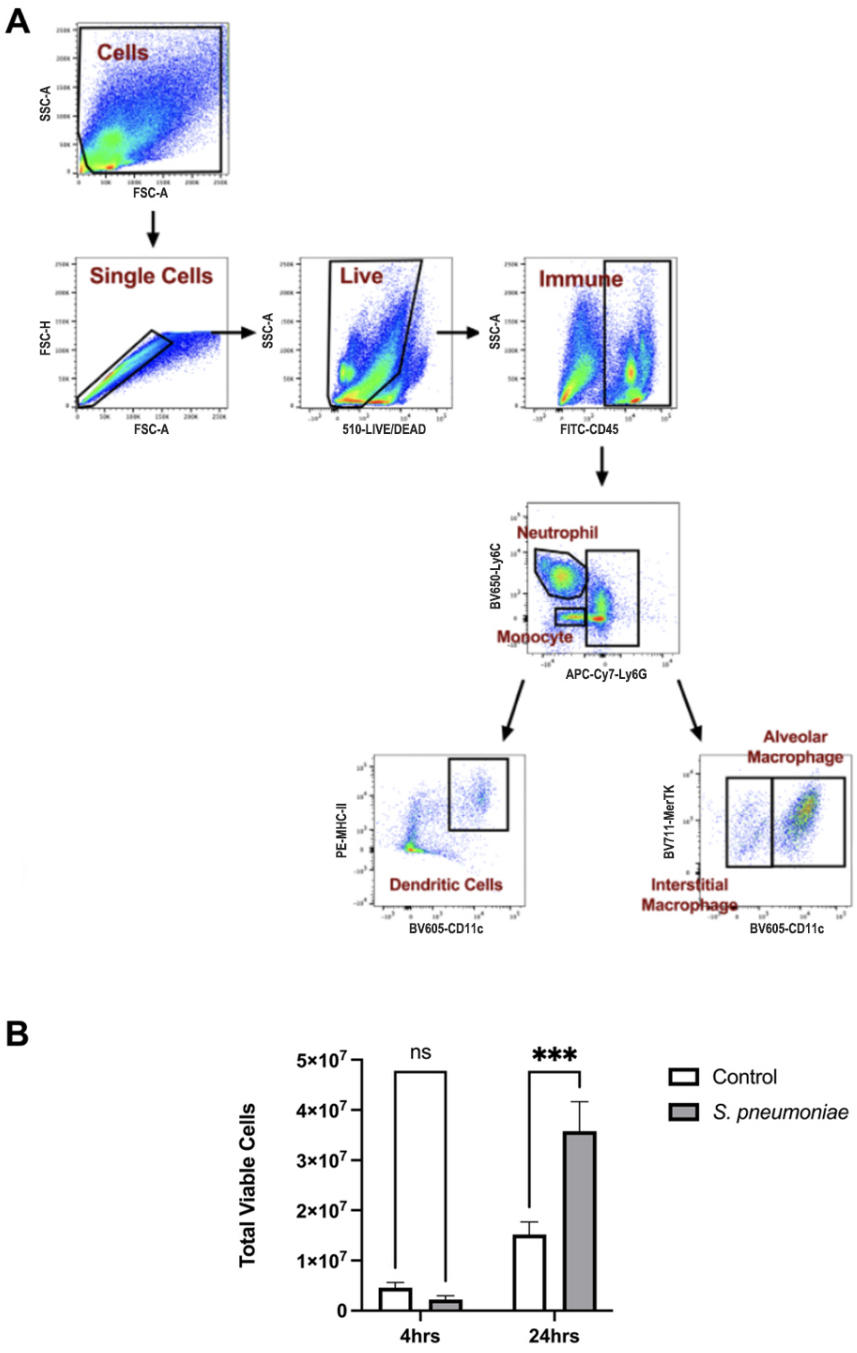


Fig. 3.17 Flow cytometry gating strategy for the phenotypic characterisation of innate immune infiltrates during pneumococcal infection. Single cell suspensions of lung parenchymal tissue were stained with the fluorochromes outlined in table 2.4. Cell populations were first gated on cells to remove debris, then singlets were isolated based on forward scatter and finally live (Aqua^{-}) cells. Immune cells were gated as CD45^{+} populations, neutrophils (CD45^{+}CD11b^{hi}Ly6C^{+}Ly6G^{+}), monocytes (CD45^{+}CD11b^{hi}Ly6C$^{int\text{-}hi}$Ly6G^{-}), DCs (CD45^{+}CD11B^{int}Ly6C^{-}CD11c^{+}MHC-II^{hi}), AMs (CD45^{+}CD11b^{int}Ly6C^{-}CD11c^{hi}MerTK^{hi}), IMs (CD45^{+}CD11b^{int}Ly6C^{-}CD11c^{lo}MerTK^{+}). Total viable cells were determined by trypan blue counting in single cell suspensions of whole lung tissue, at 4 hours and 24 hours post infection prior to staining. Data is representative of mean ± SEM, where n=5mice/group. Statistical significance was determined by Two-way ANOVA using Bonferroni's post-hoc test. *** $p < 0.001$

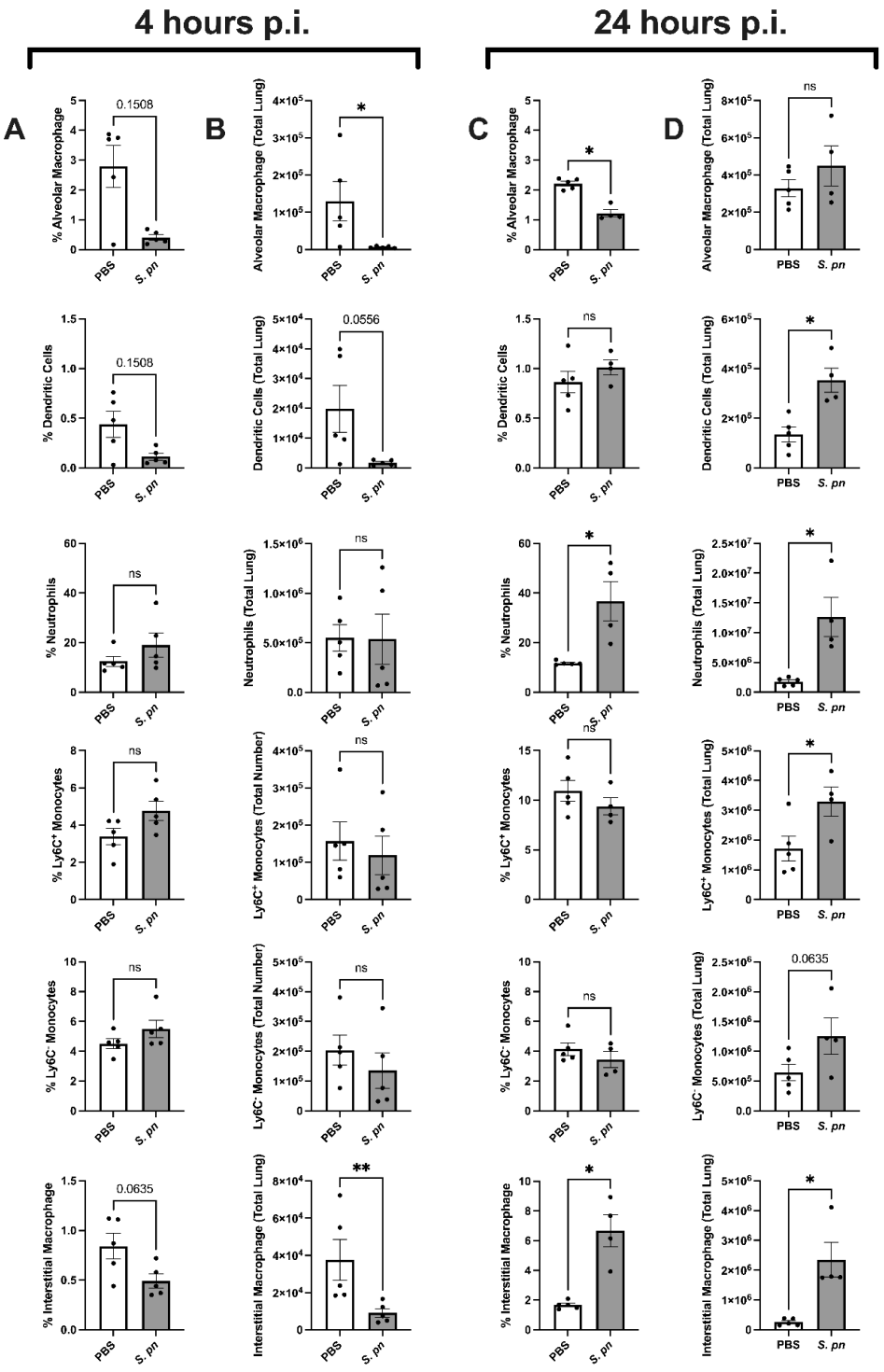


Fig. 3.18 Pneumococcal infection is characterised by an early depletion of AM and swift infiltration of neutrophils and monocytes. Male C57BL6/J mice were inoculated with *S. pneumoniae* D39, as per the protocol outlined in **section 2.2.4**. Lung tissue was harvested either 4 hours (**A, B**) or 24 hours (**C, D**) post-infection. Cells were isolated from lung parenchymal tissue and stained using the fluorochromes highlighted in **table 2.5**. Cell populations were gating as per the gating strategy outlined in **Fig. 3.17**. Percentage expressed over total live cells. Data is representative of mean ± SEM, where n=10/group. Significance was measured using Mann-Whitney test, where ns = non-significant, * $p < 0.05$, ** $p < 0.01$.

3.12 Antibiotics do not elicit direct immunomodulatory effects on THP-1 macrophage.

The next step was to determine whether butyrate could be protective in a model of antibiotic induced dysbiosis *in vivo*. Previous research suggests that antibiotics can have direct immunomodulatory effects *in vitro* in macrophage and THP-1 derived macrophages [411], [412], [413], [414], which could be a potential caveat in the model of antibiotic-induced dysbiosis. Therefore, we conducted experiments to confirm or disprove these previous reports in the context of TLR2 ligation and pneumococcal stimulation. Bode *et al*. demonstrated a direct effect of antibiotics, namely linezolid, vancomycin and daptomycin *in vitro* on differentiated human THP-1 monocytic cells [412]. THP-1 cells were chosen based on this publication to see if these results could be replicated using vancomycin, due to its efficacy *in vivo* at depleting gram positive anaerobes, particularly those responsible for SCFA synthesis and penicillin/streptomycin due to its widespread use in cell culture and its reported immunomodulatory off-target effects [412], [415], [414], [358].

THP-1 cells were differentiated using 100nM phorbol 12-myristate 13-acetate (PMA) for 48 hours to skew cells towards a phenotype reflecting monocyte-derived macrophage. Subsequently cells were pre-treated with penicillin/streptomycin (100ug/mL) or vancomycin (50ug/mL) overnight or left untreated (media control). Cells were then stimulated with the TLR2 ligand Pam3Csk4 and the heat-killed poly-valent lysate of *S. pneumoniae*, supernatants were collected at 6 hours post-stimulation for downstream analysis. Inflammatory cytokines IL-6, IL-1β and TNF-α were measured in the supernatant by ELISA. Similarly, TNF-α and the two toll-like receptors TLR2 and TLR4 were quantified by qPCR, due to reported modulatory effects of vancomycin on expression of these TLRs [412].

No significant modulation of IL-6, IL-1β and TNF-α production were noted basally or upon stimulation (**Fig. 3.19 A-F**). Ultimately, there were no observable modulatory effect of antibiotics on monocyte-derived macrophage phenotype. Thus, the previously documented immunomodulatory impact of antibiotics on the innate immune

phenotype was not confirmed and therefore this is not likely to act as a confounding variable.

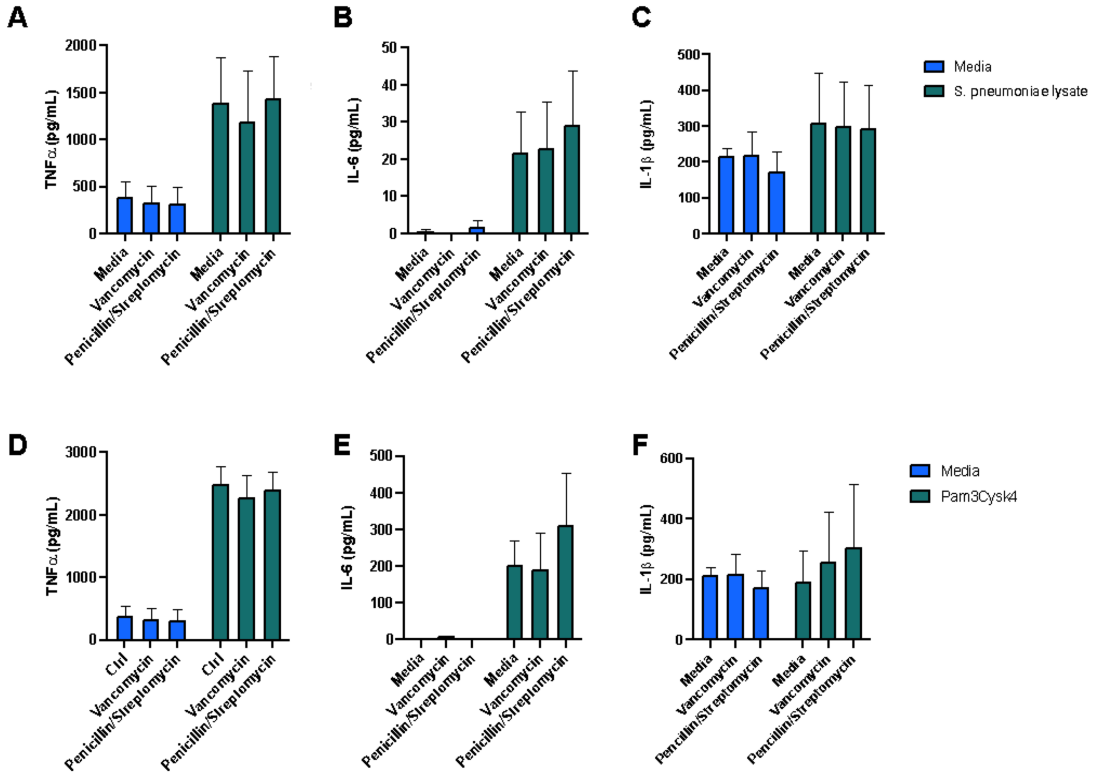


Fig. 3.19 Antibiotics do not significantly modulate inflammatory cytokine production upon stimulation in monocyte-derived macrophage. THP-1 cells were stimulated with PMA (100nM) for 48 hours. Cells were subsequently allowed to rest overnight prior to stimulation. Cells were left untreated (Media) or pre-treated with either penicillin/streptomycin (100ug/mL) or vancomycin for 24hrs. After this time cells were stimulated with media (control), Pam3Csk4 (200ng/mL) or a polyvalent heat-killed pneumococcal lysate (22.5ug/mL) for 6 hours. TNF-α **(A, D)**, IL-6 **(B, E)** and IL-1β **(C, F)** were quantified in cell supernatants by ELISA. Data is representative of mean ± SEM, where n=3 independent experiments.

3.13 Antibiotics cause a reduction of polyspecific IgA in the intestine.

Here we used a model of broad-spectrum antibiotic-induced dysbiosis, adapted from Reikvam *et al.* 2011, to examine the potential of butyrate supplementation to circumventing the deleterious effects of dysbiosis [416]. Polyspecific intestinal IgA has a crucial role in mediating intestinal homeostasis and regulation of commensal communities through direct coating of bacteria. We examined polyspecific secretory IgA in faecal pellets as a proxy of shifts in the gut microbiota composition [417], [418]. Mice were administered a broad-spectrum antibiotic cocktail containing amphotericin (100mg/kg), metronidazole (10mg/mL), vancomycin (50mg/mL), neomycin (10mg/mL) and ampicillin (10mg/kg), administered daily by oral gavage for 14 days. The anti-fungal agent amphotericin B was administered as microbiota ablation by antibiotic cocktail can result in fungal overgrowth [419] (**Fig. 3.20 A**). Oral gavage was used as it ensures delivery of a consistent antibiotic volume across animals and reduces detrimental effects product of overconsumption such as excess weight loss [420]. Mice were administered food and water *ad libitum* and weighed daily to track fluctuations in weight. An additional group received butyrate (100mM) in drinking water alongside antibiotic treatment.

Mice administered antibiotics exhibited no significant fluctuation in weight over the course of antibiotic treatment compared to that of controls (**Fig. 3.20 B**). Similarly, no significant changes in weight were observed in animals receiving butyrate supplementation alongside antibiotic treatment (**Fig. 3.20 B**). However, mice receiving antibiotics had a significantly lower detectable level of polyspecific secretory IgA in faecal matter (**Fig. 3.20 C**), this also applied to animals receiving butyrate in combination with antibiotic treatment (**Fig. 3.20 C**). Intestinal IgA has been linked to protective roles in pneumococcal infection, when synergising with anti-pneumococcal IgG [421]. However, in our model of acute pneumococcal infection animals rapidly progress to acute bronchopneumonia and invasive infection, **Fig. 3.16**, so it is unlikely that an adaptive pneumococcal-targeted antibody response has been mounted in the time frame before onset of terminal disease.

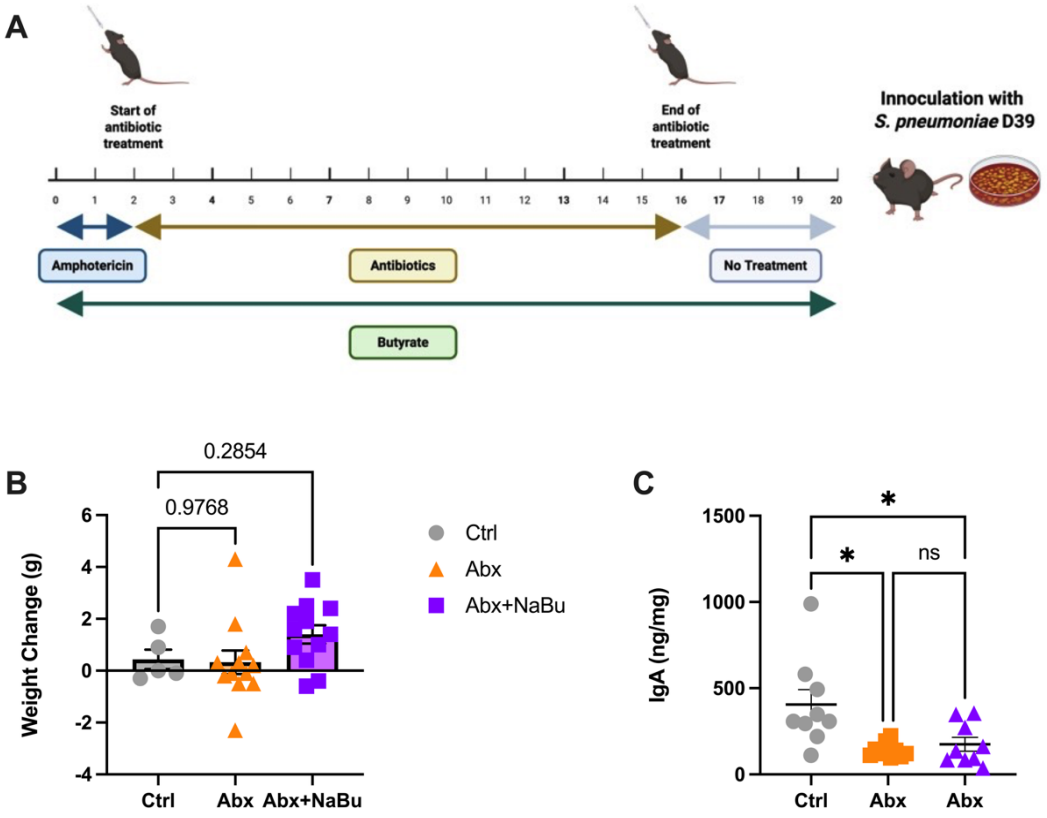


Fig. 3.20 Antibiotic treatment regimen and tracking of body weight in dysbiotic mice. Male C57BL6/J mice were administered amphotericin 1mg/kg two days prior to antibiotic treatment. Two hundred microlitres of antibiotics (Abx) at the following concentrations metronidazole 1g/L, ampicillin 1g/L, neomycin 1g/L and vancomycin 500mg/L, were administered by oral gavage daily for a period of 14 days. Mice were weighed daily and examined for signs of malaise. Data is representative of n=10 mice/group (male). Statistical analysis was performed by one-way ANOVA, ns = non-significant, * $p < 0.05$.

3.14 Dysbiosis contributes to an increased susceptibility to pneumococcal pneumonia.

It has been established that wide-scale ablation of the microbiota contributes to the pathogenesis of respiratory infection, particularly in the setting of pneumococcal pneumonia [179], [73]. Due to the variability in the basal microbiota among different housing conditions and different susceptibility of particular mouse strains to specific pneumococcal stains, we needed to confirm these results in house, prior to dietary supplementation with butyrate [422]. Mice were then treated with antibiotics and rested with no treatment for 4 days to prevent interference of the antibiotics with the infection (**Fig. 3.20 A**).

Mice were anaesthetised using ketamine/xylanzine and inoculated with approximately 7.5-8x10^8 CFU of *S. pneumoniae* serotype 2, strain D39. Initial surface body temperature was recorded using an infrared thermometer on the ventral abdomen of the mouse. Mice were sacrificed when an average score of 3 or a score of 3 in any individual category (body temperature, activity and appearance or respiratory score) was reached, indicating terminal disease and the humane endpoint of the study. Antibiotic-induced dysbiosis resulted in a heightened susceptibility to pneumococcal pneumonia. Mice administered antibiotics exhibited a sharper decline ($p = 0.0668$) in surface body temperature over the period of infection, compared to controls (**Fig. 3.21 A**). Similarly, mice administered antibiotics reached a significantly higher illness behaviour score (**Fig. 3.21 B**) and overall disease severity score (**Fig. 3.21 C**) over the course of study. Mice administered antibiotics had an overall lower survival index compared to control mice (**Fig 3.21 D**).

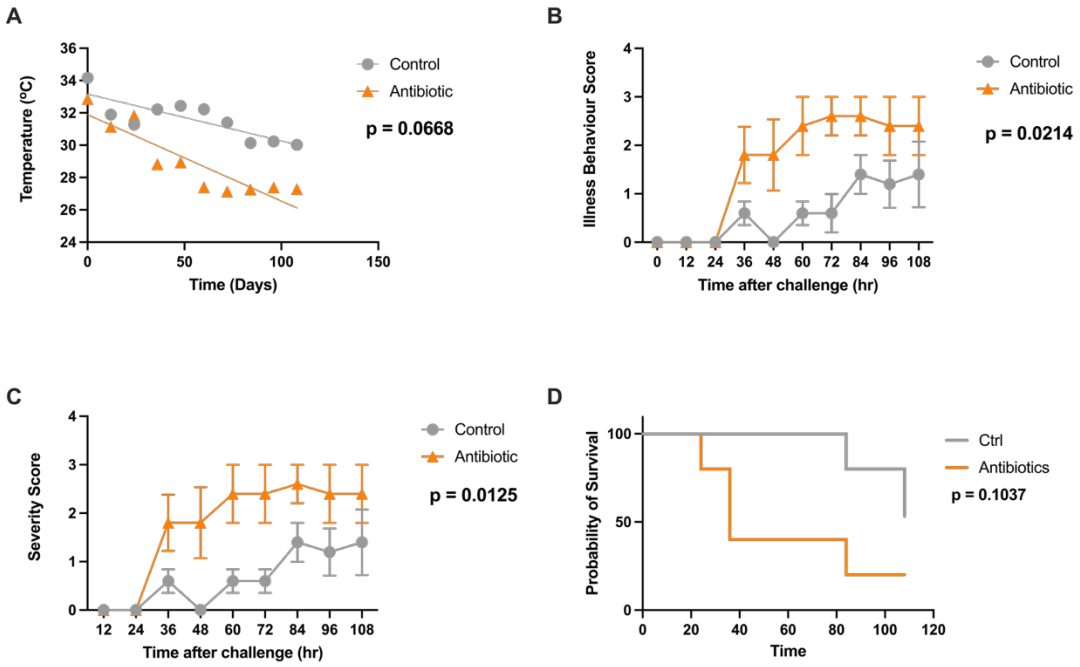


Fig 3.21 Antibiotic-induced dysbiosis of the microbiota increases susceptibility to pneumococcal pneumonia. Mice were inoculated with approximately 7.5 x 10^8 CFU of *S. pneumoniae* serotype 2, strain D39 and scored for disease severity, as per guidelines outlined in table X, until the humane endpoint was reached. Data is representative of n=5 mice/group (male). Survival analysis was performed by Kaplan-Meyer analysis (**A**), due to an initial significant difference in basal temperature, correlation analysis was performed on temperature over the course of infection (**C**). Data was analysed by Kruskal-Wallace test (**B, D**). p-values are specified on graphs.

3.15 Butyrate ameliorates the effects of dysbiosis-driven exacerbation of invasive pneumococcal infection.

The results presented in **Fig. 3.21** are in agreement with the current literature which demonstrates that antibiotic-induced intestinal dysbiosis is detrimental during pneumococcal infection [179], [73]. It is likely that ablation of commensal communities that produce short-chain fatty acids, is a contributing factor in the deleterious outcomes of dysbiosis on respiratory health and disease. Antibiotic-induced dysbiosis results in a strong phenotype of immune dysregulation [179], [73] and therefore, the ability of oral butyrate supplementation to restore immunocompetence in dysbiotic mice during pneumococcal challenge is an attractive strategy that to date has not been investigated. *In vitro* results demonstrated that butyrate enhanced the anti-microbial profile of AMs and suppressed heightened production of IL-6 in response to infection (**Figs. 3.13 and 3.14**).

A recent publication by Kullberg et al. 2025 demonstrated that i.p. administration of butyrate was protective against challenge with *K. pneumonaie* in vivo, reducing lung bacterial burden, bacterial dissemination and decreasing levels of pro-inflammatory IL-6 and neutrophil infiltration [197]. This was a promising study to support our hypothesis that butyrate was protective in dysbiotic cohorts against pneumococcal challenge *in vivo*, by aiding in the resolution of invasive pneumococcal infection through enhancement of bacterial clearance and control of excessive inflammation.

Mice were treated as before with antibiotics by daily oral gavage, as described in **section 2.2.3** and **Fig. 3.20 A**. Mice were administered butyrate (100mM) in drinking water *ad libitum* throughout the entire course of antibiotic administration and the course of infection until the humane endpoint was reached. Mice were infected as outlined in **section 2.4** and scored for disease severity, based on the criteria outlined in **table 2.6**, initially at the time of infection and at the 18-hour timepoint immediately before sacrifice. Lungs and spleens from infected animals were collected in 1mL PBS. Lungs were divided for concurrent flow cytometry analysis and CFU enumeration and each part weighed to allow for normalisation of bacterial counts and cell numbers. For CFU enumeration, tissues were mechanically lysed and a series of ten-fold serial dilutions

was prepared, dilutions were plated in triplicate on blood agar plates, as outlined in **section 2.3.4.**

In line with the survival results in **Fig. 3.21**, animals receiving antibiotic treatment alone exhibited a significant decrease in body temperature at 18 hours post infection and increases in illness behavioural score marked by decreased activity and piloerection (**Fig. 3.22 A, B, C**). Animals administered antibiotics in combination with butyrate had a significantly lower bacterial burden in the lungs compared to mice receiving antibiotics alone, comparable to levels seen in eubioitic mice (**Fig. 3.22 D**). Mice receiving oral butyrate supplementation exhibited a significantly higher temperature 18 hours post infection (**Fig. 3.22 A**) and lower temperate drops over the course of infection (**Fig. 3.22 B**), whereas the mean average temperature of the treatment groups administered antibiotics alone was 28.4°C, indicating terminal disease, where the mean average temperature of the treatment group administered antibiotics in combination with butyrate was 30°C (**Fig. 3.22 A**). Hypothermia in murine pneumococcal pneumonia has been shown to be a direct correlate of invasive disease[410]. Therefore mice in the butyrate treated group were expected to have lower bacterial burden in spleens. Notably this was the case as animals receiving butyrate supplementation alongside antibiotics had significantly a lower bacterial burden in the spleens than those receiving antibiotics with no supplementation (**Fig. 3.22 E**). No significant effects were observed between control animals (receiving water), and animals receiving both butyrate and antibiotics, across any of the readouts (**Fig. 3.22 A, B, C, D, E**).

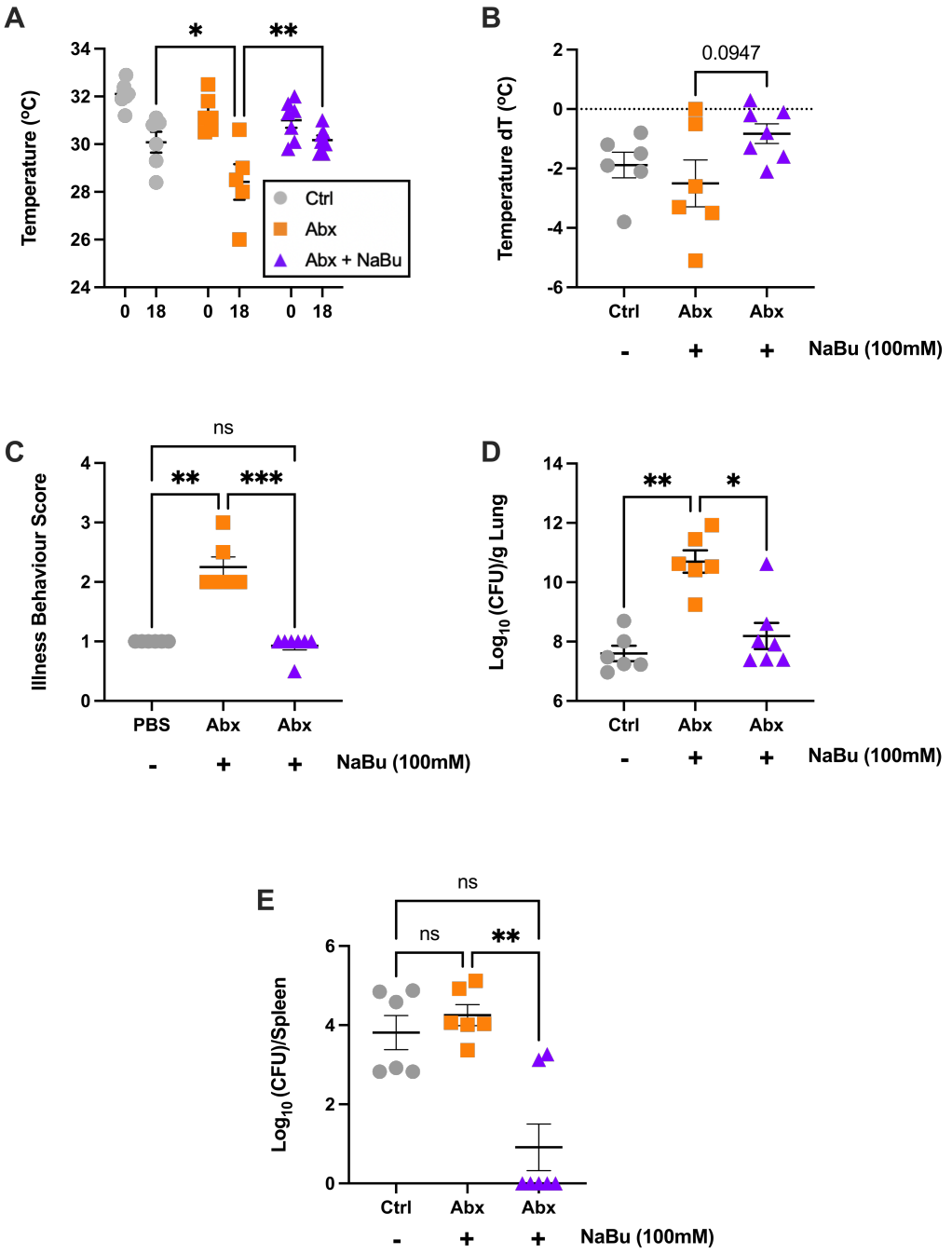


Fig. 3.22 Butyrate alleviates the deleterious effects of antibiotic-induced dysbiosis on outcomes of pneumococcal infection. Male C57BL6/J mice were administered antibiotics (ampicillin, neomycin, metronidazole and vancomycin) by oral gavage for 14 days. Mice were then taken off antibiotic treatment for three days prior to infection with *S. pneumoniae* D39, as shown in **Fig. 3.20**. Animals were scored twice daily for disease severity based on the scoring criteria highlighted in table X. Mice were sacrificed at 18 hours post infection and bacterial colonies were enumerated in the lung (**A**) and spleen (**B**). Temperatures were measured initially at time of inoculation (0 hours) and at time of sacrifice (18 hours) (**D**). Change in temperature over period of infection was considered a marker of terminal disease due to invasive pneumonia (**C**). Data is represented as logged values of CFUs, where mean ± SEM and n=6/7 per group. Statistical analysis was performed by ordinary one-way ANOVA (**B, C**) or Kruskal Wallace test (**D, E**), using Dunnett's post-hoc test, or two-way ANOVA (**A**), * $p < 0.05$, ** $p < 0.01$.

3.16 Dietary supplementation with butyrate attenuates neutrophil recruitment during invasive pneumococcal infection.

We next investigated whether butyrate supplementation could alter resident innate immune populations in the lung that could contribute to the protective effects seen. To address this, the first step was to analyse lung cell populations after butyrate supplementation but in the absence of infection to determine if butyrate could "prime" the lung environment to better cope with the lung infection. Mice were administered either water (control) or water supplemented with 100mM sodium butyrate *ad libitum* for 14 days. Mice were anesthetised and inoculated with sterile 1X PBS to maintain consistency in the treatment protocol used during infections and account for any effects introduced by the volume that would be later used to inoculate the bacteria, **section 2.2.4**. Mice were sacrificed at the end of the 14-day treatment period and lungs were collected for immunophenotyping. Phenotypic characterisation of lung single cell suspensions was carried out using the gating strategy highlighted in **Fig. 3.17**. AM were characterised as ($CD45^{+}CD11b^{int}CD11c^{hi}CD64^{hi}MerTK^{hi}$), dendritic cells ($CD11b^{int}CD11c^{hi}MHCII^{+}CD64^{-}$), neutrophils ($CD11b^{hi}$, $CD11c^{-}$, $Ly6G^{+}$), interstitial macrophage ($CD45^{+}CD11b^{int}CD11c^{lo}CD64^{+}MerTK^{+}$), $Ly6C^{hi}$ monocytes ($CD11b^{hi}$, $CD11c^{-}$, $Ly6G^{-}$, $Ly6C^{hi}$) and $Ly6C^{lo}$ monocytes ($CD11b^{hi}$, $CD11c^{-}$, $Ly6G^{+}$, $Ly6C^{lo}$).

In the absence of infection, overall lung cellularity was not impacted by butyrate compared to controls receiving water (**Fig. 3.23 A**). No significant changes were observed in mice treated with butyrate compared to controls for any of the innate immune populations studied in the lungs (**Fig. 3.23 B-G**). Having established that butyrate does not independently induce basal changes in infiltrating innate immune populations in the lungs prior to infection, we then evaluated its effects on animals rendered more susceptible to pneumococcal pneumonia by antibiotic treatment. Animals were subject to antibiotic and dietary intervention as outlined in **Fig 3.20 A** and lung cell populations were analysed as described before.

Similarly, both frequency and number of monocyte populations were significantly enhanced in dysbiotic animals (**Fig. 3.24 C, D**). Dysbiotic animals had a significantly

higher frequency and number of myeloid cells however this is largely attributed to the increases in neutrophils and monocytes (**Fig. 3.24 A, B**). In contrast, butyrate treated mice had comparable numbers of neutrophils infiltrating the lungs to mice not exposed to antibiotics (**Fig. 3.24 E, F**). Frequencies of dendritic cells and interstitial macrophage were increased animals receiving antibiotics and butyrate; however this was not recapitulated in total numbers (**Fig. 3.24 G, H, K, L**). Overall, no significant modulation in cellular dynamics were noted in dysbiotic mice receiving butyrate other than a suppression of exacerbated neutrophilic infiltration, implying that butyrate treatment could prevent uncontrolled neutrophilic inflammation.

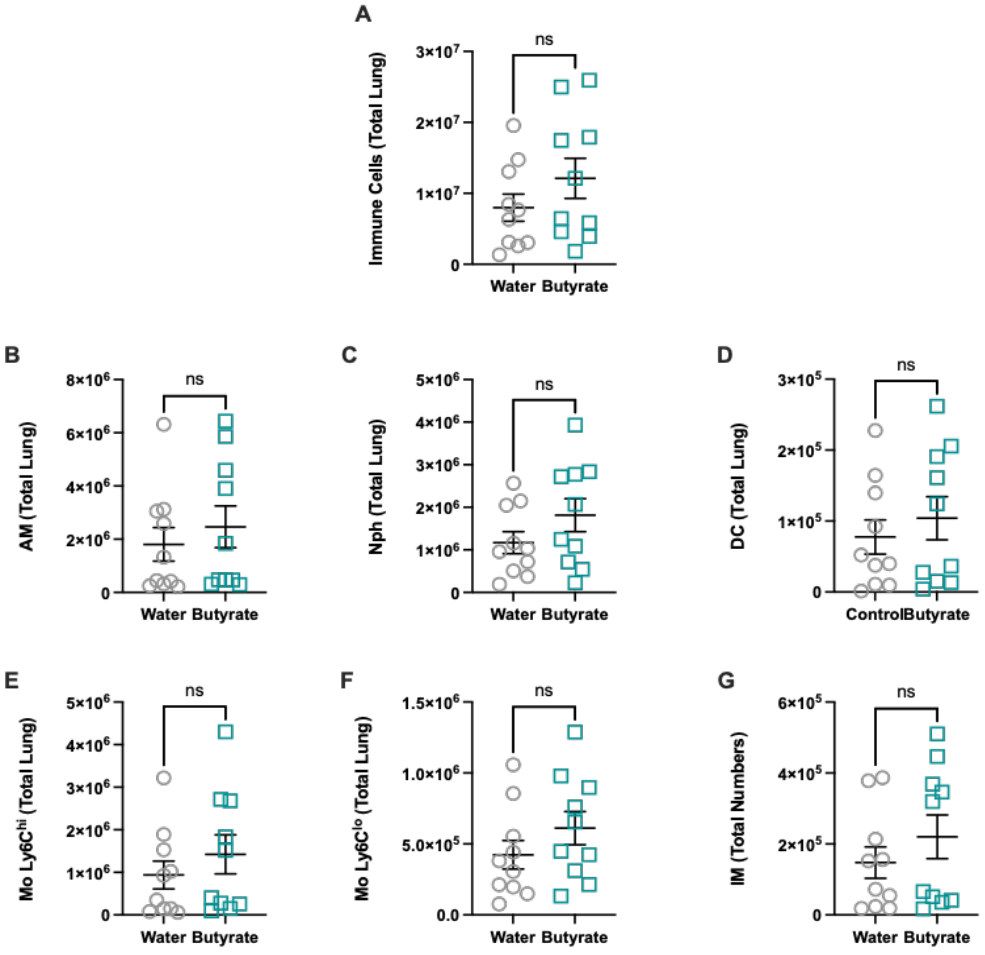


Fig. 3.23 Dietary supplementation with butyrate does not alter innate immune population in the lungs under basal conditions. Mice were administered butyrate in drinking water *ad libitum* for 14 days prior to sacrifice. Cells were isolated from lung parenchymal tissue and stained using the fluorochromes highlighted in **table 2.5**. Cell populations were gated as per the gating strategy outlined in **Fig. 3.17**. Data is representative of mean ± SEM, where n=10/group. Significance was measured using Mann-Whitney test, where ns = non-significant. Data from one experiment.

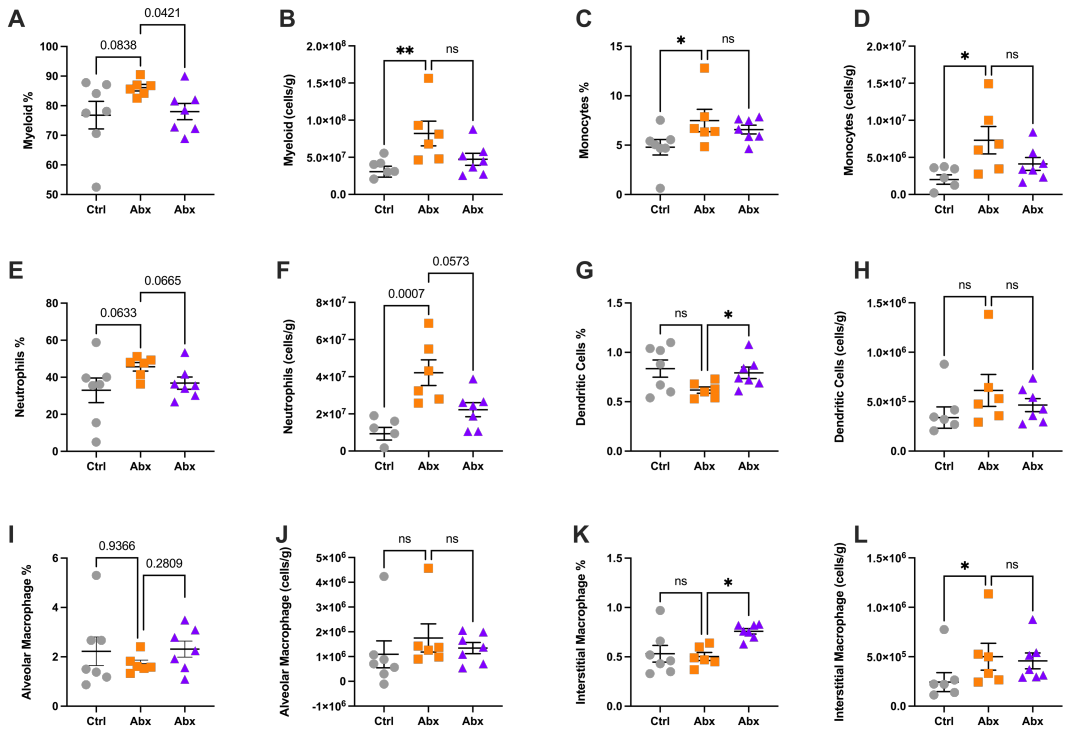


Fig. 3.24 Antibiotic-induced dysbiosis alters innate immune infiltrates during pneumococcal infection. Male C57BL6/J mice were administered antibiotics (ampicillin, neomycin, metronidazole and vancomycin) by oral gavage for 14 days, alone or in synergy with butyrate (100mM) in drinking water administered *ad libitum*. Mice were then taken off antibiotic treatment for three days prior to infection with *S. pneumoniae* D39, as outlined in **Fig. 20**. Cells were isolated from lung parenchymal tissue and stained using the fluorochromes highlighted in table X. Cell populations were gating as per the gating strategy outlined in **Fig. 3.17**. Data is representative of mean ± SEM, where n=6/7 per group. Significance was measured using Mann-Whitney test, where ns = non-significant, * $p < 0.05$, ** $p < 0.01$.

Discussion

Here we hypothesised that oral administration of butyrate as a therapeutic dietary intervention could improve outcomes of pneumococcal disease in susceptible dysbiotic cohorts. First, the optimal concentration of butyrate that would induce immunomodulatory effects on these cells without causing significant cytotoxicity was determined. Having established the optimal dose of 1mM, it was demonstrated that butyrate had a concentration dependent effect on HDACi in FLAMs **(Fig. 3.2), (Fig. 3.3)**. Significant enhancement of acetylated histone 3 and 4 was only seed in treatment of macrophage with 1mM butyrate, but not 100µM (**Fig. 3.3 A, C**). Histone deacetylase inhibition (HDACi) appears to be a prominent mechanism of epigenetic regulation elicited by SCFA, particularly for butyrate and propionate [148]. Furthermore HDACi activity underpins the imprinting of an antimicrobial phenotype in tissue resident macrophages [196], [391], [423], [148]. The HDACi activity of butyrate on FLAMs suggested that broad-scale transcriptomic changes would occur in cells treated with 1mM butyrate due to a higher degree of histone polyacetylation and subsequent chromosomal accessibility.

We went on to characterise the transcriptional profile of murine AMs exposed to butyrate alone, in combination with the TLR2 agonist Pam3Csk4 or infected with the murine adapted *S. pneumoniae* isolate, D39 by bulk mRNA sequencing. *In vitro* butyrate pre-treatment induced global transcriptomic changes in FLAMs in response to *S. pneumoniae* infection and Pam3Csk4, as outlined in section **3.7-3.11**. Gene set enrichment analysis (GSEA) highlighted pathways involved in innate host defence (**Fig. 3.7**) in cells treated with butyrate compared to controls. For cells treated with butyrate that were also stimulated with Pam3Csk or *S. pneumoniae*, differentially expressed genes demonstrating signatures of transcriptional enhancement included various antimicrobial peptides (*Ltf, Ngp, S100a9*) and IFN signalling genes (**Fig. 3.8 - Fig. 3.13**). We acknowledge that lipocalin 2 (*Lcn2*) has been associated with deleterious outcomes of pneumococcal infection, however, upregulation of *Lnc2* in butyrate treated FLAMs did not appear to impair their bactericidal capacity *in vitro* (**Fig. 3.15 A**) (will add the references offline). Similarly, while S100a9 levels are increased in patients suffering

from bacterial pneumoniae, highlighting it as a potential biomarker, however, S100a9 has an indispensable role in innate defence against the pneumococcus, with S100a9-/- mice exhibiting a significantly higher mortality in a model of pneumococcal pneumonia than WT controls [238]. This was not observed to be associated with a general upregulation in the inflammatory profile of the macrophage as genes encoding NFκB-governed cytokines were not increased, namely *Tnf*, *Il6*, *Il1B*, *Il8*. In fact, in the setting of TLR2 stimulation, butyrate treated cells exhibited significantly suppressed transcription of *Il6*, a trend which was recapitulated at the protein level in both cells exposed to TLR2 ligation and viable pneumococci (**Fig. 3.13**). This implies that butyrate promotes an anti-microbial program in AMs in response to inflammatory stimuli but does not promote an uncontrolled inflammatory phenotype. Machado *et al.* 2022 demonstrated that acetate could promote pneumococcal clearance in an inflammatory manner by an NLRP3 and glycolytic-HIF-1α axis and subsequent nitric oxide production [195]. We do acknowledge that butyrate treatment upregulated transcriptional expression of *Cxcl9* and *Cxcl10*, in response to both TLR2 ligation and *S. pneumoniae* infection. Both *Cxcl9* and *Cxcl10* were associated with higher susceptibility to nasal colonisation of *S. pneumoniae* in human challenge models as outlined by Urban *et al.* 2024 [393]. Similarly, this has been documented in murine studies showing that antagonisation of CXCL1 and CXCL2 using the selective inhibitor DF2162 improves outcomes of pneumococcal infection [394]. To determine if this could be an unanticipated deleterious effect, we further investigated the ability of butyrate supplementation to alter innate cell recruitment *in vivo* during pneumococcal challenge.

Before proceeding with the *in vivo* model, the antimicrobial transcriptomic signatures induced by butyrate treatment in FLAMs were verified at the phenotypic level using a gentamicin protection assay. At the initial time-point post infection no observable or significant changes were noted between controls and cells treated with butyrate, implying that butyrate had no significant impact on bacterial uptake. However, at 6 hours post infection a decrease was observed in cells treated with butyrate, implying a higher degree off bactericidal activity and intracellular pneumococcal clearance (**Fig. 3.15**). These effects have been demonstrated in the context of *K. pneumoniae* infection in which butyrate promoted intracellular bacterial clearance through SCFA-mediated

alterations of lysosomal function [367]. A gut-lung axis driven mechanistic feature of dysbiosis is abrogation of AM function and a lower capacity to clear infection, specifically in the response to pneumococci. However, the current data and previous reports, demonstrate that SCFAs can enhance anti-microbial functions of AMs [107], [195]. **From these insights and supporting literature we believe that butyrate improves the bactericidal function of AM and could overcome the AM phenotype seen in response to respiratory infection in dysbiotic cohorts.**

In this instance susceptibility was a consequence of broad-spectrum antibiotic-mediated systemic dysbiosis. **Butyrate administered as a dietary supplement during the induction of antibiotic-induced dysbiosis successfully alleviated disease burden in susceptible animals in agreement with our hypothesis.** Using intestinal secretory IgA as a proxy for the degree of commensal ablation, it was demonstrated that butyrate did not seem to circumvent the degree of commensal loss (**Fig. 3.20 C**). In dysbiotic animals it is likely that the gram-positive anaerobes responsible for SCFA production are lost, notably members of the *Firmicutes* phyla, *Lachnospiraceae* and *Clostridiales* cluster XIVa members, which would be likely targets of vancomycin [424], [388]. Butyrate alone appears capable of circumventing the effects of dysbiosis in response to pneumococcal infection to those at baseline it is likely that under eubioitic circumstances endogenous butyrate has a critical role in host pneumococcal defence by acting as an immunomodulatory agent via. the gut-lung axis of immune regulation (**Fig. 3.22**). However, no reduction in disease burden was noted between dysbiotic mice receiving butyrate and control (eubioitic) mice (**Fig. 3.22**). Sencio and colleagues 2020, demonstrated the therapeutic potential of acetate in overcoming the effects of dysbiosis induced by influenza A infection leading to pneumococcal superinfection [425]. **Here we provide primary evidence that butyrate alleviates the enhanced susceptibility to invasive pneumococcal pneumonia caused by antibiotic-induced dysbiosis.**

Ultimately our contributions have provided novel insights into how SCFA can rescue a gut-lung axis mediated hypo responsiveness to pneumococcal infection. This has therapeutic implications given the higher susceptibility to respiratory infection in those

presenting with dysbiosis or co-morbidities in which dysbiosis appears to be a contributing factor, such as COPD [87].

4. Exploring the immunomodulatory effects of butyrate on pneumococcal vaccination outcomes.

4. Introduction

Despite the availability of pneumococcal vaccines, invasive pneumococcal disease (IPD) remains a significant global concern, particularly in immunocompromised individuals, children and older adults. The introduction of conjugated formulations has improved pneumococcal vaccine immunogenicity and efficacy in preventing IPD [426]. However, caveats remain in the performance of current pneumococcal vaccines and the optimal direction for future pneumococcal vaccine design. Parenterally administered formulations fail to generate neutralising IgA in the nasopharyngeal and respiratory mucosa, limiting their capacity to reduce infection and transmission. While conjugated pneumococcal vaccines do reduce carriage of the serotypes included in the formulation, serotype replacement by non-vaccine types is an additional and growing concern with over 100 circulating pathogenic serotypes, with current conjugated vaccines covering up to 23 serotypes [202, 203]. Conjugation approaches have improved vaccine performance by triggering T cell activity in response to the otherwise T-cell independent pneumococcal polysaccharide antigens [295]. However, generating robust long-lived humoral and cellular-mediated immunity to the bacterium is a goal that has not yet been completely achieved [427],[295]. Considering the evidence that the microbiota provides therapeutic benefit during pneumococcal infection and in keeping with the focus on *Streptococcus pneumoniae*, as a pathogen of high clinical relevance, we aimed to design a pre-clinical model of intranasal pneumococcal immunisation. Furthermore, it has recently emerged that the commensal microbiota has a functional role in the performance of parenterally administered pneumococcal vaccines[348], [363],[421]. It has recently emerged that pneumococcal antigen-specific intestinal IgA can synergise with systemic IgG to enhance pneumococcal vaccine efficacy in a microbiota dependent manner, further supporting evidence that the host microbiota can ameliorate pneumococcal vaccine responses[421]. Gutzeit *et al.* 2025, demonstrated that $IgA^{-/-}$ animals immunised with Prevnar13® had significantly reduced PPS-specific plasma IgG1 compared to WT mice, implying a dependency on IgA for generation of IgG1 responses to T-cell dependent antigens. Suppression of IgG3 but not IgM responses was also noted in $IgA^{-/-}$ animals in response to Pneumovax23 which contains T-cell independent antigens implying a direct link between IgA and antigen-specific IgG. Indeed, it was

found that IgA constrains activation-induced expression of the inhibitory receptor PD-1 on T cells[421].

As previously highlighted in the introduction, the microbiota is a governing factor of host immunity. Many exogenous and endogenous factors influence vaccine performance; however, the microbiota presents a potential driving factor behind the heterogeneity in vaccine performance between individuals[344]. Germ-free murine models, models of broad-spectrum antibiotic-mediated ablation of the microbiota, and clinical studies, based mainly on paediatric cohorts receiving antibiotic treatment, have identified causal links between dysregulation of the commensal microbiota and impaired responses to immunisation[102], [347], [363], [346]. The mechanisms by which the microbiota provides both immunostimulatory and immunomodulatory signals is explored in detail in section 6.5.2, however, these remain to be fully elucidated[344]. The current literature suggests that the ability of the microbiota to act as an "endogenous adjuvant", providing immunostimulatory signals to the innate immune compartment[362], [363], [365],[428]. Alternatively, the microbiota may "prime" resident lymphocytes to migrate to distal anatomical effector niches[18],[360]. However, the exact mechanisms by which microbiota-derived metabolites modulate outcomes of immunisation remains incompletely understood. SCFAs have emerged as microbiota-derived agents which can elicit pleiotropic immunomodulatory activity at distal anatomical sites. These metabolic products have demonstrated therapeutic effectivity in different models of respiratory infections, namely *S. pneumoniae*, *Influenza* and *K. pneumoniae,* implicating SCFAs as key participants in the protective role of the gut-lung axis during respiratory infection[195], [112],[107]. As shown in the previous chapter, butyrate protects dysbiotic animals against invasive pneumococcal pneumonia[73], [195], [425],[429]. While research has shown that SCFAs can improve vaccine immunogenicity *in vivo*, this area of research remains in its infancy. Importantly, almost all of the current studies focus on parenteral delivery of vaccines in the setting of antibiotic-induced dysbiosis[367],[102].

Nasal immunisation could improve immunisation regimes to respiratory pathogens by generating sterilising mucosal immunity at the site of pathogen entry[308],[430]. Nasal

vaccination strategies targeting *S. pneumoniae* would be of particular importance to prevent colonisation in addition to IPD and subsequently transmission of the pathogen[201]. It is known that the microbiota promotes mucosal immune responses, Ruane *et al.* 2016 demonstrated that the microbiota regulates the ability of lung dendritic cells to induce class switch recombination to IgA in respiratory B cells[18]. Both acetate and butyrate promote IgA^+ B cells in the intestine in a T cell-independent manner suggesting a role of SCFAs in supporting mucosal IgA responses[350],[343]. Therefore, it is plausible that SCFAs can support mucosal immune responses in the respiratory tract.

Differential effects of SCFAs on B cell functions and antibody production have been reported. Kim *et al*. 2016, highlighted a role for gut-derived SCFA in supporting B cell functionality. This study reported that SCFAs promoted B cell class-switching, resulting in enhanced IgA, IgG1, IgG2a, IgG2b and IgG3, due to the enhancement of class switching genes[124]. Similarly, Wu *et al*. 2023 found that administration of butyrate could alleviate vancomycin induced hypo responsiveness to the injectable rabies vaccine by enhancing the production of plasma cells[367]. This feature of SCFA boosting the functional capacity of B cells has also been demonstrated in human cells. *In vitro*, SCFA promoted the differentiation of naïve human B cells to $CD20^-CD38^+$ plasma B cells and increased production of IgA and IgG[124]. Immunisation can alter the profile of the resident gut microbiota, as demonstrated in the context of SARS-CoV2 immunisation. Following immunisation with the injectable BBIBP-CorV vaccine, α-diversity was significantly altered, with enhancements in SCFA fermentation pathways, nucleotide fermentation and degradation pathways, pyruvate fermentation and polysaccharide biosynthesis. In this study, a positive correlation was identified between SCFA bioavailability and ACE2-RBD inhibiting antibodies[431]. This provides another example of SCFA supporting antigen-specific humoral immunity in humans. In contrast to these enhancing effects, it has been shown that high-fibre diet dependent SCFA production and additional supplementation with butyrate derivatives, can impair B cell class switching and abrogate vaccine induced antibody production[371]. Sanchez *et al.* 2020, demonstrated that while low dose SCFA can enhance antigen-specific IgG3 and IgG2b, higher concentrations of SCFA had a suppressive effect on antigen-specific responses to

both mucosal and parenteral immunisation. This feature was driven by SCFA-mediated suppression of *Aicda* and *Prdm1* expression in a HDACi dependent mechanism[371].

SCFA have differential effects on T cell functions, explored in detail in section **1.6.5**. With the stage of T cell differentiation seemingly dictating the immunomodulatory outcomes of SCFA treatment[432].

The gut-lung axis of immune regulation relates to the common mucosal immune system where mucosal sites are immunologically integrated. By this logic, the effect of the microbiota and derived metabolites on immunisation may be stronger in the context of a mucosal vaccine, than in the parenteral or systemic setting. To examine the modulatory effects on adaptive immune processes in the respiratory parenchyma, a robust adaptive response would need to be generated locally in the lung. All pneumococcal vaccines to date have been designed for parenteral delivery. Therefore, in order to examine the immunomodulatory effects of short-chain fatty acids in this context, the first step was to design an effective experimental intranasal pneumococcal vaccine and to establish a model of intramuscular vaccination with Prevnar13® to investigate the effects of butyrate supplementation in both settings. **Here we examined the potential of harnessing the gut-lung axis of immune regulation in improving pneumococcal vaccine immunogenicity through dietary intervention with oral butyrate. We further assessed the effects of butyrate on an experimental trivalent intranasal pneumococcal vaccine as well as the licensed intramuscular vaccine 13-valent Prevnar.**

Hypothesis

"The gut-lung axis of immune regulation can be harnessed to improve intranasal vaccine immunogenicity through dietary intervention with the immunomodulatory short-chain fatty acid, butyrate."

Aims:

1. To establish a pre-clinical model of intranasal pneumococcal immunisation using a polyvalent heat-killed pneumococcal lysate coupled with the experimental mucosal adjuvant double mutant heat labile toxin (dmLT).

2. To determine the capacity of dietary intervention with the SCFA butyrate to modulate outcomes of immunisation using this model.

3. To investigate the impact of dietary intervention with the SCFA, butyrate, on outcomes of immunisation using the licensed pneumococcal vaccine, Prevnar13®.

4.1 Designing a polyvalent intranasal pneumococcal vaccine.

As highlighted in the introduction, there is only one vaccine to date licensed for intranasal administration in paediatric cohorts, the live attenuated influenza vaccine (LAIV). Historically, there has been an interest in the development of a pneumococcal vaccine suitable for nasal delivery. A live attenuated *S. pneumoniae* immunisation regime proved effective in protection against recolonisation under early-phase clinical trial in the United Kingdom (ISRCTN22467293)[289]. Similarly, a nasally administered pneumococcal vaccine containing conserved bacterial proteins entered phase I clinical trials (Ab-01.12) in 2024. **The main aim of this chapter was to examine the effects of butyrate supplementation on outcomes of intranasal immunisation, with a broader initiative of harnessing the gut-lung axis of immune regulation to improve respiratory vaccine immunogenicity.**

The first step was to establish an experimental nasal pneumococcal vaccine and effective immunisation regimen. A heat-killed trivalent pneumococcal lysate (referred to as SpnL) comprising three clinically relevant and well characterised pneumococcal serotypes, E1586 (serotype 1), E1434 (serotype 3) and TIGR4 (serotype 4) was kindly provided by our collaborators, Prof. Analía Rial and Prof. José A. Chabalgoity, Department of Biotechnology, School of Medicine, University of La República, Uruguay [282],[433]. To study the full extent of SCFA dietary supplementation on vaccine immunogenicity, an immunisation model which yields robust cellular and humoral immune responses was essential. The nasal cavity is constantly exposed to a variety of antigens and harbours a resident commensal microbiota. Similar to alternative routes of mucosal immunisation, overcoming a barrier of immune tolerance is necessary to achieve effective adaptive responses with adequate longevity for protection. Mucosal vaccines need to be tailored to the route of administration and elicit adequate immunogenicity to overcome this tolerogenic immune barrier. For this reason, we considered the inclusion of a highly immunostimulatory adjuvant. Double-mutant heat labile toxin is considered the “gold standard” mucosal adjuvant in preclinical models and has also entered clinical trial development in the setting of administration by transcutaneous (NCT04826094), intradermal (NCT03548064, NCT03922061,

NCT02531685), sublingual (NCT03548064), oral (NCT02531802, NCT04232943, NCT02052934, NCT03548064, NCT01147445, NCT01739231, NCT03038243, NCT03729219) and intramuscular (NCT03404674) routes[308]. Given the success of dmLT in driving robust mucosal and systemic humoral and cellular immunity in mice, dmLT was the adjuvant of choice in our model of intranasal trivalent pneumococcal lysate immunisation.

Mice were immunised intranasally (i.n.) with 15µg of total protein per dose of the SpnL, corresponding to 5µg/dose per pneumococcal serotype, on days 0 and 14, alone (antigen control) or with 1µg of dmLT/dose. On day 21, perfused lung tissue, spleens, serum and nasal lavages were collected for downstream analysis.

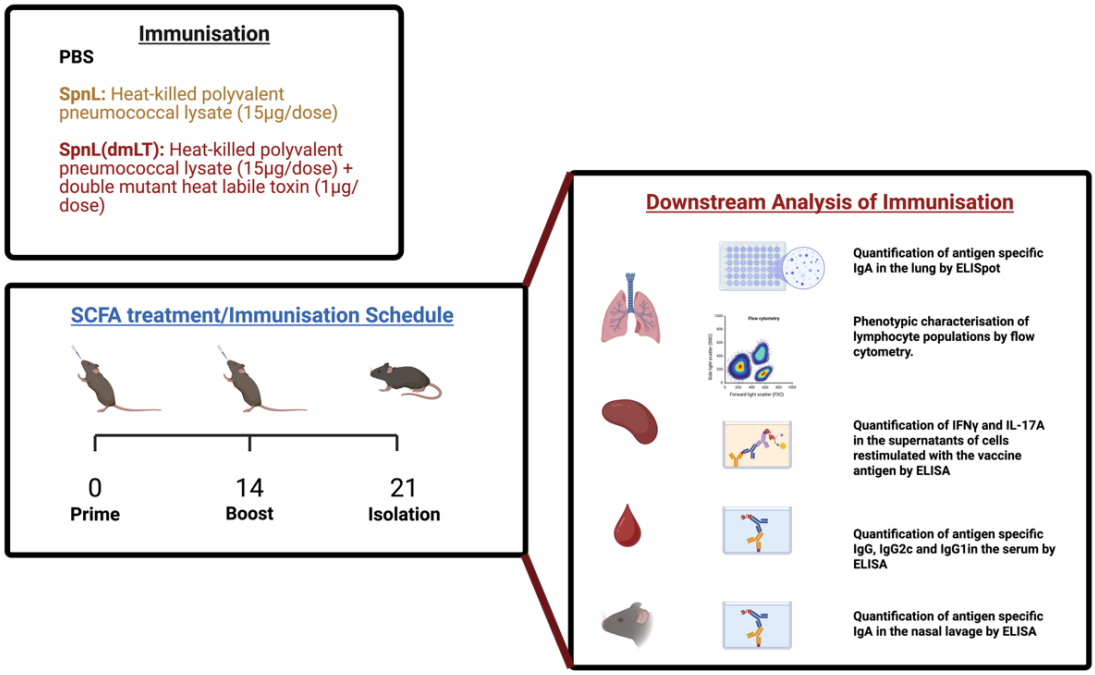


Fig. 4.1 Vaccination strategy for the experimental adjuvanted intranasal pneumococcal vaccine. Female C57BL6/J mice were immunised with a either PBS (vehicle control), polyvalent pneumococcal lysate, 15µg/dose (SpnL) or this lysate in combination with dmLT, 1µg/dose (SpnL + dmLT) on day 0 and again on day 14. Mice were sacrificed on day 21, serum was collected for analysis of systemic antibody responses. Lungs and spleens were isolated for analysis of *ex vivo* antigen-specific cytokine production, and immunophenotypic characterisation of lymphocyte populations**.** Serum, nasal washes and lung tissue was collected for analysis of antigen-specific antibody responses.

4.2 Nasal immunisation with the adjuvanted polyvalent whole-cell pneumococcal vaccine, SpnL(dmLT), generates antigen-specific IFN-γ and IL-17A in both the lung and spleen.

To first establish if this pre-clinical vaccine could generate antigen-specific cellular-mediated immune responses, the cytokine milieu, from the lungs and spleens of immunised mice was measured upon antigen recall. Single cell suspensions from spleens and lungs isolated from mice previously immunised with PBS (vehicle control), SpnL or SpnL(dmLT) were stimulated *in vitro* with SpnL at increasing concentrations (15µg/mL, 45µg/mL and 100µg/mL) for 72 hours. Anti-CD3 antibody, which will selectively target T cells through engagement of the T-cell receptor was included as a positive control for T cell-derived cytokine production. Post stimulation cell supernatants were collected and IFN-γ and IL-17A were quantified by ELISA. IFN-γ and IL-17A were chosen based on their roles in host response to pneumococcal infection as outlined in the introduction.

Antigen restimulation of both lung and splenic cells with SpnL led to production of IFN-γ and IL-17 only in mice that received SpnL or SpnL(dmLT) with undetectable or negligible cytokine production in the control group vaccinated with PBS, highlighting the response was specific to the vaccine antigens (**Fig 4.2 A-D)**. Antigen-specific IFN-γ production was significantly higher in the lung and spleen cells from mice previously vaccinated with SpnL(dmLT) compared to those that received SpnL alone in a dose-dependent manner (**Fig. 4.2 B, D**). All concentrations of antigen restimulation were successful in generating antigen-specific IL-17A upon recall in both the spleen and lung cells from mice previously vaccinated with SpnL(dmLT). Responses in the SpnL(dmLT) group were significantly higher compared with SpnL alone and demonstrated a dose-dependent trend (**Fig. 4.2 A, C**). For further experiments, 100µg/mL was chosen for antigen restimulation.

Therefore, nasal administration of the adjuvanted vaccine, SpnL(dmLT), proved successful at inducing antigen-specific IFN-γ and IL-17 producing T cells in both the lungs

and spleen, proving that our experimental vaccine was successful in driving cellular mediated immunity locally and systemically.

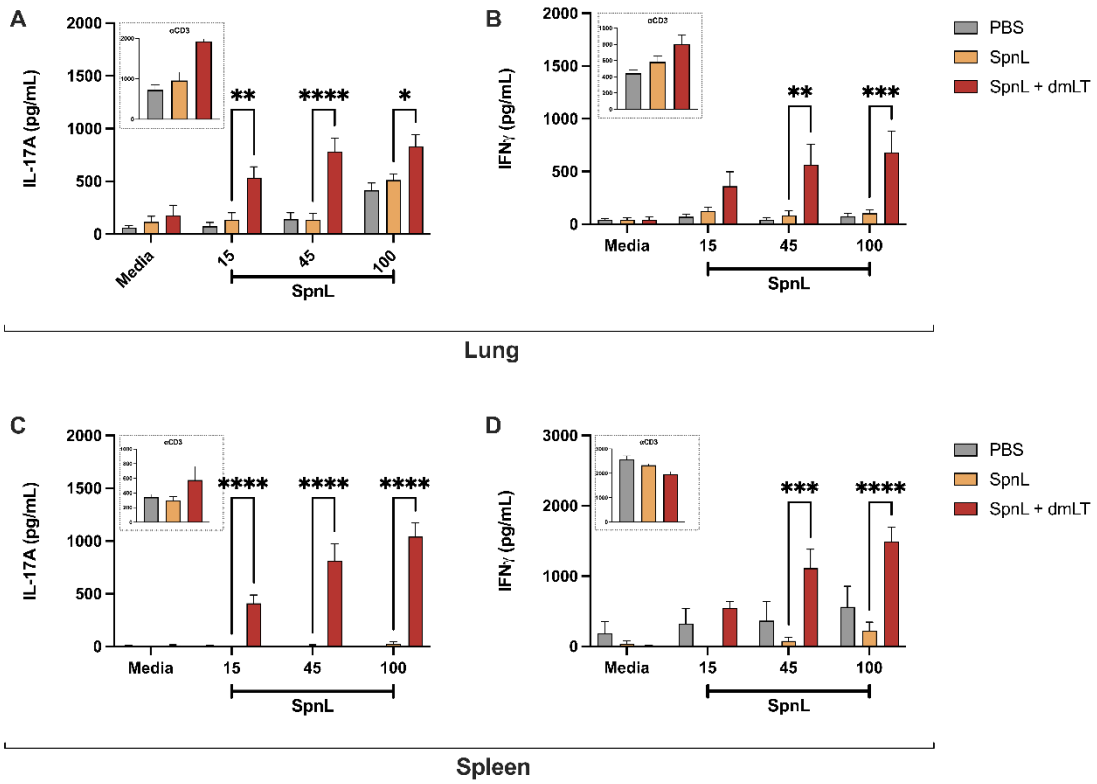


Fig. 4.2 An experimental intranasal adjuvanted pneumococcal vaccine, SpnL(dmLT) generates robust IL-17A and IFN-γ in vaccinated animals in response to antigen recall. Female C57BL6/J mice were immunised with a either PBS (vehicle control), polyvalent pneumococcal lysate, 15µg/dose (SpnL) or SpnL 15µg/dose + dmLT, 1µg/dose (SpnL(dmLT)) on days 0 and 14. Mice were sacrificed on day 21 and lung and splenic cells were isolated for downstream analysis. Single cell suspensions of lung (**A, B**) and splenic tissue (**C, D**) were plated and stimulated *ex vivo* with the polyvalent pneumococcal lysate (SpnL). Separately cells were restimulated with αCD3 as a positive control. Data is representative of mean ± SEM, with n=6/group, statistical significance was measured using two-way ANOVA using Bonferroni's post-hoc test, comparing conditions to the SpnL control. Data is representative of n=2 experimental replicates

4.3 Immunisation with the intranasal experimental polyvalent pneumococcal vaccine, SpnL(dmLT) results in increased lymphocyte populations in the lungs and drives $CD44^+CD4^+$ T effector/memory cells.

Following the success of this pre-clinical i.n. immunisation model at driving antigen-specific cytokine responses (**Fig. 4.2)**, the cellular sources of IFN-γ and IL-17 were investigated in both the lungs and spleen. Mice were immunised using the schedule and treatments outlined in **Fig. 4.1**. Upon sacrifice, lung and splenic tissue was collected, disrupted into single cell suspension and seeded at concentrations outlined in **section 2.1.7**. Single cell suspensions of these tissues were stimulated *ex vivo* with 100µg/mL of the antigenic pneumococcal lysate, SpnL, for 2 hours. Cells were subsequently exposed to Brefeldin A, the active ingredient in GolgiPlug™ in addition to stimuli (SpnL/αCD3) for a further 4 hours, to inhibit protein transport and allow intracellular detection of cytokine production by flow cytometry. Cells were subsequently stained as per the methods highlighted in **section 2.1.10**, using the fluorophores outlined in **table 3.5**. Immunophenotypic analysis was carried out by flow cytometry using the gating strategy outlined in **Fig. 4.3**. Mice immunised i.n. with SpnL(dmLT) has higher overall viable number in comparison to mice immunised with SpnL alone, as measured by trypan blue counts of perfused whole lung tissue single cell suspensions (**Fig. 4.4 A**). The frequency and number of $CD45^+$ immune cells in the lungs of SpnL(dmLT) immunised mice were significantly higher than in SpnL immunised mice (**Fig. 4.4 B, C**).

This indicated that the nasal vaccine increased the number of immune cells in tissues adjacent to the route of immunisation. B cells, characterised as $CD45^+$, $CD19^+$, $CD3^-$ were significantly increased in both frequency of total live cells and total cell numbers in the lungs of mice immunised with the adjuvanted formulation (**Fig. 4.4 D, H**). This suggests that the adjuvanted formulation, SpnL(dmLT) promotes homing or local expansion of antigen-specific B cells that could contribute to local humoral responses in addition to local cell mediated immunity. Additionally, a significant increase in both the frequency and total number of T cells, characterised as $CD45^+$, $CD3^+$, $CD19^-$ was observed in SpnL(dmLT) immunised mice (**Fig. 4.4 E, I**). Investigation of the local T cell populations identified a significant increase in $CD4^+$ T cell populations in the mice immunised with

SpnL(dmLT) (**Fig. 4.4 F, J**). In contrast no statistically significant or observable increases in the frequency or total number of $CD8^+$ T cells was observed (**Fig. 4.4 G, K**), implying the cytokine production seen in response to antigen recall was likely mediated by $CD44^{hi}CD4^+$ T cells.

T cell populations were further stratified. Alternative T cell subsets, particularly memory γδT cells have been identified as sources of IL-17A and IFN-γ, during antigen recall in the response to gram-positive bacterial infection[434],[435]. Thus, we wanted to identify if the antigen-specific cytokine production seen in response to vaccination could be in part attributed to resident γδT cell populations. Resident γδT cell total numbers were increased in the lung tissue of animals immunised with the adjuvanted formulation, SpnL(dmLT), in comparison to those immunised with the lysate alone, SpnL (**Fig. 4.4 L, M**). However, no significant increase in $IL\text{-}17A^+$ $\gamma\delta TCR^+$ T cell populations was noted in animals immunised with SpnL(dmLT) compared to those administered SpnL (**Fig. 4.4 N, O**). Furthermore, no $IFN\text{-}\gamma^+$ $\gamma\delta TCR^+$ T cell populations were identified, consequently γδT cells were eliminated as a source of antigen-specific cytokine production**,** (**Fig. 4.3**)**.** High levels of CD44 surface expression, is classically associated with effector and memory T cell phenotypes[436]. Effector/memory T cells were defined as $CD45^+$, $CD3^+$, $CD4^+$, $CD44^{hi}$ and analysed for intracellular expression of IL-17A or IFN-γ. No IL-17A or IFN-γ expression was detected in $CD44^{lo}$ or $CD44^-$ populations (**Fig. 4.3**). Instead, the source of antigen-specific IL-17A and IFN-γ from mice immunised with the adjuvanted formulation was attributed to $CD45^+CD3^+CD4^+CD44^{hi}$ cells which showed $IL\text{-}17A^+$ and $IFN\text{-}\gamma^+$ populations, which were considered Th17 and Th1 populations respectively. In both cases, expression of IL-17A and IFN-γ, appeared dependent on the adjuvanted formulation, with significant increases in these groups compared to mice receiving the antigen alone (**Fig. 4.5 A-D**).

Ultimately, the events recorded for NK cells ($CD3^-CD19^-NK1.1^+$) acquired during cytometric analysis were below the threshold considered reliable to measure this population (less than 100 events), thus this population was excluded from further analysis (**Fig. 4.3**).

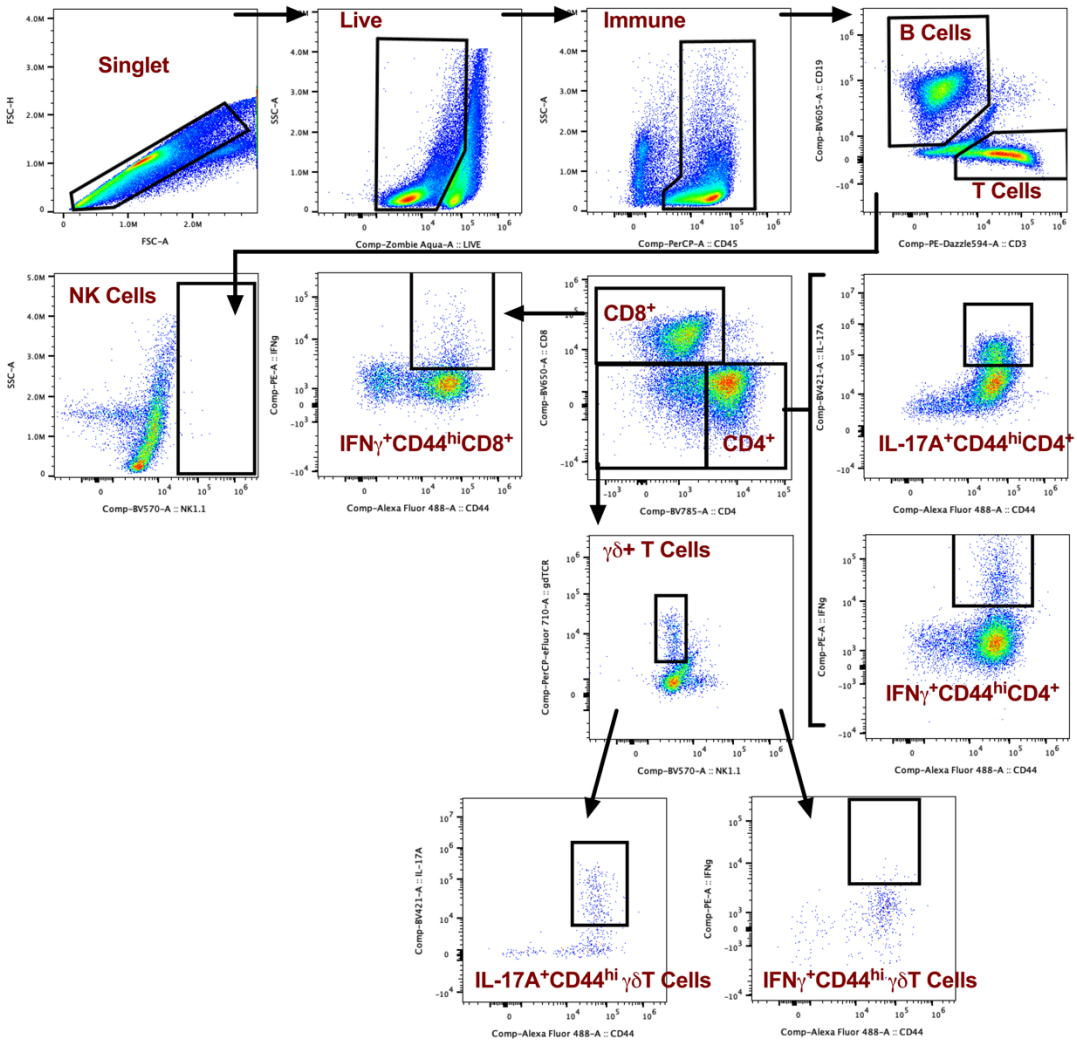


Fig. 4.3 Immunophenotyping of resident lymphocyte populations post immunisation. Lung parenchymal cells and splenocytes were isolated from immunised mice and stimulated *ex vivo* with SpnL. Cells were then stained for the surface markers outlined in **table 3.5**. Intracellular IL-17A and IFN-γ were measured by further intracellular staining. Cells were phenotypically characterised by the following co-expression patterns of surface markers all gated on live, single cells and $CD45^+$: B Cells: $CD19^+$, $CD3^-$, T cells $CD19^-$, $CD3^+$, $\gamma\delta TCR^+$ further stratified by expression of IL-17A/IFN-γ and co-expression of CD44 and CD4 or CD8 to distinguish helper and cytotoxic T cells. NK cells were phenotypically identified as ($CD3^-$, $CD19^-$, $NK1.1^+$). Gating strategy shown is representative of lung parenchymal phenotypic analysis.

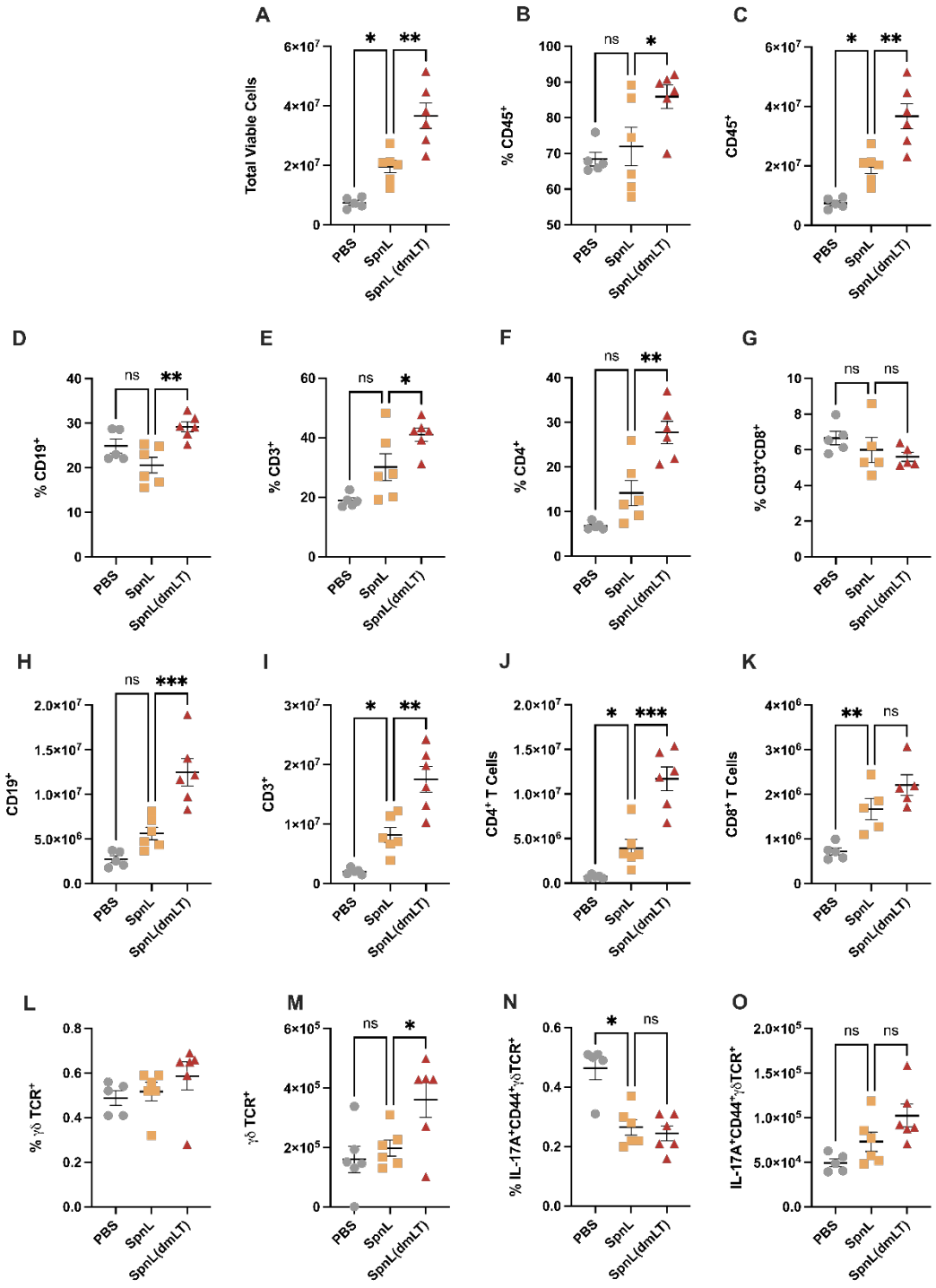


Fig. 4.4 Nasal vaccination with SpnL(dmLT) promotes increases in lymphocyte populations in the lung parenchyma. Female C57BL6/J mice were immunised based on the vaccination strategy outlined in Fig. 4.1. Lung parenchymal tissue was isolated and disrupted to a single cell suspension prior to *ex vivo* restimulation with the polyvalent pneumococcal antigen (100µg/mL) for 6 hours. Lymphocyte populations in the lungs were phenotypically characterised by flow cytometry using the gating strategy characterised in Fig. 4.3. Cell frequencies in percentage of live cells (**B, D, E, F, G, H, L, N**) and total population numbers in lung tissue (**A, H, I, J, K, M, O**) are shown. Data is representative of mean ± SEM, where n=5/6 biological replicates, statistical significance was determined by one-way ANOVA using Dunnett's post-hoc test, * $p < 0.05$, ** $p < 0.01$, *** $p < 0.005$. Representative experiment, where experiment was performed twice with consistent trends across 2 independent experiments.

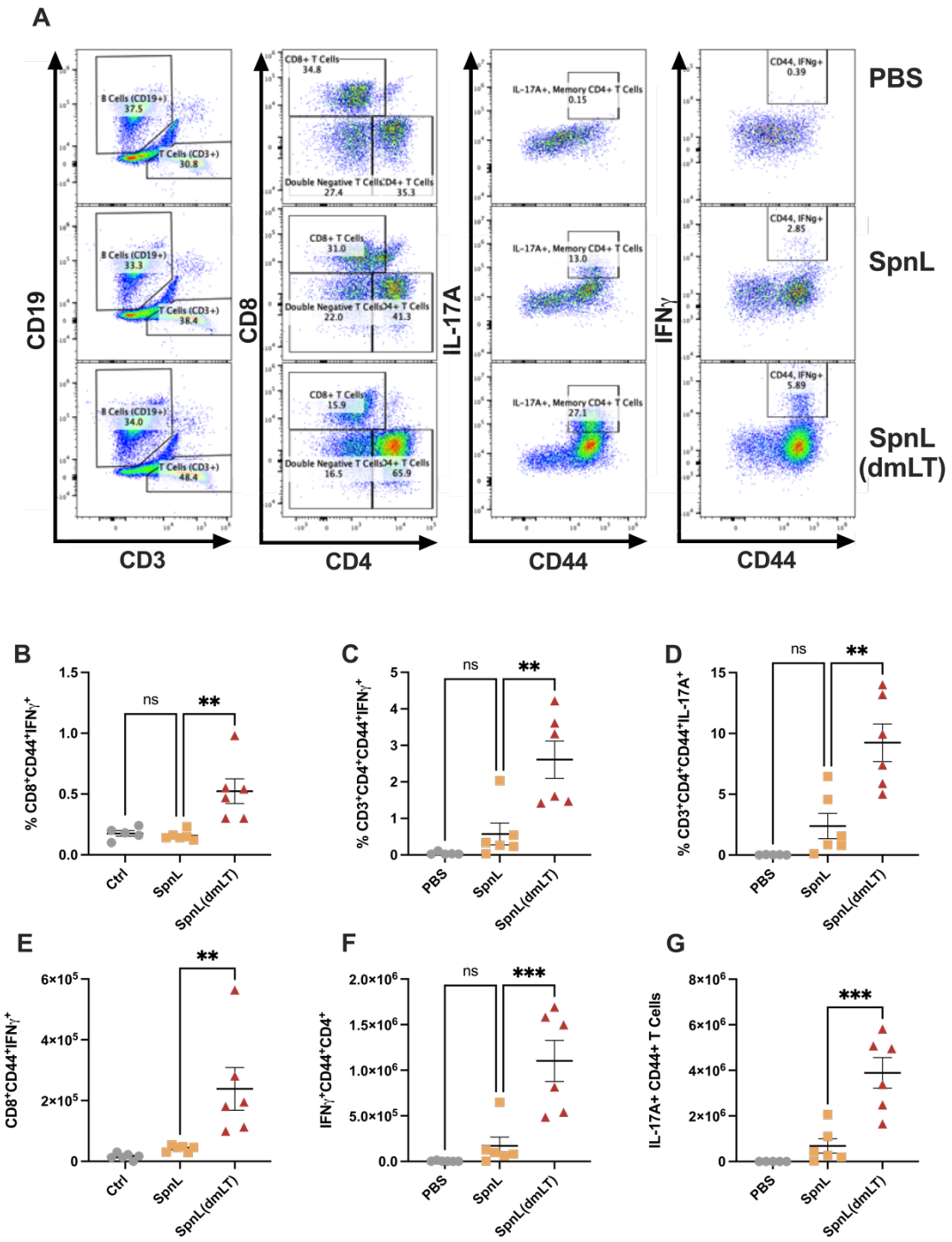


Fig. 4.5 Nasal vaccination with SpnL(dmLT) generates memory T cell populations in the lung capable of IL-17A and IFN-γ production upon antigen restimulation. Female C57BL6/J mice were immunised based on the vaccination strategy outlined in Fig. 4.1. Lung parenchymal tissue was isolated and disrupted to a single cell suspension prior to *ex vivo* restimulation with the polyvalent pneumococcal antigen (100µg/mL) for 6 hours. Lymphocyte populations in the lungs were phenotypically characterised by flow cytometry using the gating strategy characterised in Fig. 4.3. Cell frequencies in percentage of live cells (**A, B, C**) and total population numbers in lung tissue (**D, E, F**) are shown. Data is representative of mean ± SEM, where n=5/6 biological replicates, statistical significance was determined by one-way ANOVA using Dunnett's post-hoc test, * $p < 0.05$, ** $p < 0.01$, *** $p < 0.005$. Representative experiment, where experiment was performed twice with consistent trends.

4.4 Intranasal SpnL(dmLT) does not increase splenic total lymphocyte populations but leads to increased splenic effector/memory $CD4^+CD44^+$ T cell populations.

In the lungs, animals immunised with SpnL(dmLT) exhibited significant increases in $CD19^+$ B cell and $CD4^+$ T cell populations. Furthermore $CD44^+$ effector/memory T cells were significantly increased locally in the lungs and produced IL-17A and IFN-γ upon antigen recall. Given the success of this system at generating robust $CD4^+$ dominant cell-mediated immunity, the logical next step was to investigate if this applied in the systemic context. It has been widely documented that mucosal immunisation can elicit antigen-specific systemic immunity [308]. Animals were immunised as per the schedule outlined in **Fig. 4.1**. Spleens were isolated at the time of sacrifice and processed to seed single cell suspensions of splenocytes for antigen restimulation as described above in **section 4.3**. Cells were subsequently stained and analysed by flow cytometry; phenotypic characterisation was based on the gating strategy outlined in **Fig. 4.3**.

Splenocytes from mice immunised with SpnL(dmLT) exhibited similar frequencies of B and T cells (**Fig. 4.6 D, E, H, I**). However, a trending increase in total $CD19^+$ B cells (**Fig. 4.6 H**) was observed. Similarly, total T cells ($CD3^+$), $CD4^+$ T cells or $CD8^+$ T cells showed a slight visible increase in the SpnL(dmLT) group compared to SpnL alone but these were not significant across treatment groups (**Fig. 4.6 A-D**). We further investigated the ability of the adjuvanted, SpnL(dmLT), formulation to drive $CD44^+$ effector/memory T cell populations able to produce IFN-γ and IL-17 in the spleen of vaccinated mice. The inclusion of dmLT in the formulation resulted in a significant increase of Th1 cells compared to animals immunised with SpnL alone (**Fig. 4.7 F**) and a non-significant increase in frequency of Th1 cells (**Fig. 4.7 C**). Similarly, total numbers of Th17 cells were significantly increased in SpnL(dmLT) immunised animals compared to those immunised with antigen alone (**Fig. 4.7 G**) however this was not seen in the frequency of this population (**Fig. 4.7 D**). Interestingly, vaccination with unadjuvanted SpnL led to enhanced splenic Th17 memory T cell numbers when compared to PBS controls (**Fig. 4.7 D, G**).

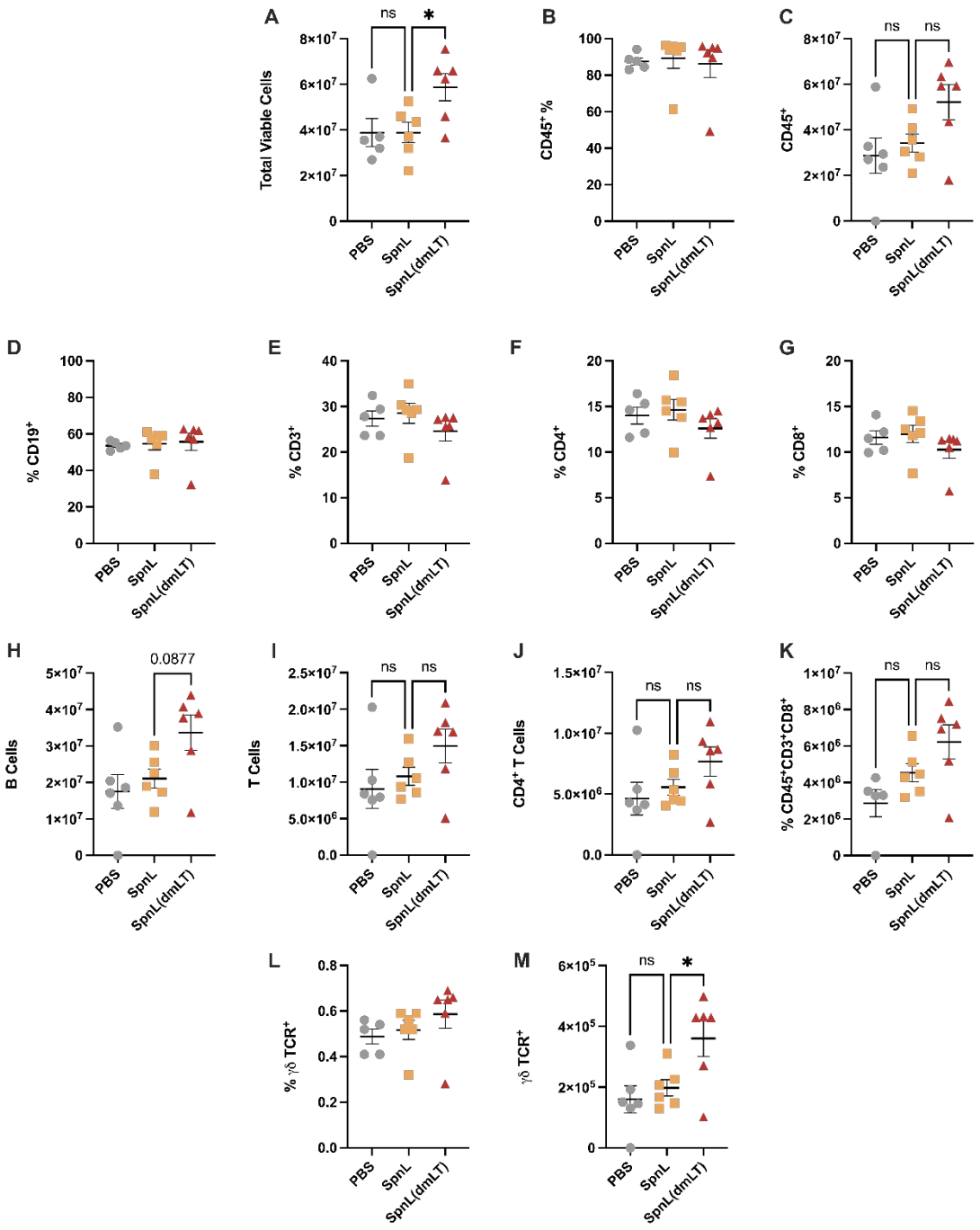


Fig. 4.6 Nasal vaccination with SpnL(dmLT) does not increase total lymphocyte populations in the spleens of immunised animals. Female C57BL6/J mice were immunised based on the vaccination strategy outlined in Fig. 4.1. Splenic tissue was isolated and disrupted to a single cell suspension prior to *ex vivo* restimulation with the polyvalent pneumococcal antigen (100µg/mL) for 6 hours. Lymphocyte populations in the spleen were phenotypically characterised by flow cytometry using the gating strategy characterised in Fig. 4.3. Cell frequencies in percentage of live cells (**B, D, E, F, G, L**) and total population numbers in lung tissue (**C, H, I, J, K, M**) are shown. Data is represented as mean ± SEM (n=5/6), statistical significance was determined by one-way ANOVA using Dunnett's post-hoc test, * $p < 0.05$, ** $p < 0.01$, *** $p < 0.005$. Representative experiment, where experiment was performed twice with consistent trends.

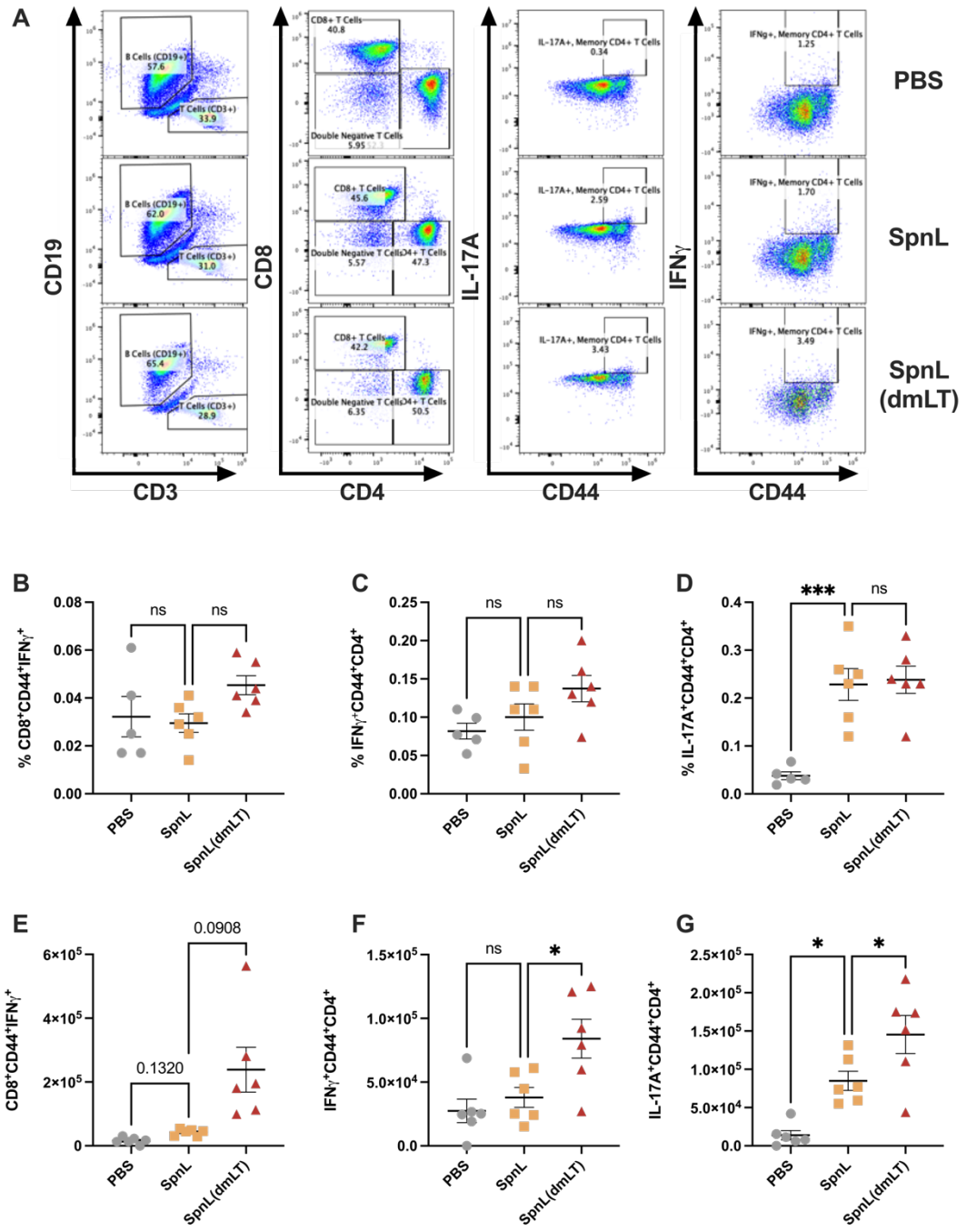


Fig. 4.7 Nasal vaccination with SpnL(dmLT) promotes memory T cell populations in the spleen capable of IL-17A and IFN-γ production upon antigen restimulation. Female C57BL6/J mice were immunised based on the vaccination strategy outlined in Fig. 4.1. Splenic tissue was isolated and disrupted to a single cell suspension prior to *ex vivo* restimulation with the polyvalent pneumococcal antigen (100µg/mL) for 6 hours. Lymphocyte populations in the spleen were phenotypically characterised by flow cytometry using the gating strategy characterised in Fig. 4.3. Cell frequencies in percentage of live cells (**B, C, D**) and total population numbers in lung tissue (**E, F, G**) are shown. Data is representative of mean ± SEM, where n=5/6 biological replicates, statistical significance was determined by one-way ANOVA using Dunnett's post-hoc test, * $p < 0.05$, ** $p < 0.01$, *** $p < 0.005$. Representative experiment, where experiment was performed twice with consistent trends.

4.5 Immunisation with SpnL(dmLT) promotes serum antigen-specific IgG antibodies.

Having demonstrated that our experimental vaccine could generate robust antigen-specific cell mediated immunity, we proceeded to evaluate the humoral responses elicited by the trivalent preparation of pneumococcal antigens combined with dmLT. The clinical correlates of pneumococcal vaccine efficacy are antibody titres targeting the outer pneumococcal polysaccharide as well as opsonophagocytic killing assay (OPKA)[437]. As outlined in section **1.5.5**, targeting non-capsular antigens could prove an effective approach to increasing coverage to non-vaccine serotypes and targeting intercellular virulence factors to further improve protection against invasive disease in susceptible cohorts[318],[295]. Therefore, we tested antibodies against SpnL which likely include antibodies against both surface and internal protein components of the bacteria, in addition to this we tested polysaccharide specific antibodies against the serotype 3 capsular polysaccharide. Animals were immunised as per the schedule highlighted in **Fig. 4.1**. Blood was collected at the time of sacrifice and allowed to coagulate before separation of serum by centrifugation. Antigen-specific antibodies were measured by ELISA against the pneumococcal lysate.

The experimental adjuvanted pneumococcal vaccine SpnL(dmLT) was capable of inducing antigen-specific serum IgG against total SpnL with significantly increased levels compared to animals immunised with SpnL alone (**Fig. 4.8 A, E**). Vaccination with SpnL alone induced lower antigen-specific IgG titres than SpnL(dmLT), yet significant antigen-specific IgG compared to control immunised animals (**Fig. 4.8, A, E**). Having noted an increase in total antigen-specific IgG, SpnL-specific IgG1 and IgG2c were measured in the serum. Again, vaccination with SpnL(dmLT) significantly enhanced SpnL-specific IgG2c and IgG1 compared to animals immunised with SpnL alone (**Fig. 4.8 B, C, F, G**). However, vaccination with SpnL alone significantly boosted SpnL specific IgG2c compared to control immunised controls but not SpnL specific IgG1 which demonstrated a trending increase (**Fig. 4.8 G**).

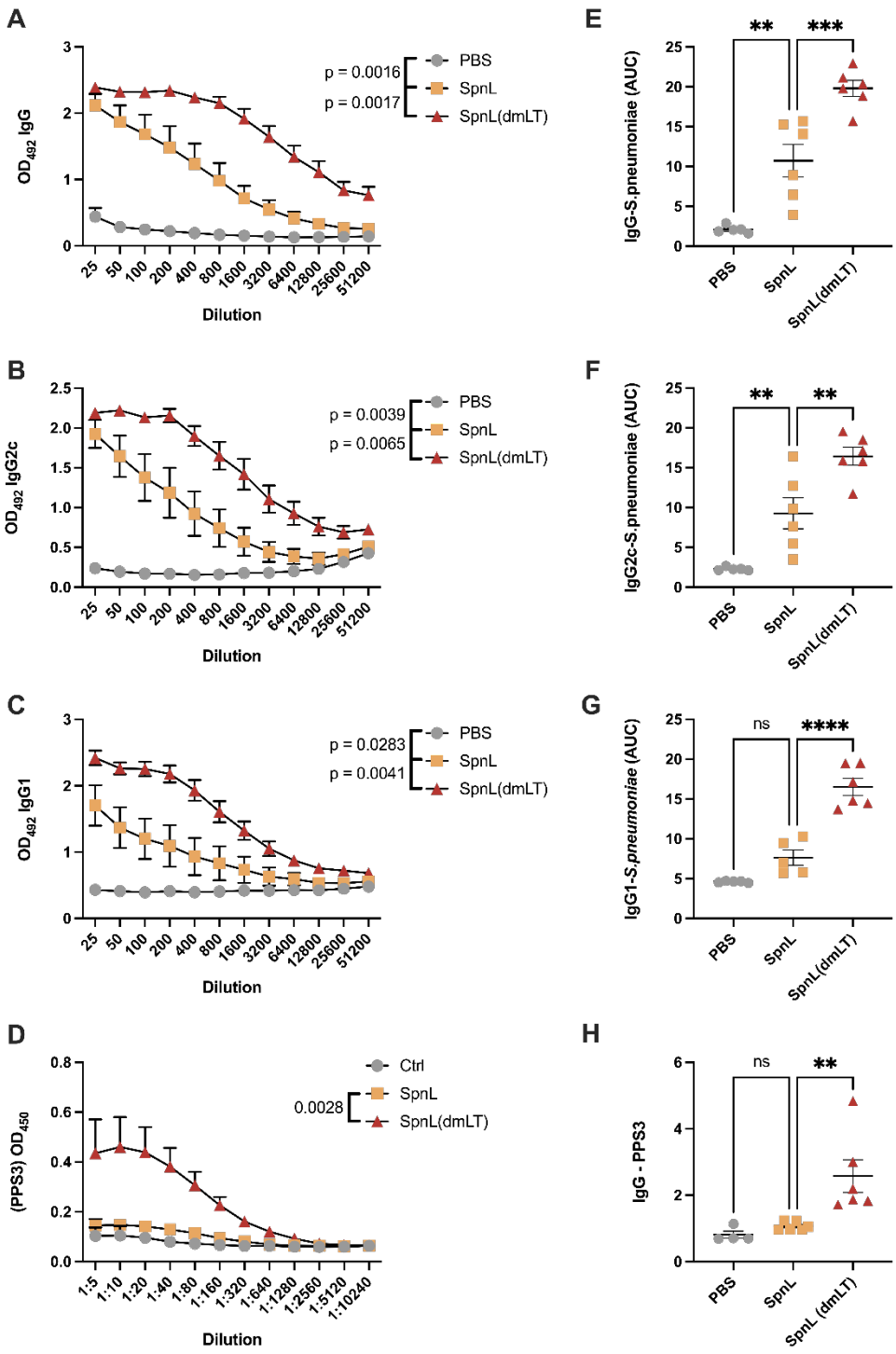


Fig. 4.8 Nasal vaccination with SpnL(dmLT) promotes antigen-specific humoral immunity, enhancing antigen-specific serum total IgG, and IgG1 and IgG2c subclasses against the trivalent SpnL. Female C57BL6/J mice were immunised based on the vaccination strategy outlined in Fig. 4.1. Serum was collected for downstream analysis, and antigen-specific IgG, IgG2c and IgG1 was quantified by ELISA to determine SpnL (**A, B, C, E, F, G**) and PPS3 (**D, H**) specific antibodies. Serum was serially diluted (**A, B, C, D**) and antibody titres were calculated as area under the curve (AUC) (**E, F, G, H**). Results shown as the mean value for individual animals. Data represents mean ± SEM, where n=5/6 biological replicates/group. Statistical significance was determined by one-way ANOVA, using Dunnett's post-hoc test, ** $p < 0.01$, *** $p < 0.005$. Representative experiment of 2independent experiments.

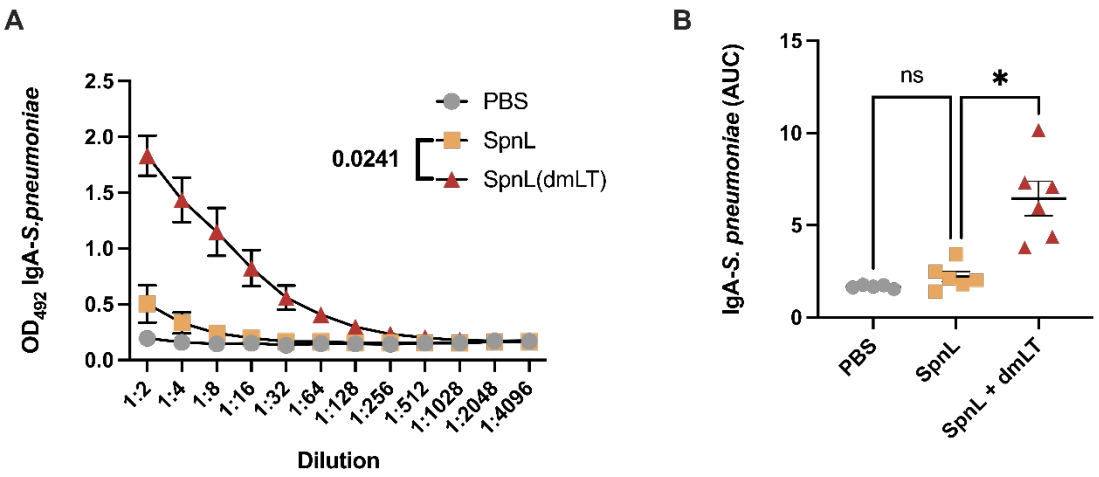


Fig. 4.9 Nasal vaccination with SpnL(dmLT) generates local antigen-specific IgA in the nasal cavity. Female C57BL6/J mice were immunised based on the vaccination strategy outlined in Fig. 4.1. Lavages of the nasal cavity were collected, and antigen-specific IgA was quantified by ELISA. Titration of nasal lavage by ELISA (**A**) and the area under the curve (AUC) (**B**) of each animal were used as proxies of IgA detection. Data is representative of mean ± SEM, where n=5/6 biological replicates/group. Statistical significance was determined by Kruskal-Wallace test, using Dunn's post-hoc test, * $p < 0.005$. Representative of one independent experiment.

4.6 SpnL(dmLT) promotes local antigen-specific IgA in the nasal tract and lungs.

Heat labile enterotoxins are highly effective at generating antigen-specific mucosal IgA in addition to systemic cellular and humoral responses, this has additionally been investigated in a pre-clinical model of nasal pneumococcal vaccination[339],[341]. Upper respiratory tract antigen-specific IgA and IgG are generated in response to challenge with *S. pneumoniae* serotype 6B and 23F in human pneumococcal carriage models, and it has been proposed that mucosal humoral responses are fundamental to protection against natural infection[291]. This further emphasises that generation of antigen-specific IgA in the nasal cavity through intranasal immunisation could overcome this upon pathogen re-encounter. *S. pneumoniae* has developed mechanisms of sub diversion of IgA via IgA protease, implying that secretory IgA is a crucial component of host defence against pneumococcal infection[438].

Therefore, we tested the ability of vaccination with SpnL(dmLT) to increase SpnL-specific IgA in nasal washes and lungs compared to those that received SpnL alone. Generation of mucosal neutralising antibodies protects against transmission and invasive respiratory infection. A high bacterial burden of nasopharyngeal colonisation is a risk factor for both transmission and the development of pneumonia through aspiration[201]. Thus, antigen-specific IgA in nasal lavages would be considered a potentially protective factor against colonisation and pneumococcal disease.

The experimental i.n. polyvalent pneumococcal vaccine was successful at generating antigen-specific secretory IgA in the nasal cavity. Antigen-specific IgA was significantly increased in nasal lavages of mice vaccinated with SpnL(dmLT) compared to SpnL alone (**Fig. 4.9 A, B**). The ability of this experimental adjuvanted vaccine to generate antigen-specific IgA in the lungs was also measured by ELISpot. Lung single cell suspensions from vaccinated or control mice were incubated in the presence of media (negative control), the polyvalent pneumococcal lysate at a concentration of 20µg/mL (antigen-specific stimulation), or LPS, a polyclonal B cell activator, to serve as a functional positive control for the detection of total IgA positive cells. Animals immunised with SpnL(dmLT) had significantly higher levels of relative spot volume (RSV) (**Fig. 4.10 B, D**) indicating a

significantly higher level of antigen-specific IgA in the lungs, compared to animals immunised with SpnL alone. Furthermore, antibody secreting cells (ASC) per million cells were also significantly upregulated in mice vaccinated with SpnL(dmLT) compared to SpnL alone (**Fig. 4.11 A, C**). This highlighted that antibody secreting cells were more abundant in animals immunised with SpnL(dmLT) compared to SpnL alone (**Fig. 4.10 B**). Similarly, polyclonal IgA was significantly increased in animals immunised with the adjuvanted formulation (**Fig. 4.10 C, D**).

Collectively, this data suggested that an adjuvanted formulation was essential for generating antigen-specific humoral responses in the nasal cavity and lung parenchyma, sites adjacent to the route of administration.

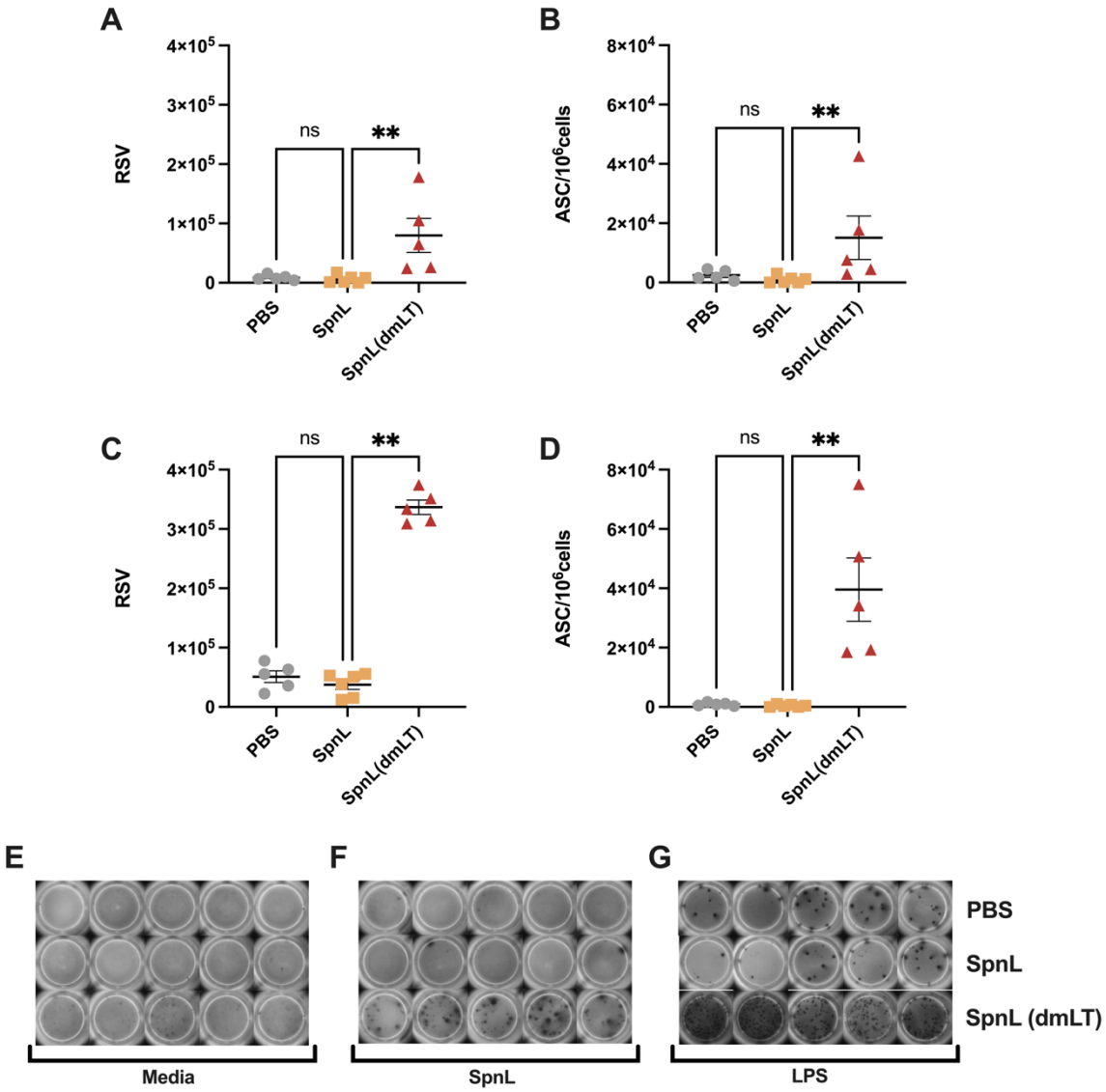


Fig. 4.10 Nasal vaccination with SpnL(dmLT)generates antigen-specific IgA in the lung parenchyma. Female C57BL6/J mice were immunised based on the vaccination strategy outlined in Fig. 4.1. Single cell suspensions of lung tissue were incubated in complete media (-ctrl) (**E**), SpnL (20µg/mL) (**A, B, F**) or LPS (*E. coli* derived R515) (**C, D, G**) as positive control for total IgA overnight, before IgA detection by ELISpot. Relative spot volume (RSV) of the wells (**B, D**) and antibody secreting cells (ASC)/10^6 cells (**A, C**) are shown. Data is representative of mean ± SEM, where n=5/6 mice/group. Statistical significance was determined by Kruskal-Wallace, using Dunn's post-hoc test, *** $p < 0.005$. Representative of 2 independent experiments.

Table. 4.1 Antigen-specific responses to SpnL(dmLT)

Site:	**Response:**	
	Cellular	***Humoral***
Serum	-	IgG, IgG2c, IgG1
Spleen	IL-17A$^+$CD44$^+$CD4$^+$ T cells (Th17) IFN-γ+CD44$^+$CD4$^+$ T cells (Th1) IFN-γ+CD44$^+$CD8$^+$ T cells	-
Nasal tract	-	sIgA
Lung	IL-17A$^+$CD44$^+$CD4$^+$ T cells IFN-γ+CD44$^+$CD4$^+$ T cells IFN-γ+CD44$^+$CD8$^+$ T cells	IgA, CD19$^+$ B Cells

4.7 Exploring the effects of SCFA-mediated modulation on pneumococcal vaccine responses.

We successfully generated a model of intranasal pneumococcal immunisation as a proof-of-concept in which we could further study the effects of dietary intervention with butyrate (**Table 4.1**). A schedule integrating dietary supplementation and the vaccine regimen was outlined as shown in **Fig. 4.11.**

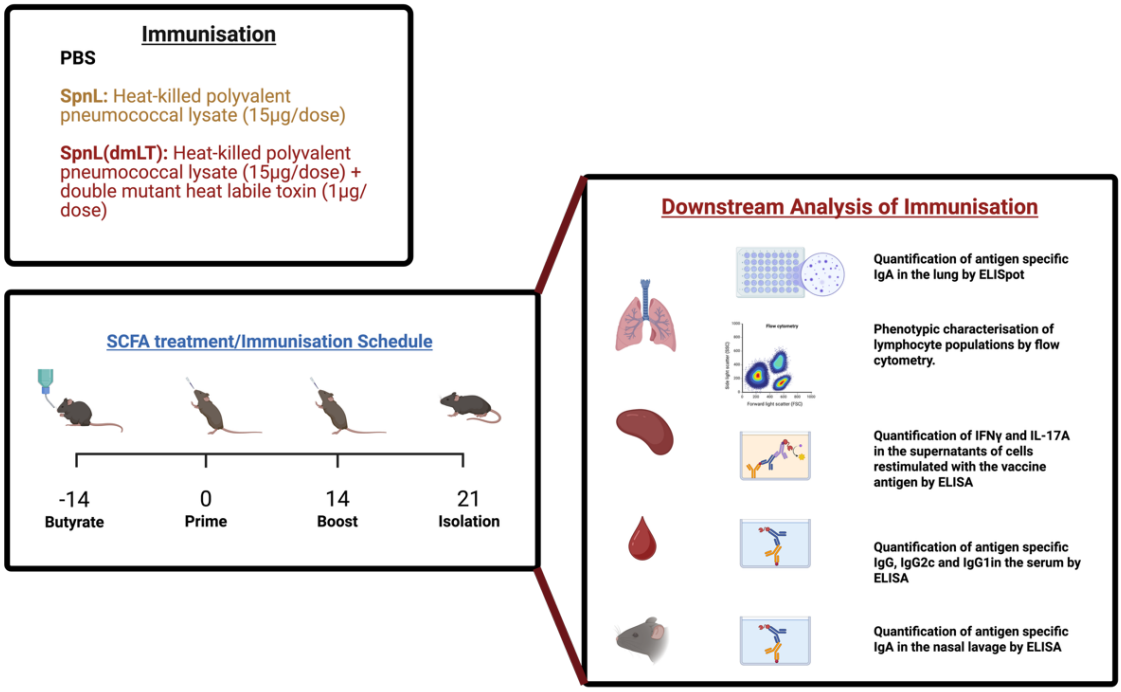


Fig. 4.11 Dietary supplementation during pneumococcal immunisation.
Female C57BL6/J mice were administered butyrate (100mM) in drinking water *ad libitum* 14 days prior to immunisation (day -14). On days 0 and 14, mice were immunised i.n. with either PBS (control), trivalent pneumococcal lysate, 15µg/dose (SpnL) or SpnL in combination with dmLT, 1µg/dose (SpnL(dmLT)). Mice were sacrificed on day 21 and tissue collected for analysis of immune responses. Serum was collected for analysis of systemic antibody responses. Lung and spleens were isolated for analysis of cytokine production, and immunophenotypic characterisation of lymphocyte populations**.** Nasal washes and lung tissue were also analysed for antigen-specific antibody responses including IgA.

4.8 Oral butyrate supplementation alters basal levels of lung and splenic IL-17A in the lung in naïve mice.

Before proceeding to assessing the effect of oral butyrate supplementation on immune responses in mice nasally vaccinated with SpnL(dmLT), we characterised the ability of butyrate to modulate levels of cytokine secretion by Th1 and Th17 cells in the lungs or spleens of naïve mice. For this, mice received 100mM butyrate in the drinking water *ad libitum*, for two weeks prior to administration of the vehicle control (PBS), intranasally and again 14 days after the initial inoculation to mimic the conditions of the future immunisation experiments. Animals were maintained on oral butyrate supplementation throughout the course of the experiment until sacrifice on day 21 (**Fig. 4.11)**. Lungs and spleens were then isolated and studied for production of T cell derived cytokines upon stimulation with media (baseline) and αCD3.

In the absence of *ex vivo* stimulation (media controls) prior oral butyrate supplementation did not alter baseline levels of IL-17A or IFN-γ, locally in the lungs or systemically in the spleens (**Fig. 4.12 A-D**). This implies that oral butyrate treatment does not modify baseline cytokine production by T lymphocytes. However, upon treatment with anti-CD3, there was a significant increase observed in production of IL-17A in the lung of naïve mice exposed to oral butyrate compared to controls (**Fig. 4.12 A**). This was not observed in splenic cells stimulated with anti-CD3 *ex vivo*, as both splenocytes from mice administered butyrate or water exhibited similar levels of IL17-A (**Fig. 4.12 C**). In the case of IFN-γ, butyrate supplementation did not alter its secretion upon αCD3 restimulation in lungs or spleens compared to drinking water alone.

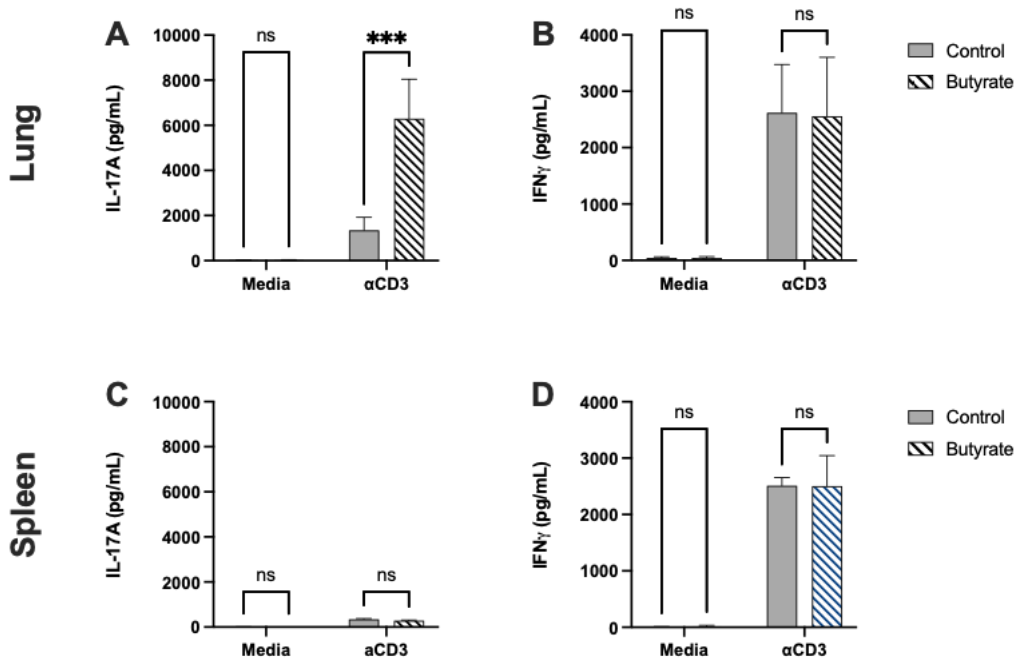


Fig. 4.12 Oral butyrate supplementation can alter resident T-cell derived lung IL-17A levels in naïve mice. Mice were administered butyrate (100mM) in drinking water ad libitum for 14 days prior to i.n. instillation with PBS. Mice were then maintained on oral butyrate supplementation and re-administered PBS i.n. 14 days post initial immunisation, prior to sacrifice on day 21. Lung parenchymal and splenic cell preparations were cultured *ex vivo* in the absence of stimulation (media) or with αCD3 200ng/mL for 72 hours. IL-17A and IFN-γ were quantified in cell supernatants by ELISA. Data is represented as mean ± SEM, n=11 biological replicates from 3 independent experiments (**A, B, C, D**). Data was analysed by two-way ANOVA, using Bonferroni's post-hoc test. *** $p < 0.005$. Representative of two independent experiments.

4.9 Butyrate supplementation alters lymphocyte populations in the lungs of immunised mice.

The next objective was to evaluate the impact of butyrate supplementation on the resident immune populations in the lungs of mice immunised with SpnL(dmLT). Butyrate was administered at 100mM in the drinking water of mice *ad libitum*, for 14 days prior to priming with SpnL(dmLT) and throughout the course of immunisation, while controls received water alone. Mice were immunised with the adjuvanted vaccine, SpnL(dmLT), on days 0 and 14. On day 21, lung and spleens were collected for downstream analysis. Single cell suspensions of these tissues were treated as outlined previously in section **4.3**, stimulated for 6 hours *ex vivo* with the pneumococcal antigen, SpnL (100µg/mL) to drive production of the cytokines and allow their detection by flow cytometry after intracellular staining. In parallel, immunophenotyping of B cells and T cell subsets was conducted.

While the frequencies of B cells ($CD19^+$), T cells ($CD3^+$), $CD4^+$ T cells ($CD3^+$, $CD4^+$) or CD8+ T cells ($CD3^+$, $CD8^+$) remained unchanged after butyrate supplementation, an overall reduction in cellularity was observed in the lungs of animals receiving oral supplementation of butyrate during immunisation compared to controls (**Fig. 4.13 A, C, E, G**), (**Fig. 4.13 A**). The lower total numbers of live cells corresponded to significantly lower overall numbers of B cells (**Fig. 4.13 G**), and trending decreases in total T cells and helper ($CD4^+$), effector ($CD8^+$) T cells and γδT cells (**Fig. 4.13 H, I, J, K**) in butyrate treated mice compared to controls.

We went on investigate the effects of butyrate treatment on the profiles of vaccine induced effector/memory $CD44^+$ T cells. For this intracellular analysis of IFN-γ and IL-17A was performed by flow cytometry on single cell suspensions obtained from lungs of mice immunised with SpnL(dmLT) while receiving butyrate supplementation or water. Strikingly, oral supplementation with butyrate significantly supressed both IFN-γ and IL-17A production in $CD44^+CD4^+$ T cells in response to SpnL stimulation compared to immunised animals that received water alone (**Fig. 4.14 C, D, E, F**).

In the case of $CD8^{+}CD44^{hi}$ cells, no significant changes were observed in both the frequency and total number of IFN-γ^{+} cells between animals receiving butyrate compared to controls (**Fig. 4.12 A, B**). Due to the low number of IL-$17A^{+}$ gamma delta T cells and lack of IFN-γ producing gamma delta T cells, we ruled these out as a tangible source of cytokine same with NK cells.

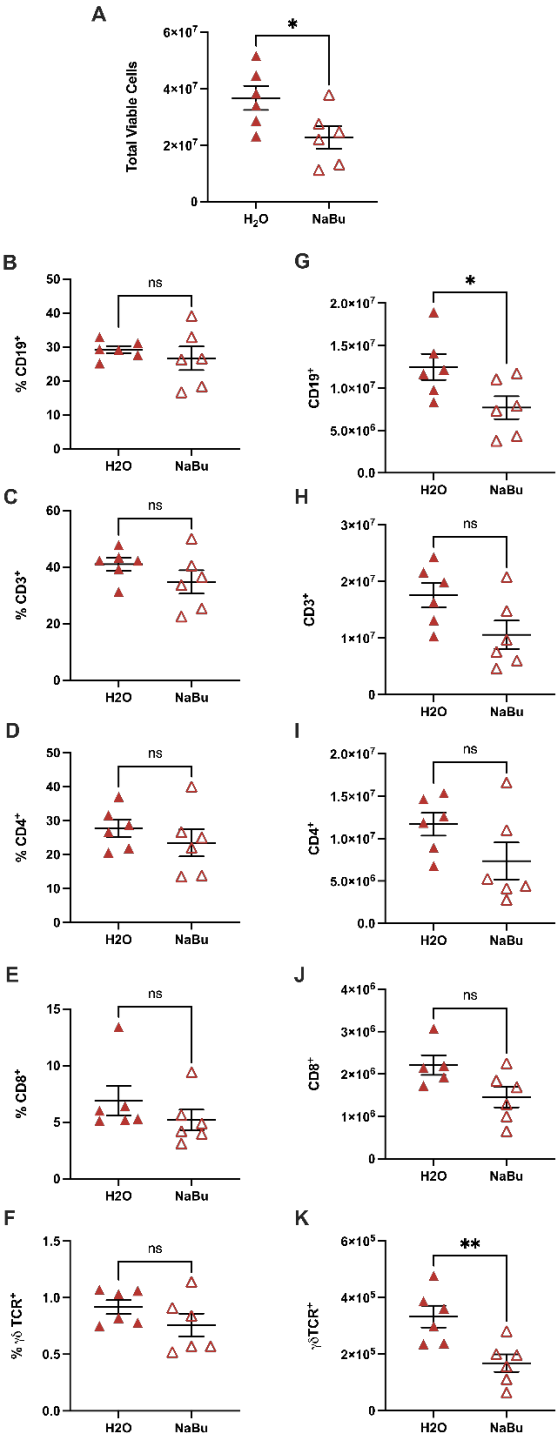


Fig. 4.13 Lymphocyte populations are decreased in the lung in immunised animals receiving dietary oral butyrate supplementation. Female C57BL6/J mice were administered butyrate (100mM) in drinking water ad libitum for 14 days prior to and during the course of nasal vaccination with SpnL(dmLT) on day 0 and again on day 14, prior to sacrifice on day 21. Lymphocyte populations were determined by flow cytometry, based on the gating strategy shown in **Fig. 4.3**. Cell frequencies (**B, C, D, E, F**) and total numbers (**G, H, I, J, K**) are shown. Data is representative of mean ± SEM, where n=5/6 replicates/group. Statistical significance was determined by Mann-Whitney test. * $P < 0.05$. Representative of two separate experiments.

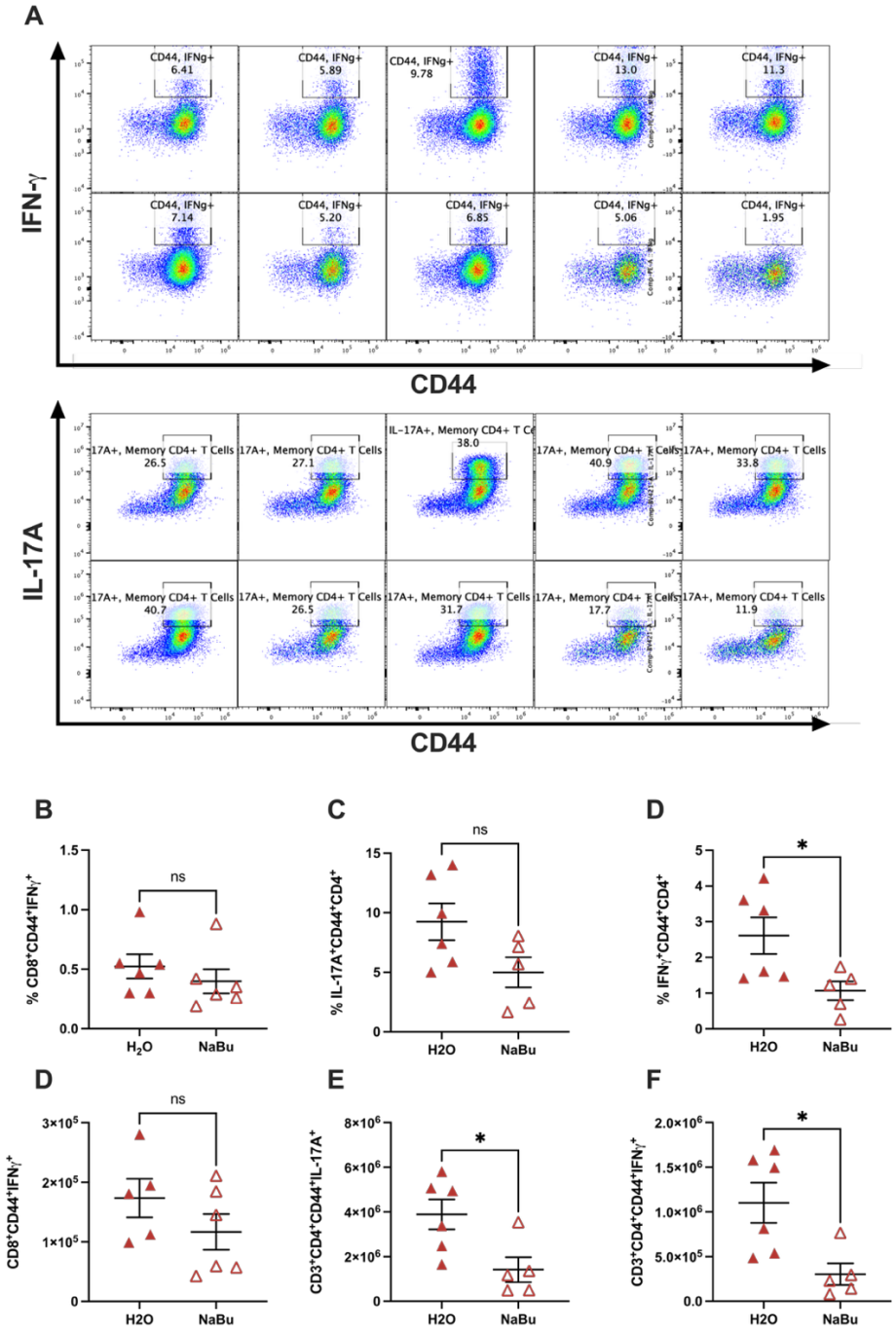


Fig. 4.14 Dietary intervention with butyrate results in lower numbers of IL-17A$^+$ and IFN-γ$^+$ CD44$^+$ memory T cells in the lungs of immunised mice. Female C57BL6/J mice were administered butyrate (100mM) in drinking water ad libitum for 14 days prior to and during the course of nasal vaccination with SpnL(dmLT) on day 0 and again on day 14, prior to sacrifice on day 21. Single cell suspensions of lungs were prepared and stimulated *ex vivo* with SpnL (100µg/mL) for 6 hours, prior to staining and immunophenotypic analysis by flow cytometry. Population analysis was based on the gating strategy outlined in Fig. 4.1. Plots are representative of Th17 and Th1 populations from 5 individual biological replicates (A) Graphs represent IFN-γ$^+$CD44$^+$CD4$^+$ (**C**), (**E**) and IL-17A$^+$ CD44$^+$CD4$^+$ (**B**), (**D**) T cell populations from immunised mice treated with water (control) or butyrate (NaBu). Data is representative of mean ± SEM, where n=5/6 biological replicates/group. Statistical significance was determined by Mann-Whitney test, * p <0.05. Data is representative of two experimental replicates.

4.10 Butyrate supplementation increases lymphocyte populations in the spleens of immunised mice.

We then examined how butyrate affected cell dynamics systemically. For this, antigen-specific cytokine production, lymphocyte frequencies and total counts were assessed in the spleens of immunised mice. As before mice received butyrate (100mM) in drinking water *ad libitum* for 14 days prior to initial immunisation and throughout the course of immunisation, **Fig. 4.11**.

Total lymphocyte populations were unaffected by dietary supplementation with butyrate. Both frequencies and total numbers of $CD19^+$ B cells, total T cells, $CD4^+$ T cells and $CD8^+$ T cells were not significantly different between butyrate treated and water controls (**Fig. 4.15 A-H**). We further investigated IL-$17A^+$ and IFN-γ+ producing lymphocyte populations in splenic tissue. Conversely to the trend seen in the lung, the frequencies of Th17, Th1 and $CD8^+CD44^+$IFN-γ^+ T cells were increased in animals receiving butyrate (**Fig. 4.16 B, C, D, E, F**). This was reflected in the total cell number of the aforementioned populations (**Fig. 4.16 G, H, I, J, K**).

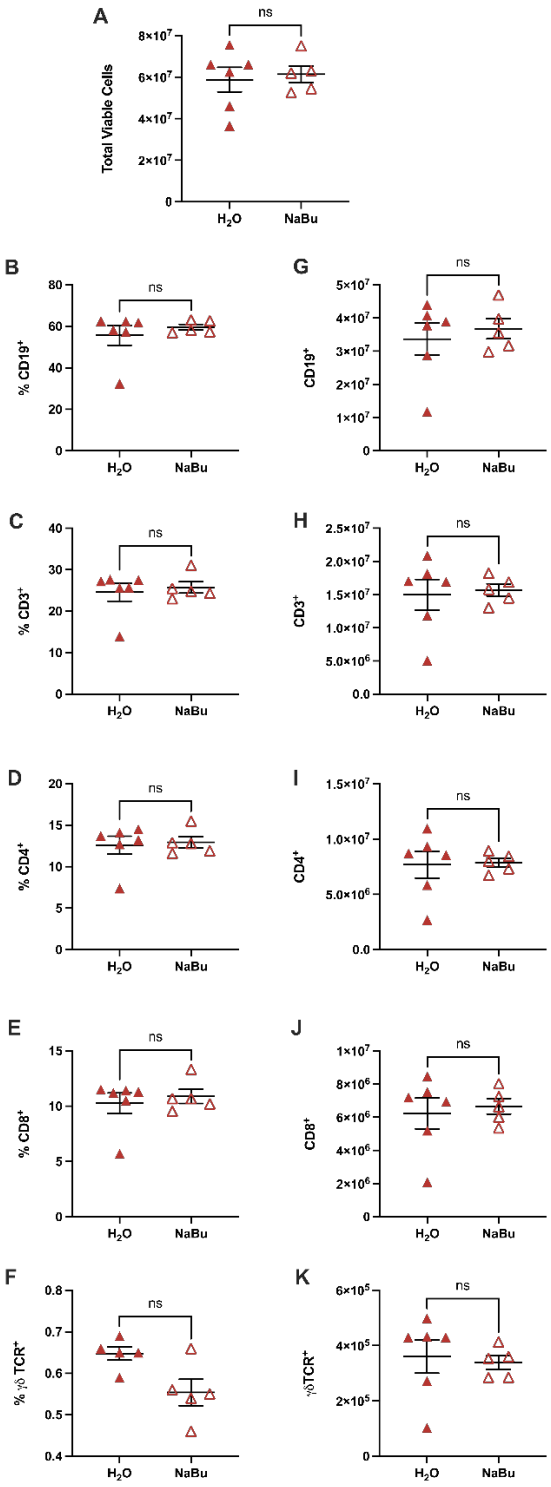


Fig. 4.15 Lymphocyte populations are unchanged in the spleen of immunised animals receiving dietary oral butyrate supplementation. Female C57BL6/J mice were administered butyrate (100mM) in drinking water ad libitum for 14 days prior to and during the course of i.n. instillation with SpnL(dmLT) on day 0 and again on day 14, prior to sacrifice on day 21. Lymphocyte populations were determined by flow cytometry, based on the gating strategy shown in Fig. 4.3. Cell frequencies (**B, C, D, E, F**) and total numbers (**G, H, I, J, K**) are shown. Data is representative of mean ± SEM, where n=5/6 replicates/group. Statistical significance was determined by Mann Whitney test, * $p < 0.05$, ** $p < 0.01$

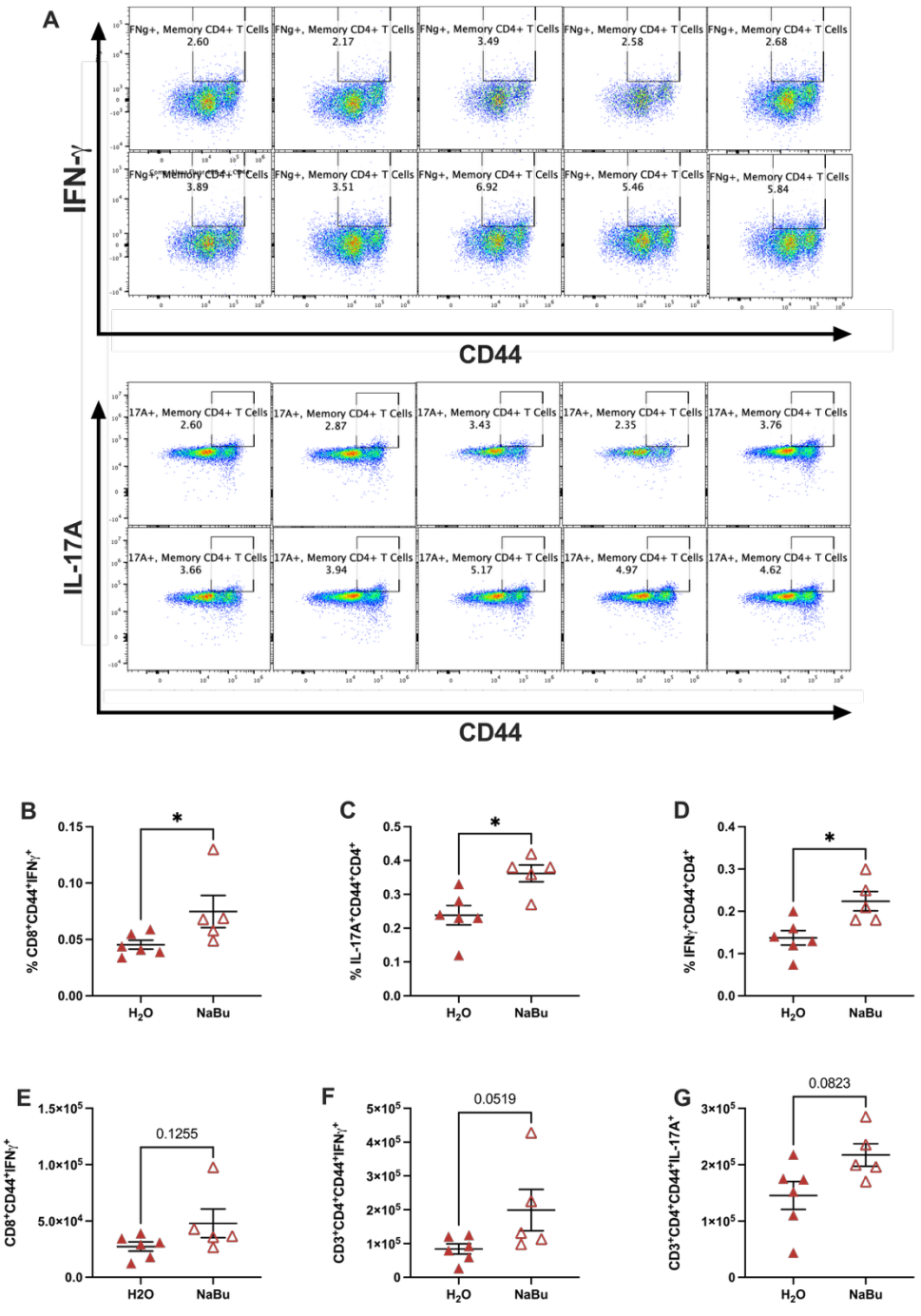
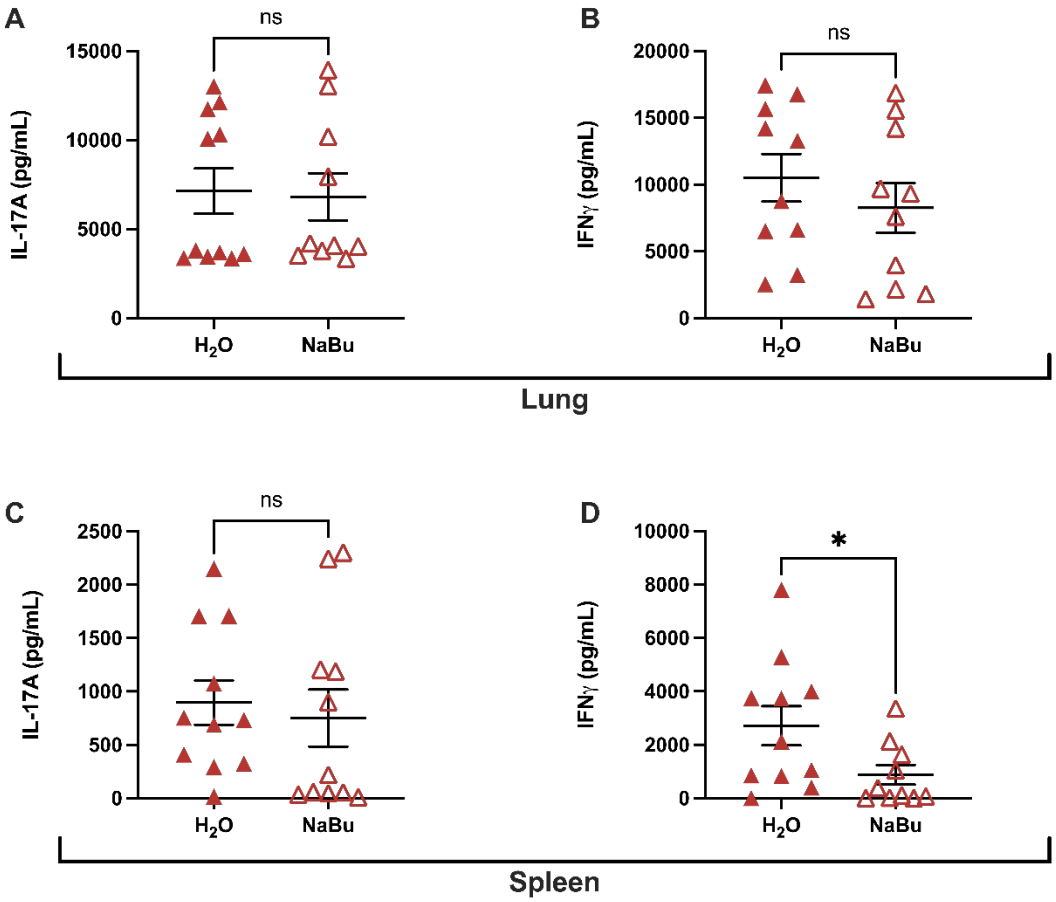


Fig. 4.16 Dietary intervention with butyrate results in higher frequencies and numbers of IL-17A$^+$ and IFN-γ$^+$ CD44$^+$ T cells in the spleens of immunised mice. Female C57BL6/J mice were administered sodium butyrate (NaBU, 100mM) in drinking water ad libitum for 14 days prior to and during the course of i.n. instillation with SpnL(dmLT) on day 0 and again on day 14, prior to sacrifice on day 21. Single cell suspensions of splenic tissue were prepared and stimulated ex vivo with SpnL (100µg/mL) for 6 hours, prior to staining and immunophenotypic analysis by flow cytometry. Population analysis was based on the gating strategy outlined in Fig. 4.1. Plots are representative of individual biological replicates from IFN-γ$^+$CD44$^+$CD4$^+$ and IL-17A$^+$ CD44$^+$CD4$^+$ T cell populations immunised mice treated with water (control) (**A**). Statistical significance was determined by Mann-Whitney test * $p < 0.05$. Representative experiment, where experiment was performed twice with consistent trends.



4.17 Butyrate supplementation results in reduced splenic IFN-γ in immunised animals in response to antigen recall. Female C57BL6/J mice were administered either water (Ctrl) or sodium butyrate (NaBu) in drinking water for 14 days prior to initial i.n. immunisation with the adjuvanted vaccine, SpnL(dmLT). Mice were boosted with the vaccine on day 14 and maintained on dietary supplements throughout the course of immunisation. Lung and splenic tissue was isolated, and single cell suspensions of these tissues were stimulated *ex vivo* with the pneumococcal antigen, SpnL (100ug/mL) for 72hrs. Secondary cytokines, IFN-γ and IL-17A were quantified in cell supernatants by ELISA. Data is representative of mean ± SEM, where n=10-11 mice/group, representative of two experimental replicates. Statistical significance was determined by student's unpaired t-test, * $p < 0.05$.

4.11 Dietary supplementation with butyrate results in reduced levels of antigen-specific antibodies in the serum of immunised mice.

Given the modulatory effects of dietary intervention with butyrate on cell mediated immunity induced by the nasal pneumococcal vaccine, we next assessed the effects of butyrate on vaccine driven antibody responses. It is recognised that the main correlate of pneumococcal vaccine efficacy are PCV specific IgG titres and the ability of these antibodies to bind capsular polysaccharide on viable bacteria for opsophagocytosis is classically measured using the "gold-standard" OPKA assay[437],[439]. Conjugated pneumococcal vaccine formulations generate higher antibody responses by enhancing follicular helper T cell (T_{fh}) participation[316],[440]. For this reason, we wanted to assess responses to SpnL and separately to the pneumococcal capsular polysaccharide.

We first focused on B cells. Both frequencies and total numbers of $CD19^+$ B cell populations in the spleens of immunised mice were comparable between controls and animals receiving butyrate supplementation, implying any changes in serum antigen-specific antibody levels were not due to a reduction in splenic B cells (**Fig. 4.15 B, G)**. However, while no reduction in the relative frequencies of lung B cells was observed **(Fig. 4.13 B)**, total B cell numbers in the lungs were lower in butyrate treated mice **(Fig. 4.13 G)**. Class switching to IgG2c in C57/BL6 mice (or equivalent IgG2a in BALB/c mice) is dependent on IFN-γ[325], [324],[326]. Thus, the observed reduction in antigen-specific IFN-γ in combination with a reduction in local $CD44^+IFN\text{-}\gamma^+$ T cell populations in the lungs could result in the suppression in antigen-specific IgG2c (**Fig. 4.17 D**), (**Fig 4.14 D, F**).

Antigen-specific antibodies against the pneumococcal lysate, SpnL in the serum of mice immunised during butyrate supplementation or water were quantified by ELISA. Total antigen-specific IgG levels were significantly lower in mice receiving butyrate treatment (**Fig. 4.18 A, B**). Antigen-specific IgG2c responses were also lower in butyrate treated mice (**Fig. 4.18 E, F**). Antigen-specific IgG1 levels were reduced, although not significantly (because of 1 high responder) in butyrate treated mice (**Fig. 4.18 C, D**).

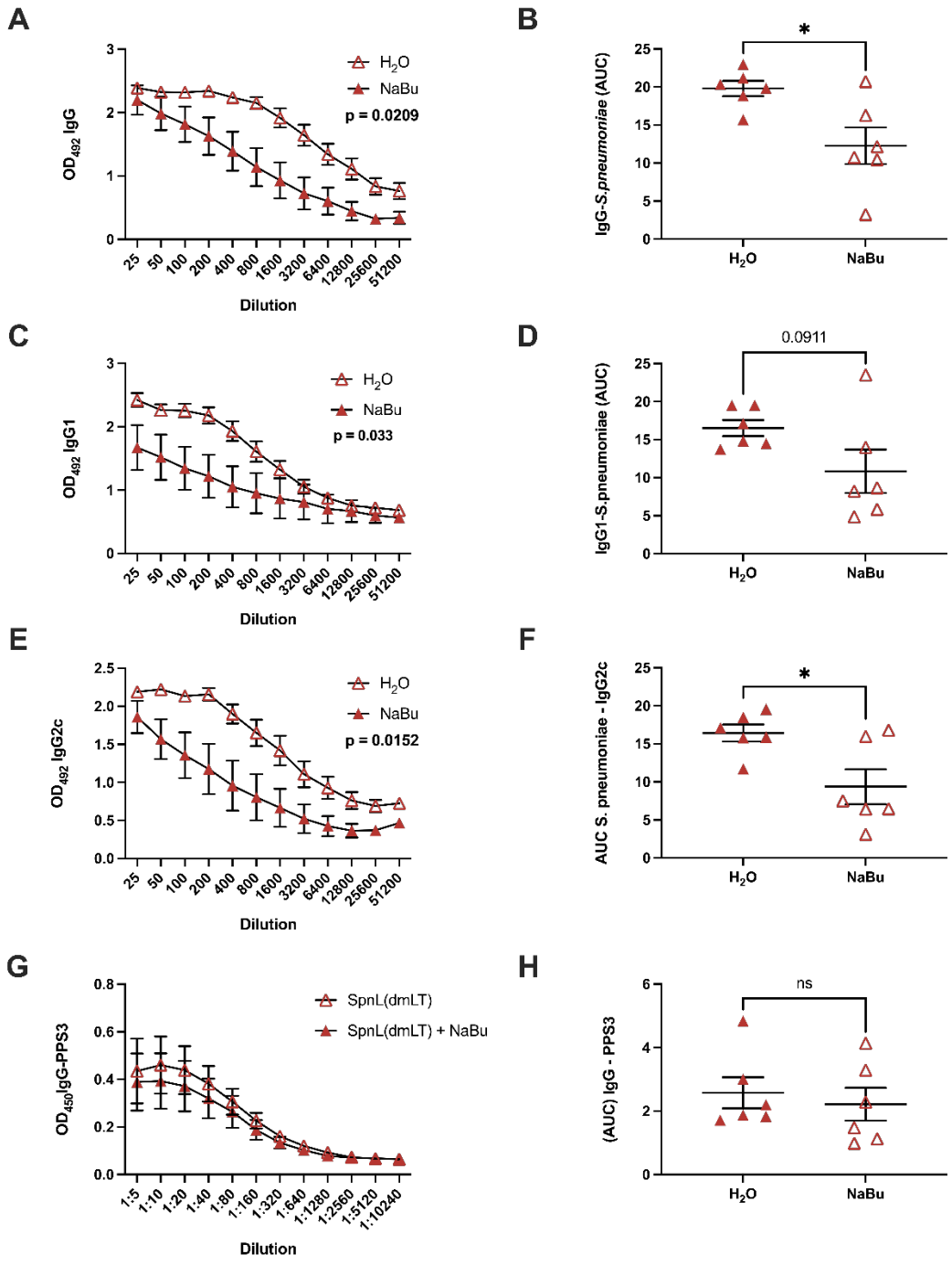


Fig. 4.18 Butyrate supplementation limits nasal vaccine induced antigen-specific serum IgG responses. Female C57BL6/J mice were administered butyrate (100mM) in drinking water ad libitum for 14 days prior to and during the course of nasal vaccination with SpnL(dmLT) on day 0 and again on day 14, prior to sacrifice on day 21. Serum was collected and antigen-specific antibodies against the pneumococcal antigen SpnL (**A, B, C, D, E, F**) or PPS3 (**G, H**) were measured by ELISA. Data is representative of mean ± SEM, where n=5/6 biological replicates/group. Statistical significance was determined by student's unpaired t-test, * $p < 0.05$. The data presented are from two independent experiments.

4.12 Butyrate supplementation results in reduced levels of antigen-specific IgA in the lung and nasal cavity of immunised mice.

Nasal vaccination with SpnL(dmLT) generates antigen-specific mucosal IgA in the lungs, as shown in **Fig. 4.10**. Given the ability of butyrate to increase polyspecific IgA in the faecal matter, and intestinal mucosa, we wanted to examine if this effect applied to the lung. Thus, we wanted to investigate the effects of butyrate supplementation on the ability of our vaccine model to generate antigen-specific IgA producing B cells in the lungs using ELISpot analysis. For this, single cell suspensions of lungs isolated from immunised animals were stimulated *ex vivo* as before with media (control), SpnL (20µg/mL) and LPS (*E. coli* R515) as a positive control and relative spot volume (RSV) of wells and antibody secreting cells (ASC)/10^6were measured. Lung ASC/10^6 total cells and RSV were lower in butyrate treated vaccinated mice (**Fig. 4.19 B**), (**Fig. 4.19 A**). This trend was mirrored in the RSV levels of total polyspecific IgA, while total ASC reduced although not significantly (**Fig. 4.20 A**)**,** (**Fig. 4.20 B**). Antigen-specific IgA was measured by ELISA in the nasal washes of immunised mice. In line with the ELISpot results, SpnL specific secretory IgA was significantly lower in vaccinated mice treated with butyrate compared to controls receiving water (**Fig. 4.21**).

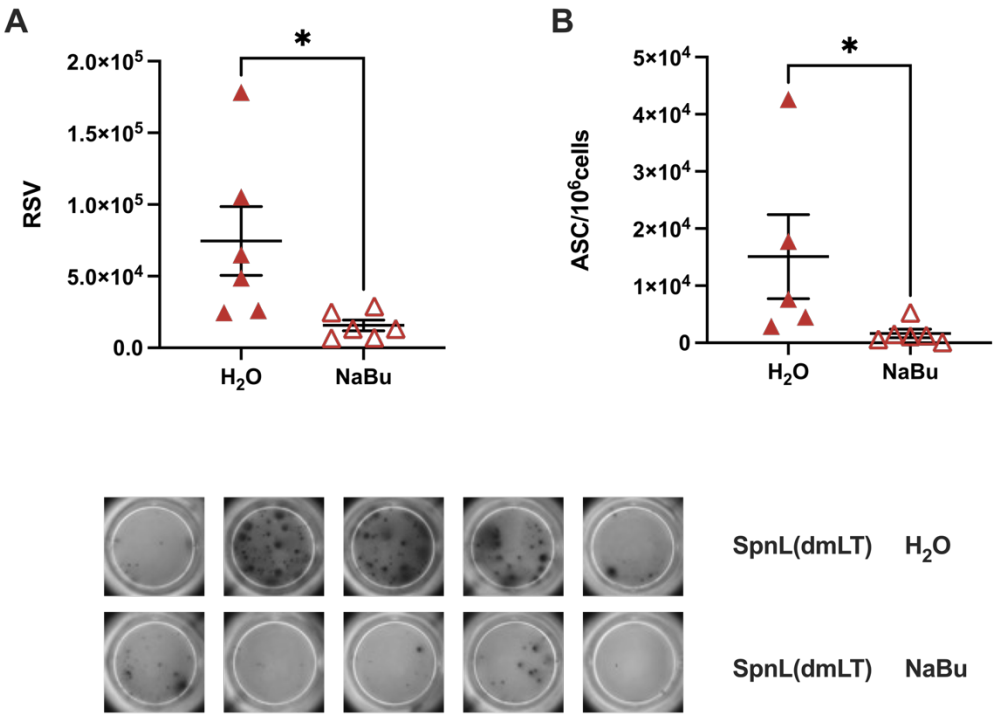


Fig. 4.19 Butyrate supplementation reduced vaccine induced antigen-specific IgA in lung parenchymal tissue. Female C57BL6/J mice were administered butyrate (100mM) in drinking water ad libitum for 14 days prior to and during the course of nasal vaccination with SpnL(dmLT) on day 0 and again on day 14, prior to sacrifice on day 21. Single cell suspensions of lung tissue were incubated in the absence of stimuli (-ctrl), or with the polyvalent pneumococcal lysate (20µg/mL) or LPS (*E. coli* derived R515) as a control for total IgA. Relative spot volume of wells (**A**) and antibody secreting cells/10^6 (**B**) was quantified in wells restimulated with the pneumococcal antigen to assess antigen-specific IgA production. Data is representative of mean ± SEM, where n=5/6 biological replicates/group. Statistical significance was determined by Mann-Whitney test, * $p < 0.05$. Representative 2 independent experiments.

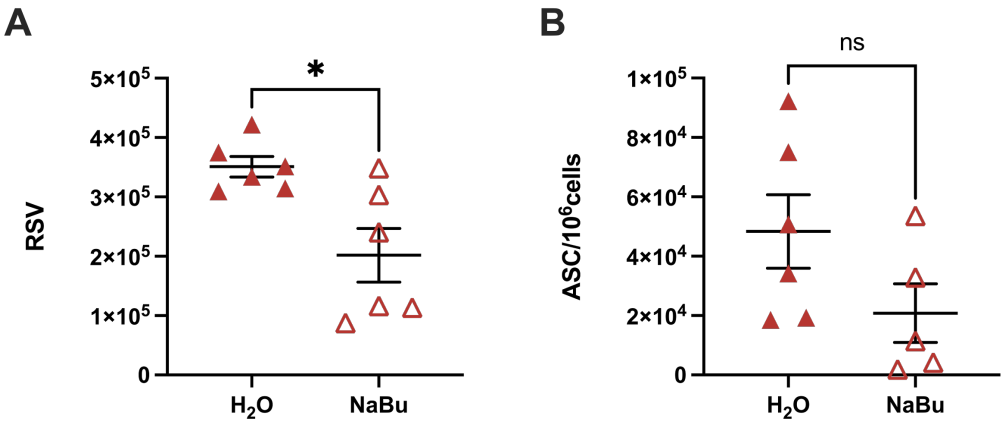


Fig. 4.20 Butyrate supplementation limits production of total IgA in the serum of immunised mice. Female C57BL6/J mice were administered butyrate (100mM) in drinking water ad libitum for 14 days prior to and during the course of nasal vaccination with SpnL(dmLT) on day 0 and again on day 14, prior to sacrifice on day 21. Single cell suspensions of lung tissue were incubated with LPS (*E. coli* derived R515) as a control for total IgA. Relative fluorescent intensity of wells (**A**) and antibody secreting cells/10^6 (**B**) was quantified in wells restimulated with pneumococcal antigen to assess antigen-specific IgA. Data is representative of mean ± SEM, where n=5/6 biological replicates/group. Statistical significance was determined by Mann-Whitney test, * p <0.05. Representative of 2 independent experiments.

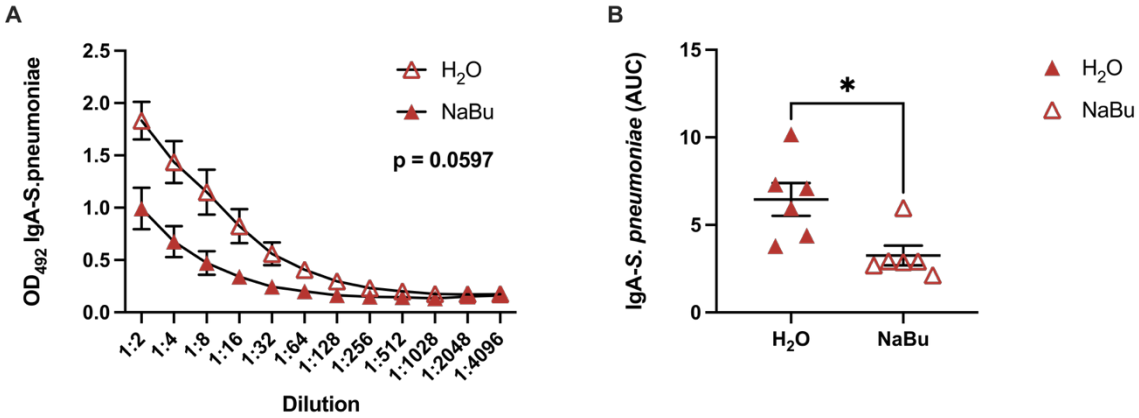


Fig. 4.21 Butyrate supplementation reduced antigen-specific IgA in the nasal cavity of immunised mice. Female C57BL6/J mice were administered butyrate (100mM) in drinking water ad libitum for 14 days prior to and during the course of nasal vaccination with SpnL(dmLT) on day 0 and again on day 14, prior to sacrifice on day 21. Lavages of the nasal cavity were collected, and antigen-specific IgA was quantified by ELISA. Titration of nasal lavage by ELISA (**A**) and the area under the titration curve (**B**) of each animal were used as proxies of IgA detection. Data is representative of mean ± SEM, where n=5/6 biological replicates/group. Statistical significance was determined by Mann-Whitney test, using Dunn's post-hoc test, * p < 0.05. Representative of 2 independent experiments.

4.13 Butyrate supplementation did not suppress antigen-specific serum IgG in mice immunised intramuscularly with the conjugated polyvalent pneumococcal vaccine, Prevnar13® but did decrease antigen-specific Th1 responses.

Butyrate supplementation potently suppressed local and systemic antigen-specific antibody production in the intranasal vaccination setting (**Fig. 4.16**). Here it was investigated if butyrate supplementation elicited similar effects in the context of intramuscular vaccination with Prevenar 13™. This would address whether this was a gut-lung axis mediated event in the context of both intranasal and parenteral pneumococcal immunisation.

Animals underwent dietary supplementation with butyrate (100mM) administered in drinking water *ad libitum* for two weeks prior to initial immunisation. Animals were then immunised with 25uL of the commercially available intramuscular pneumococcal vaccine, Prevnar13®, in the right hind limb flank. Animals were maintained on the dietary supplement throughout the entire course of immunisation. Animals were boosted two weeks post-initial immunisation and subsequently sacrificed 28 days post initial immunisation. Serum was isolated and antigen-specific antibodies targeting pneumococcal capsular polysaccharide 3 (PPS3) and pneumococcal capsular polysaccharide 4 (PPS4) were quantified by ELISA. Lungs and spleens were isolated, and single cell suspensions were prepared from these organs. Lung parenchymal cells and splenocytes were seeded and restimulated with either media (Ctrl), PPS1 (10 μg/mL, 50μg/mL, 100ug/mL), PPS3 (10μg/mL, 50μg/mL, 100 μg/mL), PPS4 (10μg/mL, 50μg/mL, 100μg/mL), CRM_{197} (7.5μg/mL) and a heat-killed polyvalent bacterial lysate, SpnL, containing *S. pneumoniae* serotype 1, 3 and 4 (10μg/mL total protein, 100μg/mL total protein).

Of the antigens used for splenocyte restimulation, only the bacterial lysate revealed antigen-specific IFN-γ production in vaccinated mice **(Fig. 4.19 E)**. All three of the *S. pneumoniae* serotypes in the polyvalent lysate were covered in the commercial vaccine. However, no antigen-specific cytokine response was detected in splenocytes restimulated with the capsular polysaccharides, PPS1, PPS3 and PPS4 at the

concentrations tested. We tested the effects of butyrate supplementation on antibody responses following vaccination with Prevnar13® by quantifying PPS3 and PPS4 specific IgG in the serum, due to limitations on the availability of PPS1 we did not measure PPS1-specific antibodies. Butyrate supplementation did not alter levels of Prevnar induced IgG against PPS3 or PPS4 (**Fig. 4.22 A, B, C, D**). However, butyrate supplementation did suppress antigen-specific IFN-γ in response to stimulation with the pneumococcal lysate SpnL (**Fig. 4.22 E**).

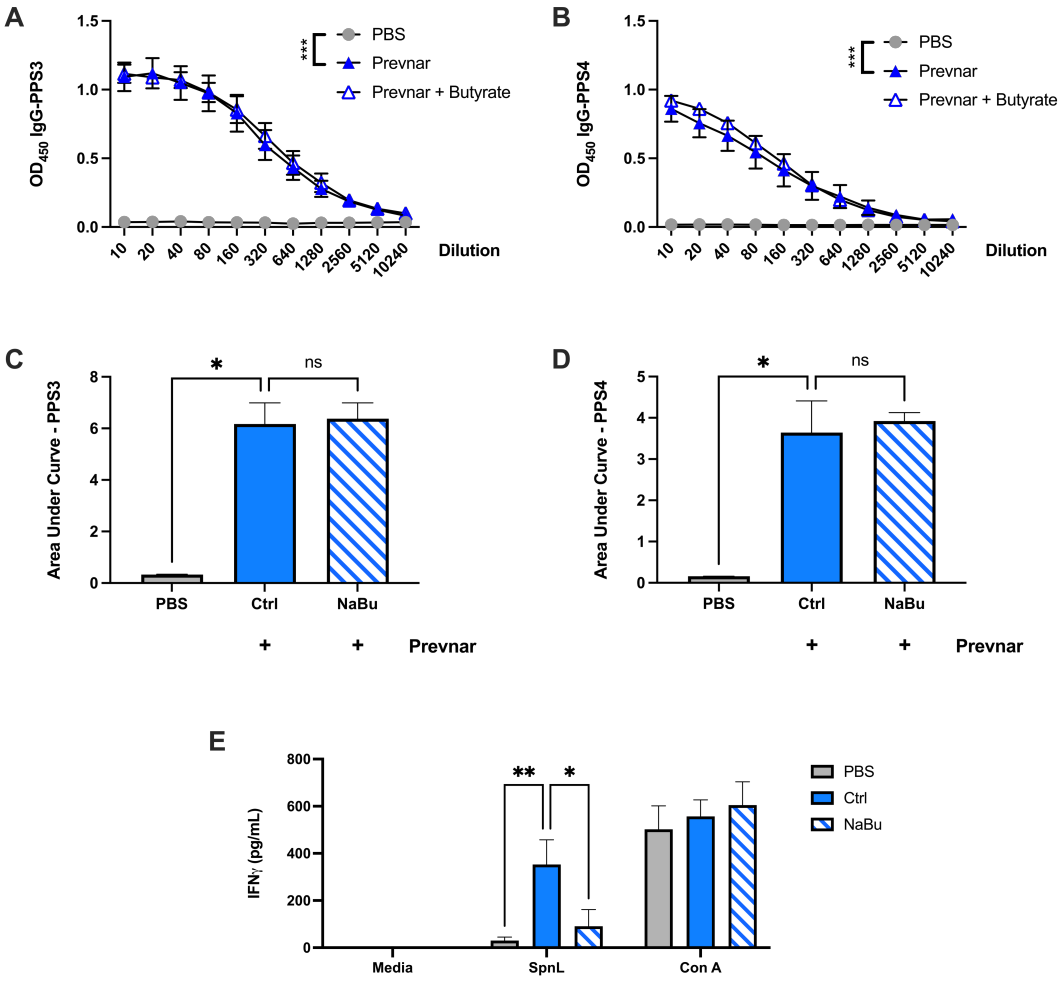


Fig. 4.22 Oral butyrate supplementation suppressed vaccine (Prevnar13®)-induced antigen-specific splenic IFN-γ but not antigen-specific IgG, Prevnar. Female mice were administered the dietary supplement and immunised as per the regimen described in Fig. A with 25uL of Prevnar. Mice were sacrificed on day 28 and serum and spleens were collected. Pneumococcal polysaccharide (from *S. pneumoniae* serotype 3 (**A, B**) and 4 (**C, D**)) specific serum IgG was quantified by ELISA. Splenocytes were plated and restimulated with a polyvalent bacterial lysate containing *S. pneumoniae* serotype 1, 3 and 4 and separately with concanavalin A as a control. Data is representative of mean ± SEM, n=5/group and analysed by Kruskal-Wallace, using Dunn's post-hoc test (A, B, C, D) and two-way ANOVA using Bonferroni's post-hoc test (E). Intramuscular injections were performed by Dr. Kiva Brennan.

Discussion

The immunomodulatory impact of the microbiota on vaccine outcomes remains a nascent area of research. As mentioned in the introduction of this chapter, vaccine performance varies widely among the global population. The microbiota is identified as a governing factor which may underpin the heterogeneity in vaccine performance between individuals, and populations, particularly relevant in the case of suboptimal vaccine performance in low-middle income countries, known as the "tropical barrier" of vaccine efficacy[441]. It is widely recognised that dysbiosis negatively impacts vaccine performance[102], [367],[363]. *In vivo* models of antibiotic-induced dysbiosis remain the archetype of studying microbiome mediated effects on outcomes of infection and immunisation, however, the direct effects of microbiota-derived immunomodulators in vaccine performance in the eubioitic setting have not been investigated to the same extent as dysbiotic models.

SCFAs are gut microbiota-derived potent pleiotropic immunomodulators, which are disseminated systemically in the portal circulation. It is plausible that varying basal levels of SCFAs in the global population can impact on vaccine immunogenicity[431]. Considering the beneficial effects of SCFAs on supporting humoral response and regulating T cell functions highlighted in section 1.7 and the introductory section of this chapter, it was hypothesised that SCFAs could improve vaccine responses. **The translational application of this could be effective at targeting substandard performance to vaccines, through the administration of a safe, affordable and widely available nutritional supplement. To date no publications have investigated the impact of dietary supplementation with SCFA on the outcomes of intranasal immunisation.**

Our first aim was to establish an intranasal pneumococcal vaccine capable of generating robust cellular and humoral immune responses with which we could investigate the effects of SCFA supplementation. Here a pre-clinical polyvalent adjuvanted pneumococcal vaccine, SpnL(dmLT), was prepared for i.n. delivery. This model proved highly successful in driving cell-mediated immunity both local to the site

of administration and systemically. Significantly increased production of IFN-γ and IL-17A was induced in lung and spleen cells isolated from animals immunised i.n. with the adjuvanted formulation, SpnL(dmLT). Complementary to this, i.n. immunisation with SpnL(dmLT) induced populations of Th17 and Th1 memory T cells upon antigen recall. Administration of SpnL(dmLT) i.n. did not exhibit significant increases in $CD8^+$ T cells in the lung, similarly no cytokine production was detected in NK cells or γδT cell populations in immunised animals. This confirmed that the significant production of cytokines seen in immunised animals in response to antigen recall was attributable exclusively to $CD44^{hi}CD4^+$ effector/memory T cell populations. Total numbers of Th17 and Th1 effector/memory T cells were increased in the spleens of animals immunised i.n. with SpnL(dmLT). This, considered alongside the generation of IL-17A and IFN-γ in *ex vivo* splenic restimulations, demonstrates the ability of this vaccine to generate systemic cell mediated immunity.

SpnL(dmLT) was additionally successful in generating humoral immunity, local to the site of mucosal administration. This was reflected in significantly increased *S. pneumoniae* specific IgA in the nasal cavity of animals immunised i.n. with SpnL(dmLT) compared to those immunised with SpnL alone. This supports the extensive literature on dmLT as a "gold standard" mucosal adjuvant and the ability of this adjuvant to support mucosal antibody responses at sites adjacent to the immunisation route[308], [339],[338]. IL-17A is required for the translocation of secretory IgA across mucosal barriers[286],[36]. It is likely that increased Th17 cells and significant enhancement of IL-17A in *ex vivo* restimulations of whole lung tissue from animals immunised with the adjuvanted preparation, SpnL(dmLT), contributes to the significant enhancement of antigen-specific IgA detected in lavages of the nasal cavity. *In vivo,* dmLT promotes systemic antigen-specific serum IgG and mucosal IgA, while also driving cell mediated immunity, particularly Th17 mediated responses[339]. Here the results following nasal vaccination with, SpnL(dmLT) support these examples from the literature. In the setting of intranasal delivery, dmLT-adjuvanted preparations have demonstrated efficacy in preclinical immunisation models targeting *Shigella flexneri* and *Clostridium tetani*, both of which are enteric pathogens, suggesting dmLT adjuvanted mucosal vaccines can elicit

mucosal responses distal to the administration route, presumably an effect of the CMIS[339].

Studies by Estupiñan and colleagues have recently explored dmLT as an effective intranasal adjuvant in the setting of pneumococcal immunisation. This pneumococcal vaccine coupled with dmLT when delivered i.n. demonstrated increased IgA^+ antibody secreting cells in the bone marrow and PPS1-specific IgA in the serum and salivary secretions[341]. However, here we demonstrate the effectiveness of the mucosal adjuvant dmLT with a whole cell pneumococcal lysate, combining three clinically relevant serotypes, which may induce a higher degree of protection due to the wider variety of both surface and intracellular antigens. Additionally, it is known that capsular polysaccharide is a factor facilitating pneumococcal shedding during active infection in a serotype specific manner, so targeting alternative pneumococcal antigens could overcome pneumococcal evasion of mucosal immunity[201]. Animals immunised i.n. with SpnL(dmLT) had significantly heightened *S. pneumoniae* specific IgA levels in the lung as measured by ELISpot. The ability of the model vaccine to generate secretory IgA in the respiratory tract suggest that this vaccine could prove successful at preventing not only pneumococcal-mediated invasive disease but also infection and transmission of the pathogen. While this still requires further investigation by live pneumococcal challenge of immunised animals, these findings confirm the value of the model for the purpose of the project and facilitate the study of the full extent of systemic and mucosal immune responses in the setting of dietary intervention.

Serum isolated from animals immunised i.n. with SpnL(dmLT) also displayed marked increases in *S. pneumoniae* specific IgG, IgG2c and IgG1 subclasses. Lung parenchymal $CD19^+$ B cell populations were significantly increased in both relative frequency and total number, albeit splenic cells demonstrated a discrete trending increase in total numbers of $CD19^+$ B cells while demonstrating no increase in the frequency of splenic $CD19^+$ B cells. This implies that the generation of both antigen-specific IgA and IgG occur predominantly at sites near where the vaccine was administered, plausibly the local draining lymph nodes such as the cervical or mediastinal lymph nodes.

Examining the effects of dietary intervention with butyrate on outcomes of vaccine-induced cellular immunity, a significant reduction in total numbers and frequencies of memory T cells, namely Th17 and Th1 T cells was observed in the lungs of animals receiving butyrate. However, in immunised mice receiving the dietary supplement, there was no significant change in secretion of IFN-γ or IL-17A (**Fig. 4.18**). It is worth noting however, that unlike the spleen, lung tissue restimulations will contain a higher contributing frequency of innate cells. This could underpin the difference seen between the cytokine producing memory T cells and the total cytokine secretion during the recall response. In contrast to the lung data, increased frequencies and numbers of Th17 and Th1 cells was noted in the spleens of immunised animals receiving butyrate supplementation compared to controls. This extended to total numbers of Th17 cells. Again, these trends were not recapitulated in terms of cytokine secretion by *ex vivo* antigen restimulation of cells. Total frequencies and numbers of memory T cell populations were comparatively lower in splenic tissue compared to the lung, implying that the vaccine favoured generation of adaptive cellular immunity local to the site of administration. However, there was a significant decrease in secretion of IFN-γ in *ex vivo* splenocyte restimulations from immunised mice receiving butyrate treatment compared to controls. Again, total numbers of Th1 cells were low considering the amount of cytokine that was generated in *ex vivo* cell restimulations. Current literature suggests that SCFAs have contrasting impacts on T cells relating to their specific phenotype, with differentiation state heavily influencing SCFA-driven outcomes. Sałkowska *et al.* 2017 demonstrated that SCFA-driven HDACi regulation of the RORγt locus was dependent on T cell differentiation state, with inhibition of HDACi-mediated RORγt inhibition occurring in naïve T cells but RORγt enhancement in fully differentiated T cells[377]. Considering this in the context of our work, it could suggest that butyrate driven suppression of the effector/memory T cell phenotype in the lung is due to butyrate-driven interference with naïve T cells in lung inductive sites prior to antigen presentation and subsequent differentiation (**Fig. 4.14**). In contrast we see the opposite trend in splenic effector/memory splenic T cell populations, in which butyrate enhanced this T cell phenotype (**Fig. 4.16**). This suggests that the primary anatomical site of the induction of antigen-specific responses is the lung, and that the enhancement of effector/memory phenotype in splenic T cell populations is attributed to the fact that

they are fully differentiated by the time they are subject to butyrate elicited immune modulation. Ultimately, kinetics of antigen presentation and differential anatomical effects of butyrate supplementation collectively influence outcomes of butyrate modulation on T cell phenotype in the vaccination setting.

Dietary supplementation with butyrate had a profound effect on intranasal vaccine mediated humoral and cellular immune responses. Antigen-specific serum IgG, IgG2c and IgG1 were decreased in animals administered butyrate compared to controls. Antigen-specific IgA in the nasal cavity was significantly reduced in immunised mice receiving butyrate supplementation. Similarly, antigen-specific IgA in lung parenchymal tissue was significantly reduced in immunised mice receiving butyrate supplementation, a trend that was recapitulated in total polyspecific IgA in the lung, as shown by ELISpot. This reduction in local antibody production was supported by a reduction in total numbers of $CD19^+$ B cells in the lungs of immunised mice receiving butyrate supplementation. This may suggest that the reduction in B cells was partially responsible for the reduction antigen-specific antibodies. The decrease in lung Th17 cells could also contribute to a reduction in pIgR-mediated transport of IgA across the nasal mucosa resulting in significantly lower antigen-specific IgA in the nasal cavity of immunised mice receiving butyrate supplementation. This would warrant measuring IL-17A production in nasal tissues. While our results were surprising given the initial hypothesis that SCFA supplementation would enhance vaccine immunogenicity, they were not completely out of line with the current literature. Sanchez *et al.* 2020 demonstrated that a high fibre diet and SCFA supplementation dampen class switch recombination, plasma cell differentiation and class-switched antibody responses, resulting in lower overall levels of antigen-specific antibody in response to local and systemic immunisation with an oral ovalbumin and cholera toxin vaccine [371].

Having established the unfavourable effects of dietary intervention with butyrate on outcomes of intranasal pneumococcal vaccination, we wanted to further examine its effects in the context of the licensed parenterally administered pneumococcal vaccine, Prevnar13®. Serum IgG anti-serotype 3 and 4 capsular polysaccharides, both of which are included in Prevnar13®, were quantified in the serum of immunised mice.

Immunisation with Prevnar13® significantly increased serum antibodies against PPS3 and PPS4. However, no significant differences in serum anti-PPS3 and PPS4 IgG were seen in immunised mice with regard to butyrate supplementation. Pneumococcal polysaccharides are T-cell independent antigens, however in this case pneumococcal capsular polysaccharides are conjugated to CRM_{197} which facilitates the engagement of T cells. In the literature, SCFA-mediated reduction in antibody responses also applied in response to both T-independent and T-dependent antigens in parenteral immunisation[371]. **This suggests that the route of immunisation is key regarding the impact of microbiota-derived metabolites on outcomes of immunisation, with more pronounced effects in the setting of mucosal immunisation.**

5. General Discussion

Research highlighting the dynamic immunological relationship between diet, the host microbiota, and host immunity has expanded at an unprecedented pace. As aforementioned, knowledge of axes of immunological crosstalk between the intestinal microbiota and peripheral anatomical immunological niches, such as the gut-liver axis, the gut-brain axis and the gut-lung axis of immune regulation, and their roles in host health and disease has been established. However, the field of research concerning SCFAs, a family of highly pleiotropic immunomodulatory microbiota-derived systemic messengers, is far from complete. This work can be stratified into two main research objectives: studying the effects of dietary supplementation with the highly immunomodulatory SCFA, butyrate on outcomes of **(1) pneumococcal pneumonia and (2) intranasal and parenteral pneumococcal vaccine efficacy**. While these two objectives have been separately dissected in the third and fourth chapters respectively, there has been one overarching theme throughout; **harnessing the gut-lung axis of immune regulation, through the use of SCFAs, to improve therapeutic and prophylactic avenues against pneumococcal disease.**

The first objective of this work focussed on the ability of butyrate to modulate alveolar macrophage functions *in vitro* and improve outcomes of pneumococcal pneumonia in a setting of dysbiosis-induced susceptibility. Here the direct anti-microbial properties of butyrate on three serotypes of *S. pneumoniae* was examined; ultimately no direct bacteriostatic or bactericidal activities were observed in any of the pneumococcal serotypes tested. It was established that 1mM butyrate pre-treatment elicited inhibition of HDACs, implying an open chromatin structure and higher rate of transcriptional activity in line with current literature [148], [196]. No published studies to date have investigated the impact of butyrate treatment on the AM transcriptome *in vitro*. Butyrate induced the expression of a range of anti-microbial genes (*Ear, Ltf, Ngp, S100a9, Rnase2b, Gm2a, Klk8, Slpi*), genes involved in type I and type III IFN signalling and some chemoattractants (*Ccr2, Cxcl9, Cxcl10*), in FLAMs in response to *S. pneumoniae* infection (**Fig. 3.9 B**), (**Fig. 3.11 A**). The effects of butyrate were then investigated at the functional level by gentamicin protection assay in FLAMs and primary human AMs *ex vivo*. The anti-microbial transcriptomic signature was recapitulated at the functional level with butyrate treated macrophage exhibiting a higher bactericidal

capacity than controls in both murine FLAMs and human AMs in response to infection. This was noted in response to infection with the murine adapted serotype 2 (D39), the clinical isolate serotype 1 (E1586) and the clinic-derived wild-type strain (TUH) (**Fig. 3.15**). We acknowledge that the ability of butyrate to drive genes involved in type I and type II IFN production and signalling would require further investigation at the functional level, however it did prove an interesting insight to be pursued in further studies (**Fig. 3.11 A**). One study has identified synergy between type I IFN induction and lysosomal function in intracellular bacterial clearance, in the context of the intracellular pathogen *Salmonella enterica* in intestinal epithelial cells [442]. Indeed, "*Lysosome*" was a functional category upregulated in GSEA KEGG analysis of butyrate treated FLAMs (**Fig. 3.8 B**). It is plausible that these could be complimentary mechanisms in the clearance of intracellular pneumococci [443]. Butyrate altered the cytokine milieu of FLAMs infected with *S. pneumoniae* or stimulation with Pam3Csk4, specifically limiting production of IL-6 (**Fig. 3.13**), (**Fig. 3.14**).

We acknowledge, pivotal insights by Kullberg *et al.* 2025 have identified the protective effects of butyrate and the butyrogenic commensal bacteria *F. prausnitzii* during acute *K. pneumoniae* infection [197]. This study further identified that *F. prausnitzii* was positively associated with shorter period of hospitalisation in CAP patient cohorts [197]. **The availability of butyrate supplements for human consumption, makes oral supplementation an effective strategy to offset the effects of dysbiosis during infection. In addition, the effects of butyrate on invasive pneumococcal infection have not yet been characterised to date.** Dysbiosis results in a heightened susceptibility to respiratory infection, demonstrated in murine models of antibiotic-induced dysbiosis, in patient cohorts suffering from chronic intestinal conditions and here in a model of antibiotic-induced dysbiosis (**Fig. 3.21**) [179], [73], [181], [374], [375], [376], [377], [378]. Butyrate supplementation ameliorated the effects of dysbiosis-driven exacerbation of invasive pneumococcal infection, attenuating disease severity, reducing the bacterial burden in the lung and limiting systemic bacterial dissemination (**Fig. 3.22**). This suggests that the increased severity in dysbiotic mice was likely due to an ablation in SCFA producing commensals and that exogenous supplementation with SCFA rescued

this phenotype. Thus, in the healthy normobiotic setting SCFAs are crucial regulatory factors in host response to pneumococcal LRTI.

Pre-biotics and probiotics have demonstrated efficacy in protecting against respiratory infection and pathology [444]. Supporting these pre-clinical murine models of FMT to circumvent susceptibility to severe bacterial LRTI has boasted promising results [179], [73]. In fact, the first successful incidence of using FMT to cure bacterial pneumonia in clinic was documented last year to treat a geriatric patient presenting with severe pneumonia caused by a combination of Covid-19 and multiple secondary bacterial infections, including pan-drug resistant *K. pneumoniae* and pan-resistant *Acetinobacter baumanii* [444]. This same patient exhibited decreases in beneficial gut bacteria notably *Prevotella*, *Ruminococcus* and *Lactobacillus*, all of which have reported roles in SCFA production, were successfully restored upon allogenic transplantation of a healthy donor microbiota [136], [137], [122], [139], [444]. It is plausible that the depletion of SCFAs, pre-FMT contributed to the worsening of disease.

Short-chain fatty acids hold significant therapeutic potential in alleviating respiratory infection and pathogenesis, demonstrated in current pre-clinical studies and in our own findings [197], [112], [445], [446]. To date, one clinical trial has been completed comparing SCFA metabolism in COPD versus healthy cohorts (NCT03327181), however with no published results. Similarly, there are several ongoing clinical trials evaluating human bioavailable concentrations of SCFA (NCT01757379). Additionally, there are clinical trials underway investigating prebiotics and SCFA-producing probiotics therapeutics in intestinal inflammation and gut health (NCT05013060), (NCT07198984), (NCT05058131). However, no clinical trials have been launched examining SCFAs as therapeutics for respiratory infection or pathology. This in addition to our findings prompts further research into the use of alternative microbiome-targeted therapies in pneumococcal infection, particularly in cases where individuals are susceptible.

The second objective of this work investigates the use of SCFA supplementation in improving the efficacy of an adjuvanted intranasal pneumococcal vaccine, SpnL(dmLT) and the commercially available vaccine Prevnar13®. Our hypothesis, given the current literature, was that SCFA, namely butyrate, would enhance vaccine immunogenicity, particularly humoral responses to these vaccines due to the ability of butyrate to

enhance B cell functionality and positively regulate secretory IgA in the intestinal tract [124], [431], [350], [367]. However, the results were in converse to our initial hypothesis.

Here, a polyvalent heat-killed pneumococcal lysate, composed of three clinically relevant *S. pneumoniae* strains, namely E1586 (serotype 1), E1434 (serotype 3) and TIGR4 (serotype 4) was combined with the experimental "gold-standard" mucosal adjuvant double mutant heat-labile toxin. This experimental vaccine yielded successful results in driving robust cellular mediated immunity, namely IL-17A and IFN-γ producing Th17 and Th1 cells respectively. The adjuvanted experimental preparation when delivered i.n. also induced local production of antigen-specific IgA in the nasal cavity and in the lung parenchymal tissue as well as systemic antibodies (**Table 4.1**). Ultimately, this provided a model of intranasal pneumococcal immunisation in which we could study the modulatory effects of the short-chain fatty acid, specifically butyrate, supplementation as a proof-of-concept. Design of effective intranasal vaccines is a challenging area of research, adjuvanted or live attenuated formulations which elicit larger immunogenicity appear to be more effective options in overcoming mucosal tolerance [308]. Here this is further demonstrated in which inclusion of dmLT dramatically enhanced antigen-specific responses to the lysate alone. The inclusion of ADP-ribosylating, or AB5 containing, enterotoxins such as CTA1DD or LTA63 in clinical i.n. vaccines have encountered off-target neurotoxic effects, resulting in Bell's palsy [336], [337]. However, attenuated derivatives of these enterotoxins including dmLT and LTA1 have re-entered the clinical pipeline as outlined in section **4.1** [340]. Our research suggests that with the addition of an immunogenic adjuvant, a whole-cell pneumococcal vaccine could provide protection against pan-serotype *S. pneumoniae* infection and promote sterilising immunity when delivered i.n., reducing the burden of carriage and as a result transmission. The reductive effects of butyrate supplementation were more apparent in the lung, with reduced Th1 and Th17 populations, total B cell numbers, IgA^+ B cells by ELISpot and sIgA in the nasal cavity (**Fig. 4.13**), (**Fig. 4.14**), (**Fig. 4.19**), (**Fig. 4.21**). Serum antigen-specific antibodies, IgG, IgG2c and IgG1 were decreased in butyrate-treated mice (**Fig. 4.18 A-F**). Interestingly capsular polysaccharide specific

antibodies were not inhibited to the same extent as total SpnL specific antibodies (**Fig. 4.18 G, H**).

Collectively, these dietary intervention studies administering butyrate during the course of immunisation yielded striking results, hence we wanted to investigate if this effect is recapitulated in the parenteral setting, using the clinically administered parenteral pneumococcal conjugate vaccine, Prevnar 13®. Dietary supplementation with butyrate did not impact humoral responses generated by Prevnar 13®. In which serum PPS3- and PPS4-specific antibodies were not inhibited in mice receiving butyrate (**Fig. 4.22 A-D**). It is known that capsular polysaccharides are T-independent antigens as noted in the efficacy of Pneumovax (PPV23) [316], [295]. However here dmLT is included in the vaccine formulation which will facilitate T cell engagement, similarly to the conjugation of pneumococcal polysaccharides to the CRM_{197} carrier protein in Prevnar13® [316], [295]. Thus, it is unlikely that PPS3- and PPS4- specific responses are occurring independently of T-cell contributions thus the modulatory effect of butyrate does not differ between the response to T-dependent and T-independent antigens. This is supported by current literature [371], [350].

The immunogenicity of the formulation and kinetics and location of antigen presentation likely weigh heavily into the differential effects observed between splenic and lung effector/memory T cell populations in response to butyrate supplementation and the differences seen between the intranasal SpnL(dmLT) vaccine and the parenteral Prevnar13® vaccine. In the setting of mucosal immunisation, butyrate had highly dynamic effects in both cellular and humoral, local and systemic antigen-specific responses. Whereas in the setting of parenteral immunisation, butyrate limited IFN-γ in response to whole cell restimulation with SpnL but had no overall impact on humoral immunity (**Fig. 4.22 E**).

Dietary intervention with butyrate resulted in decreased memory T cell populations in the lungs of immunised animals (**Fig. 4.14**). However, in converse to this, splenic Th1 and Th17 populations were increased (**Fig. 4.16**). Albeit the reduction seen in systemic, or splenic, IFN-γ production supports a systemic reduction in Th1 driven immunity (**Fig.**

4.17 C, D). While the frequency and number of systemic Th1 cells remains higher in butyrate treated animals the functionality of these cells in producing IFN-γ is likely suppressed. However, we acknowledge that there will be a limited contribution of innate cytokine milieu in the restimulations, which could be elucidated through the inclusion of a pan-myeloid marker in the phenotypic analysis of cytokine producing populations (**Fig. 4.17**).

As discussed in section **1.7.1** and **4.1**, a wide heterogeneity exists in vaccine immunogenicity, and as a result, efficacy amongst the global population. Vaccine efficacy is often compromised in lower- and middle-income countries (LMIC), seen in the case of vaccines targeting enteric pathogens, the oral polio vaccine (OPV), the oral cholera vaccine and the oral rotavirus vaccine [441]. In contrast systematic reviews have identified in past epidemiological data that immunogenicity to PCV7 in the Western Pacific Region, Southeast Asia and Africa compared to European and American regions [447], [448]. The circumstances behind this effect are multifactorial, with many socioeconomic factors such as limited access to medical assistance and clean running water, and malnutrition contributing to this effect. It also cannot be overlooked that higher middle-income countries (HMIC) have better methods of cold-chain storage, and an economic advantage in bulk purchasing of vaccines, resulting in disparities in the global roll-out of vaccines [313]. Comprehensive literature reviews have highlighted the many factors that influence efficacy of vaccination; however, the microbiota remains an outstanding factor that could underpin heterogeneity in vaccine responses amongst the global population [441]. A clinical observational study by Gill *et al.* 2022, highlighted that participants partaking in a controlled dietary intervention study with enriched resistant starch, apple cider vinegar and inulin (H-SCFA) had higher serum concentrations of both butyrate and propionate [385]. This H-SCFA cohort exhibited lower total numbers of circulating $CD4^+$ Th1, $CD8^+$ T_{fh} cells and crucially, B cells [385]. This implies diet, through metabolic activity of the microbiota is a critical regulator of systemic lymphocyte dynamics.

However, nutrition is a defining factor in vaccine efficacy, but the immunological implications remain relatively unclear. It is known that LMICs exhibit different dietary

pattens to HMICs, which is represented in the landscape of the microbiota from these two cohorts [109]. Diets in certain LMICs can be richer in dietary fibre, while HMIC diets are rich in protein, fat and refined sugar. Linking this to findings by Gill et al. 2022, a diet rich in SCFA pre-biotics could result in lower lymphocyte populations and thus lower vaccine responses, explaining the contrast in vaccine efficacy amongst the global populations [385]. **Essentially could differing levels of diet induced bioavailable SCFAs sway account for the differences seen in vaccine response amongst the global population?**

Dysbiosis has negative outcomes in disease and pathology in both the intestine and in distal organs such as the brain, liver and lungs through axes of immune regulation [449], [450], [451]. Dysbiosis can be caused by xenobiotic treatment, poor lifestyle and dietary habits or underlying comorbidities and genetic predisposition, as detailed in section **1.2.3** [88]. However, by definition, any agent capable of altering the commensal microbiota can be considered a dysbiotic factor; this includes dietary supplements, prebiotic foods and probiotics. As demonstrated here dietary supplementation with sodium butyrate has highly differential effects on outcomes of acute respiratory infection and parenteral and mucosal immunisation. The supplement industry is a multi-billion-dollar industry, expanding at a highly proliferative rate with sales of dietary supplements surpassing 220 billion US dollars in 2020 [452]. Approaches to holistic health and “wellness” are gaining increasing global popularity, with these approaches to health involving supplement and pro-biotic intake and microbiome-targeted diets, rich in pre-biotics and phytochemicals [453]. Supplements do not require European Medicines Agency (EMA, EU) or Food and Drug Administration (FDA, USA) approval prior to commercial distribution, due to their status as a food and not a medicinal product. However, as demonstrated here, uninformed consumption of dietary supplements can result in off-target effects.

This research highlights the potentially highly therapeutic benefits of SCFAs in respiratory health but also that SCFA supplementation could be a hinderance in the setting of vaccination, due to its modulatory effects on host adaptive immunity. This leads us to critically evaluate the physiological and immunological implications of

supplementation use. However, the reductions seen in Th1, Th17 and antigen-specific humoral immunity pose an alternative question, could SCFA provide therapeutic relief in autoimmune disease? Sanchez et al. 2024 demonstrated that SCFA could alleviate autoantibodies and autoimmunity in a murine model of systemic lupus [371]. Similiarly, SCFAs were capable of reducing IL-17 levels and attenuating the effects of imiquimod-induced psoriasis-like murine model, with SCFA exhibiting similarities in effect to α-IL-17 [454]. **Ultimately, this work has contributed to our current understanding of the role of the gut-lung axis of immune regulation, specifically the role of the SCFA butyrate, in host immunity. Here we build on the current knowledge of SCFAs, particularly butyrate and its potential as a therapeutic avenue in LRTI. Additionally, we provided novel insights into the role of the gut-lung axis of immune regulation, specifically the role of butyrate in outcomes of respiratory and parenteral pneumococcal immunisation.**

Future Work

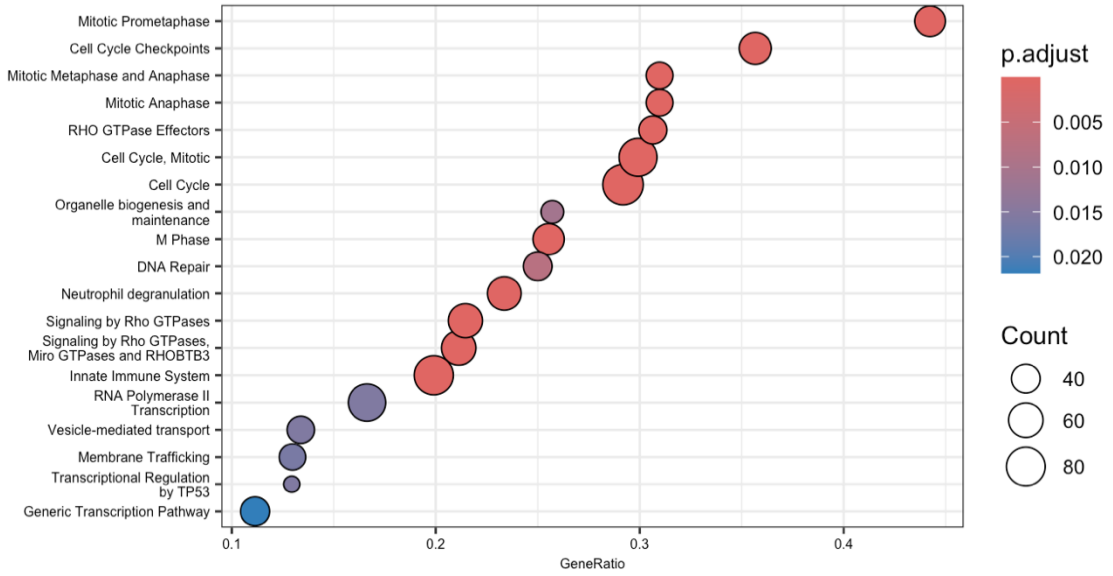
There are unexplored avenues which would provide further mechanistic insight into the effects outlined in this work.

- Characterising the effects of SCFA supplementation on the profile of the microbiota by 16S sequencing in eubioitic mice, dysbiotic mice and dysbiotic mice, to examine the presence of SCFA producing bacteria and whether exogenous supplementation with butyrate could induce shifts in the commensal microbiota.
- Lysosomal degradation is a main mechanism of intracellular bacterial clearance. Performing gentamicin protection assay using the specific inhibitor of vacuolar ATPase, bafilomycin A, which facilitates acidification of the lysosome, to evaluate the effects of butyrate on lysosomal function as a means of increasing the bactericidal capacity of the cell. Similiarly investigate the ability of butyrate to drive lysosomal ROS as a mechanism intracellular bactericidal activity and clearance, again using bafilomycin A.
- To determine the contributions of type I IFNs in potential synergy with lysosomal functions in promoting bacterial clearance as described above, except in primary macrophages isolated form $IFNAR^{-/-}$ mice.
- To evaluate if the effects of a high fibre diet (particularly enrichment of inulin, as it is a butyrogenic prebiotic) to attenuate pneumococcal pneumonia in the dysbiotic model [112].

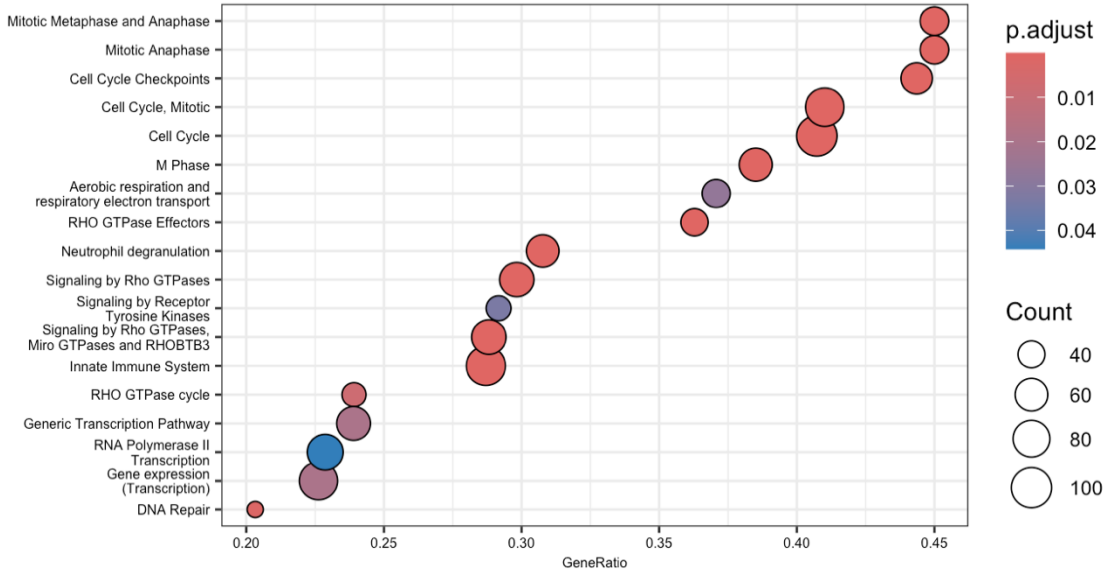
Here, butyrate limited adaptive immunity in the lung during intranasal immunisation, resulting in lower antigen-specific mucosal IgA and serum IgG, IgG2c and IgG1 antibodies. Similiarly, Th1 and Th17 responses in the lung were attenuated in mice receiving butyrate during immunisation. As discussed, both the anatomical location and kinetics of antigen presentation likely has a role in this outcome. SCFA have differing reported effects on naïve and differentiated $CD4^{+}$ T cells [432].

- To examine the effects of butyrate supplementation on the vaccination model outlined in Chapter 4, in FFAR2$^{-/-}$/FFAR3$^{-/-}$ mice to assess the contribution of this pathway in butyrate mediated effects on vaccine immunogenicity.
- To quantify expression of IgG^{+}CD38^{+} plasma B cell populations in the lung tissue, respiratory draining lymph nodes, the spleen and the gut, due to the intestinal homing capacity of lung IgA+ B cells, to examine the source of antibody production and whether plasma cell populations are readily affected by butyrate supplementation during immunisation [18].
- To determine in our own hands, the effects of SCFA on naïve and differentiated CD4^{+} T cells, derived from the lung and the spleen *ex vivo*.

Appendix:



1) GSEA enrichment analysis of butyrate pre-treated macrophage, infected with S. pneumoniae as outlined in section 3.4



2) GSEA enrichment analysis of butyrate pre-treated macrophage, stimulated with Pam3Csk4 as outlined in section 3.4

Bibliography

1. Brown, E.M., M. Sadarangani, and B.B. Finlay, *The role of the immune system in governing host-microbe interactions in the intestine.* Nat Immunol, 2013. **14**(7): p. 660-7.
2. Kim, Y.S. and S.B. Ho, *Intestinal goblet cells and mucins in health and disease: recent insights and progress.* Curr Gastroenterol Rep, 2010. **12**(5): p. 319-30.
3. Mockl, L., *The Emerging Role of the Mammalian Glycocalyx in Functional Membrane Organization and Immune System Regulation.* Front Cell Dev Biol, 2020. **8**: p. 253.
4. Johansson, M.E., et al., *Composition and functional role of the mucus layers in the intestine.* Cell Mol Life Sci, 2011. **68**(22): p. 3635-41.
5. Sun, W.W., et al., *Nanoarchitecture and dynamics of the mouse enteric glycocalyx examined by freeze-etching electron tomography and intravital microscopy.* Commun Biol, 2020. **3**(1): p. 5.
6. Vaishnava, S., et al., *Paneth cells directly sense gut commensals and maintain homeostasis at the intestinal host-microbial interface.* Proc Natl Acad Sci U S A, 2008. **105**(52): p. 20858-63.
7. Bevins, C.L. and N.H. Salzman, *Paneth cells, antimicrobial peptides and maintenance of intestinal homeostasis.* Nat Rev Microbiol, 2011. **9**(5): p. 356-68.
8. Moran, A.P., A. Gupta, and L. Joshi, *Sweet-talk: role of host glycosylation in bacterial pathogenesis of the gastrointestinal tract.* Gut, 2011. **60**(10): p. 1412-25.
9. Medina-Contreras, O., et al., *CX3CR1 regulates intestinal macrophage homeostasis, bacterial translocation, and colitogenic Th17 responses in mice.* J Clin Invest, 2011. **121**(12): p. 4787-95.
10. Jakubzick, C.V., G.J. Randolph, and P.M. Henson, *Monocyte differentiation and antigen-presenting functions.* Nat Rev Immunol, 2017. **17**(6): p. 349-362.
11. Bain, C.C. and A.M. Mowat, *Macrophages in intestinal homeostasis and inflammation.* Immunol Rev, 2014. **260**(1): p. 102-17.
12. Mazzini, E., et al., *Oral tolerance can be established via gap junction transfer of fed antigens from CX3CR1(+) macrophages to CD103(+) dendritic cells.* Immunity, 2014. **40**(2): p. 248-61.
13. Esterhazy, D., et al., *Classical dendritic cells are required for dietary antigen-mediated induction of peripheral T(reg) cells and tolerance.* Nat Immunol, 2016. **17**(5): p. 545-55.
14. Farache, J., et al., *Luminal bacteria recruit CD103+ dendritic cells into the intestinal epithelium to sample bacterial antigens for presentation.* Immunity, 2013. **38**(3): p. 581-95.
15. Rescigno, M., et al., *Dendritic cells express tight junction proteins and penetrate gut epithelial monolayers to sample bacteria.* Nat Immunol, 2001. **2**(4): p. 361-7.
16. Ruane, D., et al., *Lung dendritic cells induce migration of protective T cells to the gastrointestinal tract.* J Exp Med, 2013. **210**(9): p. 1871-88.
17. Iwata, M., et al., *Retinoic acid imprints gut-homing specificity on T cells.* Immunity, 2004. **21**(4): p. 527-38.

18. Ruane, D., et al., *Microbiota regulate the ability of lung dendritic cells to induce IgA class-switch recombination and generate protective gastrointestinal immune responses.* J Exp Med, 2016. **213**(1): p. 53-73.
19. Li, X. and Y. Zheng, *Regulatory T cell identity: formation and maintenance.* Trends Immunol, 2015. **36**(6): p. 344-53.
20. Akdis, M., et al., *Immune responses in healthy and allergic individuals are characterized by a fine balance between allergen-specific T regulatory 1 and T helper 2 cells.* J Exp Med, 2004. **199**(11): p. 1567-75.
21. Zhou, J.Y., et al., *Intestinal Tr1 Cells Confer Protection against Colitis in the Absence of Foxp3+ Regulatory T Cell-Derived IL-10.* Immunohorizons, 2023. **7**(6): p. 456-466.
22. Kespohl, M., et al., *The Microbial Metabolite Butyrate Induces Expression of Th1-Associated Factors in CD4(+) T Cells.* Front Immunol, 2017. **8**: p. 1036.
23. Mittal, S.K. and P.A. Roche, *Suppression of antigen presentation by IL-10.* Curr Opin Immunol, 2015. **34**: p. 22-7.
24. Hasnain, S.Z., et al., *IL-10 promotes production of intestinal mucus by suppressing protein misfolding and endoplasmic reticulum stress in goblet cells.* Gastroenterology, 2013. **144**(2): p. 357-368 e9.
25. van der Sluis, M., et al., *Combined defects in epithelial and immunoregulatory factors exacerbate the pathogenesis of inflammation: mucin 2-interleukin 10-deficient mice.* Lab Invest, 2008. **88**(6): p. 634-42.
26. Horn, V. and G.F. Sonnenberg, *Group 3 innate lymphoid cells in intestinal health and disease.* Nat Rev Gastroenterol Hepatol, 2024. **21**(6): p. 428-443.
27. Kang, I., Y. Kim, and H.K. Lee, *Double-edged sword: gammadelta T cells in mucosal homeostasis and disease.* Exp Mol Med, 2023. **55**(9): p. 1895-1904.
28. Wu, Z., et al., *MAIT cell homing in intestinal homeostasis and inflammation.* Sci Adv, 2025. **11**(6): p. eadu4172.
29. Thompson, E.A., et al., *Interstitial Migration of CD8alphabeta T Cells in the Small Intestine Is Dynamic and Is Dictated by Environmental Cues.* Cell Rep, 2019. **26**(11): p. 2859-2867 e4.
30. Tezuka, H., et al., *Regulation of IgA production by naturally occurring TNF/iNOS-producing dendritic cells.* Nature, 2007. **448**(7156): p. 929-33.
31. Mills, K.H.G., *IL-17 and IL-17-producing cells in protection versus pathology.* Nat Rev Immunol, 2023. **23**(1): p. 38-54.
32. Gribonika, I., et al., *Peyer's patch T(H)17 cells are dispensable for gut IgA responses to oral immunization.* Sci Immunol, 2022. **7**(73): p. eabc5500.
33. Macpherson, A.J., et al., *A primitive T cell-independent mechanism of intestinal mucosal IgA responses to commensal bacteria.* Science, 2000. **288**(5474): p. 2222-6.
34. Cerutti, A., *The regulation of IgA class switching.* Nat Rev Immunol, 2008. **8**(6): p. 421-34.
35. Tsuji, M., et al., *Preferential generation of follicular B helper T cells from Foxp3+ T cells in gut Peyer's patches.* Science, 2009. **323**(5920): p. 1488-92.
36. Hirota, K., et al., *Plasticity of Th17 cells in Peyer's patches is responsible for the induction of T cell-dependent IgA responses.* Nat Immunol, 2013. **14**(4): p. 372-9.

37. Zhong, Z., et al., *Pro- and Anti- Effects of Immunoglobulin A- Producing B Cell in Tumors and Its Triggers.* Front Immunol, 2021. **12**: p. 765044.
38. Hiemstra, P.S., P.B. McCray, Jr., and R. Bals, *The innate immune function of airway epithelial cells in inflammatory lung disease.* Eur Respir J, 2015. **45**(4): p. 1150-62.
39. Lillehoj, E.P., et al., *Cellular and molecular biology of airway mucins.* Int Rev Cell Mol Biol, 2013. **303**: p. 139-202.
40. Chatterjee, M., J.P.M. van Putten, and K. Strijbis, *Defensive Properties of Mucin Glycoproteins during Respiratory Infections-Relevance for SARS-CoV-2.* mBio, 2020. **11**(6).
41. Roy, M.G., et al., *Muc5b is required for airway defence.* Nature, 2014. **505**(7483): p. 412-6.
42. Shenoy, A.T., et al., *Antigen presentation by lung epithelial cells directs CD4(+) T(RM) cell function and regulates barrier immunity.* Nat Commun, 2021. **12**(1): p. 5834.
43. Arebro, J., et al., *Antigen-presenting epithelial cells can play a pivotal role in airway allergy.* J Allergy Clin Immunol, 2016. **137**(3): p. 957-60 e7.
44. Kiyono, H. and S. Fukuyama, *NALT- versus Peyer's-patch-mediated mucosal immunity.* Nat Rev Immunol, 2004. **4**(9): p. 699-710.
45. Zheng, M.Z.M. and L.M. Wakim, *Tissue resident memory T cells in the respiratory tract.* Mucosal Immunol, 2022. **15**(3): p. 379-388.
46. Whitsett, J.A., S.E. Wert, and T.E. Weaver, *Alveolar surfactant homeostasis and the pathogenesis of pulmonary disease.* Annu Rev Med, 2010. **61**: p. 105-19.
47. Tecle, T., S. Tripathi, and K.L. Hartshorn, *Review: Defensins and cathelicidins in lung immunity.* Innate Immun, 2010. **16**(3): p. 151-9.
48. Malur, A., et al., *Restoration of PPARgamma reverses lipid accumulation in alveolar macrophages of GM-CSF knockout mice.* Am J Physiol Lung Cell Mol Physiol, 2011. **300**(1): p. L73-80.
49. Yu, X., et al., *The Cytokine TGF-beta Promotes the Development and Homeostasis of Alveolar Macrophages.* Immunity, 2017. **47**(5): p. 903-912 e4.
50. Misharin, A.V., et al., *Flow cytometric analysis of macrophages and dendritic cell subsets in the mouse lung.* Am J Respir Cell Mol Biol, 2013. **49**(4): p. 503-10.
51. Mitsi, E., et al., *Human alveolar macrophages predominately express combined classical M1 and M2 surface markers in steady state.* Respir Res, 2018. **19**(1): p. 66.
52. Nayak, D.K., et al., *Isolation and In Vitro Culture of Murine and Human Alveolar Macrophages.* J Vis Exp, 2018(134).
53. Smith, M.R., T.J. Standiford, and R.C. Reddy, *PPARs in alveolar macrophage biology.* PPAR Res, 2007. **2007**: p. 23812.
54. Liao, X., et al., *Kruppel-like factor 4 regulates macrophage polarization.* J Clin Invest, 2011. **121**(7): p. 2736-49.
55. Pestal, K., L.C. Slayden, and G.M. Barton, *KLF family members control expression of genes required for tissue macrophage identities.* J Exp Med, 2025. **222**(5).
56. McCowan, J., et al., *The transcription factor EGR2 is indispensable for tissue-specific imprinting of alveolar macrophages in health and tissue repair.* Sci Immunol, 2021. **6**(65): p. eabj2132.

57. Hussell, T. and T.J. Bell, *Alveolar macrophages: plasticity in a tissue-specific context.* Nat Rev Immunol, 2014. **14**(2): p. 81-93.
58. Gibbings, S.L., et al., *Three Unique Interstitial Macrophages in the Murine Lung at Steady State.* Am J Respir Cell Mol Biol, 2017. **57**(1): p. 66-76.
59. McQuattie-Pimentel, A.C., G.R.S. Budinger, and M.N. Ballinger, *Monocyte-derived Alveolar Macrophages: The Dark Side of Lung Repair?* Am J Respir Cell Mol Biol, 2018. **58**(1): p. 5-6.
60. Arafa, E.I., et al., *Recruitment and training of alveolar macrophages after pneumococcal pneumonia.* JCI Insight, 2022. **7**(5).
61. Feehan, K.T., et al., *Post-resolution macrophages shape long-term tissue immunity and integrity in a mouse model of pneumococcal pneumonia.* Nat Commun, 2024. **15**(1): p. 4326.
62. Guillon, A., et al., *Pneumonia recovery reprograms the alveolar macrophage pool.* JCI Insight, 2020. **5**(4).
63. Zhang, J., et al., *Bacterial pneumonia induces senescence in resident alveolar macrophages that are outcompeted by monocytes.* Cell Rep, 2025. **44**(5): p. 115571.
64. Ingersoll, M.A., et al., *Comparison of gene expression profiles between human and mouse monocyte subsets.* Blood, 2010. **115**(3): p. e10-9.
65. Hong, H., et al., *Role of IL-25, IL-33, and TSLP in triggering united airway diseases toward type 2 inflammation.* Allergy, 2020. **75**(11): p. 2794-2804.
66. Trompette, A., et al., *Gut microbiota metabolism of dietary fiber influences allergic airway disease and hematopoiesis.* Nat Med, 2014. **20**(2): p. 159-66.
67. Braciale, T.J., J. Sun, and T.S. Kim, *Regulating the adaptive immune response to respiratory virus infection.* Nat Rev Immunol, 2012. **12**(4): p. 295-305.
68. Lyadova, I.V. and A.V. Panteleev, *Th1 and Th17 Cells in Tuberculosis: Protection, Pathology, and Biomarkers.* Mediators Inflamm, 2015. **2015**: p. 854507.
69. Kohlmeier, J.E. and D.L. Woodland, *Memory T cell recruitment to the lung airways.* Curr Opin Immunol, 2006. **18**(3): p. 357-62.
70. Ross, P.J., et al., *Relative contribution of Th1 and Th17 cells in adaptive immunity to Bordetella pertussis: towards the rational design of an improved acellular pertussis vaccine.* PLoS Pathog, 2013. **9**(4): p. e1003264.
71. Wang, Y., et al., *Cross-protective mucosal immunity mediated by memory Th17 cells against Streptococcus pneumoniae lung infection.* Mucosal Immunol, 2017. **10**(1): p. 250-259.
72. Griffin, G.K., et al., *IL-17 and TNF-alpha sustain neutrophil recruitment during inflammation through synergistic effects on endothelial activation.* J Immunol, 2012. **188**(12): p. 6287-99.
73. Brown, R.L., R.P. Sequeira, and T.B. Clarke, *The microbiota protects against respiratory infection via GM-CSF signaling.* Nat Commun, 2017. **8**(1): p. 1512.
74. D'Alessio, F.R., et al., *CD4+CD25+Foxp3+ Tregs resolve experimental lung injury in mice and are present in humans with acute lung injury.* J Clin Invest, 2009. **119**(10): p. 2898-913.
75. Turnbaugh, P.J., et al., *The human microbiome project.* Nature, 2007. **449**(7164): p. 804-10.
76. Gill, S.R., et al., *Metagenomic analysis of the human distal gut microbiome.* Science, 2006. **312**(5778): p. 1355-9.

77. Bentley, R. and R. Meganathan, *Biosynthesis of vitamin K (menaquinone) in bacteria.* Microbiol Rev, 1982. **46**(3): p. 241-80.
78. Kundra, P., et al., *Healthy adult gut microbiota sustains its own vitamin B12 requirement in an in vitro batch fermentation model.* Front Nutr, 2022. **9**: p. 1070155.
79. Cebula, A., et al., *Thymus-derived regulatory T cells contribute to tolerance to commensal microbiota.* Nature, 2013. **497**(7448): p. 258-62.
80. Miranda-Waldetario, M.C.G. and M.A. Curotto de Lafaille, *Oral tolerance to dietary antigens and Foxp3(+) regulatory T cells.* Immunol Rev, 2024. **326**(1): p. 8-16.
81. Pickard, J.M., et al., *Gut microbiota: Role in pathogen colonization, immune responses, and inflammatory disease.* Immunol Rev, 2017. **279**(1): p. 70-89.
82. Eckburg, P.B., et al., *Diversity of the human intestinal microbial flora.* Science, 2005. **308**(5728): p. 1635-8.
83. Claesson, M.J., et al., *Composition, variability, and temporal stability of the intestinal microbiota of the elderly.* Proc Natl Acad Sci U S A, 2011. **108 Suppl 1**(Suppl 1): p. 4586-91.
84. Walker, A.W., et al., *High-throughput clone library analysis of the mucosa-associated microbiota reveals dysbiosis and differences between inflamed and non-inflamed regions of the intestine in inflammatory bowel disease.* BMC Microbiol, 2011. **11**: p. 7.
85. Sha, H., et al., *Blocking coprophagy increases the levels of inflammation and depression in healthy mice as well as mice receiving fecal microbiota transplantation from disease model mice donors.* APMIS, 2023. **131**(7): p. 351-368.
86. Shanahan, F. and C.N. Bernstein, *The evolving epidemiology of inflammatory bowel disease.* Curr Opin Gastroenterol, 2009. **25**(4): p. 301-5.
87. Bowerman, K.L., et al., *Disease-associated gut microbiome and metabolome changes in patients with chronic obstructive pulmonary disease.* Nat Commun, 2020. **11**(1): p. 5886.
88. Levy, M., et al., *Dysbiosis and the immune system.* Nat Rev Immunol, 2017. **17**(4): p. 219-232.
89. Cleynen, I., et al., *Inherited determinants of Crohn's disease and ulcerative colitis phenotypes: a genetic association study.* Lancet, 2016. **387**(10014): p. 156-67.
90. Liu, Y., et al., *TLR4 regulates RORgammat(+) regulatory T-cell responses and susceptibility to colon inflammation through interaction with Akkermansia muciniphila.* Microbiome, 2022. **10**(1): p. 98.
91. Lamas, B., et al., *CARD9 impacts colitis by altering gut microbiota metabolism of tryptophan into aryl hydrocarbon receptor ligands.* Nat Med, 2016. **22**(6): p. 598-605.
92. Kamada, N., et al., *Abnormally differentiated subsets of intestinal macrophage play a key role in Th1-dominant chronic colitis through excess production of IL-12 and IL-23 in response to bacteria.* J Immunol, 2005. **175**(10): p. 6900-8.
93. Maslowski, K.M., et al., *Regulation of inflammatory responses by gut microbiota and chemoattractant receptor GPR43.* Nature, 2009. **461**(7268): p. 1282-6.

94. Spor, A., O. Koren, and R. Ley, *Unravelling the effects of the environment and host genotype on the gut microbiome.* Nat Rev Microbiol, 2011. **9**(4): p. 279-90.
95. Rochereau, N., et al., *NOD2 deficiency increases retrograde transport of secretory IgA complexes in Crohn's disease.* Nat Commun, 2021. **12**(1): p. 261.
96. Vijay-Kumar, M., et al., *Metabolic syndrome and altered gut microbiota in mice lacking Toll-like receptor 5.* Science, 2010. **328**(5975): p. 228-31.
97. Wen, L., et al., *Innate immunity and intestinal microbiota in the development of Type 1 diabetes.* Nature, 2008. **455**(7216): p. 1109-13.
98. Bosch, A., et al., *Development of Upper Respiratory Tract Microbiota in Infancy is Affected by Mode of Delivery.* EBioMedicine, 2016. **9**: p. 336-345.
99. Al Nabhani, Z., et al., *A Weaning Reaction to Microbiota Is Required for Resistance to Immunopathologies in the Adult.* Immunity, 2019. **50**(5): p. 1276-1288 e5.
100. Klein, E.Y., et al., *Global increase and geographic convergence in antibiotic consumption between 2000 and 2015.* Proc Natl Acad Sci U S A, 2018. **115**(15): p. E3463-E3470.
101. Palleja, A., et al., *Recovery of gut microbiota of healthy adults following antibiotic exposure.* Nat Microbiol, 2018. **3**(11): p. 1255-1265.
102. Swaminathan, G., et al., *Vaccine Hyporesponse Induced by Individual Antibiotic Treatment in Mice and Non-Human Primates Is Diminished upon Recovery of the Gut Microbiome.* Vaccines (Basel), 2021. **9**(11).
103. Cho, K.Y., *Association of gut microbiota with obesity in children and adolescents.* Clin Exp Pediatr, 2023. **66**(4): p. 148-154.
104. Aslam, R., et al., *Link between gut microbiota dysbiosis and childhood asthma: Insights from a systematic review.* J Allergy Clin Immunol Glob, 2024. **3**(3): p. 100289.
105. Kowalska-Duplaga, K., et al., *Differences in the intestinal microbiome of healthy children and patients with newly diagnosed Crohn's disease.* Sci Rep, 2019. **9**(1): p. 18880.
106. Akagawa, S. and K. Kaneko, *Gut microbiota and allergic diseases in children.* Allergol Int, 2022. **71**(3): p. 301-309.
107. Wu, T., et al., *Microbiota-Derived Short-Chain Fatty Acids Promote LAMTOR2-Mediated Immune Responses in Macrophages.* mSystems, 2020. **5**(6).
108. Carmody, R.N., et al., *Diet dominates host genotype in shaping the murine gut microbiota.* Cell Host Microbe, 2015. **17**(1): p. 72-84.
109. De Filippo, C., et al., *Impact of diet in shaping gut microbiota revealed by a comparative study in children from Europe and rural Africa.* Proc Natl Acad Sci U S A, 2010. **107**(33): p. 14691-6.
110. Martinez, I., et al., *Resistant starches types 2 and 4 have differential effects on the composition of the fecal microbiota in human subjects.* PLoS One, 2010. **5**(11): p. e15046.
111. Holscher, H.D., et al., *Fiber supplementation influences phylogenetic structure and functional capacity of the human intestinal microbiome: follow-up of a randomized controlled trial.* Am J Clin Nutr, 2015. **101**(1): p. 55-64.
112. Trompette, A., et al., *Dietary Fiber Confers Protection against Flu by Shaping Ly6c(-) Patrolling Monocyte Hematopoiesis and CD8(+) T Cell Metabolism.* Immunity, 2018. **48**(5): p. 992-1005 e8.

113. Raoul, P., et al., *Food Additives, a Key Environmental Factor in the Development of IBD through Gut Dysbiosis.* Microorganisms, 2022. **10**(1).
114. Rodriguez-Palacios, A., et al., *The Artificial Sweetener Splenda Promotes Gut Proteobacteria, Dysbiosis, and Myeloperoxidase Reactivity in Crohn's Disease-Like Ileitis.* Inflamm Bowel Dis, 2018. **24**(5): p. 1005-1020.
115. Xiao, H.W., et al., *Gut microbiota modulates alcohol withdrawal-induced anxiety in mice.* Toxicol Lett, 2018. **287**: p. 23-30.
116. Agus, A., K. Clement, and H. Sokol, *Gut microbiota-derived metabolites as central regulators in metabolic disorders.* Gut, 2021. **70**(6): p. 1174-1182.
117. Agus, A., J. Planchais, and H. Sokol, *Gut Microbiota Regulation of Tryptophan Metabolism in Health and Disease.* Cell Host Microbe, 2018. **23**(6): p. 716-724.
118. Li, Q., et al., *Microbial metabolite indole-3-propionic acid drives mitochondrial respiration in CD4(+) T cells to confer protection against intestinal inflammation.* Nat Metab, 2025.
119. Caparros-Martin, J.A., et al., *Bile acids in the lower airways is associated with airway microbiota changes in chronic obstructive pulmonary disease: an observational study.* BMJ Open Respir Res, 2024. **11**(1).
120. Hino, S., et al., *Mucin-Derived O-Glycans Act as Endogenous Fiber and Sustain Mucosal Immune Homeostasis via Short-Chain Fatty Acid Production in Rat Cecum.* J Nutr, 2020. **150**(10): p. 2656-2665.
121. Smith, E.A. and G.T. Macfarlane, *Dissimilatory amino Acid metabolism in human colonic bacteria.* Anaerobe, 1997. **3**(5): p. 327-37.
122. Van den Abbeele, P., et al., *Butyrate-producing Clostridium cluster XIVa species specifically colonize mucins in an in vitro gut model.* ISME J, 2013. **7**(5): p. 949-61.
123. Moon, J., et al., *Faecalibacterium prausnitzii alleviates inflammatory arthritis and regulates IL-17 production, short-chain fatty acids, and the intestinal microbial flora in experimental mouse model for rheumatoid arthritis.* Arthritis Res Ther, 2023. **25**(1): p. 130.
124. Kim, M., et al., *Gut Microbial Metabolites Fuel Host Antibody Responses.* Cell Host Microbe, 2016. **20**(2): p. 202-14.
125. Liu, Q., et al., *Lung immune tone via gut-lung axis: gut-derived LPS and short-chain fatty acids' immunometabolic regulation of lung IL-1beta, FFAR2, and FFAR3 expression.* Am J Physiol Lung Cell Mol Physiol, 2021. **321**(1): p. L65-L78.
126. Morrison, D.J. and T. Preston, *Formation of short-chain fatty acids by the gut microbiota and their impact on human metabolism.* Gut Microbes, 2016. **7**(3): p. 189-200.
127. Topping, D.L. and P.M. Clifton, *Short-chain fatty acids and human colonic function: roles of resistant starch and nonstarch polysaccharides.* Physiol Rev, 2001. **81**(3): p. 1031-64.
128. van der Beek, C.M., et al., *The prebiotic inulin improves substrate metabolism and promotes short-chain fatty acid production in overweight to obese men.* Metabolism, 2018. **87**: p. 25-35.
129. Hald, S., et al., *Effects of Arabinoxylan and Resistant Starch on Intestinal Microbiota and Short-Chain Fatty Acids in Subjects with Metabolic Syndrome: A Randomised Crossover Study.* PLoS One, 2016. **11**(7): p. e0159223.

130. Miyamoto, J., et al., *Barley beta-glucan improves metabolic condition via short-chain fatty acids produced by gut microbial fermentation in high fat diet fed mice.* PLoS One, 2018. **13**(4): p. e0196579.
131. Larsen, N., et al., *Potential of Pectins to Beneficially Modulate the Gut Microbiota Depends on Their Structural Properties.* Front Microbiol, 2019. **10**: p. 223.
132. Baxter, N.T., et al., *Dynamics of Human Gut Microbiota and Short-Chain Fatty Acids in Response to Dietary Interventions with Three Fermentable Fibers.* mBio, 2019. **10**(1).
133. Daisuke Maruyama, X.T., Thien N. M. Doan, Wen-I Liao, Tomohiro Chaki, Hiroki Taenaka, Mazharul Maishan, Brian Layden, Michael A. Matthay, Arun Prakash, *Gut Microbiome-derived Propionate Reprograms Alveolar Macrophages Metabolically and Regulates Lung Injury Responses.* bioRxiv, 2025.
134. Wolever, T.M., et al., *Guar, but not psyllium, increases breath methane and serum acetate concentrations in human subjects.* Am J Clin Nutr, 1992. **55**(3): p. 719-22.
135. Lange, O., M. Proczko-Stepaniak, and A. Mika, *Short-Chain Fatty Acids-A Product of the Microbiome and Its Participation in Two-Way Communication on the Microbiome-Host Mammal Line.* Curr Obes Rep, 2023. **12**(2): p. 108-126.
136. Miller, T.L. and M.J. Wolin, *Pathways of acetate, propionate, and butyrate formation by the human fecal microbial flora.* Appl Environ Microbiol, 1996. **62**(5): p. 1589-92.
137. Reichardt, N., et al., *Phylogenetic distribution of three pathways for propionate production within the human gut microbiota.* ISME J, 2014. **8**(6): p. 1323-35.
138. Duncan, S.H., P. Louis, and H.J. Flint, *Lactate-utilizing bacteria, isolated from human feces, that produce butyrate as a major fermentation product.* Appl Environ Microbiol, 2004. **70**(10): p. 5810-7.
139. Chen, T., et al., *Fiber-utilizing capacity varies in Prevotella- versus Bacteroides-dominated gut microbiota.* Sci Rep, 2017. **7**(1): p. 2594.
140. Frampton, J., et al., *Short-chain fatty acids as potential regulators of skeletal muscle metabolism and function.* Nat Metab, 2020. **2**(9): p. 840-848.
141. Le Poul, E., et al., *Functional characterization of human receptors for short-chain fatty acids and their role in polymorphonuclear cell activation.* J Biol Chem, 2003. **278**(28): p. 25481-9.
142. Taggart, A.K., et al., *(D)-beta-Hydroxybutyrate inhibits adipocyte lipolysis via the nicotinic acid receptor PUMA-G.* J Biol Chem, 2005. **280**(29): p. 26649-52.
143. Thangaraju, M., et al., *GPR109A is a G-protein-coupled receptor for the bacterial fermentation product butyrate and functions as a tumor suppressor in colon.* Cancer Res, 2009. **69**(7): p. 2826-32.
144. Pluznick, J., *A novel SCFA receptor, the microbiota, and blood pressure regulation.* Gut Microbes, 2014. **5**(2): p. 202-7.
145. Ritzhaupt, A., et al., *Identification and characterization of a monocarboxylate transporter (MCT1) in pig and human colon: its potential to transport L-lactate as well as butyrate.* J Physiol, 1998. **513 (Pt 3)**(Pt 3): p. 719-32.
146. Miyauchi, S., et al., *Functional identification of SLC5A8, a tumor suppressor down-regulated in colon cancer, as a Na(+)-coupled transporter for short-chain fatty acids.* J Biol Chem, 2004. **279**(14): p. 13293-6.

147. Sun, M., et al., *Microbiota metabolite short-chain fatty acids, GPCR, and inflammatory bowel diseases.* J Gastroenterol, 2017. **52**(1): p. 1-8.
148. Nshanian, M., et al., *Short-chain fatty acid metabolites propionate and butyrate are unique epigenetic regulatory elements linking diet, metabolism and gene expression.* Nat Metab, 2025. **7**(1): p. 196-211.
149. Chen, Y., et al., *Lysine propionylation and butyrylation are novel post-translational modifications in histones.* Mol Cell Proteomics, 2007. **6**(5): p. 812-9.
150. Dai, L., et al., *Lysine 2-hydroxyisobutyrylation is a widely distributed active histone mark.* Nat Chem Biol, 2014. **10**(5): p. 365-70.
151. Xie, Z., et al., *Lysine succinylation and lysine malonylation in histones.* Mol Cell Proteomics, 2012. **11**(5): p. 100-7.
152. Fellows, R., et al., *Microbiota derived short-chain fatty acids promote histone crotonylation in the colon through histone deacetylases.* Nat Commun, 2018. **9**(1): p. 105.
153. Bergman, E.N., *Energy contributions of volatile fatty acids from the gastrointestinal tract in various species.* Physiol Rev, 1990. **70**(2): p. 567-90.
154. Bugaut, M., *Occurrence, absorption and metabolism of short-chain fatty acids in the digestive tract of mammals.* Comp Biochem Physiol B, 1987. **86**(3): p. 439-72.
155. Thibault, R., et al., *Butyrate utilization by the colonic mucosa in inflammatory bowel diseases: a transport deficiency.* Inflamm Bowel Dis, 2010. **16**(4): p. 684-95.
156. Hamer, H.M., et al., *Butyrate modulates oxidative stress in the colonic mucosa of healthy humans.* Clin Nutr, 2009. **28**(1): p. 88-93.
157. Xing, X., et al., *Sodium butyrate protects against oxidative stress in HepG2 cells through modulating Nrf2 pathway and mitochondrial function.* J Physiol Biochem, 2016. **73**(3): p. 405-414.
158. Liu, K., et al., *p53 beta-hydroxybutyrylation attenuates p53 activity.* Cell Death Dis, 2019. **10**(3): p. 243.
159. Xu, S., et al., *Butyrate induces apoptosis by activating PDC and inhibiting complex I through SIRT3 inactivation.* Signal Transduct Target Ther, 2017. **2**: p. 16035.
160. Bordon, Y., *Butyrate promotes T cell 'stemness' to support immunity to melanoma.* Nat Rev Immunol, 2025. **25**(12): p. 865.
161. Rutting, S., et al., *Short-chain fatty acids increase TNFalpha-induced inflammation in primary human lung mesenchymal cells through the activation of p38 MAPK.* Am J Physiol Lung Cell Mol Physiol, 2019. **316**(1): p. L157-L174.
162. Bassis, C.M., et al., *Analysis of the upper respiratory tract microbiotas as the source of the lung and gastric microbiotas in healthy individuals.* mBio, 2015. **6**(2): p. e00037.
163. Dickson, R.P., et al., *Bacterial Topography of the Healthy Human Lower Respiratory Tract.* mBio, 2017. **8**(1).
164. Dickson, R.P., et al., *Spatial Variation in the Healthy Human Lung Microbiome and the Adapted Island Model of Lung Biogeography.* Ann Am Thorac Soc, 2015. **12**(6): p. 821-30.

165. Odendaal, M.L., et al., *Host and environmental factors shape upper airway microbiota and respiratory health across the human lifespan.* Cell, 2024. **187**(17): p. 4571-4585 e15.
166. Stearns, J.C., et al., *Culture and molecular-based profiles show shifts in bacterial communities of the upper respiratory tract that occur with age.* ISME J, 2015. **9**(5): p. 1268.
167. Quinn-Bohmann, N., et al., *Meta-analysis of the human upper respiratory tract microbiome reveals robust taxonomic associations with health and disease.* BMC Biol, 2024. **22**(1): p. 93.
168. Erb-Downward, J.R., et al., *Analysis of the lung microbiome in the "healthy" smoker and in COPD.* PLoS One, 2011. **6**(2): p. e16384.
169. Francoise, A. and G. Hery-Arnaud, *The Microbiome in Cystic Fibrosis Pulmonary Disease.* Genes (Basel), 2020. **11**(5).
170. Mikhail, S.G. and D.N. O'Dwyer, *The lung microbiome in interstitial lung disease.* Breathe (Sheff), 2025. **21**(2): p. 240167.
171. Garcia-Nunez, M., et al., *Severity-related changes of bronchial microbiome in chronic obstructive pulmonary disease.* J Clin Microbiol, 2014. **52**(12): p. 4217-23.
172. Huang, D., et al., *Association between airway microbiota and systemic inflammation markers in non-small cell lung cancer patients.* Sci Rep, 2025. **15**(1): p. 3539.
173. Zhou, X., S. Shen, and Z. Wang, *Genetic evidence of bidirectional mendelian randomization study on the causality between gut microbiome and respiratory diseases contributes to gut-lung axis.* Sci Rep, 2024. **14**(1): p. 25550.
174. Chioma, O.S., et al., *Gut microbiota modulates lung fibrosis severity following acute lung injury in mice.* Commun Biol, 2022. **5**(1): p. 1401.
175. Fouhy, F., et al., *A pilot study demonstrating the altered gut microbiota functionality in stable adults with Cystic Fibrosis.* Sci Rep, 2017. **7**(1): p. 6685.
176. Stokholm, J., et al., *Maturation of the gut microbiome and risk of asthma in childhood.* Nat Commun, 2018. **9**(1): p. 141.
177. Thorburn, A.N., et al., *Evidence that asthma is a developmental origin disease influenced by maternal diet and bacterial metabolites.* Nat Commun, 2015. **6**: p. 7320.
178. Ekbom, A., et al., *Increased risk of both ulcerative colitis and Crohn's disease in a population suffering from COPD.* Lung, 2008. **186**(3): p. 167-172.
179. Schuijt, T.J., et al., *The gut microbiota plays a protective role in the host defence against pneumococcal pneumonia.* Gut, 2016. **65**(4): p. 575-83.
180. Tian, X., et al., *Elevated Gut Microbiome-Derived Propionate Levels Are Associated With Reduced Sterile Lung Inflammation and Bacterial Immunity in Mice.* Front Microbiol, 2019. **10**: p. 159.
181. Ichinohe, T., et al., *Microbiota regulates immune defense against respiratory tract influenza A virus infection.* Proc Natl Acad Sci U S A, 2011. **108**(13): p. 5354-9.
182. Davis, C.P. and D.C. Savage, *Habitat, succession, attachment, and morphology of segmented, filamentous microbes indigenous to the murine gastrointestinal tract.* Infect Immun, 1974. **10**(4): p. 948-56.

183. Ngo, V.L., et al., *Intestinal microbiota programming of alveolar macrophages influences severity of respiratory viral infection.* Cell Host Microbe, 2024. **32**(3): p. 335-348 e8.
184. *"The deadly dance of alveolar macrophages and influenza virus". C. David, C. Verney, M. Si-Tahar and A. Guillon. Eur Respir Rev 2024; 33: 240132.* Eur Respir Rev, 2025. **34**(175).
185. Aegerter, H., B.N. Lambrecht, and C.V. Jakubzick, *Biology of lung macrophages in health and disease.* Immunity, 2022. **55**(9): p. 1564-1580.
186. Chen, L.W., P.H. Chen, and C.M. Hsu, *Commensal microflora contribute to host defense against Escherichia coli pneumonia through Toll-like receptors.* Shock, 2011. **36**(1): p. 67-75.
187. Lee, C., et al., *Sodium butyrate inhibits the NF-kappa B signaling pathway and histone deacetylation, and attenuates experimental colitis in an IL-10 independent manner.* Int Immunopharmacol, 2017. **51**: p. 47-56.
188. Saemann, M.D., et al., *Anti-inflammatory effects of sodium butyrate on human monocytes: potent inhibition of IL-12 and up-regulation of IL-10 production.* FASEB J, 2000. **14**(15): p. 2380-2.
189. Asarat, M., et al., *Short-Chain Fatty Acids Regulate Cytokines and Th17/Treg Cells in Human Peripheral Blood Mononuclear Cells in vitro.* Immunol Invest, 2016. **45**(3): p. 205-22.
190. Sun, M., et al., *Microbiota-derived short-chain fatty acids promote Th1 cell IL-10 production to maintain intestinal homeostasis.* Nat Commun, 2018. **9**(1): p. 3555.
191. Felix, K.M., et al., *Gut Microbiota Contributes to Resistance Against Pneumococcal Pneumonia in Immunodeficient Rag(-/-) Mice.* Front Cell Infect Microbiol, 2018. **8**: p. 118.
192. Khan, N., et al., *Intestinal dysbiosis compromises alveolar macrophage immunity to Mycobacterium tuberculosis.* Mucosal Immunol, 2019. **12**(3): p. 772-783.
193. Hanson, C., et al., *The Relationship between Dietary Fiber Intake and Lung Function in the National Health and Nutrition Examination Surveys.* Ann Am Thorac Soc, 2016. **13**(5): p. 643-50.
194. Szmidt, M.K., et al., *Long-term dietary fiber intake and risk of chronic obstructive pulmonary disease: a prospective cohort study of women.* Eur J Nutr, 2020. **59**(5): p. 1869-1879.
195. Machado, M.G., et al., *Acetate Improves the Killing of Streptococcus pneumoniae by Alveolar Macrophages via NLRP3 Inflammasome and Glycolysis-HIF-1alpha Axis.* Front Immunol, 2022. **13**: p. 773261.
196. Schulthess, J., et al., *The Short-chain Fatty Acid Butyrate Imprints an Antimicrobial Program in Macrophages.* Immunity, 2019. **50**(2): p. 432-445 e7.
197. Kullberg, R.F.J., et al., *Butyrate-producing gut bacterium Faecalibacterium prausnitzii protects against bacterial pneumonia.* Eur Respir J, 2025. **66**(5).
198. Xing, J., et al., *Gut microbiota-derived isovaleric acid ameliorates influenza virus infection via gut-lung axis.* NPJ Biofilms Microbiomes, 2025. **11**(1): p. 116.
199. Collaborators, G.B.D.A.R., *Global mortality associated with 33 bacterial pathogens in 2019: a systematic analysis for the Global Burden of Disease Study 2019.* Lancet, 2022. **400**(10369): p. 2221-2248.

200. Collaborators, G.B.D.L.R.I., *Estimates of the global, regional, and national morbidity, mortality, and aetiologies of lower respiratory infections in 195 countries, 1990-2016: a systematic analysis for the Global Burden of Disease Study 2016.* Lancet Infect Dis, 2018. **18**(11): p. 1191-1210.
201. Weiser, J.N., D.M. Ferreira, and J.C. Paton, *Streptococcus pneumoniae: transmission, colonization and invasion.* Nat Rev Microbiol, 2018. **16**(6): p. 355-367.
202. Ganaie, F., et al., *A New Pneumococcal Capsule Type, 10D, is the 100th Serotype and Has a Large cps Fragment from an Oral Streptococcus.* mBio, 2020. **11**(3).
203. Pimenta, F., et al., *New Pneumococcal Serotype 15D.* J Clin Microbiol, 2021. **59**(5).
204. Executive, H.S., *Community Acquired Pneumonia Antibiotic Treatment in the Community (Adults).*
205. Miller, W.R. and C.A. Arias, *ESKAPE pathogens: antimicrobial resistance, epidemiology, clinical impact and therapeutics.* Nat Rev Microbiol, 2024. **22**(10): p. 598-616.
206. Organisation, W.H., *WHO updates list of drug-resistant bacteria most threatening to human health*.
207. Li, J., et al., *Streptococcus pneumoniae beta-lactam resistance: epidemiological trends, molecular drivers, and innovative control strategies in the post-pandemic era.* Clin Microbiol Rev, 2025. **38**(3): p. e0008225.
208. Wang, J.L., et al., *Global trends in non-susceptibility rates of Streptococcus pneumoniae isolates to ceftriaxone: Data from the antimicrobial testing leadership and surveillance (ATLAS) programme, 2016-21.* Int J Antimicrob Agents, 2024. **63**(2): p. 107072.
209. Gonzales, B.E., et al., *Increase of Macrolide-Resistance in Streptococcus pneumoniae Strains After the Introduction of the 13-Valent Pneumococcal Conjugate Vaccine in Lima, Peru.* Front Cell Infect Microbiol, 2022. **12**: p. 866186.
210. Darkwah, S., et al., *Pneumococcal serotypes and their association with death risk in invasive pneumococcal disease: a systematic review and meta-analysis.* Front Med (Lausanne), 2025. **12**: p. 1566502.
211. Maeda, H. and K. Morimoto, *Global distribution and characteristics of pneumococcal serotypes in adults.* Hum Vaccin Immunother, 2025. **21**(1): p. 2469424.
212. Luck, J.N., H. Tettelin, and C.J. Orihuela, *Sugar-Coated Killer: Serotype 3 Pneumococcal Disease.* Front Cell Infect Microbiol, 2020. **10**: p. 613287.
213. Donati, C., et al., *Structure and dynamics of the pan-genome of Streptococcus pneumoniae and closely related species.* Genome Biol, 2010. **11**(10): p. R107.
214. Tettelin, H., et al., *Complete genome sequence of a virulent isolate of Streptococcus pneumoniae.* Science, 2001. **293**(5529): p. 498-506.
215. Berge, M.J., et al., *A programmed cell division delay preserves genome integrity during natural genetic transformation in Streptococcus pneumoniae.* Nat Commun, 2017. **8**(1): p. 1621.

216. Choi, E.H., et al., *Capsular Polysaccharide (CPS) Release by Serotype 3 Pneumococcal Strains Reduces the Protective Effect of Anti-Type 3 CPS Antibodies.* Clin Vaccine Immunol, 2016. **23**(2): p. 162-7.
217. Vidal, J.E., et al., *The LuxS-dependent quorum-sensing system regulates early biofilm formation by Streptococcus pneumoniae strain D39.* Infect Immun, 2011. **79**(10): p. 4050-60.
218. Dessing, M.C., et al., *Role played by Toll-like receptors 2 and 4 in lipoteichoic acid-induced lung inflammation and coagulation.* J Infect Dis, 2008. **197**(2): p. 245-52.
219. Komori, M., et al., *Pneumococcal peptidoglycan-polysaccharides regulate Toll-like receptor 2 in the mouse middle ear epithelial cells.* Pediatr Res, 2011. **69**(2): p. 101-5.
220. Schroder, N.W., et al., *Lipoteichoic acid (LTA) of Streptococcus pneumoniae and Staphylococcus aureus activates immune cells via Toll-like receptor (TLR)-2, lipopolysaccharide-binding protein (LBP), and CD14, whereas TLR-4 and MD-2 are not involved.* J Biol Chem, 2003. **278**(18): p. 15587-94.
221. Letiembre, M., et al., *Toll-like receptor 2 deficiency delays pneumococcal phagocytosis and impairs oxidative killing by granulocytes.* Infect Immun, 2005. **73**(12): p. 8397-401.
222. Moffitt, K., et al., *Toll-like receptor 2-dependent protection against pneumococcal carriage by immunization with lipidated pneumococcal proteins.* Infect Immun, 2014. **82**(5): p. 2079-86.
223. Dessing, M.C., et al., *Toll-like receptor 2 does not contribute to host response during postinfluenza pneumococcal pneumonia.* Am J Respir Cell Mol Biol, 2007. **36**(5): p. 609-14.
224. Knapp, S., et al., *Toll-like receptor 2 plays a role in the early inflammatory response to murine pneumococcal pneumonia but does not contribute to antibacterial defense.* J Immunol, 2004. **172**(5): p. 3132-8.
225. Davis, K.M., S. Nakamura, and J.N. Weiser, *Nod2 sensing of lysozyme-digested peptidoglycan promotes macrophage recruitment and clearance of S. pneumoniae colonization in mice.* J Clin Invest, 2011. **121**(9): p. 3666-76.
226. Richard, A.L., et al., *TLR2 signaling decreases transmission of Streptococcus pneumoniae by limiting bacterial shedding in an infant mouse Influenza A co-infection model.* PLoS Pathog, 2014. **10**(8): p. e1004339.
227. Mogensen, T.H., et al., *Live Streptococcus pneumoniae, Haemophilus influenzae, and Neisseria meningitidis activate the inflammatory response through Toll-like receptors 2, 4, and 9 in species-specific patterns.* J Leukoc Biol, 2006. **80**(2): p. 267-77.
228. Albiger, B., et al., *Toll-like receptor 9 acts at an early stage in host defence against pneumococcal infection.* Cell Microbiol, 2007. **9**(3): p. 633-44.
229. Dessing, M.C., et al., *Toll-like receptor 2 contributes to antibacterial defence against pneumolysin-deficient pneumococci.* Cell Microbiol, 2008. **10**(1): p. 237-46.
230. McNeela, E.A., et al., *Pneumolysin activates the NLRP3 inflammasome and promotes proinflammatory cytokines independently of TLR4.* PLoS Pathog, 2010. **6**(11): p. e1001191.

231. Liu, T., et al., *NF-kappaB signaling in inflammation.* Signal Transduct Target Ther, 2017. **2**: p. 17023-.
232. Pahl, H.L., *Activators and target genes of Rel/NF-kappaB transcription factors.* Oncogene, 1999. **18**(49): p. 6853-66.
233. Feng, S., et al., *Absent in melanoma 2 inflammasome is required for host defence against Streptococcus pneumoniae infection.* Innate Immun, 2019. **25**(7): p. 412-419.
234. Fang, R., et al., *Type I interferon signaling regulates activation of the absent in melanoma 2 inflammasome during Streptococcus pneumoniae infection.* Infect Immun, 2014. **82**(6): p. 2310-7.
235. Houldsworth, S., P.W. Andrew, and T.J. Mitchell, *Pneumolysin stimulates production of tumor necrosis factor alpha and interleukin-1 beta by human mononuclear phagocytes.* Infect Immun, 1994. **62**(4): p. 1501-3.
236. Koppe, U., et al., *Streptococcus pneumoniae stimulates a STING- and IFN regulatory factor 3-dependent type I IFN production in macrophages, which regulates RANTES production in macrophages, cocultured alveolar epithelial cells, and mouse lungs.* J Immunol, 2012. **188**(2): p. 811-7.
237. Herring, S.E., et al., *Mitochondrial ROS production by neutrophils is required for host antimicrobial function against Streptococcus pneumoniae and is controlled by A2B adenosine receptor signaling.* PLoS Pathog, 2022. **18**(11): p. e1010700.
238. Ostermann, L., et al., *S100A9 is indispensable for survival of pneumococcal pneumonia in mice.* PLoS Pathog, 2023. **19**(7): p. e1011493.
239. Sprenkeler, E.G.G., et al., *S100A8/A9 Is a Marker for the Release of Neutrophil Extracellular Traps and Induces Neutrophil Activation.* Cells, 2022. **11**(2).
240. De Filippo, K., et al., *A new protective role for S100A9 in regulation of neutrophil recruitment during invasive pneumococcal pneumonia.* FASEB J, 2014. **28**(8): p. 3600-8.
241. Shaper, M., et al., *PspA protects Streptococcus pneumoniae from killing by apolactoferrin, and antibody to PspA enhances killing of pneumococci by apolactoferrin.* Infect Immun, 2004. **72**(9): p. 5031-40.
242. Angulo-Zamudio, U.A., et al., *Lactoferrin Disaggregates Pneumococcal Biofilms and Inhibits Acquisition of Resistance Through Its DNase Activity.* Front Microbiol, 2019. **10**: p. 2386.
243. Koppe, U., N. Suttorp, and B. Opitz, *Recognition of Streptococcus pneumoniae by the innate immune system.* Cell Microbiol, 2012. **14**(4): p. 460-6.
244. Flemming, H.C., et al., *Biofilms: an emergent form of bacterial life.* Nat Rev Microbiol, 2016. **14**(9): p. 563-75.
245. Leitch, E.C. and M.D. Willcox, *Synergic antistaphylococcal properties of lactoferrin and lysozyme.* J Med Microbiol, 1998. **47**(9): p. 837-42.
246. Leitch, E.C. and M.D.P. Willcox, *Elucidation of the antistaphylococcal action of lactoferrin and lysozyme.* J Med Microbiol, 1999. **48**(9): p. 867-871.
247. Ellison, R.T., 3rd and T.J. Giehl, *Killing of gram-negative bacteria by lactoferrin and lysozyme.* J Clin Invest, 1991. **88**(4): p. 1080-91.
248. Marques, E. and M. Gallazzini, *Lipocalins.* Curr Biol, 2024. **34**(14): p. R670-R672.
249. Warszawska, J.M., et al., *Lipocalin 2 deactivates macrophages and worsens pneumococcal pneumonia outcomes.* J Clin Invest, 2013. **123**(8): p. 3363-72.

250. Boix-Palop, L., et al., *Evaluation of Plasma Lipocalin-2 as a Predictor of Etiology and Severity in Adult Patients with Community-Acquired Pneumonia.* Microorganisms, 2023. **11**(5).
251. Tjabringa, G.S., et al., *Human cathelicidin LL-37 is a chemoattractant for eosinophils and neutrophils that acts via formyl-peptide receptors.* Int Arch Allergy Immunol, 2006. **140**(2): p. 103-12.
252. Merres, J., et al., *Role of the cathelicidin-related antimicrobial peptide in inflammation and mortality in a mouse model of bacterial meningitis.* J Innate Immun, 2014. **6**(2): p. 205-18.
253. Zec, K., et al., *Comparative transcriptomic and proteomic signature of lung alveolar macrophages reveals the integrin CD11b as a regulatory hub during pneumococcal pneumonia infection.* Front Immunol, 2023. **14**: p. 1227191.
254. Ryckman, C., et al., *Proinflammatory activities of S100: proteins S100A8, S100A9, and S100A8/A9 induce neutrophil chemotaxis and adhesion.* J Immunol, 2003. **170**(6): p. 3233-42.
255. Knapp, S., et al., *Alveolar macrophages have a protective antiinflammatory role during murine pneumococcal pneumonia.* Am J Respir Crit Care Med, 2003. **167**(2): p. 171-9.
256. Dockrell, D.H., et al., *Alveolar macrophage apoptosis contributes to pneumococcal clearance in a resolving model of pulmonary infection.* J Immunol, 2003. **171**(10): p. 5380-8.
257. Kruckow, K.L., et al., *Acute organ injury and long-term sequelae of severe pneumococcal infections.* Pneumonia (Nathan), 2023. **15**(1): p. 5.
258. Munoz-Wolf, N., et al., *Sublingual flagellin protects against acute pneumococcal pneumonia in a TLR5-dependent and NLRC4-independent fashion.* Future Microbiol, 2016. **11**: p. 1167-77.
259. Ivanov, S., et al., *Key role for respiratory CD103(+) dendritic cells, IFN-gamma, and IL-17 in protection against Streptococcus pneumoniae infection in response to alpha-galactosylceramide.* J Infect Dis, 2012. **206**(5): p. 723-34.
260. Domon, H., et al., *Neutrophil Elastase Subverts the Immune Response by Cleaving Toll-Like Receptors and Cytokines in Pneumococcal Pneumonia.* Front Immunol, 2018. **9**: p. 732.
261. Yanagihara, K., et al., *Effects of specific neutrophil elastase inhibitor, sivelestat sodium hydrate, in murine model of severe pneumococcal pneumonia.* Exp Lung Res, 2007. **33**(2): p. 71-80.
262. Nakamatsu, M., et al., *Role of interferon-gamma in Valpha14+ natural killer T cell-mediated host defense against Streptococcus pneumoniae infection in murine lungs.* Microbes Infect, 2007. **9**(3): p. 364-74.
263. Kawakami, K., et al., *Critical role of Valpha14+ natural killer T cells in the innate phase of host protection against Streptococcus pneumoniae infection.* Eur J Immunol, 2003. **33**(12): p. 3322-30.
264. Paudel, S., et al., *CXCL1 regulates neutrophil homeostasis in pneumonia-derived sepsis caused by Streptococcus pneumoniae serotype 3.* Blood, 2019. **133**(12): p. 1335-1345.
265. Metzemaekers, M., M. Gouwy, and P. Proost, *Neutrophil chemoattractant receptors in health and disease: double-edged swords.* Cell Mol Immunol, 2020. **17**(5): p. 433-450.

266. Ottonello, L., et al., *CCL3 (MIP-1alpha) induces in vitro migration of GM-CSF-primed human neutrophils via CCR5-dependent activation of ERK 1/2.* Cell Signal, 2005. **17**(3): p. 355-63.
267. Serbina, N.V. and E.G. Pamer, *Monocyte emigration from bone marrow during bacterial infection requires signals mediated by chemokine receptor CCR2.* Nat Immunol, 2006. **7**(3): p. 311-7.
268. Ellis, G.T., et al., *TRAIL+ monocytes and monocyte-related cells cause lung damage and thereby increase susceptibility to influenza-Streptococcus pneumoniae coinfection.* EMBO Rep, 2015. **16**(9): p. 1203-18.
269. Olliver, M., et al., *Human monocytes promote Th1 and Th17 responses to Streptococcus pneumoniae.* Infect Immun, 2011. **79**(10): p. 4210-7.
270. Barthelemy, A., et al., *Exogenous Activation of Invariant Natural Killer T Cells by alpha-Galactosylceramide Reduces Pneumococcal Outgrowth and Dissemination Postinfluenza.* mBio, 2016. **7**(6).
271. Murray, M.P., et al., *Stimulation of a subset of natural killer T cells by CD103(+) DC is required for GM-CSF and protection from pneumococcal infection.* Cell Rep, 2022. **38**(2): p. 110209.
272. Xu, R., et al., *TNFR2(+) regulatory T cells protect against bacteremic pneumococcal pneumonia by suppressing IL-17A-producing gammadelta T cells in the lung.* Cell Rep, 2023. **42**(2): p. 112054.
273. Bradley, L.M., et al., *Matrix metalloprotease 9 mediates neutrophil migration into the airways in response to influenza virus-induced toll-like receptor signaling.* PLoS Pathog, 2012. **8**(4): p. e1002641.
274. Horn, K.J., et al., *Neutrophil responsiveness to IL-10 impairs clearance of Streptococcus pneumoniae from the lungs.* J Leukoc Biol, 2024. **115**(1): p. 4-15.
275. Neill, D.R., et al., *T regulatory cells control susceptibility to invasive pneumococcal pneumonia in mice.* PLoS Pathog, 2012. **8**(4): p. e1002660.
276. Zhang, Q., et al., *Characterisation of regulatory T cells in nasal associated lymphoid tissue in children: relationships with pneumococcal colonization.* PLoS Pathog, 2011. **7**(8): p. e1002175.
277. Szabo, S.J., et al., *A novel transcription factor, T-bet, directs Th1 lineage commitment.* Cell, 2000. **100**(6): p. 655-69.
278. Szabo, S.J., et al., *Distinct effects of T-bet in TH1 lineage commitment and IFN-gamma production in CD4 and CD8 T cells.* Science, 2002. **295**(5553): p. 338-42.
279. Schulz, E.G., et al., *Sequential polarization and imprinting of type 1 T helper lymphocytes by interferon-gamma and interleukin-12.* Immunity, 2009. **30**(5): p. 673-83.
280. Ruan, S., et al., *Th1 promotes M1 polarization of intestinal macrophages to regulate colitis-related mucosal barrier damage.* Aging (Albany NY), 2023. **15**(14): p. 6721-6735.
281. Mills, C.D., et al., *Pillars Article: M-1/M-2 Macrophages and the Th1/Th2 Paradigm. J. Immunol. 2000. 164: 6166-6173.* J Immunol, 2017. **199**(7): p. 2194-2201.
282. Marques, J.M., et al., *Protection against Streptococcus pneumoniae serotype 1 acute infection shows a signature of Th17- and IFN-gamma-mediated immunity.* Immunobiology, 2012. **217**(4): p. 420-9.

283. Harrington, L.E., et al., *Interleukin 17-producing CD4+ effector T cells develop via a lineage distinct from the T helper type 1 and 2 lineages.* Nat Immunol, 2005. **6**(11): p. 1123-32.
284. Sutton, C., et al., *A crucial role for interleukin (IL)-1 in the induction of IL-17-producing T cells that mediate autoimmune encephalomyelitis.* J Exp Med, 2006. **203**(7): p. 1685-91.
285. Lu, Y.J., et al., *Interleukin-17A mediates acquired immunity to pneumococcal colonization.* PLoS Pathog, 2008. **4**(9): p. e1000159.
286. Cao, A.T., et al., *Th17 cells upregulate polymeric Ig receptor and intestinal IgA and contribute to intestinal homeostasis.* J Immunol, 2012. **189**(9): p. 4666-73.
287. Onishi, R.M. and S.L. Gaffen, *Interleukin-17 and its target genes: mechanisms of interleukin-17 function in disease.* Immunology, 2010. **129**(3): p. 311-21.
288. Mitsi, E., et al., *Agglutination by anti-capsular polysaccharide antibody is associated with protection against experimental human pneumococcal carriage.* Mucosal Immunol, 2017. **10**(2): p. 385-394.
289. Hill, H., et al., *A Randomized Controlled Clinical Trial of Nasal Immunization with Live Virulence Attenuated Streptococcus pneumoniae Strains Using Human Infection Challenge.* Am J Respir Crit Care Med, 2023. **208**(8): p. 868-878.
290. Robinson, R.E., et al., *Human Infection Challenge with Serotype 3 Pneumococcus.* Am J Respir Crit Care Med, 2022. **206**(11): p. 1379-1392.
291. Wright, A.K., et al., *Human nasal challenge with Streptococcus pneumoniae is immunising in the absence of carriage.* PLoS Pathog, 2012. **8**(4): p. e1002622.
292. Nikolaou, E., et al., *Experimental Human Challenge Defines Distinct Pneumococcal Kinetic Profiles and Mucosal Responses between Colonized and Non-Colonized Adults.* mBio, 2021. **12**(1).
293. Collins, A.M., et al., *First human challenge testing of a pneumococcal vaccine. Double-blind randomized controlled trial.* Am J Respir Crit Care Med, 2015. **192**(7): p. 853-8.
294. Poolman, J., et al., *Pneumococcal serotype 3 otitis media, limited effect of polysaccharide conjugate immunisation and strain characteristics.* Vaccine, 2009. **27**(24): p. 3213-22.
295. Duke, J.A. and F.Y. Avci, *Emerging vaccine strategies against the incessant pneumococcal disease.* NPJ Vaccines, 2023. **8**(1): p. 122.
296. Song, J.Y., M.H. Nahm, and M.A. Moseley, *Clinical implications of pneumococcal serotypes: invasive disease potential, clinical presentations, and antibiotic resistance.* J Korean Med Sci, 2013. **28**(1): p. 4-15.
297. Hanage, W.P., et al., *Invasiveness of serotypes and clones of Streptococcus pneumoniae among children in Finland.* Infect Immun, 2005. **73**(1): p. 431-5.
298. Moscoso, M., E. Garcia, and R. Lopez, *Biofilm formation by Streptococcus pneumoniae: role of choline, extracellular DNA, and capsular polysaccharide in microbial accretion.* J Bacteriol, 2006. **188**(22): p. 7785-95.
299. Watson, O.J., et al., *Global impact of the first year of COVID-19 vaccination: a mathematical modelling study.* Lancet Infect Dis, 2022. **22**(9): p. 1293-1302.
300. Watanabe, H., et al., *Antimicrobial susceptibility and serotype distribution of Streptococcus pneumoniae and molecular characterization of multidrug-resistant serotype 19F, 6B, and 23F Pneumococci in northern Thailand.* J Clin Microbiol, 2003. **41**(9): p. 4178-83.

301. Pollard, A.J. and E.M. Bijker, *Publisher Correction: A guide to vaccinology: from basic principles to new developments.* Nat Rev Immunol, 2021. **21**(2): p. 129.
302. Pichichero, M.E., *Protein carriers of conjugate vaccines: characteristics, development, and clinical trials.* Hum Vaccin Immunother, 2013. **9**(12): p. 2505-23.
303. Zhao, T., et al., *Vaccine adjuvants: mechanisms and platforms.* Signal Transduct Target Ther, 2023. **8**(1): p. 283.
304. Prevention, C.o.D.C.a. *Shingles Vaccine*. 2025; Available from: https://www.cdc.gov/shingles/vaccines/index.html.
305. Laurens, M.B., *RTS,S/AS01 vaccine (Mosquirix): an overview.* Hum Vaccin Immunother, 2020. **16**(3): p. 480-489.
306. Coccia, M., et al., *Cellular and molecular synergy in AS01-adjuvanted vaccines results in an early IFNgamma response promoting vaccine immunogenicity.* NPJ Vaccines, 2017. **2**: p. 25.
307. Stone, A.E., et al., *Fentanyl conjugate vaccine by injected or mucosal delivery with dmLT or LTA1 adjuvants implicates IgA in protection from drug challenge.* NPJ Vaccines, 2021. **6**(1): p. 69.
308. Lavelle, E.C. and R.W. Ward, *Mucosal vaccines - fortifying the frontiers.* Nat Rev Immunol, 2022. **22**(4): p. 236-250.
309. Abramson, J.S., *Intranasal, cold-adapted, live, attenuated influenza vaccine.* Pediatr Infect Dis J, 1999. **18**(12): p. 1103-4.
310. Prevelance, C.o.D.C.a. *Pneumococcal Disease Surveillance and Trends*. 2024; Available from: https://www.cdc.gov/pneumococcal/php/surveillance/index.html.
311. Black, S., et al., *Efficacy, safety and immunogenicity of heptavalent pneumococcal conjugate vaccine in children. Northern California Kaiser Permanente Vaccine Study Center Group.* Pediatr Infect Dis J, 2000. **19**(3): p. 187-95.
312. Colijn, C., J. Corander, and N.J. Croucher, *Designing ecologically optimized pneumococcal vaccines using population genomics.* Nat Microbiol, 2020. **5**(3): p. 473-485.
313. Cohen, J., Kupferschmidt K., *Fairer Shares.* Science, 2021.
314. Wahl, B., et al., *Burden of Streptococcus pneumoniae and Haemophilus influenzae type b disease in children in the era of conjugate vaccines: global, regional, and national estimates for 2000-15.* Lancet Glob Health, 2018. **6**(7): p. e744-e757.
315. Li, J., et al., *Cross reactivity within pneumococcal serogroups 6 and 15 following adult vaccination with pneumococcal conjugate vaccine V116.* Commun Med (Lond), 2025. **5**(1): p. 443.
316. Jha, V. and E.N. Janoff, *Complementary Role of CD4+ T Cells in Response to Pneumococcal Polysaccharide Vaccines in Humans.* Vaccines (Basel), 2019. **7**(1).
317. Clutterbuck, E.A., et al., *Serotype-specific and age-dependent generation of pneumococcal polysaccharide-specific memory B-cell and antibody responses to immunization with a pneumococcal conjugate vaccine.* Clin Vaccine Immunol, 2008. **15**(2): p. 182-93.

318. Kadioglu, A., et al., *The role of Streptococcus pneumoniae virulence factors in host respiratory colonization and disease.* Nat Rev Microbiol, 2008. **6**(4): p. 288-301.
319. Wilson, R., et al., *Protection against Streptococcus pneumoniae lung infection after nasopharyngeal colonization requires both humoral and cellular immune responses.* Mucosal Immunol, 2015. **8**(3): p. 627-39.
320. Cockeran, R., R. Anderson, and C. Feldman, *The role of pneumolysin in the pathogenesis of Streptococcus pneumoniae infection.* Curr Opin Infect Dis, 2002. **15**(3): p. 235-9.
321. Hollingshead, S.K. and D.E. Briles, *Streptococcus pneumoniae: new tools for an old pathogen.* Curr Opin Microbiol, 2001. **4**(1): p. 71-7.
322. Oleszycka, E., et al., *The vaccine adjuvant alum promotes IL-10 production that suppresses Th1 responses.* Eur J Immunol, 2018. **48**(4): p. 705-715.
323. Jordan, M.B., et al., *Promotion of B cell immune responses via an alum-induced myeloid cell population.* Science, 2004. **304**(5678): p. 1808-10.
324. Finkelman, F.D., et al., *IFN-gamma regulates the isotypes of Ig secreted during in vivo humoral immune responses.* J Immunol, 1988. **140**(4): p. 1022-7.
325. Snapper, C.M., C. Peschel, and W.E. Paul, *IFN-gamma stimulates IgG2a secretion by murine B cells stimulated with bacterial lipopolysaccharide.* J Immunol, 1988. **140**(7): p. 2121-7.
326. Munoz-Wolf, N., et al., *Non-canonical inflammasome activation mediates the adjuvanticity of nanoparticles.* Cell Rep Med, 2023. **4**(1): p. 100899.
327. Robla, S., et al., *A chitosan-based nanosystem as pneumococcal vaccine delivery platform.* Drug Deliv Transl Res, 2021. **11**(2): p. 581-597.
328. Xu, J.H., et al., *Mucosal immunization with PsaA protein, using chitosan as a delivery system, increases protection against acute otitis media and invasive infection by Streptococcus pneumoniae.* Scand J Immunol, 2015. **81**(3): p. 177-85.
329. Xu, J., et al., *Intranasal vaccination with chitosan-DNA nanoparticles expressing pneumococcal surface antigen a protects mice against nasopharyngeal colonization by Streptococcus pneumoniae.* Clin Vaccine Immunol, 2011. **18**(1): p. 75-81.
330. Carroll, E.C., et al., *The Vaccine Adjuvant Chitosan Promotes Cellular Immunity via DNA Sensor cGAS-STING-Dependent Induction of Type I Interferons.* Immunity, 2016. **44**(3): p. 597-608.
331. Longet, S., et al., *An oral alpha-galactosylceramide adjuvanted Helicobacter pylori vaccine induces protective IL-1R- and IL-17R-dependent Th1 responses.* NPJ Vaccines, 2019. **4**: p. 45.
332. Davitt, C.J.H., et al., *Alpha-galactosylceramide enhances mucosal immunity to oral whole-cell cholera vaccines.* Mucosal Immunol, 2019. **12**(4): p. 1055-1064.
333. Mizel, S.B. and J.T. Bates, *Flagellin as an adjuvant: cellular mechanisms and potential.* J Immunol, 2010. **185**(10): p. 5677-82.
334. Munoz, N., et al., *Mucosal administration of flagellin protects mice from Streptococcus pneumoniae lung infection.* Infect Immun, 2010. **78**(10): p. 4226-33.
335. Porte, R., et al., *A Toll-Like Receptor 5 Agonist Improves the Efficacy of Antibiotics in Treatment of Primary and Influenza Virus-Associated*

Pneumococcal Mouse Infections. Antimicrob Agents Chemother, 2015. **59**(10): p. 6064-72.
336. Mutsch, M., et al., *Use of the inactivated intranasal influenza vaccine and the risk of Bell's palsy in Switzerland.* N Engl J Med, 2004. **350**(9): p. 896-903.
337. Lewis, D.J., et al., *Transient facial nerve paralysis (Bell's palsy) following intranasal delivery of a genetically detoxified mutant of Escherichia coli heat labile toxin.* PLoS One, 2009. **4**(9): p. e6999.
338. Norton, E.B., et al., *Characterization of a mutant Escherichia coli heat-labile toxin, LT(R192G/L211A), as a safe and effective oral adjuvant.* Clin Vaccine Immunol, 2011. **18**(4): p. 546-51.
339. Clements, J.D. and E.B. Norton, *The Mucosal Vaccine Adjuvant LT(R192G/L211A) or dmLT.* mSphere, 2018. **3**(4).
340. Valli, E., et al., *LTA1 is a safe, intranasal enterotoxin-based adjuvant that improves vaccine protection against influenza in young, old and B-cell-depleted (muMT) mice.* Sci Rep, 2019. **9**(1): p. 15128.
341. Molina Estupinan, J.L., et al., *The adjuvants dmLT and mmCT enhance humoral immune responses to a pneumococcal conjugate vaccine after both parenteral or mucosal immunization of neonatal mice.* Front Immunol, 2022. **13**: p. 1078904.
342. Stone, A.E., et al., *Route and antigen shape immunity to dmLT-adjuvanted vaccines to a greater extent than biochemical stress or formulation excipients.* Vaccine, 2023. **41**(9): p. 1589-1601.
343. Isobe, J., et al., *Commensal-bacteria-derived butyrate promotes the T-cell-independent IgA response in the colon.* Int Immunol, 2020. **32**(4): p. 243-258.
344. Lynn, D.J., Benson, S.C., Lynn, M.A., Pulendran, B., *Modulation of immune responses to vaccination by the microbiota: implications and potential mechanisms.* Nature Reviews Immunology, 2022(22): p. 33–46.
345. Hagan, T., et al., *Antibiotics-Driven Gut Microbiome Perturbation Alters Immunity to Vaccines in Humans.* Cell, 2019. **178**(6): p. 1313-1328 e13.
346. Lamouse-Smith, E.S., A. Tzeng, and M.N. Starnbach, *The intestinal flora is required to support antibody responses to systemic immunization in infant and germ free mice.* PLoS One, 2011. **6**(11): p. e27662.
347. Harris, V.C., et al., *Effect of Antibiotic-Mediated Microbiome Modulation on Rotavirus Vaccine Immunogenicity: A Human, Randomized-Control Proof-of-Concept Trial.* Cell Host Microbe, 2018. **24**(2): p. 197-207 e4.
348. Chapman, T.J., et al., *Antibiotic Use and Vaccine Antibody Levels.* Pediatrics, 2022. **149**(5).
349. Takeuchi, T., et al., *Acetate differentially regulates IgA reactivity to commensal bacteria.* Nature, 2021. **595**(7868): p. 560-564.
350. Wu, W., et al., *Microbiota metabolite short-chain fatty acid acetate promotes intestinal IgA response to microbiota which is mediated by GPR43.* Mucosal Immunol, 2017. **10**(4): p. 946-956.
351. Furusawa, Y., et al., *Commensal microbe-derived butyrate induces the differentiation of colonic regulatory T cells.* Nature, 2013. **504**(7480): p. 446-50.
352. Arpaia, N., et al., *Metabolites produced by commensal bacteria promote peripheral regulatory T-cell generation.* Nature, 2013. **504**(7480): p. 451-5.

353. Zaiatz-Bittencourt, V., et al., *Butyrate limits human natural killer cell effector function.* Sci Rep, 2023. **13**(1): p. 2715.
354. Luu, M., et al., *Microbial short-chain fatty acids modulate CD8(+) T cell responses and improve adoptive immunotherapy for cancer.* Nat Commun, 2021. **12**(1): p. 4077.
355. Rosenberg, J. and J. Huang, *CD8(+) T Cells and NK Cells: Parallel and Complementary Soldiers of Immunotherapy.* Curr Opin Chem Eng, 2018. **19**: p. 9-20.
356. Carlini, F., et al., *Butyrate enhances CD56(bright) NK cell-driven killing of activated T cells and modulates NK cell chromatin accessibility.* Genes Immun, 2025. **26**(4): p. 342-351.
357. Perez, M., et al., *Microbiota-Derived Short-Chain Fatty Acids Boost Antitumoral Natural Killer Cell Activity.* J Clin Med, 2024. **13**(13).
358. Dupraz, L., et al., *Gut microbiota-derived short-chain fatty acids regulate IL-17 production by mouse and human intestinal gammadelta T cells.* Cell Rep, 2021. **36**(1): p. 109332.
359. Fricke, W.F., et al., *Type 2 immunity-dependent reduction of segmented filamentous bacteria in mice infected with the helminthic parasite Nippostrongylus brasiliensis.* Microbiome, 2015. **3**: p. 40.
360. Bradley, C.P., et al., *Segmented Filamentous Bacteria Provoke Lung Autoimmunity by Inducing Gut-Lung Axis Th17 Cells Expressing Dual TCRs.* Cell Host Microbe, 2017. **22**(5): p. 697-704 e4.
361. Gauguet, S., et al., *Intestinal Microbiota of Mice Influences Resistance to Staphylococcus aureus Pneumonia.* Infect Immun, 2015. **83**(10): p. 4003-14.
362. Oh, J.Z., et al., *TLR5-mediated sensing of gut microbiota is necessary for antibody responses to seasonal influenza vaccination.* Immunity, 2014. **41**(3): p. 478-492.
363. Lynn, M.A., et al., *Early-Life Antibiotic-Driven Dysbiosis Leads to Dysregulated Vaccine Immune Responses in Mice.* Cell Host Microbe, 2018. **23**(5): p. 653-660 e5.
364. Nakaya, H.I., et al., *Systems biology of vaccination for seasonal influenza in humans.* Nat Immunol, 2011. **12**(8): p. 786-95.
365. Kim, D., et al., *Corrigendum: Nod2-mediated recognition of the microbiota is critical for mucosal adjuvant activity of cholera toxin.* Nat Med, 2016. **22**(8): p. 961.
366. Ivanov, II and D.R. Littman, *Segmented filamentous bacteria take the stage.* Mucosal Immunol, 2010. **3**(3): p. 209-12.
367. Wu, Q., et al., *Short-Chain Fatty Acids Alleviate Vancomycin-Caused Humoral Immunity Attenuation in Rabies-Vaccinated Mice by Promoting the Generation of Plasma Cells via Akt-mTOR Pathway.* J Virol, 2023. **97**(7): p. e0065623.
368. Dufort, F.J., et al., *Glucose-dependent de novo lipogenesis in B lymphocytes: a requirement for atp-citrate lyase in lipopolysaccharide-induced differentiation.* J Biol Chem, 2014. **289**(10): p. 7011-7024.
369. Fagone, P., et al., *Phospholipid biosynthesis program underlying membrane expansion during B-lymphocyte differentiation.* J Biol Chem, 2007. **282**(10): p. 7591-605.

370. Caro-Maldonado, A., et al., *Metabolic reprogramming is required for antibody production that is suppressed in anergic but exaggerated in chronically BAFF-exposed B cells.* J Immunol, 2014. **192**(8): p. 3626-36.
371. Sanchez, H.N., et al., *B cell-intrinsic epigenetic modulation of antibody responses by dietary fiber-derived short-chain fatty acids.* Nat Commun, 2020. **11**(1): p. 60.
372. Lauro, M.L., J.M. Burch, and C.L. Grimes, *The effect of NOD2 on the microbiota in Crohn's disease.* Curr Opin Biotechnol, 2016. **40**: p. 97-102.
373. Heinken, A., J. Hertel, and I. Thiele, *Metabolic modelling reveals broad changes in gut microbial metabolism in inflammatory bowel disease patients with dysbiosis.* NPJ Syst Biol Appl, 2021. **7**(1): p. 19.
374. Jacobsen, H.A., et al., *Increased risk of obstructive lung disease in inflammatory bowel disease: A population-based cohort study.* United European Gastroenterol J, 2024. **12**(4): p. 477-486.
375. Long, M.D., et al., *Increased risk of pneumonia among patients with inflammatory bowel disease.* Am J Gastroenterol, 2013. **108**(2): p. 240-8.
376. Herrlinger, K.R., et al., *Alterations in pulmonary function in inflammatory bowel disease are frequent and persist during remission.* Am J Gastroenterol, 2002. **97**(2): p. 377-81.
377. Smith, R.A., et al., *Patients With Inflammatory Bowel Disease Are at Increased Risk of Hospitalization Due to Respiratory Syncytial Virus.* Am J Gastroenterol, 2024. **119**(8): p. 1545-1554.
378. Kantso, B., et al., *Inflammatory Bowel Disease Patients Are at Increased Risk of Invasive Pneumococcal Disease: A Nationwide Danish Cohort Study 1977-2013.* Am J Gastroenterol, 2015. **110**(11): p. 1582-7.
379. Kan, H., et al., *Dietary fiber, lung function, and chronic obstructive pulmonary disease in the atherosclerosis risk in communities study.* Am J Epidemiol, 2008. **167**(5): p. 570-8.
380. Thomas, S.T., et al., *Fetal Liver-Derived Alveolar-like Macrophages: A Self-Replicating Ex Vivo Model of Alveolar Macrophages for Functional Genetic Studies.* Immunohorizons, 2022. **6**(2): p. 156-169.
381. Chang, K.C., N. Nagarajan, and Y.H. Gan, *Short-chain fatty acids of various lengths differentially inhibit Klebsiella pneumoniae and Enterobacteriaceae species.* mSphere, 2024. **9**(2): p. e0078123.
382. Jacobson, A., et al., *A Gut Commensal-Produced Metabolite Mediates Colonization Resistance to Salmonella Infection.* Cell Host Microbe, 2018. **24**(2): p. 296-307 e7.
383. Silva, C., et al., *Short-Chain Fatty Acids Promote Mycobacterium avium subsp. hominissuis Growth in Nutrient-Limited Environments and Influence Susceptibility to Antibiotics.* Pathogens, 2020. **9**(9).
384. Lim, S., et al., *Serotype-Dependent Inhibition of Streptococcus pneumoniae Growth by Short-Chain Fatty Acids.* J Microbiol Biotechnol, 2024. **34**(1): p. 47-55.
385. Gill, P.A., et al., *A randomized dietary intervention to increase colonic and peripheral blood SCFAs modulates the blood B- and T-cell compartments in healthy humans.* Am J Clin Nutr, 2022. **116**(5): p. 1354-1367.

386. dos Santos, M.P., et al., *Sodium butyrate enhances the cytotoxic effect of antineoplastic drugs in human lymphoblastic T-cells.* Leuk Res, 2009. **33**(2): p. 218-21.
387. Salimi, V., et al., *Sodium butyrate promotes apoptosis in breast cancer cells through reactive oxygen species (ROS) formation and mitochondrial impairment.* Lipids Health Dis, 2017. **16**(1): p. 208.
388. Konishi, H., et al., *The butyrate derived from probiotic Clostridium butyricum exhibits an inhibitory effect on multiple myeloma through cell death induction.* Sci Rep, 2025. **15**(1): p. 11919.
389. Sealy, L. and R. Chalkley, *The effect of sodium butyrate on histone modification.* Cell, 1978. **14**(1): p. 115-21.
390. Chang, P.V., et al., *The microbial metabolite butyrate regulates intestinal macrophage function via histone deacetylase inhibition.* Proc Natl Acad Sci U S A, 2014. **111**(6): p. 2247-52.
391. Huang, C., et al., *The effect of short-chain fatty acids on M2 macrophages polarization in vitro and in vivo.* Clin Exp Immunol, 2022. **207**(1): p. 53-64.
392. Schmeck, B., et al., *Pneumococci induced TLR- and Rac1-dependent NF-kappaB-recruitment to the IL-8 promoter in lung epithelial cells.* Am J Physiol Lung Cell Mol Physiol, 2006. **290**(4): p. L730-L737.
393. Urban, B.C., et al., *Inflammation of the nasal mucosa is associated with susceptibility to experimental pneumococcal challenge in older adults.* Mucosal Immunol, 2024. **17**(5): p. 973-989.
394. Tavares, L.P., et al., *CXCR1/2 Antagonism Is Protective during Influenza and Post-Influenza Pneumococcal Infection.* Front Immunol, 2017. **8**: p. 1799.
395. Nilsen, N.J., et al., *A role for the adaptor proteins TRAM and TRIF in toll-like receptor 2 signaling.* J Biol Chem, 2015. **290**(6): p. 3209-22.
396. Stack, J., et al., *TRAM is required for TLR2 endosomal signaling to type I IFN induction.* J Immunol, 2014. **193**(12): p. 6090-102.
397. Terawaki, S., et al., *RUN and FYVE domain-containing protein 4 enhances autophagy and lysosome tethering in response to Interleukin-4.* J Cell Biol, 2015. **210**(7): p. 1133-52.
398. Valecka, J., et al., *RUFY4 exists as two translationally regulated isoforms, that localize to the mitochondrion in activated macrophages.* R Soc Open Sci, 2021. **8**(7): p. 202333.
399. Prieto, L.I., S.I. Graves, and D.J. Baker, *Insights from In Vivo Studies of Cellular Senescence.* Cells, 2020. **9**(4).
400. Prieto, L.I., et al., *Senescent alveolar macrophages promote early-stage lung tumorigenesis.* Cancer Cell, 2023. **41**(7): p. 1261-1275 e6.
401. Kell, D.B., E.L. Heyden, and E. Pretorius, *The Biology of Lactoferrin, an Iron-Binding Protein That Can Help Defend Against Viruses and Bacteria.* Front Immunol, 2020. **11**: p. 1221.
402. Zakrzewicz, D., et al., *Host-derived extracellular RNA promotes adhesion of Streptococcus pneumoniae to endothelial and epithelial cells.* Sci Rep, 2016. **6**: p. 37758.
403. Boehmer, D. and I. Zanoni, *Interferons in health and disease.* Cell, 2025. **188**(17): p. 4480-4504.

404. Yum, S., et al., *TBK1 recruitment to STING activates both IRF3 and NF-kappaB that mediate immune defense against tumors and viral infections.* Proc Natl Acad Sci U S A, 2021. **118**(14).
405. Jefferies, C.A., *Regulating IRFs in IFN Driven Disease.* Front Immunol, 2019. **10**: p. 325.
406. Nyazika, T.K., et al., *Intracellular survival of Streptococcus pneumoniae in human alveolar macrophages is augmented with HIV infection.* Front Immunol, 2022. **13**: p. 992659.
407. Kadioglu, A., et al., *Sex-based differences in susceptibility to respiratory and systemic pneumococcal disease in mice.* J Infect Dis, 2011. **204**(12): p. 1971-9.
408. Georges, H., et al., *Epidemiological features and prognosis of severe community-acquired pneumococcal pneumonia.* Intensive Care Med, 1999. **25**(2): p. 198-206.
409. Falagas, M.E., E.G. Mourtzoukou, and K.Z. Vardakas, *Sex differences in the incidence and severity of respiratory tract infections.* Respir Med, 2007. **101**(9): p. 1845-63.
410. Bast, D.J., et al., *Novel murine model of pneumococcal pneumonia: use of temperature as a measure of disease severity to compare the efficacies of moxifloxacin and levofloxacin.* Antimicrob Agents Chemother, 2004. **48**(9): p. 3343-8.
411. Vujkovic-Cvijin, I., et al., *Host variables confound gut microbiota studies of human disease.* Nature, 2020. **587**(7834): p. 448-454.
412. Bode, C., et al., *Linezolid, vancomycin and daptomycin modulate cytokine production, Toll-like receptors and phagocytosis in a human in vitro model of sepsis.* J Antibiot (Tokyo), 2015. **68**(8): p. 485-90.
413. Zimmermann, P., et al., *The Immunomodulatory Effects of Macrolides-A Systematic Review of the Underlying Mechanisms.* Front Immunol, 2018. **9**: p. 302.
414. Ryu, A.H., et al., *Use antibiotics in cell culture with caution: genome-wide identification of antibiotic-induced changes in gene expression and regulation.* Sci Rep, 2017. **7**(1): p. 7533.
415. Hoverstad, T., et al., *Influence of oral intake of seven different antibiotics on faecal short-chain fatty acid excretion in healthy subjects.* Scand J Gastroenterol, 1986. **21**(8): p. 997-1003.
416. Reikvam, D.H., et al., *Depletion of murine intestinal microbiota: effects on gut mucosa and epithelial gene expression.* PLoS One, 2011. **6**(3): p. e17996.
417. Macpherson, A.J. and T. Uhr, *Induction of protective IgA by intestinal dendritic cells carrying commensal bacteria.* Science, 2004. **303**(5664): p. 1662-5.
418. Bunker, J.J., et al., *Innate and Adaptive Humoral Responses Coat Distinct Commensal Bacteria with Immunoglobulin A.* Immunity, 2015. **43**(3): p. 541-53.
419. Dollive, S., et al., *Fungi of the murine gut: episodic variation and proliferation during antibiotic treatment.* PLoS One, 2013. **8**(8): p. e71806.
420. Bongers, K.S., et al., *Antibiotics cause metabolic changes in mice primarily through microbiome modulation rather than behavioral changes.* PLoS One, 2022. **17**(3): p. e0265023.
421. Gutzeit, C., et al., *Gut IgA functionally interacts with systemic IgG to enhance antipneumococcal vaccine responses.* Sci Adv, 2025. **11**(7): p. eado9455.

422. Kerr, A.R., et al., *Role of inflammatory mediators in resistance and susceptibility to pneumococcal infection.* Infect Immun, 2002. **70**(3): p. 1547-57.
423. Davie, J.R., *Inhibition of histone deacetylase activity by butyrate.* J Nutr, 2003. **133**(7 Suppl): p. 2485S-2493S.
424. Huang, S., et al., *Lachnospiraceae-derived butyrate mediates protection of high fermentable fiber against placental inflammation in gestational diabetes mellitus.* Sci Adv, 2023. **9**(44): p. eadi7337.
425. Sencio, V., et al., *Gut Dysbiosis during Influenza Contributes to Pulmonary Pneumococcal Superinfection through Altered Short-Chain Fatty Acid Production.* Cell Rep, 2020. **30**(9): p. 2934-2947 e6.
426. Lewnard, J.A., et al., *Childhood vaccines and antibiotic use in low- and middle-income countries.* Nature, 2020. **581**(7806): p. 94-99.
427. Geno, K.A., et al., *Pneumococcal Capsules and Their Types: Past, Present, and Future.* Clin Microbiol Rev, 2015. **28**(3): p. 871-99.
428. Chilton, P.M., et al., *Adjuvant activity of naturally occurring monophosphoryl lipopolysaccharide preparations from mucosa-associated bacteria.* Infect Immun, 2013. **81**(9): p. 3317-25.
429. Antunes, K.H., et al., *Short-chain fatty acid acetate triggers antiviral response mediated by RIG-I in cells from infants with respiratory syncytial virus bronchiolitis.* EBioMedicine, 2022. **77**: p. 103891.
430. Kiyono, H. and P.B. Ernst, *Nasal vaccines for respiratory infections.* Nature, 2025. **641**(8062): p. 321-330.
431. Tang, B., et al., *Correlation of gut microbiota and metabolic functions with the antibody response to the BBIBP-CorV vaccine.* Cell Rep Med, 2022. **3**(10): p. 100752.
432. Salkowska, A., et al., *Differentiation stage-specific effect of histone deacetylase inhibitors on the expression of RORgammaT in human lymphocytes.* J Leukoc Biol, 2017. **102**(6): p. 1487-1495.
433. Collection, A.T.C. *Streptococcus pneumoniae (Klein) Chester - BAA-334 ™*. Available from: https://www.atcc.org/products/baa-334.
434. Lalor, S.J. and R.M. McLoughlin, *Memory gammadelta T Cells-Newly Appreciated Protagonists in Infection and Immunity.* Trends Immunol, 2016. **37**(10): p. 690-702.
435. Murphy, A.G., et al., *Correction: Staphylococcus aureus Infection of mice expands a population of memory gammadelta T cells that are protective against subsequent infection.* J Immunol, 2015. **194**(9): p. 4588.
436. Baaten, B.J., et al., *CD44 regulates survival and memory development in Th1 cells.* Immunity, 2010. **32**(1): p. 104-15.
437. Ryman, J., et al., *Predicting vaccine effectiveness against invasive pneumococcal disease in children using immunogenicity data.* NPJ Vaccines, 2022. **7**(1): p. 140.
438. Janoff, E.N., et al., *Pneumococcal IgA1 protease subverts specific protection by human IgA1.* Mucosal Immunol, 2014. **7**(2): p. 249-56.
439. standardization., W.H.O.E.c.o.b., *Recommendations to assure the quality, safety and efficacy of pneumococcal conjugate vaccines*, in *Geneva: Replacement of WHO Technical Report Series, No 927, Annex 2; 2009*. p. 91–151.

440. Sterrett, S., et al., *Peripheral CD4 T follicular cells induced by a conjugated pneumococcal vaccine correlate with enhanced opsonophagocytic antibody responses in younger individuals.* Vaccine, 2020. **38**(7): p. 1778-1786.
441. Lynn, D.J., et al., *Modulation of immune responses to vaccination by the microbiota: implications and potential mechanisms.* Nat Rev Immunol, 2022. **22**(1): p. 33-46.
442. Zhang, H., et al., *Type I interferon remodels lysosome function and modifies intestinal epithelial defense.* Proc Natl Acad Sci U S A, 2020. **117**(47): p. 29862-29871.
443. Wee, Y.S., et al., *Interferon-inducible transmembrane proteins of the innate immune response act as membrane organizers by influencing clathrin and v-ATPase localization and function.* Innate Immun, 2012. **18**(6): p. 834-45.
444. Zhuang, L., et al., *Fecal microbiota transplantation in severe pneumonia: a case report on overcoming pan-drug resistant Klebsiella pneumoniae infection.* Front Med (Lausanne), 2024. **11**: p. 1451751.
445. Antunes, K.H., et al., *Microbiota-derived acetate protects against respiratory syncytial virus infection through a GPR43-type 1 interferon response.* Nat Commun, 2019. **10**(1): p. 3273.
446. Hu, L., et al., *Gut microbiota-derived acetate attenuates lung injury induced by influenza infection via protecting airway tight junctions.* J Transl Med, 2024. **22**(1): p. 570.
447. Park, D.E., et al., *The differential impact of coadministered vaccines, geographic region, vaccine product and other covariates on pneumococcal conjugate vaccine immunogenicity.* Pediatr Infect Dis J, 2014. **33 Suppl 2**(Suppl 2 Optimum Dosing of Pneumococcal Conjugate Vaccine For Infants 0 A Landscape Analysis of Evidence Supportin g Different Schedules): p. S130-9.
448. Choe, Y.J., et al., *Associations between geographic region and immune response variations to pneumococcal conjugate vaccines in clinical trials: A systematic review and meta-analysis.* Int J Infect Dis, 2020. **92**: p. 261-268.
449. Loh, J.S., et al., *Microbiota-gut-brain axis and its therapeutic applications in neurodegenerative diseases.* Signal Transduct Target Ther, 2024. **9**(1): p. 37.
450. Dang, A.T. and B.J. Marsland, *Microbes, metabolites, and the gut-lung axis.* Mucosal Immunol, 2019. **12**(4): p. 843-850.
451. Pabst, O., et al., *Gut-liver axis: barriers and functional circuits.* Nat Rev Gastroenterol Hepatol, 2023. **20**(7): p. 447-461.
452. Djaoudene, O., et al., *A Global Overview of Dietary Supplements: Regulation, Market Trends, Usage during the COVID-19 Pandemic, and Health Effects.* Nutrients, 2023. **15**(15).
453. Hossain, M.S., et al., *Dietary Phytochemicals in Health and Disease: Mechanisms, Clinical Evidence, and Applications-A Comprehensive Review.* Food Sci Nutr, 2025. **13**(3): p. e70101.
454. Chen, Y.J., et al., *Short-chain fatty acids ameliorate imiquimod-induced skin thickening and IL-17 levels and alter gut microbiota in mice: a metagenomic association analysis.* Sci Rep, 2024. **14**(1): p. 17495.